Budapest University of Technology and Economics

PhD Thesis

Non-perturbative Methods in Quantum Field Theories

Author:
Péter Mati

Supervisor:
Prof. Antal Jakovác

Department of Theoretical Physics

April 2015

Abstract

Non-perturbative Methods in Quantum Field Theories

by Péter Mati

The non-perturbative aspects of quantum field theories (QFT) seem to be indispensable to understand the qualitative behaviour of strongly interacting physical systems. In my thesis we are going to discuss two different non-perturbative approach. One of them is the 2PI (Two-Particle Irreducible) functional technique combined with the Dyson-Schwinger equation. Essentially, it is based on resumming a particular class of Feynman diagrams, in a well-controlled, systematic way. This is going to be applied to the Bloch-Nordsieck model (at zero and finite temperature) which can be considered as the low frequency limit of Quantum Electrodynamics. The second is the Functional (or Exact) Renormalisation Group (FRG) approach. Here, the Wilsonian idea is used: by integrating out the rapid degrees of freedom, an effective description of the theory is obtained, which is proved useful in the investigation of the phase diagram and critical behaviour of the system under consideration. We will explore the fixed point structure of the O(N) model in various dimensions.

Acknowledgements

I would like to thank my supervisor, Antal Jakovác, who gave me all his support during these years and many ideas with his brilliant insight on physics.
I also thank Zsolt Szép, who always gave me selfless help when I needed.
I would like to thank the support of the MTA-DE Particle Physics Research Group, too. And within the group, a special thanks goes to István Nándori who made possible our joint research.
I thank András Patkós the discussions and the help he provided when I needed advice regarding physical problems.
I also would like to thank Daniel Litim the semester that I could spend at the University of Sussex under his supervision.
And of course, I would like to thank all my family members and friends, who gave me constant support during the years ...

Contents

Abstract ii

Acknowledgements iii

Contents iv

Abbreviations ix

1 Introduction 1
- 1.1 Perturbation Theory . . . 2
- 1.2 Renormalisation . . . 6
  - 1.2.1 Traditional way . . . 6
  - 1.2.2 The modern approach . . . 8
- 1.3 Basics of the functional formalism of QFT . . . 11
- 1.4 Outline of the thesis . . . 14

2 Exploring Quantum Electrodynamics in the Infrared 17
- 2.1 The infrared catastrophe . . . 18
- 2.2 The Bloch-Nordsieck model . . . 24
  - 2.2.1 The breakdown of the perturbation series . . . 25
  - 2.2.2 Two-Particle Irreducible (2PI) resummation in the Bloch-Nordsieck model . . . 27
    - 2.2.2.1 Analytic study of the 2PI equations . . . 29
    - 2.2.2.2 Numerical solution . . . 30
  - 2.2.3 Dyson-Schwinger equations and Ward identities . . . 33
- 2.3 The Bloch-Nordsieck model at finite temperature . . . 38
  - 2.3.1 The finite temperature formalism . . . 38
  - 2.3.2 Dyson-Schwinger equations in the Bloch-Nordsieck model at finite temperature . . . 40
  - 2.3.3 Calculation of $\mathcal{J}$ . . . 43
  - 2.3.4 Renormalisation . . . 44
  - 2.3.5 Zero velocity case . . . 45
  - 2.3.6 Finite velocity case . . . 51
    - 2.3.6.1 Small time behaviour . . . 52
    - 2.3.6.2 Large time behaviour . . . 52

2.3.6.3 Solution for $t \in (0, \infty)$ . . . 53
2.3.7 Discussion of earlier results . . . 55
2.4 Applying the 2PI technique at finite temperature . . . 57
2.4.1 The 2PI equations at finite temperatures . . . 58
2.4.2 One-loop correction at $T \neq 0$ . . . 59
2.4.3 Non-zero temperature calculations in the 2PI framework . . . 60
2.4.4 2PI results . . . 62
2.4.5 The zero velocity case . . . 62
2.4.6 The finite velocity case . . . 68
2.5 Chapter summary . . . 69

3 The Functional Renormalisation Group Study of the O(N) model 73
3.1 Coarse-graining and the Wilsonian approach . . . 74
3.1.1 Criticality and fixed points . . . 76
3.1.2 The Wilson-Polchinski approach . . . 78
3.1.3 The effective average action . . . 81
3.1.4 Approximations of the effective average action . . . 86
3.2 The O(N) model in the framework of FRG . . . 87
3.3 The O(N) model and the spontaneous breaking of symmetry . . . 90
3.4 Mermin-Wagner-Hohenberg-Coleman theorem for the O(N) model in the framework of FRG . . . 92
3.4.1 MW theorem for finite N . . . 92
3.4.2 MW theorem for the spherical model . . . 95
3.5 The phase structure of the O(N) model . . . 96
3.5.1 The Vanishing Beta Function curves . . . 96
3.5.2 VBF curves for $D \leq 2$ . . . 100
3.5.2.1 Continuous symmetries ($N \geq 2$) . . . 100
3.5.2.2 $\mathbb{Z}_2$ symmetry ($N = 1$) . . . 104
3.5.3 VBF curves for $2 < D < 4$ . . . 106
3.5.4 VBF curves for $D \geq 4$ . . . 110
3.5.4.1 Triviality of the O(N) model in $D > 4$ . . . 112
3.5.4.2 Triviality of the O(N) model in $D = 4$ . . . 115
3.5.5 The N dependence and the large-N limit . . . 119
3.5.5.1 N dependence for O(N) theories in $D \leq 2$ . . . 119
3.5.5.2 N dependence in $2 < D < 4$ . . . 120
3.5.5.3 N dependence in $D \geq 4$ . . . 121
3.5.6 The fractal dimensions . . . 125
3.6 Chapter summary . . . 126

4 Summary and thesis statements 129

A One-loop integral in the Bloch-Nordsieck model 133

B The 2PI functional technique 135

C Basics of the finite temperature field theory in CTP formalism 139

C.1 Propagators 140
C.2 Equilibrium 142

D Local operator equations **145**
D.1 The Dyson-Schwinger equation 145
D.2 The vertex function 146
D.3 Ward identities 147

E BN model calculations at $T > 0$ **149**
E.1 The calculation of Eq. (2.116) 149
E.2 The calculation of Eq. (2.137) 150

F One-loop correction in the BN model at finite temperature **151**

G Derivation of the RG equations **157**
G.1 The exact RG equations 157
G.1.1 RG equation for $W_k[J]$ 158
G.1.2 RG equation for $\Gamma_k[\phi]$ 158
G.1.3 The RG equation in the LPA for the O(N) model 160

H Proof of the nested formula **161**

Bibliography **167**

Abbreviations

QFT	**Q**uantum **F**ield **T**heory
PT	**P**erturbation **T**heory
1PI	**One**-**P**article **I**rreducible
2PI	**Two**-**P**article **I**rreducible
RG	**R**enormalisation **G**roup
FRG	**F**unctional **R**enormalisation **G**roup
BN	**B**loch-**N**ordsieck
IR	**I**nfra**R**ed
UV	**U**ltra**V**iolet
MW	**M**ermin **W**agner(-Coleman)
LHS	**L**eft **H**and **S**ide
RHS	**R**ight **H**and **S**ide

Dedicated to my family and many friends....

Chapter 1

Introduction

The subatomic particles behave in such ways that seem completely bizarre from the human perspective, and at some point we even lose our intuition based on everyday classical physics. To understand contemporary theoretical physics R. P. Feynman said once: "If you want to learn about nature, to appreciate nature, it is necessary to understand the language that she speaks in". The mathematical model was manifested under the name of Quantum Field Theory (QFT) and has proved to be the most successful strategy in the description of elementary particle interactions, and as such is regarded as a fundamental part of modern theoretical physics. In most textbooks the emphasis is on the effectiveness of the theory, which at present essentially means perturbative QFT. Undoubtedly an extraordinary success was achieved by the perturbative description of quantum electrodynamics and of the Standard Model of electroweak interactions, the theoretical predictions are in an impressive agreement with the experimental results. However, one must not consider PT as the fundamental definition of QFT, rather it must be looked at a systematic technique to approximate the full theory taking into account the errors in a controlled way. It is well known that everything that can be done in the framework of free field theory is mathematically correct. Once we want to introduce interactions between fields things are getting complicated. In fact, we do not at present have a rigorously defined interacting quantum field theory for a four-dimensional space-time, although there are such theories in lower dimensions (conformal field theories). One short way to put the main difficulty is to say that the central theoretical object of a quantum field theory, the functional integral [9] has at present no rigorous mathematical definition, except in special or simple cases such as non-interacting theories. However, perturbation theory can give us an efficient and conceptually meaningful technique for calculating physically interesting quantities, but in return one needs to partially give up the rigour (and comfort) that mathematics provide.

The following sections in the Introduction are based on [1–5]. The structure of this

chapter is as follows. First we discuss PT in nutshell, then we proceed to the concept of renormalisation. At the end of the chapter we give a very brief introduction to the basic concepts in QFT. The outline of the thesis is given in the last section.

1.1 Perturbation Theory

In quantum theory, we typically solve a problem by finding the states of definite energy and their corresponding values of energy, i.e. we diagonalise the Hamiltonian of the system. Unfortunately, in most of the cases we are unable to perform this operation exactly. But let us assume that our Hamiltonian H can be written in the following way:

$$H = H_0 + H_{int}, \tag{1.1}$$

where both of the operators are hermitian of course, and we can look at the term H_{int} as a perturbation term which depends on a coupling constant ($H_{int} = gH'_{int}$). The time evolution operators that are generated by the unperturbed and the perturbed Hamiltonian, respectively, read:

$$U_0(t) = e^{-iH_0t}, \tag{1.2}$$

$$U(t) = e^{-iHt}. \tag{1.3}$$

At this point it is convenient to switch to the interaction picture in which the observables (operators) are evolving according to the unperturbed Hamiltonian ($O_I(t) = U_0(t)^\dagger O_S U_0(t)$), and the state vectors evolve as follows:

$$\psi_I(t) = V(t)\psi_S(0), \qquad V(t) \equiv U_0(t)^\dagger U(t). \tag{1.4}$$

Where the subscript "S" is for the Schrödinger picture. The main advantage of the interaction picture is that it yields the solution of the time evolution operator in terms of a power series in the coupling constant. As a matter of fact, $V(t,t')$ is responsible for the time evolution of the state vectors in the interaction picture:

$$\psi_I(t) = V(t,t')\psi_I(t'), \qquad V(t,t') \equiv V(t)V(t')^{-1}. \tag{1.5}$$

Now, $V(t,t')$ satisfies the differential equation:

$$i\partial_t V(t,t') = H_I(t)V(t,t'), \tag{1.6}$$

where $H_I(t) \equiv H_I^{int}(t)$, i.e. the interaction part of the Hamiltonian in the interaction picture. This differential equation is equivalent to the following integral equation:

$$V(t,t') = 1 - i\int_{t'}^{t} ds H_I(s)V(s,t'). \tag{1.7}$$

The iterative solution of Eq. (1.7) will provide a power series in the coupling for $V(t,t')$. Moreover, from this result we can extract information about the S-matrix, since it is defined by the asymptotic limits of $V(t)^{-1}$ (which are the so-called Møller operators and make the connections between the in/out states):

$$\Omega^{\pm} = \lim_{t\to\mp\infty} V(t)^{-1}, \tag{1.8}$$

and the scattering matrix is: $S = \Omega^{-}\Omega^{+} = \lim_{t\to\infty,\ t'\to-\infty} V(t,t')$.
Now, it is possible to express the scattering matrix with V(t,t') through its power series in the coupling g.

$$\begin{aligned} S &= \lim_{\epsilon\to 0}\lim_{t\to\infty,\ t'\to-\infty}\sum_{n=0}^{\infty}(-i)^n\int_{t'}^{t}dt_1\int_{t'}^{t_1}dt_2...\int_{t'}^{t_{n-1}}dt_n e^{-\epsilon(|t_1|+|t_2|...+|t_n|)}H_I(t_1)H_I(t_2)...H_I(t_n) \\ &= \lim_{\epsilon\to 0}\sum_{n=0}^{\infty}\frac{(-i)^n}{n!}\int_{-\infty}^{\infty}dt_1\int_{-\infty}^{\infty}dt_2...\int_{-\infty}^{\infty}dt_n e^{-\epsilon(|t_1|+|t_2|...+|t_n|)}T\left(H_I(t_1)H_I(t_2)...H_I(t_n)\right). \end{aligned} \tag{1.9}$$

The operator $T(.)$ is the time ordering operator:

$$T(H_I(t_1)H_I(t_2)) = \theta(t_1-t_2)H_I(t_1)H_I(t_2) + \theta(t_2-t_1)H_I(t_2)H_I(t_1), \tag{1.10}$$

where $\theta(t) = 1$ if $t > 0$ and 0 otherwise. In Eq. (1.9) the factor $e^{-\epsilon\sum_n|t_n|}$ is called the adiabatic switching on, and it enables us to evaluate the limits $t\to\infty$ and $t'\to-\infty$ term-by-term.
In QFTs the interaction Hamiltonian is defined by an integral of a Lorentz scalar (which respects locality) over the three spatial dimensions:

$$H_I(t) = \int d^3x h_I(x). \tag{1.11}$$

Altogether one find the (formally) closed formula for the scattering matrix, which is called the Dyson-series:

$$S = \sum_{n=0}^{\infty}\frac{(-i)^n}{n!}\int_{-\infty}^{\infty}d^4x_1...\int_{-\infty}^{\infty}d^4x_n T\left(h_I(x_1)...h_I(x_n)\right) \equiv Te^{-i\int d^4x h_I(x)} \tag{1.12}$$

The exponential expression mathematically does not make too much sense and it is rather formal. It is only used as shorthand notation for the Dyson-series.
The perturbation series in Eq. (1.12) in most of the cases does not converge at all, moreover the integrals defined in each individual term by expanding the series will diverge, too. The divergence of the integrals can be solved in the framework of renormalisation theory, which we will consider later on. Even if we assume that each term is finite in the series, there is still no guarantee for the series to be convergent. However, the essence of perturbation theory tells us to not to look at the series as a whole, but rather consider the partial sums which define effective approximations for the operator S. More precisely, the theory should generate numbers from the matrix element of the approximated S operator which must be comparable with those that are obtained from experimental measurements. Let us assume that we would like to compute a measurable physical quantity Q which can be represented from the theory with the series $\sum_{n=0}^{\infty} q_n$. The most important Ansatz here is the following: If the first few terms of $\sum_{n=0}^{\infty} q_n$ decrease in magnitude (that is $|q_{n+1}|/|q_n| \leq 1$) as n increases, the corresponding partial sums of $\sum_{n=0}^{\infty} q_n$ is being accepted as effective approximations of the physical quantity Q. As it was mentioned above, even if each q_n can be made finite by renormalisation procedure, it is not sure that the terms are small. For QED it happens to be a good effective approximation, however for the strong interaction (at low energies) it is not. A simple mathematical example can illustrate the situation. Let us consider the following series:

$$\sum_{n=0}^{\infty} \frac{(-100)^n}{n!}, \tag{1.13}$$

$$\sum_{n=0}^{\infty} \frac{n!}{(-100)^n}. \tag{1.14}$$

The first one converges to e^{-100}, however if we look at the first few partial sums they are far away from being an acceptable approximation of the limit: $1, -99, 4901, ...$ The second series in Eq. (1.13) is not convergent. However, considering the partial sums for some lower orders it will give: $1, 0.99, 0.9902, 0.990194$. This gives a nice approximation for the integral:

$$\int_0^{\infty} dt \, \frac{100\, e^{-t}}{t + 100} = 0.99019422. \tag{1.15}$$

The trick here is that one can expand $\frac{1}{1+t/100}$ into a geometric series and evaluating the integral term by term would generate the desired series in Eq. (1.13). However, one should not change the order of integration with the summation since the radius of convergence for the geometric series is $|t| < 100$. But if we do so, then our expression

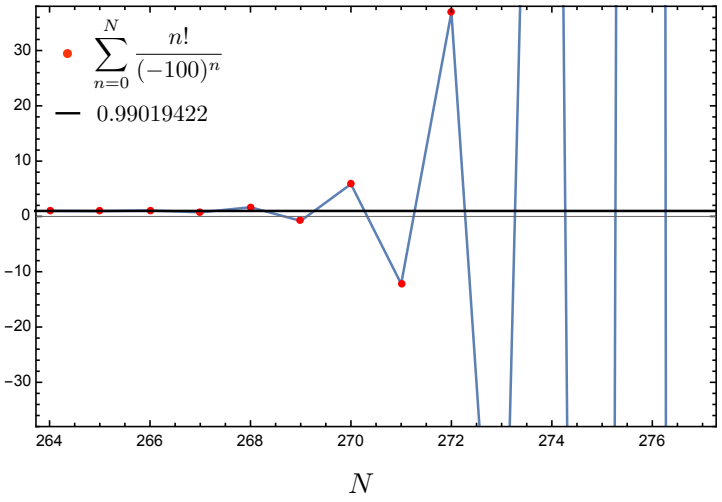

FIGURE 1.1: The partial sums of the series Eq. (1.14) is shown as a function of the truncation order N. The black line is the numerical value of the integral Eq. (1.15). One can see that the series provides a nice approximation up to the order of truncation $N = 268$.

will diverge, however, the series $\sum_n n!/(-100)^n$ will give an excellent approximation of the integral till the order $n = 100$ is reached, where the error in magnitude start to grow. For $n > 268$ the terms $n!/(100)^n > 1$, and as a consequence, the series start the to diverge widely, providing unreliable approximations of the integral (see Fig. 1.1). It can be shown that

$$\int_0^\infty dt \, \frac{xe^{-t}}{t+x} = e^x x\Gamma(0,x), \tag{1.16}$$

where $\Gamma(0,x)$ is the corresponding incomplete gamma function. Hence, in general we can say that the sum $\sum_n n!/(-x)^n$ is the asymptotic series of Eq. (1.16).

The success of this sort of perturbative analysis is two-sided. On the one hand, we can see an astounding agreement with experimental measurements as we already mentioned for example in QED: the accuracy that is achieved by the prediction in quantum electrodynamics of the magnetic moment of the electron is one part in 10^{10} [6]. On the other hand, there are serious mathematical problems: not only that the perturbation series may not converge for most of the theories, but there are quantum field theories for which they are not even asymptotic series and we know that they do not converge. The convergence of the perturbative series is not the only mathematical difficulty that one has to face in QFTs. As it was mentioned above, often each term in the Dyson-series has an infinite value which made physicist more concerned at the time. The question of infinities is the quantum field theory's most notorious problem, which was addressed

and solved by the renormalisation procedure, applied with great success firstly to QED in the pioneering work of Dyson, Feynman, Schwinger and Tomonaga between $1947-50$.

1.2 Renormalisation

1.2.1 Traditional way

In classical physics there seems to be no problem with the definition of the coupling of the interaction, calculating from a measurement. For instance, let us consider a charged test particle entering an electrostatic field. The force that is acting on it can be described by the gradient of the electrostatic potential which is proportional to the inverse of the squared distance:

$$F = -\nabla U(r) \propto -\frac{e}{r^2}. \tag{1.17}$$

From this, it is straightforward to express the coupling constant (i.e. the electric charge) $e = -4\pi\epsilon_0 r^2 F$, where we introduced the vacuum permittivity as ϵ_0. In QFT we can not do this so easily: one will get corrections from quantum fluctuations, and they will depend on which energy scale our experimental measurement is performed. We can have the following oversimplified picture in mind: every particle is surrounded by virtual particles as quantum fluctuations, and when they scatter on each other the harder the collision the deeper into the cloud of virtual particles we can see. In the following, we are going to use the notation μ for this energy scale, and call it the renormalisation scale. Hence, we can say that the coupling that we can calculate using our measurement as an input is $g = g(g_0, \mu)$. In the argument we have written g_0, which corresponds to the bare coupling. The bare coupling is, in fact, a parameter that we used to define our interaction in the Lagrangian (or Hamiltonian). Our aim is to match the theoretical parameter that we introduced, i.e. the bare coupling, to our measurement. For that reason we must invert the relation in order to be able to predict what kind of parameter we will need to choose in the theory to fit the measurement: $g_0 = g_0(g, \mu)$. Now, at this point, we need to go back to the Dyson-series obtained from PT, Eq. (1.12). We agreed that the interaction Hamiltonian is given as a function of the coupling. Now, as a consequence the perturbation series is a power series in the coupling. The whole machinery can be implemented in the framework of Lagrangians and in momentum space. Actually, the description in momentum (or Fourier) space is much more suitable since, being a well-defined quantum number, it characterises the given quantum states. It can be shown that each term in the perturbation series (apart from the first term of course) contains integrals like $\int_{k_0}^{\infty} dk k^a$, which may well be divergent, too. In brief this means that

in the given order of the perturbation series a virtual excitation arises with momentum in the $[k_0, \infty)$ range, which gives a quantum correction to the quantity under consideration. At this point comes the renormalisation procedure into the picture to extract some finite answer from our formulas. First, we must get rid of the infinities, which can be achieved in the easiest way by introducing an integral cut-off Λ as the upper limit of the integral. If we choose to work in the real space, then this cut-off can be considered as an inverse distance due to the definition of the de Broigle wavelength: $\Lambda \sim 1/a$, where a has a dimension of distance. Now, our theory can be seen as space-time was discretised, and our whole model would have been placed on an imaginary lattice. In fact, there exist such QFTs, where we do not need to perform this cut-off artificially, since a natural length scale characterises our theory, such as the lattice spacing in solid state physics or the intermolecular distance. On the contrary, if we believe that the space-time is a continuum, truncating the upper limit is not well justified in general, hence we need to take the limit $a \to 0$ (or equivalently $\Lambda \to \infty$), in order to obtain a coupling which is cut-off independent. We need to mention here that there are several regularisation techniques besides the cut-off: the Pauli-Villars regularisation introduces a particle with huge mass that cancel the UV infinities; the recently most popular is the gauge invariance respecting dimensional regularisation, which treats the dimension of the space-time as a continuous variable in a way that the integral is rendered convergent, and explicitly separates the singularity. For details see the reference [7], where it is also proved that all regularisation schemes are, in fact, equivalent.

However, as it was discussed, the presence of an artificial cut-off at a given energy scale made our theory dependent from a human choice explicitly. Nevertheless, our whole theory based on mathematical models designed by human, but once we agreed in the usage of one of these models to approximate the reality, we should avoid inconsistencies coming from an explicit human choice in the framework of the chosen model. However, it is justifiable to do so in some cases, even in QED: in the case of the Lamb shift the electrons Compton wavelength seems to be a natural lower limit to the lowest characteristic length scale a (cf. [8]). But in most of the cases, we cannot assume that processes at lower length scale do not contribute, hence we need to take the continuum limit ($a \to 0$). The actual procedure of getting rid of the cut-off is called the renormalisation. So, at this point in a regularised theory we have for the coupling $g_0 = g_0(g, \mu, \Lambda)$. Now, it is a question whether the limit $\lim_{\Lambda\to\infty}$ can be performed at a fixed $g(\mu)$ observed at the energy scale μ. If this limit happens to be finite, we say that the theory under consideration is "finite", otherwise it is not. The more usual situation is to find this limit to be infinite, like in QED. This means that in the framework of perturbative renormalisation QED is not a well defined quantum field theory, although its experimental predictions are incredibly accurate. So, independently from the result of the limit above, we can say that a theory is renormalisable if that limit exists whether being finite or infinite.

For a single coupling in the Lagrangian, Dyson formulated its criterion in the most simple way, which is called the power-counting criterion. By dimensional analysis it is easy to obtain the mass dimension of the coupling under consideration. Let us suppose that our coupling has the dimension $[g]$. It can be shown that this interaction term is renormalisable if $[g] \geq$ and non-renormalisable if $[g] < 0$. In fact the former situation can be split into two classes again by considering the coupling with $[g] = 0$ renormalisable and $[g] > 0$ super-renormalisable. The couplings with $[g] < 0$ are non-renormalisable couplings, and as such, it will produce infinite many divergent terms in the perturbation series, hence it would need infinite many counter-terms associated to these terms [7]. By infinite many, in this case, we mean infinitely many kind. The counter terms are defined as new terms in the Lagrangian and they are responsible for the cancellation of the infinities during the renormalisation procedure. However, one can look at these counter terms as new extra couplings introduced in our QFT, and formulate the following line of thought: in our theory, even if we choose some bare couplings to be zero, the corresponding physical coupling might be non-zero. For instance, let us consider a Lagrangian in which we define a massless particle, hence we do not include a bare mass into our formula. However, measuring its physical mass at some momentum scale could give us non-zero result. In this situation one can say that the particle acquires a dynamical mass through the interaction. This means that we might need to add some extra terms to he Lagrangian in order to make our theory successful. If we manage to do this by including a finite number of extra terms, we can call the theory "renormalisable", contrary, if we would need to include infinite many from those terms our QFT is called "non-renormalisable".

1.2.2 The modern approach

This final thought of the previous section leads us to the concept of renormalisation group. The idea was first imposed by K.G. Wilson [14] (who won the Nobel prize for it in 1982) and it goes as follows: we are not concerned about the limiting behaviour of the coupling in the continuum, rather we will be interested in its dependence on the scale. Let us set up the stage: we have a Lagrangian with N bare couplings $\mathbf{G}^0 = \{g_1^0, g_2^0, ..., g_N^0\}$. To do actual calculations we will need to introduce, as well, a cut-off scale Λ in momentum space. The interactions above this energy scale are being neglected, as it was explained above. Having defined these numbers, it is possible to compute the physical couplings $\mathbf{G} = \{g_1, g_2, ..., g_N\}$ at a given energy scale μ through the relation:

$$\mathbf{G} = f(\mathbf{G}^0, \Lambda, \mu) \simeq \mathbf{G} = \hat{f}(\mathbf{G}^0, a, l). \tag{1.18}$$

Here, the variables (Λ and μ) of f have energy dimension, and they correspond, actually, to inverse length scales: from the cut-off we have the inverse lattice spacing ($\Lambda \sim 1/a$) and for the arbitrary energy scale, we have an inverse arbitrary length scale ($\mu \sim 1/l$). Now, we fix the bare couplings and the cut-off but we adjust μ which defines the actual value of the physical coupling at a given energy scale. We can imagine this to happen in an N-dimensional space, and as the μ as parameter varies, the value of the physical coupling runs on a given trajectory embedded in $\mathbb{R}^N$. These trajectories are usually called as the renormalisation group flows, with the running coupling constants, but we will discuss this later in more detail. So, what would happen with a non-renormalisable theory if we tried to apply the idea of the renormalisation group to it? We would start with a Lagrangian with N couplings in it: some of them would be renormalisable, but there must be at least one which is not. If we start to scale down the energy μ, we will find that the physical couplings corresponding to the unrenormalisable terms are approaching zero. So, it seems that at low energy (meaning large distances) the non-renormalisable couplings become irrelevant. This is an incredibly important fact, because it may explain why the QFT, that seems to describe our world (namely the Standard Model or SM), is renormalisable. Indeed, it may well be that on extremely small distances, we would find a world where, for example, the effect of quantum gravity would not be negligible, but at larger distances the SM seem to be a reasonably accurate approximation of our reality and, according to the RG, the non-renormalisable interactions will look very weak. Wilson's arguments show that this circumstance explains the renormalisability of QED and other QFTs in elementary particle physics. Whatever the Lagrangian of QED was at the fundamental scale (Λ), as long as the couplings corresponding to its interactions are sufficiently small, it is legitimate for the theory to be described by a renormalisable effective Lagrangian at the energies of our experiments. Of course, it is reasonable to check the limiting behaviour of such RG running of the couplings. Basically, we need to take two limits in Eq. (1.18), namely when $\mu \to \Lambda$ and evidently when $\mu \to 0$. The first limit describes its ultraviolet limit (UV) the second the infrared (IR) behaviour, and the limits themselves are being called the UV and IR fixed points of the theory, respectively. The UV limit can even be taken to infinity, where for super-renormalisable and asymptotically free theories it gives $\lim_{\Lambda\to\infty} \mathbf{G} = 0$, which describes a non-interacting quantum field theory. This situation is called asymptotic freedom. Contrary, the scenario $\lim_{\Lambda\to\infty} \mathbf{G} \neq 0$ defines an interacting quantum field theory in the continuum, and it is called the asymptotic safety. The existence of such theory would be extremely important from theoretical point of view: an interacting QFT could be established in mathematically consistent way. Similarly, we can find free theories in the IR limit of the non-renormalisable theories, and also of some renormalisable theories like QED.

Wilson's idea is not only good for treating non-renormalisable theories, but it points out

a very deep connection with a more general phenomenon, namely the second order phase transition. The statement in brief is the following: every second order phase transition corresponds to an IR fixed point of the renormalisation group flow. In the following, we are going to illustrate why. Let us shortly discuss the second order phase transition in a ferromagnetic material, which we can define by an interacting spin lattice system with spin up and spin down states. At temperatures above a certain point, called the Curie temperature, the ferromagnet will not be magnetised, we call this the ordered phase. Below this, so-called, critical point (T_c), the system will break the $\mathbb{Z}_2$ symmetry, and the magnetisation of the system will point either up or down (this is the phenomenon of spontaneous symmetry breaking). The behaviour of the magnet exactly at the fixed point can be well characterised by the 2-point correlation function. That is, we define a random variable at each site x of the lattice which will be denoted by $S(x)$. It can take a value from the set $\{-1, 1\}$, which corresponds to the up and down states. Of course, in the symmetric phase the mean value is $\langle S(x)\rangle = 0$. The 2-point correlation function is $\langle S(x)S(y)\rangle$ and this quantity characterises our system the most. Away from the critical temperature, we will find that the spins, positioned at x and y on the lattice, will have an exponentially decaying correlation $\langle S(x)S(y)\rangle \propto \exp(-|x-y|/\xi)$, where ξ is the correlation length. However, at the critical point it turns into a power law $\langle S(x)S(y)\rangle \propto 1/|x-y|^d$. We call d a critical exponent (which is related to the correlation function), and we will discuss it later on. The power law behaviour is interesting since it means that the system is invariant under scaling transformation. That is, if we zoom out more and more, we will find the same structure at every scale. One can imagine this like a random fractal: we start from a larger distance, where we will find a domain of spins pointing up, when we magnify it and take a closer look, we will find another domain inside the previous one, which will contain spins pointing down, now we take an even closer look and we find spins pointing to the opposite direction, and so on. In fact, we can find the same fractal structure until we reach the natural length scale, the lattice spacing, which will play the role of the cut-off a in this case. These scaling solutions indeed can be described by a fixed point of the RG equation: a fixed point of a running coupling means that its running stops somewhere. We usually describe this by the beta function of the coupling: $\beta(g) = \mu\, \mathrm{d}\beta/\mathrm{d}\mu$. At a fixed point $\beta(g) = 0$, hence the running coupling becomes independent of the scale at that point. If this is so, it means that our theory is scale invariant at the critical point, and it exhibits that random fractal structure we described above.

Now, we can see that the philosophy behind renormalisation has changed a lot since it was first introduced.

1.3 Basics of the functional formalism of QFT

In this section we are going to review the functional approach to quantum field theories. In this formalism we introduce the functional integral which is being considered as the central object of QFT, however, at present it does not have a mathematical rigorous definition, except in special or simple cases such as the free field theory, or when we define our theory on a lattice. Despite the difficulties around the functional integration, we are still able to use this tool to extract the important physics which lay behind our theory. For the sake of simplicity, we are going to present the functional approach using a single scalar field $\varphi(x)$ in D dimensions, but this formalism can be generalised for an arbitrary QFT.

The fundamental objects of a QFT are the n-point correlation functions of the quantum fields. Sometimes the 2-point correlation functions are loosely called propagators or Green's functions, and throughout the thesis we are also going to use them in this respect. These correlation functions are obtained from the weighted average of a product of n field operators at different space-time points, taking into account all possible field configurations. In the Euclidean formalism we define our theory in a vector space with Euclidean metric. This transformation can be achieved by replacing the time coordinate with a pure imaginary number, i.e. $t \to -i\tau$, where, of course, τ is real. By doing this, the Lorentz-invariant square of a four-vector simply changes to the length of a vector in $\mathbb{R}^4$: $x_\mu x^\mu = t^2 - \mathbf{x}^2 \to -(t^2 + \mathbf{x}^2)$. This procedure is called the Wick-rotation, since we rotate our real quantity from the real line to the imaginary axis in the complex plane. In Euclidean QFT, the fields are weighted with an exponential of the action $S[\varphi] = \int d^4x\, \mathcal{L}(\varphi, \partial_\mu \varphi)$:

$$\langle \varphi(x_1), \varphi(x_2), ..., \varphi(x_n) \rangle := \mathcal{N} \int \mathcal{D}\varphi(x) \prod_{i=1}^{n} \varphi(x_i) e^{-S[\varphi]}. \tag{1.19}$$

Here we introduced $\mathcal{N}$ as a normalisation factor. In the RHS we used the notation of the functional integration, however the integration measure $\mathcal{D}\varphi(x)$ cannot be considered as a well defined mathematical object in the continuum. Nevertheless, we have a well established theory on lattice ([10]), so, we know that the functional integral presented in Eq. (1.19) exist when we perform this operation with a regularised measure $\mathcal{D}_R\varphi(x)$. In fact, we needed the Euclidean metric to make this integral numerically more controllable, otherwise the imaginary unit i would make this integral extremely oscillatory. The regularised action (with $\mathcal{D}_R\varphi(x)$) must be invariant under the symmetry transformation U of the theory: $S_R[U^\dagger \varphi U] = S_R[\varphi]$. We must assume this to hold for the continuum limit, too. We also need to assume that the theory that we obtained through the computation using the Euclidean metric can be analytically continued back to the Minkowski

space.

All the correlation functions derivable from the generating functional:

$$Z := \int \mathcal{D}\varphi e^{-S[\varphi]+\int J\varphi}, \tag{1.20}$$

where $J\varphi \equiv \int d^D x J(x)\varphi(x)$ and $J(x)$ represents a classical source associated to the quantum field $\varphi(x)$. The n-point correlation functions are obtained by taking the functional derivative of Z at vanishing source:

$$\langle \varphi(x_1), \varphi(x_2), ..., \varphi(x_n)\rangle = \frac{1}{Z[0]} \left.\frac{\delta^n Z[J]}{\delta J(x_1)\delta J(x_2)...\delta J(x_n)}\right|_{J=0}. \tag{1.21}$$

We are usually interested in the so-called connected n-point functions whose generator can be obtained by taking the logarithm of $Z[J]$:

$$W[J] = \ln Z[J]. \tag{1.22}$$

For an n-point correlation function being connected is interpreted in the sense of the cluster decomposition theorem ([11]), which means that the function vanishes at large space-like separations. An n-point function contains all the partitions which can be made using the connected n-point functions:

$$\langle \varphi(x_1), \varphi(x_2), ..., \varphi(x_n)\rangle = \sum_{\#\text{ of partitions}} \left\langle \prod_{i=0}^{n} \varphi(x_i) \right\rangle_{\text{con}} \prod_{j=0}^{n-i} \langle \varphi(x_j)\rangle_{\text{con}}. \tag{1.23}$$

Here the subscript "con" corresponds for the connected propagators. Since in the following we are only going to deal with connected correlators, we will neglect the superscript from our notation. In classical mechanics, the equations of motion can be derived from the action by the principle of stationary action. In quantum theory this is not the case, here the amplitude of all possible trajectories is added up in the path integral. However, if the action is replaced by the effective action, the equations of motion for the vacuum expectation values (VEV) of the fields can be derived from the stationarity requirement of the effective action. The effective action is defined through the Legendre transformation[1] of $W[J]$:

$$\Gamma[\phi] := \sup_J \left(\int J\phi - W[J] \right). \tag{1.24}$$

We will show that the variable of Γ is nothing else but the VEV of the field, $\langle\varphi(x)\rangle = \phi(x)$. Evaluating the variation of the expression in the bracket above at J_{sup} (which is

[1] The sign convention in Eq. (1.24) is usually used by the FRG community.

the source for Eq. (1.24) being its supremum), it vanishes:

$$\frac{\delta}{\delta J}\left(\int J\phi - W[J]\right)\Big|_{J=J_{\text{sup}}} = 0. \tag{1.25}$$

Indeed, the variation of $W[J]$ by J will provide the VEV of the quantum field in the presence of the source:

$$\phi = \frac{\delta W[J]}{\delta J} = \frac{1}{Z[J]}\frac{\delta Z[J]}{\delta J} = \langle\varphi\rangle_J . \tag{1.26}$$

Now, we can understand the role of Γ by taking its variation respect to the classical field $\phi(x)$ using the result above:

$$\frac{\delta\Gamma}{\delta\phi(x)} = J(x) + \int_y \frac{\delta J(y)}{\delta\phi(x)}\phi(y) - \int_y \frac{\delta W[J(y)]}{\delta J(y)}\frac{\delta J(y)}{\delta\phi(x)} = J(x). \tag{1.27}$$

This shows that the variation of the effective action provides the quantum equation of motion in the presence of a classical source J. This is very similar to the action principle, hence the name effective action, but contrary to the classical case, the equation describes the dynamics of the VEV of the quantum field taking into account all the quantum fluctuations.

The exact effective action can be only obtained in very special cases, therefore, we need to rely on approximations in order to extract some results. The vertex expansion is one of the most common form which we can use:

$$\Gamma[\phi] = \sum_{n=0}^{\infty}\frac{1}{n!}\int d^D x_1 \int d^D x_2 ... \int d^D x_n \Gamma^{(n)}(x_1, x_2, ..., x_n)\phi(x_1), \phi(x_2), ..., \phi(x_n). \tag{1.28}$$

We call Γ^n the One-Particle Irreducible (1PI) proper vertices. This name comes from the Feynman diagrams: it can be shown that the effective action is in fact the generating functional of the 1PI n-point functions, which diagrammatically correspond to connected graphs that remain connected by cutting any of their internal lines. We see at the expression in Eq. (1.28) is highly non-local, although it is being thought as the generalisation of the classical action which contains only local terms. However, we can give a quasi-local form to $\Gamma[\phi]$, by expanding each VEV of the field $\phi(x_j)$ $(j \neq 1)$ around the space-time point x_1 into Taylor series:

$$\phi(x_j) = \phi(x_1) + \partial_\mu\phi(x_1)(x_1 - x_j)^\mu + \frac{1}{2}\partial_\mu\partial_\nu\phi(x_1)(x_1 - x_j)^\mu(x_1 - x_j)^\nu + ... \tag{1.29}$$

Now, we integrate out for all the space-time points x_j with $j \geq 2$ and ordering the derivatives in an ascendant way. We obtain:

$$\Gamma[\phi] = \int d^D x \left(U(\phi) + \frac{1}{2} Z(\phi)(\partial_\mu \phi)^2 + Y(\phi, \{(\partial_\mu \phi)^{2n}\}_{n=2}^{\infty}) \right). \tag{1.30}$$

Here, we relabelled x_1 to x. $U(\phi)$ and $Z(\phi)$ are analytic functions of ϕ, called the effective potential and wave function renormalisation, respectively. The higher order of the fields derivative has been collected into Y. This is the so-called derivative (or gradient) expansion of the effective action. However, there exists a further simplification, namely, when we assume that ϕ is roughly a constant in space-time, hence the derivatives of it vanish. The equation we end up with is the following:

$$\Gamma[\phi] = \Omega U(\phi), \tag{1.31}$$

where Ω is constant, and it corresponds to the volume of the space-time on which the integration was performed. The effective potential $U(\phi)$ can be shown to be nothing else but the quantum generalisation of the classical potential [9]. We will use the functional formalism introduced above throughout the next chapters.

1.4 Outline of the thesis

This work focuses on two non-perturbative techniques applied to QFTs. In Chapter 2 we will give an analysis of the IR regime of the QED. We will derive the exact solution for the the Bloch-Nordsieck (BN) model [31, 32], using resummation techniques. The BN model was invented to resolve the problem of the infrared catastrophe, which will be explained in details in the next chapter. Different level of approximations are given both at zero and at finite temperatures. It turns out that the fermionic propagator can be given in an analytic way using the 2PI (Two-Particle Irreducible) resummation combined with the exact Ward identities which closes the infinite tower of the hierarchical Dyson-Schwinger equations. At finite temperature the simple 2PI formalism provides a result which can be matched with the exact calculations by using a mapping between the coupling constant defined in the 2PI theory (α_{2PI}) and the exact coupling (α_{ex}). We can use this relation to give the running of the 2PI coupling respect to the temperature, where the a Landau pole is recovered.
In Chapter 3 a brief introduction to the Functional Renormalisation Group is given (FRG) (cf. [92, 93]). The technique is applied to study the phase structure of the O(N) models. A proof of the Mermin-Wagner-Hohenberg-Coleman theorem is shown in the framework of the FRG in the Local Potential Approximation (LPA), both for finite

and large-N. A technique using the so-called Vanishing Beta Function curves is given in order to examine the results when the effective potential is expanded into Taylor series. This polynomial approximation will generate "fake" fixed points which has been neglected so far using physical arguments. Here, we will discuss a method, which is based more on mathematical grounds, in order to extract the physical fixed points. For $D \leq 4$ the known results are recovered for $D \geq 4$ triviality is shown. In the large-N limit for theories in dimensions $4 < D < 6$ a new fixed point candidate is found, which is currently being an up-to-date research topic [52, 53].
The dissertation based on the following articles:

- Resummations in the Bloch-Nordsieck model,
  A. Jakovac, P. Mati,
  Phys. Rev. D **85**, e-Print: arXiv:1112.3476 [hep-ph];

- Spectral function of the Bloch-Nordsieck model at finite temperature,
  A. Jakovac, P. Mati,
  Phys. Rev. D **87**, 125007, e-Print: arXiv:1301.1803 [hep-th];

- Validating the 2PI resummation: The Bloch-Nordsieck example,
  A. Jakovac, P. Mati,
  Phys. Rev. D **90**, 045038, e-Print: arXiv:1405.6576 [hep-th];

- Truncation Effects in the Functional Renormalisation Group Study of Spontaneous Symmetry Breaking,
  N. Defenu, P. Mati, I.G. Marián, I. Nándori, A. Trombettoni,
  e-Print: arXiv:1410.7024 [hep-th]
  The article is under publication at JHEP.

- The Vanishing Beta Function curves from the Functional Renormalisation Group,
  P. Mati,
  e-Print: arXiv:1501.00211 [hep-th]
  To be published in PRD (currently under consideration in the second round, only minor revisions were required by the referee in the first round).

Chapter 2

Exploring Quantum Electrodynamics in the Infrared

In this chapter we are going to investigate the IR limit of Quantum Electrodynamics which is famous of being plagued by infrared divergences. This phenomenon is known as the "infrared catastrophe", but it can be found in any QFT which involves massless fields. The development of QFTs started around 1930 with QED, therefore, in most of the cases the subjects of the computations were electromagnetic quantities. The methods used for the calculations were mostly the direct extension of the PT from quantum mechanics that we discussed briefly in the last chapter. Physicist back then, who were doing computations in QED, immediately faced infrared divergences when calculating first order perturbative corrections to the Bremsstrahlung process, due to the low frequency photon contributions. The core of the problem lays in the fundamental definition of QED, namely, that we assume the existence of a free theory, i.e. the existence of asymptotic states. However, such states are difficult to define in a theory where we have long range interactions. As a consequence, one cannot truly define the asymptotic states described by the Fock representation of free theory Hilbert space, on which the PT is performed. Thus we need to search for a non-perturbative solution to prevent these difficulties. An alternative option is provided by Bloch and Nordsieck in 1937 in their remarkable work on treating the infrared problem [31]. The divergencies are caused by the fact that in a scattering process an infinite amount of long wavelength photons are emitted, and these low energy excitations of the photon field are always present around the electron in the form of a "photon cloud". This shows us essentially that the observed particle is in fact very different from the one we call the bare particle: they can be considered as dressed "quasi particle" objects whose interactions cannot be described through PT entirely.

In this chapter we will show the emergence of the infrared catastrophe and then we

will introduce the Bloch-Nordsieck (BN) model, which was designed in order to imitate the low energy regime of QED. In Section 2.2 we will discuss the breakdown of the PT and then we will present the result for the fermionic propagator in the framework of the Two-Particle Irreducible (2PI) resummation, which corresponds to a quasi particle description. However, it is possible to obtain the exact full solution by improving the 2PI formalism using the Ward-Takahashi identities. We will give the full solution for the BN model at finite temperature which can be obtained in a closed analytic form, too (Sec. 2.3). In the last section of the chapter (Sec. 2.4) the 2PI resummed results are provided at finite temperature. Interestingly, one is able to match the coupling constant defined in the 2PI resummed theory to the full solution at finite temperature giving rise to an interesting non-perturbative running of the 2PI coupling with temperature. Section 2.2, 2.3 and 2.4 are based on [40], [41] and [42], respectively.

2.1 The infrared catastrophe

This section is based on Chapter 4 of [12] and Chapter 19 of [13]. In the following, we are going to give an example of the infrared divergencies in a semi-classical model, where the quantised electromagnetic field is interacting with a classical source. It will be shown that the asymptotic states cannot be considered as free states, actually they correspond to so-called coherent states. We are going to use the adiabatic switching on, which we mentioned already in Chapter 1, but in short it means that the interaction is being switched on only for a finite amount of time during the scattering process. We can see that this hypothesis is already in contradiction with the nature of the long range interactions, however this is how people usually treat the scattering processes. We are going to work in the Fock space representation of the incoming photons and determine the final state of the process, governed by the interaction with the classical source when the initial state was the vacuum.
The equation of motion of the quantised electromagnetic field in the Feynman gauge has the form:

$$\partial_\mu F^{\mu\nu} = \Box A^\nu = j^\nu. \tag{2.1}$$

Where $F^{\mu\nu} := \partial^\mu A^\nu - \partial^\nu A^\mu$ is the field strength tensor and A^μ is the photon field operator. The solution to this equation can be obtained as:

$$A^\mu(x) = A_0^\mu + \int d^4y\, G(x-y) j^\mu(y). \tag{2.2}$$

On the RHS the term A_0^μ corresponds to the free field operator and G is the Green's function corresponding to Eq. (2.1) and it is specified by the boundary conditions. Namely,

we can use the advanced and retarded Green's functions to obtain the solution:

$$\begin{aligned} A^\mu(x) &= A^\mu_{in}(x) + \int d^4y\, G_{ret}(x-y) j^\mu(y) \\ &= A^\mu_{out}(x) + \int d^4y\, G_{adv}(x-y) j^\mu(y). \end{aligned} \tag{2.3}$$

The various Green's functions are obtained considering different integration path on the complex plane:

$$G_{ret/adv}(x) = -\int \frac{d^4p}{(2\pi)^4} \frac{e^{-ipx}}{(p_0^2 \pm i\epsilon - \mathbf{p}^2)} = \frac{1}{2\pi}\theta(\pm x_0)\delta(x^2). \tag{2.4}$$

The constants of the integration with subscript *in* and *out* are for the photon field before and after the interaction with the source j, i.e. they are defined as the following limits:

$$\begin{aligned} \lim_{x_0 \to -\infty} A^\mu(x) &= A^\mu_{in}(x), \\ \lim_{x_0 \to \infty} A^\mu(x) &= A^\mu_{out}(x). \end{aligned} \tag{2.5}$$

We are looking for the unitary operator S that maps the *in* fields to the *out* field:

$$A^\mu_{out} = S^{-1} A^\mu_{in} S. \tag{2.6}$$

We can formulate this canonical transformation between the *in* and *out* states as follows: $|\text{out}\rangle = S\,|\text{in}\rangle$. Now, we are interested in the probability that the final state remains the vacuum after the interaction with the classical source j. That is, we are looking for the probability amplitude:

$$\langle \text{out } 0 \,|\, \text{in } 0\rangle = \langle \text{in } 0|\, S\, |\text{in } 0\rangle = \langle \text{out } 0|\, S\, |\text{out } 0\rangle \tag{2.7}$$

Now, the desired probability is $p_0 = |\langle \text{out } 0 \,|\, \text{in } 0\rangle|^2$. The probabilities like p_1, p_2,etc. (one photon, two photons, etc.) can be obtained in an analogous way. This tells us that the operator S contains all the information about the final state.
From Eq. (2.4) we can derive the following expression:

$$\begin{aligned} A^\mu_{out}(x) &= S^{-1} A^\mu_{in}(x) S \\ &= A^\mu_{in}(x) + \int d^4y \left(G_{ret}(x-y) - G_{adv}(x-y)\right) j^\mu(y) \\ &\equiv A^\mu_{in}(x) + \int d^4y \left(G_-(x-y)\right) j^\mu(y) \\ &\equiv A^\mu_{in}(x) + A^\mu_{cl}(x). \end{aligned} \tag{2.8}$$

Thus, it can be seen that the vector potential is a sum of an incident term and the classical radiation emitted by the source j. Based on the canonical commutation relation

corresponding to the vector potential, the second term in Eq. (2.8) can be rewritten as:

$$G_{-}(x-y) = g^{\mu\nu}\left(G_{ret}(x-y) - G_{adv}(x-y)\right) = -i[A^{\mu}_{in}(x), A^{\nu}_{in}(y)]. \tag{2.9}$$

And hence from Eq. (2.8):

$$S^{-1}A^{\mu}_{in}(x)S = A^{\mu}_{in}(x) - i\int d^4y[A^{\mu}_{in}(x), A_{in}(y)j(y)]. \tag{2.10}$$

The equation above can be solved for S by using the Hadamard's lemma[1] and yields:

$$S = e^{-i\int d^4x A_{in}(x)j(x)} = e^{-i\int A_{out}(x)j(x)}. \tag{2.11}$$

By decomposing the field operator into positive and negative frequency components:

$$A^{\mu}_{in}(x) = A^{\mu(+)}_{in}(x) + A^{\mu(-)}_{in}(x). \tag{2.12}$$

The commutator between the positive and the negative frequency component is the following:

$$\left[A^{\mu(-)}_{in}(x),\, A^{\nu(+)}_{in}(y)\right] = g^{\mu\nu}\int \frac{d^4k}{(2\pi)^3} e^{-ik(x-y)}\theta(k^0)\delta\left(k^2\right). \tag{2.13}$$

Using the Baker-Campbell-Hausdorff formula[2] one is able to rewrite Eq. (2.11) in terms of the decomposed field operator (Eq. (2.12)):

$$S = e^{-i\int d^4x A^{(-)}_{in}(x)j(x)} e^{-i\int d^4x A^{(+)}_{in}(x)j(x)} e^{\frac{1}{2}\int\int d^4x\, d^4y\left[A^{(-)}_{in}(y)j(y),\, A^{(+)}_{in}(x)j(x)\right]}. \tag{2.14}$$

The last exponent in the equation above can be written as:

$$\frac{1}{2}\int\int d^4x\, d^4y\, \left[A^{(-)}_{in}(y)j(y),\, A^{(+)}_{in}(x)j(x)\right] = \frac{1}{2}\int \frac{d^3k}{2k^0(2\pi)^3} J^*(k)\, J(k)|_{k^0=|\mathbf{k}|}\,, \tag{2.15}$$

where we introduced $J(k)$ as the Fourier transform (and its complex conjugate J^*) of the classical source $j^{\mu}(x)$. We have the following relations for $J(k)$:

$$J^{\mu}(k) = J^{\mu}(-k), \qquad k_{\mu}J^{\mu} = 0, \tag{2.16}$$

which show the real character and the conservation of $j(x)$. Let us decompose $J(k)$ as follows:

$$J^{\mu}(k) = k^{\mu}J_l(k) + J^{\mu}_{tr}(k), \tag{2.17}$$

[1] $e^{A}Be^{-A} = \sum_{n=0}^{\infty}\frac{1}{n!}[A,[A,[...[A,B]]...]]$.

[2] $e^{A}e^{B} = e^{A+B+\frac{1}{2}[A,B]}$ iff [A,[A,B]]=[B,[B,A]]=0.

where $J_l(k)$ is a scalar, hence the first term is parallel with k^μ and the second term is a space-like vector orthogonal to k^μ. For example, if $k = (k^0, \mathbf{k})$ then we can introduce the following space-like four-vectors $\epsilon_1 = (0, \mathbf{e}_1)$ and $\epsilon_2 = (0, \mathbf{e}_2)$ with $\mathbf{e}_1^2 = \mathbf{e}_2^2 = 1$ and $\mathbf{e}_1\mathbf{e}_2 = \mathbf{e}_1\mathbf{k} = \mathbf{e}_2\mathbf{k} = 0$. We can choose then $J^\mu_{tr}(k) = -\sum_{i=1,2} J_i(k)\epsilon_i^\mu$ with $J_i(k) = \epsilon_i J(k)$. Using this decomposition for the transverse part and the fact that in the integral of Eq. (2.15) only the light-like momenta give contributions (hence $k^2 = 0$), it can be shown:

$$J^*(k)J(k) = J^*_{tr}(k)J_{tr}(k) = -\left(|J_1(k)|^2 + |J_2(k)|^2\right). \tag{2.18}$$

Therefore, Eq. (2.14) can be written in the following way:

$$S = e^{-i\int d^4x A^{(+)}_{in}(x)j(x)} e^{-i\int d^4x A^{(-)}_{in}(x)j(x)} e^{-\frac{1}{2}\int \frac{d^3k}{2k^0(2\pi)^3}(|J_1(k)|^2+|J_2(k)|^2)}. \tag{2.19}$$

Now, we have obtained the desired form of the S matrix element of Eq. (2.7), and thus we can calculate the probability of the process by taking the absolute value square of Eq. (2.19):

$$p_0 = |\langle \text{out } 0 \,|\, \text{in } 0\rangle|^2 = |\langle \text{in } 0 \,|\, S \,|\, \text{in } 0\rangle|^2 = e^{-\int \frac{d^3k}{2k^0(2\pi)^3}\left(|J_1(k)|^2+|J_2(k)|^2\right)}. \tag{2.20}$$

In fact, this can be generalised to a process with an arbitrary photon number in the final state: the detailed derivation can be found in [12]. The corresponding probability of emitting n photons during the process can be shown to be the following expression:

$$p_n = \frac{1}{n!}\left[\int \frac{d^3q}{2q^0(2\pi)^3}\left(|J_1(q)|^2 + |J_2(q)|^2\right)\right]^n e^{-\int \frac{d^3k}{2k^0(2\pi)^3}\left(|J_1(k)|^2+|J_2(k)|^2\right)}. \tag{2.21}$$

Let us define the average number of emitted photons by:

$$\bar{n} = \int \frac{d^3k}{2k^0(2\pi)^3}\left(|J_1(k)|^2 + |J_2(k)|^2\right). \tag{2.22}$$

This enables us to identify the probability distribution defined by the emission process. It is described by Poisson statistics:

$$p_n = \frac{\bar{n}}{n!}e^{-\bar{n}}. \tag{2.23}$$

The Poission distribution claims the statistical independence of successive emissions which also manifests in the factorised form of the scattering amplitude in the case of n photon emission. Of course, the distribution is normalised in a way that the total probability of emitting infinite number of photons ads up to one, hence the average number of emitted photons is $\sum_n np_n = \bar{n}$.

In the following, we are going to examine the final state. We can start from $t \to \infty$, when we have the vacuum of the free theory, $|\text{in } 0\rangle$, which is basically an eigenvector of the annihilation part of the A^{μ}_{in} field operator with zero eigenvalue:

$$A^{\mu(+)}_{in}(x)\,|\text{in } 0\rangle = 0. \tag{2.24}$$

Now, if we consider its relation to the *out* photon field operator in Eq. (2.8), we will find:

$$A^{\mu(+)}_{out}(x)\,|\text{in } 0\rangle = S^{-1}A^{\mu(+)}_{in}(x)S\,|\text{in } 0\rangle = A^{\mu(+)}_{cl}(x)\,|\text{in } 0\rangle\,, \tag{2.25}$$

where $A^{\mu(+)}_{cl}(x)$ is the positive frequency part of the classical vector potential. So, we found that it is an eigenstate of the *out* field operator, too, but not necessarily with a zero eigenvalue (function). This we call a coherent state and it is responsible for the Poisson photon statistics in the final state. Hence, the vacuum expectation value of the out field yields:

$$\left\langle \text{in } 0 \,\middle|\, A^{\mu(+)}_{out}(x) \,\middle|\, \text{in } 0 \right\rangle = A^{\mu}_{cl}(x). \tag{2.26}$$

This last equation tells us that in the final state the field is just the classical field.
On the other hand, we can examine the amount of the average emitted radiation, which reads as:

$$\begin{aligned} \bar{E} &= \langle \text{in } 0\,|\,H(A_{out})\,|\,\text{in } 0\rangle = \left\langle \text{in } 0 \,\middle|\, S^{-1}H(A_{in})S \,\middle|\, \text{in } 0 \right\rangle \\ &= \left\langle \text{in } 0 \,\middle|\, S^{-1}\int \frac{d^3k}{2k^0(2\pi)^3}\,k^0 \sum_{\lambda=1}^{2} a^{\lambda,\dagger}_{in}(k)a^{\lambda}_{in}(k)\,S \,\middle|\, \text{in } 0 \right\rangle. \end{aligned} \tag{2.27}$$

Here, we introduced the operators $a^{\lambda,(\dagger)}_{in}(k)$, which are the annihilation and creation operators of the state with momentum k on the Fock space defined for the incoming photons, polarised in one of the two transverse direction $\lambda = 1, 2$. From Eq. (2.8) it follows that they transform in the following way:

$$a^{\lambda,\dagger}_{out}(k) = Sa^{\lambda,\dagger}_{in}(k)S^{-1} = a^{\lambda,\dagger}_{in}(k) - iJ_{\lambda}(k). \tag{2.28}$$

Thus, inserting this expression into Eq. (2.27) gives the average emitted energy as:

$$\bar{E} = \frac{1}{2}\int \frac{d^3k}{(2\pi)^3}\left(|J_1(k)|^2 + |J_2(k)|^2\right), \tag{2.29}$$

which can be shown to coincide with the emitted energy by a classical radiation (cf. [12]). Now, we can compare this result to the emitted average number of photons in Eq. (2.22). There is one difference between the two expressions, namely a $1/k^0$ factor in

the integrand. Indeed, in the phase space element $d^3k/(2k^0(2\pi)^3)$ the average number of emitted photons reads as:

$$d\bar{n} = \frac{d^3k}{\hbar k^0}\left(|J_1(k)|^2 + |J_2(k)|^2\right). \tag{2.30}$$

For pedagogical reasons, here we plugged back the $\hbar$ into the equation, since each photon quanta carries $\hbar k^0$ energy, otherwise, of course, it is set to one. Indeed, from Eq. (2.29) the average emitted energy by the photons in this phase space element is:

$$d\bar{E} = \hbar k^0 d\bar{n}. \tag{2.31}$$

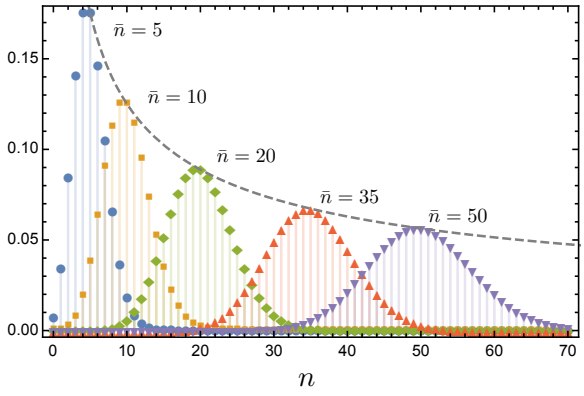

FIGURE 2.1: Possion distributions are shown for various values of the parameter $\bar{n}$, the emitted average photon number. The distribution converges to zero as $\bar{n}$ grows, which is a consequence of the diverging number of emitted soft photons.

The relation above has a very important consequence: if we have measured a finite amount of energy for photons with very low frequency, i.e. $k^0 \to 0$, $d\bar{n}$ must blow up in order to keep the LHS finite in Eq. (2.31). This is the so-called infrared catastrophe. Mathematically not only the average number of the emitted photons will diverge but the Poisson distribution itself gets in trouble, too (see Fig. 2.1):

$$\lim_{\bar{n}\to\infty} p_0 = \lim_{\bar{n}\to\infty} |\langle 0 \text{ out} \,|\, 0 \text{ in}\rangle|^2 = \lim_{\bar{n}\to\infty} e^{-\bar{n}} = 0. \tag{2.32}$$

As a consequence every matrix element between in-and-out states vanishes. From this we can see that it is impossible to construct a Fock space for the *out* states from the *in* states: there does not exist a unitary S operation which would map the two Hilbert space onto each other. This phenomenon is due to the inequivalence of the representation of the vacuum states, which happens naturally in a system with infinite degrees of freedom under specific circumstances (here $\bar{n} = \infty$).

In the following section we are going to consider the infrared phenomenon in the Bloch-Nordsieck model, which was designed to mimic the low frequency (infrared) regime of the QED.

2.2 The Bloch-Nordsieck model

Bloch and Nordsieck developed a model (1937) for the description of the ultra low frequency limit of the QED in order to solve the infrared problem. They have shown that the exact solution of the model does not require perturbation theory, although one could get back the perturbative results by expanding the analytic expression into a power series at the end of the computation.
First, we will discuss the theory itself. The BN model is a simplification of the QED Lagrangian, where the Dirac matrices γ^μ are replaced by a four-vector u^μ:

$$\mathcal{L} = -\frac{1}{4}F_{\mu\nu}F^{\mu\nu} + \bar{\Psi}(iu_\mu D^\mu - m)\Psi, \qquad iD_\mu = i\partial_\mu - eA_\mu, \quad F_{\mu\nu} = \partial_\mu A_\nu - \partial_\nu A_\mu. \tag{2.33}$$

The singled-out four-vector u_μ represents the four-velocity of the fermion. The fermion wave function here has only one component and $\bar{\Psi} = \Psi^*$. We are interested in the fermion propagator which, in the path integral representation, has the following form

$$i\mathcal{G}(x) = \left\langle T\Psi(x)\bar{\Psi}(0)\right\rangle = \frac{1}{Z}\int \mathcal{D}\bar{\Psi}\mathcal{D}\Psi\mathcal{D}A_\mu e^{iS[\bar{\Psi},\Psi,A]}\Psi(x)\bar{\Psi}(0). \tag{2.34}$$

At the tree level it reads:

$$\mathcal{G}_0(p) = \frac{1}{u_\mu p^\mu - m + i\varepsilon}. \tag{2.35}$$

Since it has a single pole, there are no antiparticles in the model, and also the Feynman propagator is the same as the retarded propagator. The lack of antiparticles also means that all closed fermion loops are zero[3]. As a consequence, the photon self-energy is zero (no vacuum polarisation), and thus the free photon propagator equals to the exact one. In Feynman gauge therefore the *exact* photon propagator is

$$G_{\mu\nu}(k) = \frac{-g_{\mu\nu}}{k^2 + i\varepsilon}. \tag{2.36}$$

In the following we will show first that the perturbation series in the framework of the BN model is plagued with IR divergencies, but this is the case in general for spinor QED, too. Then we proceed with the 2PI resummation, which gives an approximate, but non-perturbative result, free of IR divergences. Finally, we will present the solution

[3]This statement can be best seen in real time representation. There a chain of fermion propagators, because of the retardation, is proportional to $\Theta(t_1 - t_2)\ldots\Theta(t_{n-1} - t_n)$. In a closed loop $t_n = t_1$, therefore, the product of theta functions is zero almost everywhere.

of the Dyson-Schwinger equations with an Ansatz for the vertex function. We show that the last method is exact and provides the same solution which is known from literature [31, 32]. This observation, however, leads us to a proposal for how the 2PI resummation can be improved in a generic model in order to catch the IR physics correctly.

2.2.1 The breakdown of the perturbation series

In this section we will provide the one-loop perturbative result for the fermion propagator in the BN model. Reducing the Dirac spinor to a one component fermion is well justified, considering the fact that all the contributions to the fermion self-energy come from ultra-soft photons [31, 32]. Indeed, at this energy scale photons do not have enough energy even to flip the spin of the fermion, not to mention the pair creation. Here, we are going to work in counter-term formalism. In Feynman gauge the Lagrangian reads (using that the photon self-energy is zero):

$$\mathcal{L} = -\frac{1}{2}(\partial_\mu A_\nu)^2 + \bar{\Psi}(i\partial_0 - m)\Psi - e\bar{\Psi}A_0\Psi + \delta Z\bar{\Psi}i\partial_0\Psi - \delta Z_m m\bar{\Psi}\Psi - \delta e\bar{\Psi}A_0\Psi. \quad (2.37)$$

The fermionic part of the Lagrangian is Lorentz-covariant, therefore we can relate the results with different u^μ choice by Lorentz transformation. This makes possible to work with $u = (u_0, 0, 0, 0)$ without loss of generality. In fact, we can perform a Lorentz-transformation where $\Lambda u = (u_0, 0, 0, 0)$. If u^μ is a 4-velocity then $u_0 = 1$; if it is of the form $u = (1, \mathbf{v})$, then it is $u_0 = \sqrt{1 - \mathbf{v}^2}$. After rescaling the field as $\Psi \to \Psi/\sqrt{u_0}$ and the mass as $m \to u_0 m$, the Lagrangian reads

$$\mathcal{L} = -\frac{1}{4}F_{\mu\nu}F^{\mu\nu} + \bar{\Psi}(iD_0 - m)\Psi. \quad (2.38)$$

This is the Lagrangian which will be used mostly in this chapter later on. If necessary, the complete u dependence can be recovered easily.
For the fermion self-energy the one-loop diagram is the bubble with the contribution:

$$\begin{aligned} -i\Sigma_{1loop}(p_0, m) &= (-ie)^2 \int \frac{d^4k}{(2\pi)^4}\, iG_{00}(k)\, i\mathcal{G}(p-k) \\ &= -e^2u^2 \int \frac{d^4k}{(2\pi)^4}\, \frac{1}{k^2 + i\varepsilon}\, \frac{1}{p_0 - k_0 - m + i\varepsilon}. \end{aligned} \quad (2.39)$$

Here, we have a p_0 dependence only, since we are working in the special reference frame that we introduced above, and for which the product $u_\mu p^\mu = p_0$ for every four-vector p^μ. The result will change only in its argument if we choose a different reference frame: $\Sigma(p_0) \to \Sigma(up)$. This statement holds for all the computations performed at zero temperature.

Moreover, we have wave function and mass renormalisation counter-terms

$$\Sigma_{ct}(p_0) = -\delta Z p_0 + \delta Z_m m. \tag{2.40}$$

The complete one-loop self-energy is $\Sigma_{1loop} + \Sigma_{ct}$. In the calculation we have to take care of the non-standard form of the free fermion propagator. The details of the computation performed using dimensional regularisation ($D = 3 - 2\epsilon$) can be found in Appendix A, as a result we obtain

$$\Sigma_{1loop}(p_0, m) = \frac{\alpha}{\pi}(p_0 - m)\left[-\ln\frac{m - p_0}{\mu} + \mathcal{D}_\varepsilon\right], \tag{2.41}$$

where $\alpha = e^2/(4\pi)$, μ is the renormalisation scale and

$$\mathcal{D}_\varepsilon = \frac{1}{2\varepsilon} + 1 + \frac{1}{2}(\ln\pi - \Gamma_E). \tag{2.42}$$

For renormalisation, we have to subtract the divergences with the help of the counter-terms, the finite parts are fixed by the renormalisation scheme. In the $\overline{\text{MS}}$ scheme we choose the counter-terms to be

$$\delta Z_{1,\overline{\text{MS}}} = \delta Z_{m,\overline{\text{MS}}} = \frac{\alpha}{\pi}\mathcal{D}_\varepsilon, \tag{2.43}$$

which results in

$$\Sigma^{ren}_{1loop}(p_0, m) = -\frac{\alpha}{\pi}(p_0 - m)\ln\frac{m - p_0}{\mu}. \tag{2.44}$$

We can define a discontinuity of a function $f(x)$ on the complex plane through the formula

$$\underset{x}{\text{Disc}}\, f(x) = \lim_{\epsilon\to 0} f(x + i\epsilon) - f(x - i\epsilon). \tag{2.45}$$

The discontinuity of the renormalised self-energy reads

$$\underset{p_0}{\text{Disc}}\, \Sigma^{ren}_{1loop}(p_0, m) = 2\alpha\,(p_0 - m)\Theta(p_0 - m). \tag{2.46}$$

For the one-loop propagator we obtain

$$\mathcal{G}(p_0) = \frac{1}{p_0 - m - \Sigma(p)} = \frac{1}{p_0 - m}\,\frac{1}{1 + \dfrac{\alpha}{\pi}\ln\dfrac{m - p_0}{\mu}}. \tag{2.47}$$

The spectral function $\text{Disc}_{p_0}\, i\mathcal{G}$ reads

$$\varrho(p_0) = \frac{\Theta(p_0 - m)}{p_0 - m}\,\frac{2\alpha}{\left(1 + \dfrac{\alpha}{\pi}\ln\dfrac{p_0 - m}{\mu}\right)^2 + \alpha^2}. \tag{2.48}$$

The fermionic spectral function needs to satisfy the sum rule $\int_{\mathbb{R}} dp_0 \varrho(p_0) = 1$, which is the consequence of the equal time anticommutation relations. This spectral function is normalisable, since

$$\int_{-\infty}^{\infty} \frac{dp_0}{2\pi} \varrho(p_0) = \frac{\pi}{\alpha}. \tag{2.49}$$

However, the question of the integrability of the spectral function for the exact result is more subtle. We will see this later on. On the other hand the one-loop result is not reliable when $|\ln(p_0 - m)/\mu| \ll \frac{\pi}{\alpha}$, i.e. in the vicinity of the mass shell as well as in the large p_0 regime. The former can be considered as the fingerprint of the IR catastrophe: the accumulation of the soft photon contributions cause a singular behaviour close to the mass shell, hence each higher term in the perturbation series would give larger and larger "corrections" to the fermion propagator which would make the series to diverge very fast. In order to have a better description of these kinematical regimes, we need a resummation of certain class of Feynman diagrams which will be provided in the framework of the so-called 2PI functional techniques.

2.2.2 Two-Particle Irreducible (2PI) resummation in the Bloch-Nordsieck model

The 2PI formalism provides a consistent resummation framework known for a long time [15]. The basic idea is to replace the free propagator in the perturbation theory with the exact one which is approximated self-consistently with fixed-loop skeleton diagrams. The so-defined resumed perturbation theory is renormalisable [16]-[26], and can be applied to study different physical questions from non-equilibrium [22], [23], thermodynamics [20], [24],[28],[29] and different systems like O(N) model [25], [26] or gauge theories [27]. Although the 2PI approximation is constructed by physical arguments, and we expect better results (i.e. closer to the exact one) after the 2PI resummation, a priori it is not sure that one really achieves this goal. Probably the finite lifetime effects are well represented by 2PI resummation both in equilibrium [20] as well in non-equilibrium, where the 2PI is close to the Boltzmann-equation approximation [30]. But if the deep IR regime is important, where multi-particle excitations also play crucial role, the picture is far to be so clean. To make the case even worse, in most gauge theory models there is hard to make exact statements about the IR behaviour of the model. A detailed discussion of the 2PI functional formalism can be found in Appendix B.

The idea is to use the exact propagators in the perturbation theory, which propagator is determined self-consistently using skeleton diagrams as resummation patterns. The one-loop bubble diagram in the present case generates the resummation of all the "rainbow" diagrams. To obtain an expression for the 2PI resummation we apply the technique

of [20]: we use the one-loop formula (2.39), interpret the appearing propagators as full propagators, and finally perform renormalisation of the divergent parts with the same counter-terms as in the one-loop case (the actual values will be different).

The tree level photon propagator is exact, therefore we can write

$$\Sigma(p) = -ie^2 \int \frac{d^4k}{(2\pi)^4} \frac{\mathcal{G}(p-k)}{k^2 + i\varepsilon}. \tag{2.50}$$

Using a spectral representation for the fermion propagator (using the fact that now the Feynman propagator is the retarded one and that the fermion spectral function is $\varrho(\omega < 0) = 0$) we find

$$\Sigma(p_0, m) = -ie^2 \int_0^\infty \frac{d\omega}{2\pi} \int \frac{d^4k}{(2\pi)^4} \frac{1}{k^2 + i\varepsilon} \frac{\varrho(\omega)}{p_0 - k_0 - \omega + i\varepsilon}. \tag{2.51}$$

From this form it is clear that we obtain the weighted one-loop result, i.e.

$$\Sigma(p_0, m) = \int_0^\infty \frac{d\omega}{2\pi} \varrho(\omega) \Sigma_{1loop}(p_0, \omega). \tag{2.52}$$

Implicitly we always understood $\rho(\omega)$ to be dependent on the mass m. In particular, if $\varrho(\omega) = 2\pi\delta(\omega - m)$, then we get back the one-loop self-energy. At this point it is worth to examine the UV divergence structure of the 2PI approximation. UV divergences may occur in Eq. (2.52) for large values of ω: using Eq. (2.41) we find that the large ω behaviour of the one-loop self-energy reads:

$$\Sigma_{1loop}(p_0, \omega) = \frac{\alpha}{\pi}\omega \left(\ln \frac{\omega}{\mu} - \mathcal{D}_\varepsilon \right) + \frac{\alpha}{\pi} \left(-\ln \frac{\omega}{\mu} + \mathcal{D}_\varepsilon \right) p_0 + \mathcal{O}\left(\frac{p_0^2}{\omega} \right), \tag{2.53}$$

with $\mathcal{D}_\varepsilon$ given in Eq. (2.42). Since ϱ is integrable for large ω values, therefore, the $\mathcal{O}(\omega^{-1})$ contribution is already finite. Thus, the divergence structure of the self-energy is $A + Bp_0$, just like for the free case, and so the same type of counter-terms are needed, although as a result of the resummation the values are different. This is a manifestation of the general case of counter-term renormalisability of 2PI resummations [20].

2.2.2.1 Analytic study of the 2PI equations

First we try to examine Eq. (2.52) with analytic methods. We differentiate it with respect to p_0 to find

$$\frac{\partial^2\Sigma}{\partial p_0^2} = -\frac{\alpha}{\pi}\int_0^\infty \frac{d\omega}{2\pi}\frac{\varrho(\omega)}{p_0-\omega+i\varepsilon} = -\frac{\alpha}{\pi}\mathcal{G}. \tag{2.54}$$

Since

$$\frac{\partial\Sigma_{1loop}^{ren}}{\partial p_0} = \frac{\alpha}{\pi}\left(-\ln\frac{\omega-p_0-i\varepsilon}{\mu}-1\right), \qquad \frac{\partial^2\Sigma_{1loop}^{ren}}{\partial p_0^2} = -\frac{\alpha}{\pi}\frac{1}{p_0-\omega+i\varepsilon}. \tag{2.55}$$

But $\mathcal{G}^{-1} = p_0 - m - \Sigma$, so we find for $\mathcal{G}^{-1}$:

$$\frac{d^2\mathcal{G}^{-1}}{dp_0^2}\mathcal{G}^{-1} = \frac{\alpha}{\pi}. \tag{2.56}$$

To solve the equation, first we should realise that the $\alpha = 0$ and $\alpha \neq 0$ cases are very different. If $\alpha = 0$ then $(\mathcal{G}^{-1})'' = 0$ and the propagator behaves as $\mathcal{G} = Z/(p_0 - \tilde{m})$ with some wave function renormalisation constant Z and mass $\tilde{m}$. This agrees with the free case.

If $\alpha \neq 0$ then we can redefine the variables with an arbitrary Ω scale as

$$E := \Omega\sqrt{\frac{2\alpha}{\pi}}\,(m-p_0), \qquad \chi := -\Omega\mathcal{G}^{-1}, \tag{2.57}$$

then we find

$$2\frac{d^2\chi}{dE^2}\chi = 1. \tag{2.58}$$

This equation does not depend on the coupling any more. The coupling constant dependence shows up in the integration constants which are the manifestation of the renormalisation scheme. We shall also note that the equation does not give information about the sign of E and χ, because for $E \to -E$ or $\chi \to -\chi$ the equation remains the same. The chosen signs in Eq. (2.57) turn out later to be the physical choice.

We introduce

$$y = \frac{d\chi}{dE} \quad\Rightarrow\quad \frac{d^2\chi}{dE^2} = \frac{dy}{dE} = \frac{dy}{d\chi}\frac{d\chi}{dE} = y\frac{dy}{d\chi}. \tag{2.59}$$

This means that we can write for y:

$$2y\chi\frac{dy}{d\chi} = 1 \quad\Rightarrow\quad y = \frac{d\chi}{dE} = \sqrt{\ln\chi + y_0}, \tag{2.60}$$

with an integration constant y_0. Therefore

$$\int_1^{\chi} \frac{d\chi'}{\sqrt{\ln \chi'} + y_0} = E. \tag{2.61}$$

There could appear an integration constant also here on the RHS: $E - E_0$. But recalling that $E \sim p_0 - m$, we see that E_0 corresponds to a mass shift: if the mass remains the tree level one, that is m, then $E_0 = 0$.

This is the (implicit) solution of the 2PI equations. We see that for real χ the left hand side is real and positive, moreover for $\chi(E = 0) = 1$. The $E < 0$ part corresponds to imaginary values of χ. Since the equation itself is real, if χ is a solution, then χ^* is a solution, too. This means that the imaginary part is in fact the (half) discontinuity of the solution.

We see that irrespective of the value of y_0, at $E = 0$, i.e. on the mass shell, $\chi = 1$ and so $\mathcal{G} = -\Omega$ finite. This yields difficulties when we try to apply renormalisation conditions on the self-energy. Namely, if we keep the mass shell unchanged (this would correspond to the choice of E_0 above), then the renormalisation of the self-energy would mean $\Sigma(p_0 = m) = 0$ and $\Sigma'(p_0 = m) =$ finite. Then, however, near the mass shell the propagator should always behave as $\sim 1/(p_0 - m)$, i.e. *infinite* at the mass shell. This means that the physical renormalisation process requires $\Omega \to \infty$. In this case the propagator behaves near the mass shell as:

$$\mathcal{G} = \frac{-\Omega}{1 + \Omega y_0 \sqrt{\frac{2\alpha}{\pi}}(m - p_0)} \overset{\substack{\Omega\to\infty \\ y_0 = \sqrt{\pi/(2\alpha)}}}{\longrightarrow} \frac{1}{p_0 - m}, \tag{2.62}$$

because if χ is close to 1 then the logarithmic term can be neglected in Eq. (2.61), and we find $\chi = 1 + y_0 E$.

For large values of χ, on the other hand, y_0 can be neglected. Then the integral can be evaluated as

$$\sqrt{\pi}\,\mathrm{erfi}(\sqrt{\ln \chi}) = E. \tag{2.63}$$

For large χ values the expression above behaves as

$$\frac{\chi}{\sqrt{\ln \chi}} = E, \qquad \text{for large} \quad E,\, \chi. \tag{2.64}$$

2.2.2.2 Numerical solution

Let us turn now to the numerical study of the system, based on [20] and [36]: we determine the discontinuity of the self-energy self-consistently. The discontinuity of

Eq. (2.52) now reads

$$\underset{p_0}{\mathrm{Disc}}\,\Sigma(p_0,m)=\frac{\alpha}{\pi}\int_0^{p_0}d\omega(p_0-\omega)\varrho(\omega). \tag{2.65}$$

Note that the upper limit of the integration goes till p_0 because of the theta function in the discontinuity of the self-energy. Knowing the discontinuity of the self-energy, we can use the Kramers-Kronig relation to restore the complete self-energy:

$$\Sigma(p_0,m)=\int_{-\infty}^{\infty}\frac{d\omega}{2\pi}\frac{\mathrm{Disc}_\omega\; i\Sigma(\omega,m)}{p_0-\omega+i\varepsilon}. \tag{2.66}$$

While Eq. (2.65) is a completely finite expression, in the Kramers-Kronig relation we will find divergences. This corresponds to the divergences of the self-energies which must be made finite by applying the appropriate counter-terms. Technically one can regularise the integral in Eq. (2.66) and then make it finite with counter-terms, or use the (twice) subtracted form of the Kramers-Kronig relation. To see how it works, we determine the one-loop result from the tree level spectral function and the dimensional regularisation of the Kramers-Kronig equations (interpreting $\omega\to\sqrt{\omega^2}$):

$$-2\alpha\mu^{2\varepsilon}\int\frac{d^{1-2\varepsilon}\omega}{(2\pi)^{1-2\varepsilon}}\;\frac{\omega-m}{p_0-\omega+i\epsilon}=\frac{\alpha}{2\pi}(p_0-m)\left[\frac{1}{\varepsilon}-2\ln\frac{m-p_0}{\mu}+\ln\pi+1\right]. \tag{2.67}$$

The divergence structure is the same, and also the $\overline{\mathrm{MS}}$ scheme result is the same as in Eq. (2.41) (the different finite parts are due to the different regularisation method).
Now, we can set up an algorithm to solve Eq. (2.65). We choose an arbitrary spectral function as a starting one (practically the free spectral function), then follow the steps:

step 1: compute the discontinuity of the self-energy using Eq. (2.65);

step 2: compute the complete self-energy using the Kramers-Kronig relation Eq. (2.66);

step 3: renormalise the self-energy with local counter-terms. To fix the counter-terms we used on-mass-shell (OM) renormalisation scheme, i.e. the real part of the self-energy at the mass shell is zero and its derivative is also zero

$$\mathrm{Re}\,\Sigma(p_0=m)=0,\qquad \left.\frac{d\,\mathrm{Re}\,\Sigma(p_0)}{dp_0}\right|_{p_0=m}=0. \tag{2.68}$$

We note here that releasing the first condition yields a mass shift, releasing the second condition yields a finite wave function renormalisation. But in all renormalisation schemes it will remain true that near the (renormalised) mass shell the propagator behaves as $\mathcal{G}(p_0\approx m)=\zeta/(p_0-m)$ (ζ being a positive real number).

step 4: construct the new spectral function from the discontinuity of the propagator knowing the real and imaginary part of the self-energy as

$$\varrho(p_0) = \frac{2\,\mathrm{Im}\,\Sigma(p_0)}{(p_0 - m - \mathrm{Re}\,\Sigma(p_0))^2 + (\mathrm{Im}\,\Sigma(p_0))^2}. \tag{2.69}$$

step 5: continue with step 1 until the process converges.

Integrations in the above algorithm are performed numerically. This strategy was applied successfully to the ϕ^4 model in [20]. The direct application of this strategy, however, this times fails. Numerically what we can observe is that the spectral function becomes more and more shallow, and pointwise it goes to zero: $\lim_{n\to\infty} \varrho_n(p_0) = 0$ for $\forall\, p_0$. In order to see a convergence, we had to use a supplementary step in the iteration after step 4:

step 4': use a rescaling of the generated spectral function:

$$\varrho(p_0) \to A\varrho(B\,p_0), \tag{2.70}$$

with appropriate A and B which can ensure convergence. These appropriate values can be found by inspection, but the actual values are not too important (we used $A = 73$ and $B = 11$ in our numerics). In this way finally we succeeded to see convergence in the spectral function. The numerical reason of the pointwise vanishing 2PI spectral function is that the exact spectral function has a discontinuity at the mass shell, and – apart from this single point – it has always a negative derivative. Numerically, however, we cannot have a jump, since in all regularisations Eq. (2.65) yields $\varrho(p_0 \approx m) \sim (p_0 - m)^n$, where $n \geq 2$. Since the exact curve starts to bend downwards, the recursion tries to lower the spectral function in order to have smaller derivative near the mass shell. Since the spectral function has to be positive, these requirements can be satisfied only with $\varrho = 0$. With the continuous rescaling, we can achieve that the numerically badly conditioned part, the vicinity of the mass shell, becomes smaller and smaller.

The numerical results for the real part and the discontinuity of the fermion propagator can be seen in Fig. 2.2. In Fig. 2.3 the expected asymptotics are fitted to the numerical result that is obtained for the fermionic propagator in Eq. (2.62) and in Eq. (2.64). Note that since from the 2PI solution the coupling drops out, there is no need to specify its value for the presented results. The figure also proves implicitly that the strategy to resolve the aforementioned numerical problem with the 2PI equation was correct. Comparing the 1-loop and the 2PI the improvement is evident: the IR problem near the

mass shell which made the 1-loop calculation unreliable, *seems* to be cured. However, even though the 2PI result behaves well in the IR it is not closer to the exact solution which we will derive in the next section.

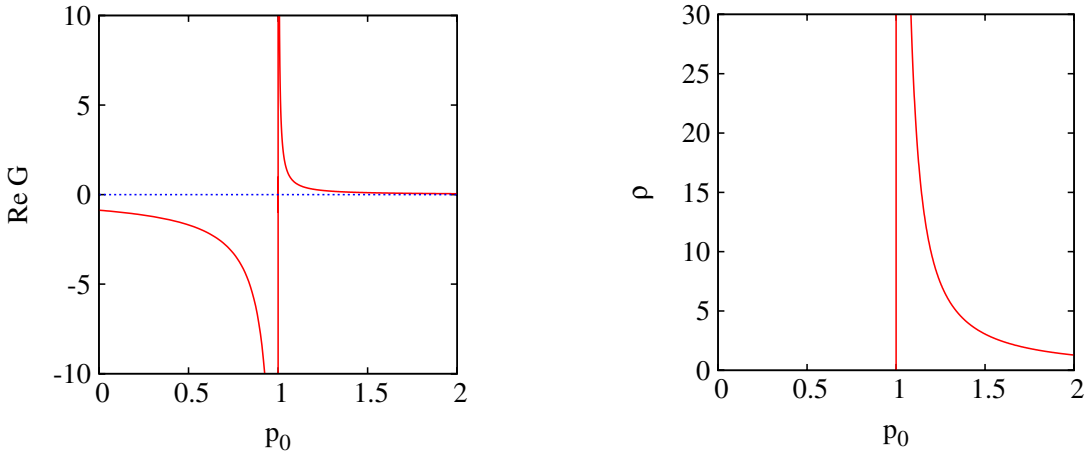

FIGURE 2.2: The real part (left panel) and discontinuity (spectral function) of the 2PI fermion propagator (right panel). The mass shell is set to $m = 1$.

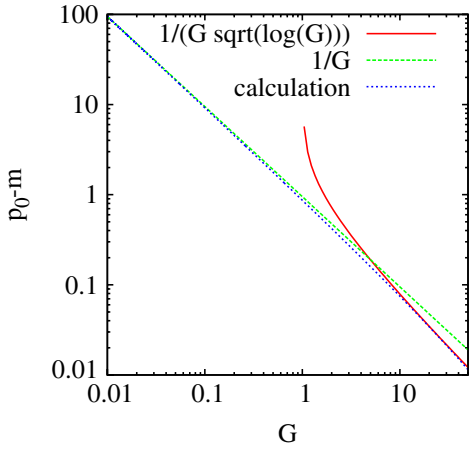

FIGURE 2.3: The expected asymptotics plotted on the data. The green curve fits on the small momentum regime with Eq. (2.62). The red curve shows the large momentum behaviour of the propagator with Eq(.2.64), where $\chi \propto \mathcal{G}$. Since inverting the relation Eq. (2.64) is rather difficult, it is more convenient to give the inverse function instead, that is why the plot is not in the form of $\mathcal{G}$ vs. $p_0 - m$. Note that on the plot label $\mathcal{G}$ is noted by capital G.

2.2.3 Dyson-Schwinger equations and Ward identities

Next we are going to consider the Dyson-Schwinger equation derived in Appendix D.1. For the BN model in Feynman gauge it can be written as

$$\Sigma(p) = -ie^2 \int \frac{d^4k}{(2\pi)^4} G(k)\mathcal{G}(p-k)u_\mu \Gamma^\mu(k; p-k, p), \tag{2.71}$$

where Γ^μ is the vertex function (see Appendix D.2). For the vertex function there is another exact equation, coming from the current conservation (see Appendix D.3). This results in the Ward identity analogous to the QED case [1]:

$$k_\mu \Gamma^\mu(k; p-k, p) = \mathcal{G}^{-1}(p) - \mathcal{G}^{-1}(p-k). \tag{2.72}$$

In this model, however, the vertex function is proportional to u^μ. In principle, the Lorentz-index in this model can come from u^μ or from any of the momenta. But, since the fermion propagator depends on the 4-momentum in the form $u_\mu p^\mu$, the fermion-photon vertex does not depend on the momentum components which are orthogonal to u^μ. Therefore the Lorentz-index which comes from k^μ in fact comes from the longitudinal part of k^μ, i.e. proportional to u^μ. So we can write $\Gamma^\mu(k; p-k, p) = u^\mu \Gamma(k; p-k, p)$. This gives us the possibility to determine the vertex function *exactly* by using the Ward identities [37]. The Ward identity for the current conservation yields then in case when $u = (1, 0, 0, 0)$:

$$\begin{aligned} k_\mu \Gamma^\mu(k; p-k, p) &= k_0 \Gamma(k; p-k, p) = \mathcal{G}^{-1}(p) - \mathcal{G}^{-1}(p-k) \\ \Gamma(k; p-k, p) &= \frac{\mathcal{G}^{-1}(p) - \mathcal{G}^{-1}(p-k)}{k_0}. \end{aligned} \tag{2.73}$$

Therefore, we find

$$\Sigma(p_0, m) = -ie^2 \int \frac{d^4k}{(2\pi)^4} \frac{G_{00}(k)}{k_0} \mathcal{G}(p-k) \left(\mathcal{G}^{-1}(p) - \mathcal{G}^{-1}(p-k) \right). \tag{2.74}$$

This is an exact equation in the BN model. Now, we will solve this equation in the renormalised theory. The finding is that the result is identical to the BN solution known from the literature ([31, 32]).
In the second term $\mathcal{G}^{-1}(p-k)$ drops out, resulting in an integral

$$-ie^2 \int \frac{d^4k}{(2\pi)^4} \frac{G_{00}(k)}{k_0} = 0, \tag{2.75}$$

because of the $k_0 \to -k_0$ symmetry. What remains is

$$\Sigma(p_0, m) = \mathcal{G}^{-1}(p)(-ie^2) \int \frac{d^4k}{(2\pi)^4} \frac{G_{00}(k)}{k_0} \mathcal{G}(p-k). \tag{2.76}$$

This form is true in the original model, we shall now find the renormalised form. First we adapt the wave function renormalisation for the fermionic fields which changes the bare propagator to $1/(Zp_0 - (m + \delta m))$ where $Z = 1 + \delta Z$. We will assume that the mass shell remains the same, then $m + \delta m = Zm$. The free propagator $1/(p_0 - m)$ gets a wave function renormalisation correction factor $1/Z$. We will use also the notation

$e_b = e + \delta e$. The full propagator then reads

$$\mathcal{G}^{-1}(p) = Z(p_0 - m) - \Sigma(p), \tag{2.77}$$

Using Eq. (2.76) we find the equation

$$\mathcal{G}(p) = \frac{\zeta(p_0)}{p_0 - m + i\varepsilon}, \tag{2.78}$$

where

$$\zeta(p_0) = \frac{1 + J(p_0)}{Z} \qquad \text{and} \quad J(p_0) = -ie_b^2 \int \frac{d^4k}{(2\pi)^4} \frac{G(k)}{k_0} \mathcal{G}(p-k). \tag{2.79}$$

$\zeta(p_0)$ can be interpreted as a running wave function renormalisation constant. With the spectral representation we have:

$$J(p_0) = \int_0^\infty \frac{d\omega}{2\pi}\, \varrho(\omega)\, I_1(\omega - p_0 - i\varepsilon), \qquad \text{where} \quad I_1(a) = ie_b^2 \int \frac{d^4k}{(2\pi)^4} \frac{1}{k_0^2 - \mathbf{k}^2 + i\varepsilon} \frac{1}{k_0} \frac{1}{a + k_0}. \tag{2.80}$$

In the Appendix A we evaluate $I_1(p_0)$, and we find

$$J(p_0) = \frac{e_b^2}{4\pi^2} \int_{-\infty}^{\infty} \frac{d\omega}{2\pi}\, \varrho(\omega) \left[\mathcal{D}_\varepsilon - \ln \frac{\omega - p_0 - i\varepsilon}{\mu} \right]. \tag{2.81}$$

We plug it into Eq. (2.79), then, assuming that spectral function fulfils the sum rule, after some algebraic manipulation we find

$$\zeta(p_0) = \frac{\dfrac{1}{\alpha_b} + \dfrac{1}{\pi}\mathcal{D}_\varepsilon - \dfrac{1}{\pi} \displaystyle\int_{-\infty}^{\infty} \frac{d\omega}{2\pi}\, \varrho(\omega)\, \ln \frac{\omega - p_0 - i\varepsilon}{\mu}}{Z/\alpha_b}. \tag{2.82}$$

We may assume that the explicit integral is not UV divergent (it can be checked a posteriori). Then the above equation can be made finite by requiring

$$\frac{1}{\alpha_b} + \frac{1}{\pi}\mathcal{D}_\varepsilon = \frac{1}{\alpha_r}, \qquad \frac{Z}{\alpha_b} = \frac{z_r}{\alpha_r}. \tag{2.83}$$

where α_r and z_r are finite. This form can be interpreted physically as the appearance of the renormalised coupling α_r and the finite wave function renormalisation z_r. We note that the coupling constant renormalisation equation in Eq. (2.83) agrees with the formula providing the non-perturbative coupling constant renormalisation in the O(N)

models [38]. Now, we find

$$\zeta(p_0) = \frac{1}{z_r}\left(1 - \frac{\alpha_r}{\pi}\int\limits_{-\infty}^{\infty}\frac{d\omega}{2\pi}\,\varrho(\omega)\,\ln\frac{\omega - p_0 - i\varepsilon}{\mu}\right). \tag{2.84}$$

This function depends on the arbitrary renormalisation scale μ, but the physics, of course, must be μ independent. This can be achieved by appropriately changing the z_r and α_r constant when we change μ. The μ-independence of $\zeta(p_0)$ requires (using the sum rule for ϱ):

$$\begin{aligned}\frac{d\zeta(p_0)}{d\ln\mu} = &- \frac{1}{z_r^2}\frac{dz_r}{d\ln\mu}\left(1 - \frac{\alpha_r}{\pi}\int\limits_{-\infty}^{\infty}\frac{d\omega}{2\pi}\,\varrho(\omega)\,\ln\frac{\omega - p_0 - i\varepsilon}{\mu}\right)\\ &- \frac{1}{z_r\pi}\frac{d\alpha_r}{d\ln\mu}\int\limits_{-\infty}^{\infty}\frac{d\omega}{2\pi}\,\varrho(\omega)\,\ln\frac{\omega - p_0 - i\varepsilon}{\mu} + \frac{1}{z_r}\frac{\alpha_r}{\pi} = 0.\end{aligned} \tag{2.85}$$

This can be satisfied if

$$-\frac{1}{z_r^2}\frac{dz_r}{d\ln\mu} + \frac{1}{z_r}\frac{\alpha_r}{\pi} = 0, \qquad \frac{1}{z_r^2}\frac{dz_r}{d\ln\mu}\frac{\alpha_r}{\pi} - \frac{1}{z_r\pi}\frac{d\alpha_r}{d\ln\mu} = 0. \tag{2.86}$$

The second equation means $z_r = \alpha_r/\alpha_0$, where α_0 is a constant; the first equation then reads

$$\frac{d\ln z_r}{d\ln\mu} = \frac{\alpha_r}{\pi} \quad\Rightarrow\quad \frac{d\alpha_r}{d\ln\mu} = \frac{\alpha_r^2}{\pi}. \tag{2.87}$$

And thus

$$-\frac{1}{\alpha_r(\mu)} + \frac{1}{\alpha_r(\mu_0)} = \frac{1}{\pi}\ln\frac{\mu}{\mu_0} \quad\Rightarrow\quad \alpha_r(\mu) = \frac{\alpha_r(\mu_0)}{1 + \dfrac{\alpha_r(\mu_0)}{\pi}\ln\dfrac{\mu_0}{\mu}}. \tag{2.88}$$

What we obtained here is nothing else but the non-perturbative running of the coupling in this model. Using the normalisability of ϱ we finally find

$$\zeta(p_0) = \frac{\alpha_0}{\pi}\int\limits_{-\infty}^{\infty}\frac{d\omega}{2\pi}\,\varrho(\omega)\,\ln\frac{\Lambda}{\omega - p_0 - i\varepsilon}, \qquad \Lambda = \mu e^{\frac{\pi}{\alpha_r}}. \tag{2.89}$$

The constant α_0 and the scale Λ are renormalisation group independent quantities (i.e. independent of the scale μ), these characterise the renormalisation scheme. The appearance of a scale Λ is the manifestation of dimensional transmutation. Now, instead of that scale Λ, it is worth to use M for which $\mathrm{Re}\,\zeta(M) = 0$. Clearly, $M \approx \Lambda$ if $\Lambda \gg m$.

Then differentiating ζ with respect to p_0, we find

$$\frac{d\zeta(p_0)}{dp_0} = \frac{\alpha_0}{\pi}\int_{-\infty}^{\infty}\frac{d\omega}{2\pi}\,\frac{\varrho(\omega)}{p_0-\omega+i\varepsilon} = \mathcal{G}(p_0) \quad \Rightarrow \quad \zeta(p_0) = \frac{\alpha_0}{\pi}\int_{p_0}^{M} d\omega\,\mathcal{G}(\omega). \tag{2.90}$$

This gives finally

$$(p_0-m)\mathcal{G}(p) = \frac{\alpha_0}{\pi}\int_{p_0}^{M} d\omega\,\mathcal{G}(\omega). \tag{2.91}$$

By differentiation with respect to p_0 we find

$$(p_0-m)\mathcal{G}' + \mathcal{G} = -\frac{\alpha_0}{\pi}\mathcal{G} \quad \Rightarrow \quad \mathcal{G}(p) = g_0(p_0-m)^{-1-\frac{\alpha_0}{\pi}}, \tag{2.92}$$

where g_0 is an arbitrary constant playing the role of the wave function renormalisation factor. This is indeed the solution of Bloch and Nordsieck [31, 32], now in terms of the renormalised quantities. We can also compute the exact spectral function of the theory

$$\underset{p_0}{\mathrm{Disc}}\,\mathcal{G}(p) = \Theta(p_0-m)\,\frac{g_0(1-e^{2i\alpha_0})}{(p_0-m)^{1+\frac{\alpha_0}{\pi}}}. \tag{2.93}$$

The discontinuity can take complex values, too, hence it is well justified to consider its absolute value instead, which gives

$$\rho(p) = \Theta(p_0-m)\,\frac{2g_0\sin(\alpha_0)}{(p_0-m)^{1+\frac{\alpha_0}{\pi}}}. \tag{2.94}$$

Interestingly, one can observe a periodic behaviour in the coupling, which is present in the finite temperature result, too (see Section 2.3). From Eq. (2.94) we can immediately see that it is not normalisable. The only way to achieve the sum rule is demanding $g_0 \to 0$. But then we are faced with a $0\times\infty$ expression. A possible solution is that one should always use a regularised version of the spectral function (or propagator), maintaining the sum rule, and only at the end of the calculation is one allowed to release the regularisation.

The most important fact regarding the BN propagator is that all the contribution of the quantised electromagnetic field now is being encoded in the exponent α_0/π, the fermion propagator has been dressed up with the photon cloud. The lesson of this analysis is that the deep IR physics seems to be well described by the Dyson-Schwinger equation supplemented with the Ward identities. As we have seen, this strategy is renormalisable and exact in case of the Bloch-Nordsieck model. However, the vertex resummation provided by the the procedure described above cannot be found in the case of the pure 2PI resummation, which could not give the exact solution. We can look at this new type of resummation as an improved version of the 2PI resummation.

In the following section we are going to present the results for the finite temperature case of the BN model.

2.3 The Bloch-Nordsieck model at finite temperature

At finite temperature the model is studied less often. In the seminal papers of Blaizot and Iancu [45, 46] the authors examined the large time behaviour of the fermion propagator with the Hard Thermal Loop (HTL) improved photon propagator. Using this result, Weldon worked out a spectral function which is valid in the vicinity of the mass shell [47]. With a different approach, Fried *et al.* studied the time dependence of the momentum loss of a hard incoming fermionic particle [48]. The main goal of this section is to work out the complete spectral function of the BN model for all momenta, and see how the short time dynamics, resembling the $T \to 0$ limit, goes over to the long time damping. Because of the relative simplicity of the model, we can even give analytic solutions for certain parameters, while for other, analytically not reachable parameter values, we used a well controlled numerical procedure. Another goal is to extend our Dyson-Schwinger formalism combined with Ward identities [40], which works excellently at zero temperature, to finite temperatures. With the help of this, the complete renormalisation process remains fully under control.

2.3.1 The finite temperature formalism

We are interested in the finite temperature fermion propagator. To determine it, we use the real time or Keldysh formalism (for details, see [49] and Appendix C). Here, the time variable runs over a contour containing forward and backward running sections (C_1 and C_2). The propagators are subject to boundary conditions which can be expressed as the KMS (Kubo-Martin-Schwinger) relations (see Appendix C). The physical time can be expressed through the contour time $t = \mathcal{T}(\tau)$. This makes possible to work with fields living on a definite branch of the contour, $\Psi_a(t, \mathbf{x}) = \Psi(\tau_a, \mathbf{x})$ where $\mathcal{T}(\tau_a) = t$, and $\tau_a \in C_a$ for $a = 1, 2$; and similarly for the gauge fields. The propagators are matrices in this notation, in particular the fermion and the photon propagator, respectively, reads as:

$$\begin{aligned} i\mathcal{G}_{ab}(x) &= \left\langle T_{\mathcal{C}} \Psi_a(x) \Psi_b^\dagger(0) \right\rangle , \\ iG_{\mu\nu,ab}(x) &= \langle T_{\mathcal{C}} A_{\mu a}(x) A_{\nu b}(0) \rangle , \end{aligned} \tag{2.95}$$

where $T_{\mathcal{C}}$ denotes ordering with respect to the contour variable (contour time ordering). For a generic propagator G_{11} corresponds to the Feynman propagator, and, since the

C_2 contour times are always larger than the C_1 contour times, $G_{21} = G^{>}$ and $G_{12} = G^{<}$ are the Wightman functions. The KMS relation for a bosonic/fermionic propagator reads $G_{12}(t, \mathbf{x}) = \pm G_{21}(t - i\beta, \mathbf{x})$ which has the following solution in Fourier space (with $k = (k^0, \mathbf{k})$)

$$\begin{aligned} iG_{12}(k) &= \pm n_{\pm}(k_0)\varrho(k), \\ iG_{21}(k) &= (1 \pm n_{\pm})(k_0)\varrho(k), \end{aligned} \tag{2.96}$$

where

$$n_{\pm}(k_0) = \frac{1}{e^{\beta k_0} \mp 1} \quad \text{and} \quad \varrho(k) = iG_{21}(k) - iG_{12}(k) \tag{2.97}$$

are the distribution functions (Bose-Einstein (+) and Fermi-Dirac (-) statistics), and the spectral function, respectively. It is sometimes advantageous to change to the R/A formalism with field assignments $\Psi_{1,2} = \Psi_r \pm \Psi_a/2$. Then, one has $G_{aa} = 0$ for both the fermion and the photon propagators. The relation between the propagators in the Keldysh formalism and the R/A propagators reads

$$G_{rr} = \frac{G_{21} + G_{12}}{2}, \quad G_{11} = G_{ra} + G_{12}, \quad \varrho = iG_{ra} - iG_{ar}. \tag{2.98}$$

The G_{ra} propagator is the retarded, the G_{ar} is the advanced propagator, G_{rr} is usually called the Keldysh propagator in the framework of the R/A formalism (not to confuse with the propagators *i*n the Keldysh formalism).

At zero temperature, as we could see in Section 2.2, the fermionic free Feynman propagator in the BN model has a single pole which means that there are no antiparticles in the model. Consequently, all closed fermion loops are zero, thus there is no self-energy correction to the photon propagator at zero temperature, as we already discussed it. The interpretation of the u parameter as the fixed four-velocity of the fermion implies that the Bloch-Nordsieck model describes that regime where the soft photon fields do not have energy even for changing the velocity of the fermion (no fermion recoil). This leads to the interpretation that the fermion is a hard probe of the soft photon fields, and as such it is not part of the thermal medium [46]. The finite temperature one-loop correction to the fermion propagator (see Appendix F) confirms this physical picture. So, we will set $\mathcal{G}_{12} = 0$, therefore the closed fermion loops as well as the photon self-energy remain zero even at finite temperature. Another, mathematical reason, why we must not consider dynamical fermions – which could show up in fermion loops – is that the spin-statistics theorem [1] forbids a one-component dynamical fermion field.
This means that now the *exact* photon propagator reads in Feynman gauge at finite

temperature

$$G_{ab,\mu\nu}(k) = -g_{\mu\nu}G_{ab}(k),$$
$$G_{ra} = \frac{1}{k^2}\bigg|_{k_0\to k_0+i\varepsilon}. \tag{2.99}$$

And the *exact* photon spectral function is

$$\varrho(k) = 2\pi\,\mathrm{sgn}(k_0)\delta(k^2). \tag{2.100}$$

All other propagators can be expressed using the identities in Eq. (2.96) and in Eq. (2.98).

2.3.2 Dyson-Schwinger equations in the Bloch-Nordsieck model at finite temperature

The derivation of the Dyson-Schwinger equations at non-zero temperature can be found in Appendix D.1 where we applied the CTP (Closed Time Path) formalism (see Appendix C). Thus, one can express the equation for the fermion self-energy with the two-component notation as it can be seen in Fig. 2.4. In terms of analytic formulas it reads:

$$\Sigma_{ab}(x,y) = i\alpha_a e^2 u_\mu \sum_{c,d=1}^{2} \int d^4w d^4z\, \mathcal{G}_{ac}(x,w)G^{\mu\nu}_{ad}(x,z)\Gamma_{\nu;dcb}(z;w,y), \tag{2.101}$$

where $\alpha_a = (-1)^{a+1}$. In Fourier space it is:

$$\Sigma_{ab}(p) = i\alpha_a e^2 u_\mu \sum_{c,d=1}^{2} \int \frac{d^4k}{(2\pi)^4}\, \mathcal{G}_{ac}(p-k)G^{\mu\nu}_{ad}(k)\Gamma_{\nu;dcb}(k;p-k,p). \tag{2.102}$$

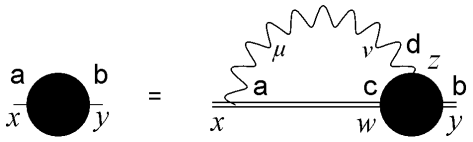

FIGURE 2.4: The Dyson-Schwinger equations in real time formalism. The bold letters for space-time points, the regular letters are the Keldysh indices and the Greek letters denote the Lorentz indices.

This equation is the non-zero temperature equivalent of Eq. (2.71), the only difference here is that, since we evaluate each operator on a given time contour, we need to indicate them, thus we use the lower indices for this purpose.
The vertex function in this case can be derived in a similar manner, too (see Appendix

D.2). The fact that the vertex function is proportional to u^μ is crucial again, in order to be able to apply the Ward identities in a way we did already in the zero temperature computation. The derivation of Ward identities at finite temperature is a straightforward generalisation of the formula that we have at zero temperature. This can be found in Appendix D.3. It is easy to rewrite it in the two-component formalism, taking into account that to satisfy the delta functions requirement the time arguments must be on the same contour. One finds in Fourier space

$$k_\mu \Gamma^\mu_{abc}(k;p,q) = \left[\delta_{ab}\mathcal{G}^{-1}_{bc}(q) - \delta_{ac}\mathcal{G}^{-1}_{bc}(p)\right] (2\pi)^4 \delta(k+p-q). \tag{2.103}$$

In the Bloch-Nordsieck model, because of the special property of the vertex function expressed in Eq. (D.10), the vertex function is *completely* determined by the fermion propagator in the form:

$$\Gamma_{abc}(k;p,q) = \frac{1}{uk}\left[\delta_{ab}\mathcal{G}^{-1}_{bc}(q) - \delta_{ac}\mathcal{G}^{-1}_{bc}(p)\right]\Big|_{p=q-k}, \tag{2.104}$$

therefore the Dyson-Schwinger equations for the fermion propagator become closed.

We will use Feynman gauge, and denote the photon propagator as $G_{\mu\nu} = -g_{\mu\nu}G$. Then this closed equation can be written as

$$\begin{aligned}
\Sigma_{ac}(p) &= -ie^2U^2\alpha_a \sum_{a',b'=1}^{2} \int \frac{d^4k}{(2\pi)^4}\frac{1}{uk} G_{aa'}(k)\mathcal{G}_{ab'}(p-k) \\
&\quad \times \left[\delta_{a'b'}(\mathcal{G}^{-1})_{b'c}(p) - \delta_{a'c}(\mathcal{G}^{-1})_{b'c}(p-k)\right] \\
&= -ie^2U^2\alpha_a \left[\sum_{a'=1}^{2}(\mathcal{G}^{-1})_{a'c}(p)\int \frac{d^4k}{(2\pi)^4}\frac{1}{uk}G_{aa'}(k)\mathcal{G}_{aa'}(p-k)\right. \\
&\quad \left. - \delta_{ac}\int \frac{d^4k}{(2\pi)^4}\frac{1}{uk}G_{aa}(k)\right],
\end{aligned} \tag{2.105}$$

where $U^2 = u_0^2 - \mathbf{u}^2$. In particular

$$\begin{aligned}
\Sigma_{11}(p) &= -ie^2U^2\left[\sum_{a'=1}^{2}(\mathcal{G}^{-1})_{a'1}(p)\int \frac{d^4k}{(2\pi)^4}\frac{1}{uk}G_{1a'}(k)\mathcal{G}_{1a'}(p-k) - \int \frac{d^4k}{(2\pi)^4}\frac{G_{11}(k)}{uk}\right] \\
\Sigma_{12}(p) &= -ie^2U^2\sum_{a'=1}^{2}(\mathcal{G}^{-1})_{a'2}(p)\int \frac{d^4k}{(2\pi)^4}\frac{1}{uk}G_{1a'}(k)\mathcal{G}_{1a'}(p-k).
\end{aligned} \tag{2.106}$$

Instead of G_{11} and G_{22}, it is more aesthetic to work with the retarded and advanced propagators (the relations are given in Eq. (2.98)). Since in the R/A formalism $G_{aa} = 0$,

the retarded propagator satisfies a homogeneous self-energy relation

$$G_{ra}(p) = G^{(0)}_{ra}(p) + G^{(0)}_{ra}(p)\Sigma_{ar}(p)G_{ra}(p), \tag{2.107}$$

while the propagators in the $1,2$ components mix. From the definitions we easily find

$$\begin{aligned} \Sigma_{ar} &= \Sigma_{11} + \Sigma_{12}, \\ \mathcal{G}_{ar} &= \mathcal{G}_{11} - \mathcal{G}_{12}. \end{aligned} \tag{2.108}$$

Therefore we have, using Eq. (2.106) and Eq. (2.98)

$$\Sigma_{ar}(p) = \mathcal{J}(p)\mathcal{G}^{-1}_{ra}(p) - \Delta M, \tag{2.109}$$

where

$$\begin{aligned} \mathcal{J}(p) &= -ie^2U^2 \int \frac{d^4k}{(2\pi)^4} \frac{1}{uk} \left(G_{21}(k)\mathcal{G}_{ra}(p-k) - G_{ra}(k)\mathcal{G}_{12}(p-k)\right), \\ \Delta M &= -ie^2U^2 \int \frac{d^4k}{(2\pi)^4} \frac{G_{11}(k)}{uk}. \end{aligned} \tag{2.110}$$

One can immediately find that $\Delta M = 0$. The photon propagator G_{11} is even for $k \to -k$, which is true in general, but now we can prove by inspecting the free propagator which is exact in our case

$$iG_{11}(k) = \frac{i}{k^2 + i\varepsilon} + (n(k_0) + \Theta(-k_0))2\pi \,\mathrm{sgn}(k_0)\, \delta(k^2). \tag{2.111}$$

For the first term the $k \to -k$ symmetry is evident, in the second one we should use the identity $n(k_0) + n(-k_0) + 1 = 0$. Therefore, with the change of the integration variable $(k \to -k)$, the G_{11} propagator remains the same while uk changes sign, so ΔM changes sign, too. As a consequence $\Delta M = 0$.

The Bloch-Nordsieck model, as all four-dimensional interacting quantum field theories, contains divergences. To obtain a finite result, we need wave function, mass and coupling constant renormalisation. Since the above expressions have contained the original parameters of the Lagrangian, we should rewrite them in terms of the renormalised quantities. From now on the parameters m and e will denote the renormalised ones, while m_0 and e_0 are the bare quantities. Renormalisation goes like in the zero temperature case in Section 2.2: assuming that the renormalised mass $m = Zm_0$ where Z is the fermion wave function renormalisation constant (this is ensured by the Ward identities) we can write $\mathcal{G}^{-1}_{ra} = Z(up - m) - \Sigma_{ar}$, and from Eq. (2.109) we find

$$\mathcal{G}_{ra}(p) = \frac{\zeta(p)}{up - m}, \qquad \text{where} \qquad \zeta(p) = \frac{1 + \mathcal{J}(p)}{Z}. \tag{2.112}$$

2.3.3 Calculation of $\mathcal{J}$

In the expression of $\mathcal{J}$ in Eq. (2.110) appears $\mathcal{G}_{12}(k)$. As we discussed earlier, for the sake of physical and mathematical consistency of the model, we must assume that the fermion describes a hard probe and is not a dynamical field, which means that we must set $\mathcal{G}_{12}(k) = 0$. Then from Eq. (2.110) we can easily recover the zero temperature result we found in Section 2.2. At finite temperature, we have

$$\mathcal{J}(p) = -ie^2U^2 \int \frac{d^4k}{(2\pi)^4} \frac{1}{uk} G_{21}(k)\mathcal{G}_{ra}(p-k). \tag{2.113}$$

Next, we prove by recursion that the solution for $\mathcal{G}_{ra}$ depends solely on $w = up - m$. It is true at tree level where $\mathcal{G}_{ra}^{-1} = up - m$. So let us assume that $\mathcal{G}_{ra}(p) = \bar{\mathcal{G}}_{ra}(up - m)$. Then

$$\mathcal{J}(p) = -ie^2U^2 \int \frac{d^4k}{(2\pi)^4} \frac{1}{uk} G_{21}(k)\bar{\mathcal{G}}_{ra}(up - m - uk), \tag{2.114}$$

implying $\mathcal{J}(p) = \bar{\mathcal{J}}(up-m)$. Equation (2.112) tells us that if $\mathcal{J}$ depends only on $up-m$, then $\mathcal{G}_{ra}$ also depends only on $up - m$. With this statement the recursion is closed.
Since in the BN model the free photon propagator is exact, we shall write it into Eq. (2.113). Using Eq. (2.96) for the G_{21} propagator, and applying the Landau prescription ($w \to w + i\varepsilon$), we find

$$\bar{\mathcal{J}}(w) = e^2U^2 \int \frac{d^4k}{(2\pi)^4} \frac{1}{uk} \left(1 + n(k_0)\right) \frac{2\pi}{2k} \left(\delta(k_0 - k) - \delta(k_0 + k)\right) \bar{\mathcal{G}}_{ra}(w - uk). \tag{2.115}$$

This result, as we shall show in Section 2.3.7, is consistent with the results of [45, 46]. The integral in Eq. (2.115) can be brought to the form (see Appendix E):

$$\bar{\mathcal{J}}(w) = \frac{-\alpha}{\pi} \int_{-\infty}^{\infty} dq\, f(q,u)\, \bar{\mathcal{G}}_{ra}(w - q), \tag{2.116}$$

where $\alpha = e^2/(4\pi)$ and

$$f(q,u) = \frac{u_0(1-v^2)}{2v} \int_{u_0(1-v)}^{u_0(1+v)} \frac{ds}{us^2} \left(1 + n\left(\frac{q}{s}\right)\right) = \frac{u_0(1-v^2)}{2vq\beta} \ln \frac{e^{\beta q/(u_0(1-v))} - 1}{e^{\beta q/(u_0(1+v))} - 1}, \tag{2.117}$$

where $u = u_0(1, \mathbf{v})$ and $v = |\mathbf{v}|$ (i.e. $\mathbf{v}$ is the velocity $\mathbf{v} = \mathbf{u}/u_0$). The integration variables q and s are related to the absolute value of $\mathbf{k}$ the angle between $\mathbf{k}$ and $\mathbf{u}$, respectively. At zero temperature $f(q) = \Theta(q)$. At $v = 0$ we find

$$f(q, \boldsymbol{u} = 0) = 1 + n(q). \tag{2.118}$$

2.3.4 Renormalisation

In Eq. (2.116) we find ultraviolet (UV) divergences. From the expression of $f(q,u)$ (Eq. (2.117)) we see that for large momenta the thermal distribution functions always decrease exponentially, thus yielding a UV finite result. So, all the UV singularity is in the $T=0$ part, discussed already in Section 2.2 and in [40].

To apply the renormalised treatment at finite temperature, we recall some results from Section 2.2. At $T=0$ Eq. (2.116) can be written in spectral representation and with dimensional regularisation as

$$\begin{aligned}\bar{\mathcal{J}}_0(w) &= \frac{-\alpha}{\pi}\int_0^\infty dq\,\bar{\mathcal{G}}_{ra}(w-q) = \frac{\alpha}{\pi}\int_{-\infty}^{\infty}\frac{dw'}{2\pi}\,\bar{\varrho}(w')\int_0^\infty dq\,\frac{1}{q+w'-w-i\varepsilon}\\ &= \frac{\alpha}{\pi}\int_{-\infty}^{\infty}\frac{dw'}{2\pi}\,\bar{\varrho}(w')\left[\mathcal{D}_\varepsilon - \ln\frac{w'-w-i\varepsilon}{\mu}\right],\end{aligned} \tag{2.119}$$

where

$$\mathcal{D}_\varepsilon = \frac{1}{2\varepsilon}+\frac{1}{2}\ln(4\pi)+\frac{1}{2}P_{1/2} \tag{2.120}$$

($P_{1/2}=-1.96351$ is the value of the polygamma function with $0,1/2$ arguments, that is $\Psi_0(1/2)$).

As we discussed in the previous section, the divergent term is necessary both for the coupling constant and for the wave function renormalisation. Repeating the procedure of Section 2.2.3, we can write, assuming normalisability of $\bar{\varrho}$

$$\bar{\zeta}(w) = \frac{1+\bar{\mathcal{J}}(w)}{Z} = \frac{\frac{4\pi^2}{e_0^2}+\mathcal{D}_\varepsilon+\bar{\mathcal{J}}_{fin}(w)}{\frac{4\pi^2 Z}{e_0^2}}, \tag{2.121}$$

where $\bar{\mathcal{J}}_{fin}(w)$ is finite. We introduce as in Eq. (2.83)

$$\frac{4\pi^2}{e_0^2}+\mathcal{D}_\varepsilon = \frac{4\pi^2}{e^2}, \qquad \frac{4\pi^2 Z}{e_0^2} = \frac{4\pi^2 z_r}{e^2}, \tag{2.122}$$

where z_r and e now are finite (renormalised) values. Using renormalisation group invariance, we can write for the complete finite temperature contribution

$$\bar{\zeta}(w) = \frac{\bar{e}^2}{4\pi^2}\left[\int_{-\infty}^{\infty}\frac{dw'}{2\pi}\,\bar{\varrho}(w')\ln\frac{\Lambda}{w'-w-i\varepsilon} - \int_{-\infty}^{\infty}dq\,(f(q,u)-\Theta(q))\,\bar{\mathcal{G}}_{ra}(w-q)\right], \tag{2.123}$$

where $\bar{e}$ is a RG invariant coupling, $\Lambda = \mu \exp(\frac{4\pi^2}{e^2})$ is the momentum scale of the Landau-pole. Introducing for the first term in the square bracket

$$I(w) = \int_{-\infty}^{\infty} \frac{dw'}{2\pi}\, \bar{\varrho}(w') \ln \frac{\Lambda}{w' - w - i\varepsilon}, \tag{2.124}$$

we can express its derivative as:

$$\frac{I(w)}{dw} = -\int_{-\infty}^{\infty} \frac{dw'}{2\pi}\, \frac{\bar{\varrho}(w')}{w - w' + i\varepsilon} = -\bar{\mathcal{G}}_{ra}(w). \tag{2.125}$$

The imaginary part of $I(w)$ term is zero for $w < 0$, moreover for $w = 0$ it is negative (at least for large Λ), while for $w \to -\infty$ it is positive. So there exists a value $w = -M$ for which it is zero. Then we can write:

$$I(w) = -\int_{-M}^{w} dq\, \bar{\mathcal{G}}_{ra}(q). \tag{2.126}$$

The scale M replaces the scale Λ. Assuming that $M \gg T$ we can change the integration limits and integrate from $-M$ to M in the second term in Eq.2.123, too. Then we find

$$\bar{\zeta}(w) = -\frac{\bar{e}^2}{4\pi^2} \int dq\, f(q,u)\, \bar{\mathcal{G}}_{ra}(w - q), \tag{2.127}$$

where the integral symbol means $\int = \int_{-M}^{M}$. If it does not cause problem, we will send $M \to \infty$. The zero temperature part is the same as in Section 2.2.3.

In conclusion, by combining Eq. (2.112) with Eq. (2.127), the renormalised equation reads:

$$w\bar{\mathcal{G}}(w) = -\frac{\alpha}{\pi} \int dq\, f(q,u)\, \bar{\mathcal{G}}(w - q), \tag{2.128}$$

where $f(q,u)$ is given by Eq.((2.117)). Since this equation is linear, the same will be true for the spectral function (with different normalisation conditions)

$$w\bar{\varrho}(w) = -\frac{\alpha}{\pi} \int dq\, f(q,u)\, \bar{\varrho}(w - q). \tag{2.129}$$

2.3.5 Zero velocity case

For $v = 0$, $u_0 = 1$ we find from Eq. (2.129) and Eq. (2.118)

$$w\bar{\varrho}(w) = -\frac{\alpha}{\pi} \int dq\, (1 + n(q))\bar{\varrho}(w - q). \tag{2.130}$$

By sending the limits of the integration to infinity, we realise that the integral on the RHS is a convolution. Therefore, we change to Fourier space where it becomes a product, and the LHS will be $i\partial_t \bar{\varrho}(t)$. Using the Fourier transform of $1 + n(q)$

$$\int \frac{dw}{2\pi} e^{-iwt} \frac{e^{\beta w}}{e^{\beta w} - 1} = \frac{-iT}{2\tanh(\pi t T)} \tag{2.131}$$

we obtain the differential equation

$$i\partial_t \bar{\varrho}(t) = \frac{iT\alpha}{\tanh(\pi t T)} \bar{\varrho}(t). \tag{2.132}$$

This has the following solution:

$$\bar{\varrho}(t) = \bar{\varrho}_0 \left(\sinh \pi t T\right)^{\alpha/\pi}. \tag{2.133}$$

Before we proceed, we shall discuss this result. First we can easily obtain the $T = 0$ result, since for $t \ll \frac{1}{T}$ the sinh function can be approximated linearly, and we get $\bar{\varrho}(t) \sim t^{\alpha/\pi}$. On the other hand this result is rather weird; it describes forever increasing correlation instead the physically sensible loss of correlation. Since we find the same result by performing the computation at zero temperature, this is not an artefact of the finite temperature calculation. In accordance with Blaizot and Iancu [45, 46], we should not consider this expression as the physical response function. Mathematically, we can argue that we are not in the physically sensible analytic domain, the time dependent spectral function is not square-integrable for a real α value, as it should be. We must therefore go over to the physical analytic domain, where the Fourier-transformation is well defined.

For the analytic continuation we consider Eq. (2.182) valid as long as it yields sensible formulae, which is the case for *complex* α values. With this assumption the spectral function in the Fourier space will be an analytic function in α. For real α values the spectral function will be interpreted as an analytic continuation. We will see that this procedure indeed provides sensible results.

To perform the inverse Fourier transformation on $\bar{\varrho}(t)$ in Eq. (2.182), we apply Laplace transformation. With $s_\pm = \pm iw$ we find

$$\int_{-\infty}^{\infty} dt\, e^{iwt} \bar{\varrho}(t) = \int_0^{\infty} dt\, e^{-s_- t} \bar{\varrho}(t) + \int_0^{\infty} dt\, e^{-s_+ t} \bar{\varrho}(-t) = \bar{\varrho}_+(s_-) + (-1)^{\alpha/\pi} \bar{\varrho}_+(s_+), \tag{2.134}$$

where

$$\bar{\varrho}_+(s) = \bar{\varrho}_0 \int_0^\infty dt\, e^{-st} \left(\sinh \pi t T\right)^{\alpha/\pi} = \bar{\varrho}_0 \frac{\Gamma\left(1+\frac{\alpha}{\pi}\right)}{2^{1+\alpha/\pi}\pi T} \frac{\Gamma\left(\frac{\beta s}{2\pi} - \frac{\alpha}{2\pi}\right)}{\Gamma\left(1+\frac{\beta s}{2\pi}+\frac{\alpha}{2\pi}\right)}. \tag{2.135}$$

Since the gamma function satisfies Euler's reflection formula $\Gamma(1-z)\Gamma(z) = \pi/\sin \pi z$, we can write with $s = \pm iw$:

$$\left.\frac{\Gamma\left(\frac{\beta s}{2\pi} - \frac{\alpha}{2\pi}\right)}{\Gamma\left(1+\frac{\beta s}{2\pi}+\frac{\alpha}{2\pi}\right)}\right|_{s=\pm iw} = \frac{\pi}{\left|\Gamma\left(1+\frac{\alpha}{2\pi}+i\frac{\beta w}{2\pi}\right)\right|^2 \sin\left(\frac{\alpha}{2} \mp i\frac{\beta w}{2}\right)}. \tag{2.136}$$

To obtain the full spectral function Eq. (2.134) we need to perform the following sum, which is done in detail in Appendix E:

$$\frac{\pi}{\left|\Gamma\left(1+\frac{\alpha}{2\pi}+i\frac{\beta w}{2\pi}\right)\right|^2}\left(\frac{1}{\sin\left(\frac{\alpha}{2}-i\frac{\beta w}{2}\right)} + \frac{(-1)^{\alpha/\pi}}{\sin\left(\frac{\alpha}{2}+i\frac{\beta w}{2}\right)}\right) = \frac{2e^{i\alpha/2}e^{\beta w/2}\sin\alpha}{\cosh(\beta w)-\cos\alpha}. \tag{2.137}$$

Thus, we get the following expression for the spectral function:

$$\bar{\varrho}^*(w) = \bar{\varrho}_0 \frac{2e^{i\alpha/2}\beta \sin\alpha\, e^{\beta w/2}}{\cosh(\beta w)-\cos\alpha} \frac{1}{\left|\Gamma\left(1+\frac{\alpha}{2\pi}+i\frac{\beta w}{2\pi}\right)\right|^2}. \tag{2.138}$$

Here, we can see that we obtained a complex valued function. This was the case at zero temperature, too (cf. Eq. (2.93)). We can get rid of the phase factor $e^{i\alpha/2}$ by taking the absolute value $\bar{\varrho} = |\bar{\varrho}^*|$. Then, we get for the (real) spectral function

$$\bar{\varrho}(w) = \frac{N_\alpha \beta |\sin\alpha|\, e^{\beta w/2}}{\cosh(\beta w)-\cos\alpha} \frac{1}{\left|\Gamma\left(1+\frac{\alpha}{2\pi}+i\frac{\beta w}{2\pi}\right)\right|^2}, \tag{2.139}$$

where N_α is a normalisation factor which incorporates the constant $\bar{\varrho}_0$, and its precise numerical value can be determined by the sum rule

$$\int \frac{dw}{2\pi}\, \bar{\varrho}(w) = 1. \tag{2.140}$$

In Fig. 2.5 we can see the shape of the spectral function for different $\alpha = e^2/4\pi$ values and for different temperatures.

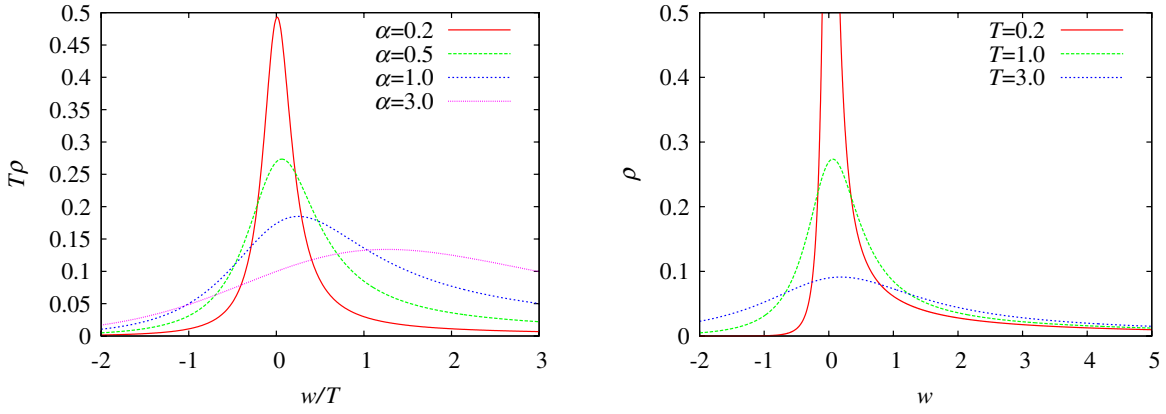

(A) (B)

FIGURE 2.5: (A) The exact, normalised spectral function at $v = 0$. Common features are the dominantly exponential decrease for $w \to -\infty$, power law decrease $\sim w^{-1-\alpha/\pi}$ for $w \to \infty$ and at the peak at finite curvature $\sim \alpha$. (B) The temperature dependence of the spectral function at $v = 0$ and $\alpha = 0.5$. In the limit $T \to 0$ it is singular at the point $w = 0$.

To discuss this result we make the following observations:

- $\bar{\varrho}(w)$ is a function of βw only, which is understandable, since there is no other scale in the system which could form a dimensionless combination.

- For $\alpha \to 0$, we find
$$\frac{e^{\beta w/2}|\sin\alpha|}{\cosh(\beta w) - \cos\alpha} \to 2\pi\delta(w), \tag{2.141}$$
so we recover the free case. It is interesting, that this behaviour periodically returns for $\alpha = 2\pi n$.

- For large values of w which is equivalent to the small temperature case we can use the asymptotic form of the Γ function for complex arguments with large absolute value:
$$\Gamma(x) = e^{-x}x^x\left(x^{-1/2} + \mathcal{O}(x^{-3/2})\right). \tag{2.142}$$
Then we find, up to normalisation factors
$$\bar{\varrho}(\beta w \gg 1) \sim \frac{e^{\beta w}}{\cosh(\beta w)}\frac{1}{w^{1+\frac{\alpha}{\pi}}} \overset{T\to 0}{\longrightarrow} \Theta(w)w^{-1-\frac{\alpha}{\pi}}. \tag{2.143}$$
This is the well-known exact solution by Bloch and Nordsieck at zero temperature. Note that the Θ function came out correctly from the formula. At finite but small temperatures, for negative arguments we observe exponential decrease.
This form also shows how at zero temperature we obtain zero wave function renormalisation factor that we discussed at the end of the Section 2.2.3 (g_0 in Eq. (2.94)).

The normalisation factor (c.f. Eq. (2.139)) is proportional to β, while the asymptotic form is $(\beta w)^{-1-\frac{\alpha}{\pi}}$. Then approaching zero temperature we obtain $T^{\frac{\alpha}{\pi}} w^{-1-\frac{\alpha}{\pi}}$, which means a renormalisation factor vanishing as $\sim T^{\frac{\alpha}{\pi}}$ for $T \to 0$.

- Now, let us consider the $w \to 0$ limit, i.e. the vicinity of the mass shell. We can expand $\bar{\varrho}$ into a power series

$$\bar{\varrho}(w) = \frac{4\bar{\varrho}(0)CT^2}{(w - CT)^2 + \left(\frac{4}{C} - 1\right) C^2T^2 + \mathcal{O}(w^3)}, \tag{2.144}$$

where

$$\frac{1}{C} = \frac{1}{2} + \frac{2}{1 - \cos\alpha} + \frac{1}{\pi^2}\Psi^2(1 + \frac{\alpha}{2\pi}), \tag{2.145}$$

and $\Psi(x)$ is the digamma function. The maximum of this function is at CT, the width is $CT\sqrt{4C^{-1} - 1}$. Since, however, the function is not symmetric, these parameters cannot be interpreted as a thermal mass and thermal width. For that we need to examine the real time dependence.

- For the real time dependence we use the fact that, according to Eq. (2.139), $\varrho(p) = \beta f_0(\beta(p_0 - m))$, which means that $\varrho(t) = e^{-imt}\tilde{f}_0(Tt)$. Omitting the oscillating phase (i.e. if we consider the envelope of $\varrho(t)$), we recover the Fourier transform of f_0. The real time dependence obtained from the inverse Fourier transform of Eq. (2.139) differs from Eq. (2.182). This is because we performed an analytic continuation to the physically sensible analytic domain. The numerical inverse Fourier transform of the normalised spectral function (and, because $iG_{ra}(t) = \Theta(t)\varrho(t)$, for $t > 0$ this is also the real time dependence of the retarded Green's function) can be seen in Fig. 2.6. At small times we expect to recover the zero temperature result. Indeed, we observe $\bar{\varrho}(t) = (1 - A(Tt)^{\alpha/\pi})e^{-imt}$ asymptotic form (for $\alpha = 0.5$ this is valid up to $Tt < 0.4$), the power law time dependence is characteristic to the zero temperature result. At $t = 0$ the value of the spectral function is 1, this is because of normalisation. Note however, that naively at zero temperature we would obtain a time dependence of the form $\sim t^{\alpha/\pi}e^{-imt}$, describing growth of correlation and violating the normalisation condition. Interpreting the zero temperature result as $T \to 0$ limit, we could cure this apparent inconsistency of the model. At strictly $T = 0$ we get back the physically sensible oscillating solution $\varrho(t) = e^{-imt}$. For large times (for $tT > 1$) the time dependence is $\sim e^{-\alpha Tt}$, which agrees with [45, 46]. Comparing it to Eq. (2.182) we see that instead of an exponential rise we found an exponential decay, but with the same coefficient. This can be understood by noting that if we have a pole at $w = w_0$ in the momentum space, meaning e^{-iw_0t} exponential time dependence, this pole is present in the spectral function in position w_0^*, too. The physical retarded Green's

function can have poles in the lower half plane, therefore we find in our case only the $w_0 = -i\alpha T$ pole, giving exponential damping.

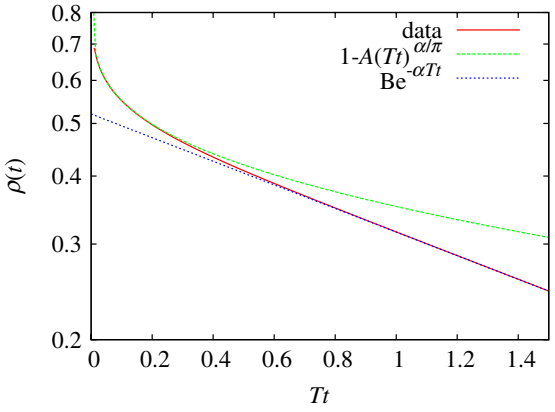

FIGURE 2.6: Time dependence of the (envelope of the) retarded Green's function (or, equivalently, the spectral function) for $v = 0$ at $\alpha = 0.5$ on a logarithmic y-scale. For small times we find $1 - A(Tt)^{\alpha/\pi}$, corresponding to the zero temperature time dependence. For large times it turns into an exponential damping of the form $\exp(-\alpha T t)$.

For the justification of the analytic continuation we also used a different method. We expanded the t-dependent result Eq. (2.182) into power series using

$$\begin{aligned}(\sinh x)^{\alpha/\pi} &= \left(\frac{1}{2}\right)^{\frac{\alpha}{\pi}} \sum_{k=0}^{\infty} \left[\Theta(x)(-1)^k \binom{\frac{\alpha}{\pi}}{k} e^{x(\frac{\alpha}{\pi}-k)} e^{-xk} \right. \\ &\quad \left. + \Theta(-x)(-1)^{\frac{\alpha}{\pi}-k} \binom{\frac{\alpha}{\pi}}{k} e^{-x(\frac{\alpha}{\pi}-k)} e^{xk}\right]. \end{aligned} \tag{2.146}$$

Now, the inverse Fourier transformation acts on a pure exponential function. We use the formula

$$\int_0^\infty dt\, e^{\pm iwt - st} = \frac{1}{s \mp iw} \tag{2.147}$$

which is true, of course, if $s > 0$, but this is the formula for the analytic continuation, too. Then the result of the Fourier transformation, with appropriate normalisation to ensure reality of ϱ is:

$$\varrho(w) \sim \sum_{k=0}^{\infty} (-1)^k \binom{\frac{\alpha}{\pi}}{k} \left[\frac{(-1)^{-\alpha/2\pi}}{s_k + iw} + \frac{(-1)^{\alpha/2\pi}}{s_k - iw}\right], \tag{2.148}$$

where $s_k = \pi T(2k - \alpha/\pi)$. Using the $(-1)^{\alpha/2\pi} = \cos\frac{\alpha}{2} + i\sin\frac{\alpha}{2}$ definition we find after a simple calculation

$$\varrho(w) \sim \sum_{k=0}^{\infty}(-1)^k \binom{\frac{\alpha}{\pi}}{k} \frac{s_k(1+\cos\alpha) - w\sin\alpha}{s_k^2 + w^2}, \qquad s_k = \pi T\left(2k - \frac{\alpha}{\pi}\right). \tag{2.149}$$

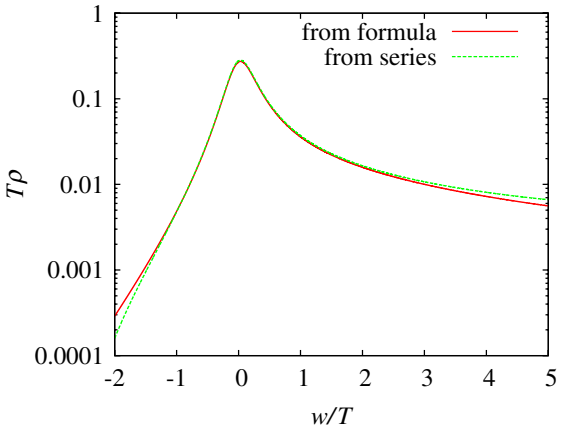

FIGURE 2.7: Comparison of the logarithm spectral function at $\alpha = 0.5$ calculated from Eq. (2.139) and from Eq. (2.149). The two results agree well.

The sum shows a fast convergence, and we can compare the result of the two calculations in Fig. 2.7. We can see that the two methods of analytic continuation yield consistent result in the central peak regime. To understand the small deviations at the edges, we remark that if α is real then $\bar{\varrho}(t = 0) = 0$ (c.f. Eq. (2.182)). In Fourier space this means $\int dw\bar{\varrho}(w) = 0$, therefore it can not be positive for all momenta. Using the second method, the position where the spectral function turns into negative values is, fortunately, at large $|w/T|$ values, therefore the peak is unaffected. The only precursor of the sign changing is the slight decrease at the edges of the plot. In our first method we started from complex α values, where $\lim_{t\to 0}\bar{\varrho}(t) = \bar{\varrho}_0 \neq 0$, then the normalisation does not require negative values for $\bar{\varrho}(w)$.

2.3.6 Finite velocity case

If $v \neq 0$, we find from Eq. (2.129) using Eq. (2.117) the following formula

$$w\bar{\varrho}(w) = -\frac{\alpha}{\pi}\frac{u_0(1-v^2)}{2v}\int_{u_0(1-v)}^{u_0(1+v)}\frac{ds}{s^2}\int dq\,(1+n(\tfrac{q}{s}))\,\bar{\varrho}(w-q). \tag{2.150}$$

The q-ntegral on the RHS is again a convolution, and formally we can use the same method as in the $v = 0$ case. We find

$$\partial_t \bar{\varrho}(t) = \frac{\alpha}{\pi} \frac{u_0(1-v^2)}{2v} \int_{u_0(1-v)}^{u_0(1+v)} \frac{ds}{s^2} \frac{Ts}{\tanh(\pi t T s)} \bar{\varrho}(t), \tag{2.151}$$

which has the solution

$$\bar{\varrho}(t) = \bar{\varrho}(0) \exp\left[\frac{\alpha}{\pi} \frac{u_0(1-v^2)}{2v} \int_{u_0(1-v)}^{u_0(1+v)} \frac{ds}{s^2} \ln(\sinh \pi t T s) \right]. \tag{2.152}$$

We cannot perform analytically neither the integral nor its Fourier transform. But we can determine many features by investigating the expressions for small and large values of t.

2.3.6.1 Small time behaviour

Since at small t we can make the approximation $\sinh \pi t T s \simeq \pi t T s$, one has:

$$\frac{u_0(1-v^2)}{2v} \int_{u_0(1-v)}^{u_0(1+v)} \frac{ds}{s^2} \ln(\sinh \pi t T s) \simeq \frac{u_0(1-v^2)}{2v} \int_{u_0(1-v)}^{u_0(1+v)} \frac{ds}{s^2} \ln(\pi t T s) = \ln(\pi T t) + \text{const.}, \tag{2.153}$$

where the constant comes from the integral of $s^{-2} \ln s$, and being a finite quantity, it goes into the normalisation. After exponentiation we find

$$\bar{\varrho}(t) \sim (Tt)^{\alpha/\pi}, \tag{2.154}$$

which is the zero temperature result. So, as we expected the short time or large frequency regime reproduces the zero temperature case, and thus it is velocity-independent.

2.3.6.2 Large time behaviour

Here, the function sinh can be approximated by the exponential, and so for large t

$$\ln \sinh \pi T t s \simeq \pi T t s - \ln 2. \tag{2.155}$$

The $\ln 2$ yields a constant factor which goes into the normalisation. The rest gives, including the prefactors

$$\alpha T t \frac{u_0(1-v^2)}{2v} \int_{u_0(1-v)}^{u_0(1+v)} \frac{ds}{s} = \alpha_{eff}(u) T t, \tag{2.156}$$

where

$$\alpha_{eff}(u) = \alpha \frac{u_0(1-v^2)}{2v} \ln\left(\frac{1+v}{1-v}\right). \tag{2.157}$$

From this form we obtain for the spectral function in the asymptotic limit:

$$\bar{\varrho}(t) = C e^{\alpha_{eff}(u) T t}. \tag{2.158}$$

We can easily check that $\lim_{v\to 0} \alpha_{eff}(u) = \alpha$. Therefore, the $v \to 0$ limit is analytic. Since in the asymptotic time regime we simply get the substitution rule $\alpha \to \alpha_{eff}(u)$ as compared to the $v = 0$ case, the analysis of the vicinity of the peak of the spectral function and the large time dependence will also remain valid in the finite velocity case but with a modified value of the coupling. In particular, since $\alpha_{eff}(u) < \alpha$, we obtain a smaller damping, larger lifetime for $v > 0$ cases. Physically this property is the consequence of the decreasing cross section at larger energies. In the ultrarelativistic limit $v \to 1$ the damping disappears.

2.3.6.3 Solution for $t \in (0, \infty)$

For intermediate times we will use a well-controlled numerical method to find the spectral function, once the analytic behaviour for large t is identified. We express the wanted $\bar{\varrho}_u(t)$ as a product of the known $\bar{\varrho}_{u=0}(t; \alpha_{eff})$ (from Eq. (2.157)) and a correction factor

$$\bar{\varrho}(t) \sim Z(t) \bar{\varrho}_{u=0}(t; \alpha_{eff}), \tag{2.159}$$

where

$$Z(t) \equiv \frac{\exp\left[\dfrac{\alpha u_0(1-v^2)}{2\pi v} \displaystyle\int_{u_0(1-v)}^{u_0(1+v)} \frac{ds}{s^2} \ln(\sinh \pi t T s)\right]}{(\sinh \pi T t)^{\frac{\alpha_{eff}(u)}{\pi}}}. \tag{2.160}$$

After a short algebra we find

$$Z(t) = \exp\left\{ \frac{\alpha u_0(1-v^2)}{2\pi v} \int_{u_0(1-v)}^{u_0(1+v)} \frac{ds}{s^2} \ln \frac{\sinh \pi T t s}{(\sinh \pi T t)^s} \right\}. \tag{2.161}$$

The ratio defined in this way is symmetric: $Z(t) = Z(-t)$. For small t arguments it behaves as $Z(t) \sim (Tt)^{\frac{\alpha-\alpha_{eff}(u)}{\pi}}$ and, since $\alpha \geq \alpha_{eff}(u)$, we also know that $Z(t=0) = 0$. At large t we find $\lim_{t\to\infty} Z(t) = 1$. We can determine it numerically, for a specific v it can be seen in Fig. 2.8.

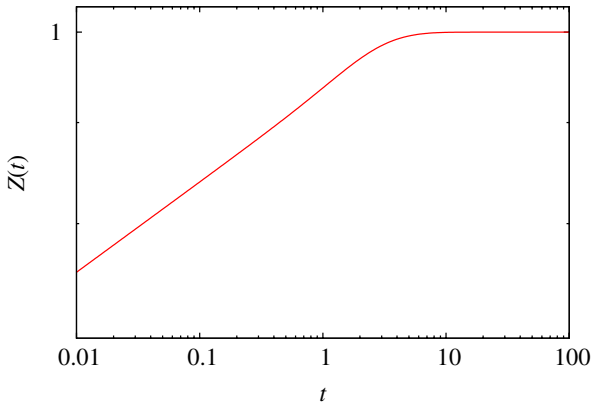

FIGURE 2.8: The $Z(t)$ function on a logarithmic plot. For small times it is a power, for larger times it flattens out. The shape of the plotted curve can be considered as a generic behaviour of $Z(t)$ (for arbitrary v and α).

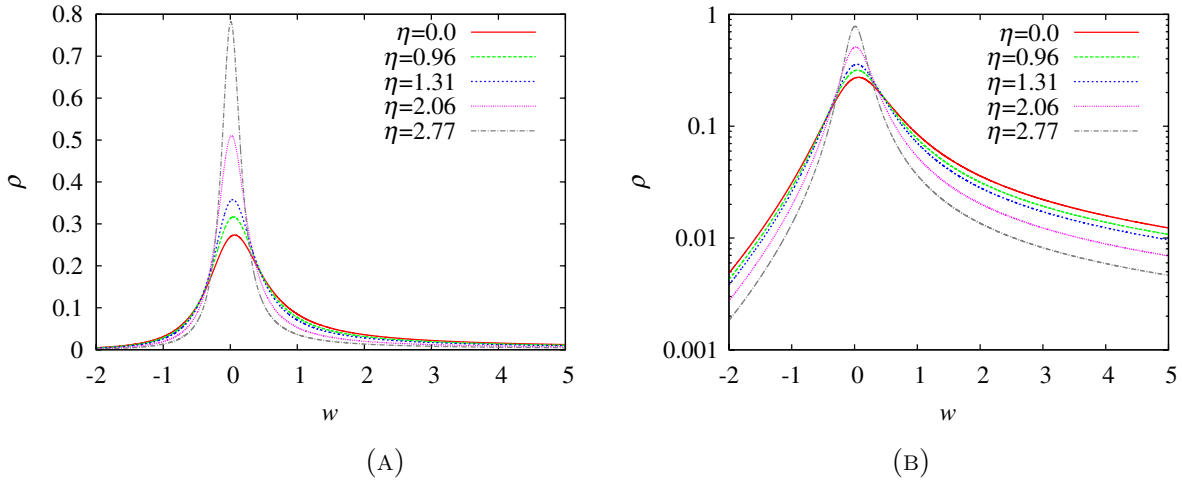

FIGURE 2.9: Velocity dependence of the spectral function for $\alpha = 0.5$. The η values are rapidities, $v = \tanh \eta$. (A) is a linear-linear plot to show that the peak region becomes more and more peaked with increasing η (v). The log-log in (B) plot demonstrates that the asymptotics remain the same.

We can numerically Fourier transform $Z(t)$, and perform a convolution in the Fourier space with the $\bar{\varrho}_{v=0}(w)$ function Eq. (2.182). This ensures that we use the same analytic continuation for the different velocity cases. As a result we obtain Fig. 2.9. We can observe that the peak becomes narrower for larger velocities, corresponding to a decreasing α_{eff} value. At large momentum the asymptotics is the same for all velocities (for a given α), because the zero temperature result is insensitive to the value of v.

Here, again we can work out the real time dependence. We now write

$$\varrho_u(p) = u_0 \beta f_u(\beta(p_0 u_0 - \mathbf{pu} - m)) \tag{2.162}$$

and find

$$\varrho_u(t) = e^{-i\mathbf{vp}t - imt/u_0} \tilde{f}_u\left(\frac{tT}{u_0}\right). \tag{2.163}$$

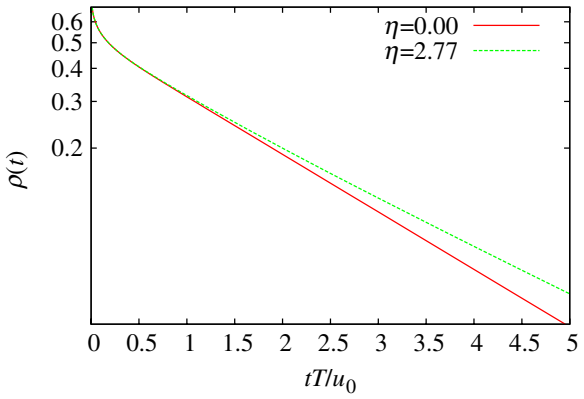

FIGURE 2.10: Comparison of the real time dependence of the retarded Green's function (or, equivalently, the spectral function) for zero and finite velocity at $\alpha = 0.5$ on logarithmic y scale. The η values are rapidities, $v = \tanh \eta$. The small time behaviour does not change, at large times the exponential damping is described by $\exp(-\alpha_{eff}(u)Tt)$.

The result of the numerical inverse Fourier transform can be seen in Fig. 2.10. At small times the spectral function (retarded Green's function) is velocity independent, this is the zero temperature asymptotics. For large times ($Tt \gg 1$) the time dependence turns into $\sim e^{-\alpha_{eff}(u)Tt}$.

2.3.7 Discussion of earlier results

We can compare our results to the earlier ones in the literature. The long time asymptotics of the finite temperature solution of the Bloch-Nordsieck model was already discussed in [45, 46]. They followed a different, functional approach. Still, the two methods lead to the same intermediate result. Neglecting renormalisation effects (which is treated later in [45, 46]), our Eq. (2.112) together with Eq. (2.115) yields, using the notation $w = up - m$

$$w\mathcal{G}_{ra}(w) = e^2 U^2 \int \frac{d^4k}{(2\pi)^4} \frac{1}{uk} (1 + n(k_0)) \bar{\varrho}(k)\, \bar{\mathcal{G}}_{ra}(w - uk), \tag{2.164}$$

where $\bar{\varrho}(k) = \frac{2\pi}{2k}(\delta(k_0 - k) - \delta(k_0 + k))$ is the photon spectral function. After Fourier transformation, we find exponentiation of the real time contributions

$$\mathcal{G}_{ra}(t) = \mathcal{G}_{ra}(t = 0)e^{F(t)}, \tag{2.165}$$

where

$$F(t) = -e^2U^2 \int \frac{d^4k}{(2\pi)^4} (1 + n(k_0))\bar{\varrho}(k) \frac{1 - e^{-iukt}}{(uk)^2} = -it\Phi_0 + it\Phi(t) + \ln \Delta(t), \tag{2.166}$$

where Φ_0, $\Phi(t)$ and $\ln \Delta(t)$ are real quantities, corresponding to the notation of [46]. Using $U^2 = 1$ this means

$$\begin{aligned}
\Phi(t) &= -e^2 \int \frac{d^4k}{(2\pi)^4} \frac{\bar{\varrho}(k)}{uk} \left[1 - \frac{\sin ukt}{ukt}\right] \\
\Phi_0 &= -e^2 \int \frac{d^4k}{(2\pi)^4} \frac{\bar{\varrho}(k)}{uk} \\
\Delta &= \exp\left\{-e^2 \int \frac{d^4k}{(2\pi)^4} n(k_0)\bar{\varrho}(k) \frac{1 - \cos ukt}{(uk)^2}\right\}.
\end{aligned} \tag{2.167}$$

These expressions agree with the equations (2.24) and (2.25) of [46] (the constant phase Φ_0 has no physical meaning).

The analysis of this formula, however, differs in our case and in [45, 46]. We restrict ourselves to the original Bloch-Nordsieck model, and used the free photon spectral function. In [45, 46] the authors used HTL-improved photon spectral function (cf. their Eq.(3.1) and (3.2)). As it turns out, the most important contribution comes from the small frequency limit of the continuum (Landau damping) part. This explains why the asymptotic time behaviour differs in our case and in the case of [45, 46] ($\exp(-\alpha_{eff}(v)Tt)$ vs. $\exp(-Ct \log t)$).

In [48] Fried *et al.* use again a different formalism. Since they examine a different physical situation, the comparison is much more difficult. What is clear, however, that they also use the original version of the model, and also find an exponentially damping solution.

It is very interesting that in [50] the authors found the same $\exp(-\alpha Tt \log t)$ like solution as was the case in [45, 46], although with a different line of thought. They use the dynamical renormalisation group idea [51], where the secular terms are melted into finite time dependence of the renormalised parameters. Clearly, they cannot consider all photonic diagrams, only those, which contribute to the renormalisation group (RG) equations. There, the logarithmic enhancement of the damping can be interpreted physically as an eternally growing cross section of the incoming hard particle which collects more and more soft photons around itself. The analysis of the pure Bloch-Nordsieck model results in a finite damping, which means that in this model the initial growth

of the cross section eventually stops, the soft photon cloud saturates. The physical interpretation of the saturation probably is that the multi-photon contributions arriving from different space-time points become incoherent. The two scenarios, one with ever growing photon cloud, the other with saturation, are both approximations of the real QED (RG, HTL and free photon approximations, respectively). The question of which one is finally manifested in QED, in particular in the ultrarelativistic limit, can be answered only after a full analysis of the complete QED where all these effects are present. In the next section we will compute the fermionic spectral function in the framework of the 2PI formalism at finite temperature. The goal is to benchmark the results of the 2PI procedure by we comparing them to the exact ones.

2.4 Applying the 2PI technique at finite temperature

In the previous section we derived the spectral function of the BN model at finite temperature exactly, and in the zero velocity case we could even obtain a closed analytic form, consistent with the analytic solution of the zero temperature study. A natural continuation of this analysis is to compare at finite temperature the results that we can achieve by the using 2PI technique with those of the exact one. In Section 2.2 we found that although the 2PI solution of the BN model is meaningful in the IR and does not blow up like the result that we can get in PT, it does not provide a satisfactory agreement with the exact one. In this section we will show that the 2PI technique does work well in the case when we consider the problem at non-zero temperature, provided that a rescaling of the coupling constant is done, which essentially can give us the running of the 2PI coupling with the temperature. Being precise: there exists a mapping between the coupling constants of the 2PI and those of the exact results in such a way that the two spectral functions overlap almost entirely. This is a highly non-trivial result, since the exact spectral function is an asymmetric function of the frequency, rather different from a simple Lorentzian. The most important message towards the 2PI community is that our result validates the 2PI approximation method at non-zero temperature and only a finite reparametrisation of the theory is needed.

From the perturbative point of view the 2PI technique resums the two particle irreducible diagrams, but the coupling constant and also the higher point functions remain unchanged. So, for a certain 2PI diagram there exists another infinite set of diagrams providing coupling constant modification. In the sense of the renormalisation group we may try to take into account the sum of these diagrams effectively as a temperature dependent (running) coupling constant. Since we now know the value of an observable exactly (the electron spectral function for any frequency and temperature in a given

gauge), the best method to extract the temperature dependent coupling is to compare the 2PI and the exact results, which will be done in the present section.

2.4.1 The 2PI equations at finite temperatures

We are working again in the real time formalism, hence the Green's functions in this picture are going to have a matrix structure like in the previous section. We choose the R/A basis for the matrix representation to calculate the retarded self-energy.

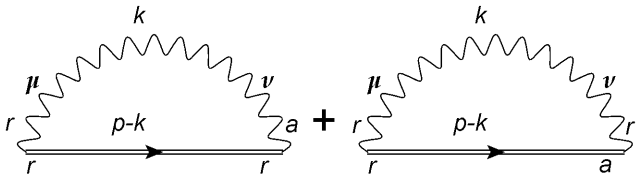

FIGURE 2.11: The diagrammatic representation of the self-energy. The wavy line corresponds to the free (here also the exact) photon propagator with a loop momentum k and the double solid line is for the exact fermion propagator with momentum $p-k$. Both the polarization and the R/A indices are shown.

First, we are going to consider the one-loop correction then, we present a derivation of the 2PI resummed spectral function at finite temperature. To evaluate its self-consistent equations we will use a numerical approach which is similar to those we discussed above for the $T = 0$ case. The integral equation for the retarded self-energy at non-zero temperature in Feynman gauge reads as:

$$\Sigma_{ar}(p) = ie^2 \int \frac{d^4k}{(2\pi)^4} \left[G_{rr}(k)\mathcal{G}_{ra}(p-k) + G_{ra}(k)\mathcal{G}_{rr}(p-k) \right]. \tag{2.168}$$

Where G and $\mathcal{G}$ stands for the propagator of the photon and the fermion, respectively. In Fig. 2.11 we can see the pictorial representation of the fermion self-energy using Feynman diagrams. Now, taking the discontinuity of the self-energy we obtain:

$$\underset{p_0}{\text{Disc}}\, \Sigma_{ar}(p) = e^2 \int \frac{d^4k}{(2\pi)^4} \left[G_{rr}(k)\rho_f(p-k) + \rho_\gamma(k)\mathcal{G}_{rr}(p-k) \right]. \tag{2.169}$$

Here, ρ_f and ρ_γ are the spectral functions of the fermion and the photon fields, respectively. In general, we can express the rr propagators with the spectral function and the distribution function of the corresponding spin statistics (the Bose-Einstein and Fermi-Dirac distributions, respectively):

$$\mathcal{G}_{rr}(p) = \left(\frac{1}{2} - n_f(p_0) \right) \rho_f(p), \tag{2.170}$$

$$G_{rr}(p) = \left(\frac{1}{2} + n_b(p_0) \right) \rho_\gamma(p). \tag{2.171}$$

When inserting these expressions into Eq. (2.169), we get

$$\begin{aligned}\underset{p_0}{\mathrm{Disc}}\,\Sigma_{ar}(p) &= e^2\int\frac{d^4k}{(2\pi)^4}\left[\left(\frac{1}{2}+n_b(k_0)\right)\rho_\gamma(k)\rho_f(p-k)\right.\\ &\quad\left.+\,\rho_\gamma(k)\left(\frac{1}{2}-n_f(p_0-k_0)\right)\rho_f(p-k)\right]\\ &= e^2\int\frac{d^4k}{(2\pi)^4}\,\left(1+n_b(k_0)-n_f(p_0-k_0)\right)\rho_\gamma(k)\rho_f(p-k). \quad (2.172)\end{aligned}$$

In the last step of Eq. (2.172) we get the most general form of the discontinuity in terms of the spectral functions.

2.4.2 One-loop correction at $T \neq 0$

For the detailed computation of the one-loop correction, see Appendix F, here we are only going to present the results.
In the case of the one-loop calculation we have to insert the spectral function of the free theory, for both the fermion and gauge fields, into Eq. (2.172). By performing this substitution, our equation reads as

$$\begin{aligned}\underset{p_0}{\mathrm{Disc}}\,\Sigma_{ar}(p) &= e^2\int\frac{d^4k}{(2\pi)^4}\,\left(1+n_b(k_0)-n_f(p_0-k_0)\right)\\ &\quad\times 2\pi\,\mathrm{sgn}\,k_0\delta(k_0^2-\mathbf{k}^2)2\pi\delta\left(u_0(p_0-k_0)-\mathbf{u}(\mathbf{p}-\mathbf{k})-m\right)\\ &= \frac{e^2}{8\pi^3}\int_0^\infty d\mathbf{k}^2\int_{-1}^{1}dx\frac{(2\pi)^2}{2|\mathbf{k}|}\left[(1+n_b(|\mathbf{k}|)-n_f(p_0-|\mathbf{k}|)\right)\\ &\quad\times\,\delta\left(u_0p_0-\mathbf{up}-u_0|\mathbf{k}|-|\mathbf{u}||\mathbf{k}|x-m\right)+\\ &\quad+\left(n_b(|\mathbf{k}|)+n_f(p_0+|\mathbf{k}|)\right)\delta\left(u_0p_0-\mathbf{up}+u_0|\mathbf{k}|-|\mathbf{u}||\mathbf{k}|x-m\right)\Big].\end{aligned} \quad (2.173)$$

Here, we introduced the variable x which stands for the cosine of the angle between the two spatial three-vectors $\mathbf{u}$ and $\mathbf{k}$. For the sake of simplicity in the following we are going to use the notations $pu \equiv p_0u_0 - \mathbf{pu}$ for the scalar product in Minkowski space and $k \equiv |\mathbf{k}|, u \equiv |\mathbf{u}|$.

First, we perform the angular integration for x:

$$\underset{p_0}{\mathrm{Disc}}\,\Sigma_{ar}(p) = \frac{e^2}{4\pi u}\left(\Theta(pu-m)\int\limits_{\frac{pu-m}{u+u_0}}^{\frac{pu-m}{u-u_0}} dk\,(1+n_b(k)-n_f(p_0-k)) + \Theta(m-pu)\int\limits_{\frac{m-pu}{u+u_0}}^{\frac{m-pu}{u-u_0}} dk\,(n_b(k)+n_f(p_0+k))\right). \tag{2.174}$$

Now, we are going to use the fact that the fermion in this system is a hard probe, thus it is not part of the heat-bath [45, 46]. This manifests already in Eq. (2.172) where we need to set the Fermi-Dirac distribution to zero; otherwise we would face inconsistencies, when we would try to take the $T \to 0$ limit (see Appendix F). Thus, likewise in the exact calculation in Section 2.3

$$n_f \equiv 0 \text{ (in the framework of the BN model).} \tag{2.175}$$

In that case Eq. (F.10) simplifies in the following way:

$$\underset{p_0}{\mathrm{Disc}}\,\Sigma_{ar}(p) = \frac{e^2}{4\pi u}\int\limits_{\frac{pu-m}{u+u_0}}^{\frac{pu-m}{u-u_0}} dk\,(1+n_b(k))\,. \tag{2.176}$$

By evaluating the integral, one gets a result consistent with the $T=0$ case:

$$\underset{p_0}{\mathrm{Disc}}\,\Sigma_{ar}(p) = \frac{e^2}{2\pi}\Theta(pu-m)(pu-m) + \frac{Te^2}{4\pi u}\ln\left(\frac{1-e^{-\beta\frac{pu-m}{u-u_0}}}{1-e^{-\beta\frac{pu-m}{u+u_0}}}\right). \tag{2.177}$$

This gives the desired result for the $T \to 0$ limit, namely

$$\underset{p_0}{\mathrm{Disc}}\,\Sigma_{ar}(p) = \frac{e^2}{2\pi}\Theta(pu-m)(pu-m). \tag{2.178}$$

2.4.3 Non-zero temperature calculations in the 2PI framework

Now, we are going to derive the 2PI resummed result for the finite temperature theory. Let us consider Eq. (2.107) and Eq. (2.168). Instead of calculating the one-loop correction by inserting free propagators, we are going to use the self-consistent fermion propagator, defining in this way a self-consistent system of integral equations. We stick to the physical picture that the fermion is not part of the thermal medium cf. Eq. (2.175). Using the calculation in Eq. (2.172) we arrive to an expression for the discontinuity of

the self-energy for a general fermion propagator:

$$\begin{aligned}\underset{p_0}{\mathrm{Disc}}\,\Sigma_{ar}(p) &= e^2\int\frac{d^4k}{(2\pi)^4}\,(1+n_b(k_0))\,\rho_\gamma(k)\rho_f(p-k)\\ &= e^2\int\frac{d^4k}{(2\pi)^4}\,(1+n_b(k_0))\,\frac{2\pi}{2k}(\delta(k_0-k)-\delta(k_0+k))\bar{\rho}_f(up-uk-m).\end{aligned} \tag{2.179}$$

Here, we used the free photon propagator as above and for the general spectral function of the fermion we introduced the notation $\rho_f(p)=\bar{\rho}_f(up-m)$. After some algebra, we find

$$\underset{p_0}{\mathrm{Disc}}\,\Sigma_{ar}(p)=\frac{e^2}{8\pi^2}\int_{-\infty}^{\infty}dk\int_{-1}^{1}dxkn_b(k)\bar{\rho}_f(w+(u_0+ux)k). \tag{2.180}$$

Here, we defined $w:=up-m$, and x represents the angle between the spatial parts of k^μ and u^μ, so xku is the scalar product of two three-dimensional vectors like in the one-loop calculation. Actually, this can be written in a more elegant, and for the numerical implementation, a more useful way. Hence, we introduce the variable z as the argument of the function $\bar{\rho}_f$:

$$\underset{p_0}{\mathrm{Disc}}\,\Sigma_{ar}(p) = \frac{e^2}{8\pi^2}\frac{1}{u}\int_{-\infty}^{\infty}dk\int_{w+(u_0-u)k}^{w+(u_0+u)k}dz\bar{\rho}_f(z)n_b(k)=\frac{e^2}{8\pi^2}\frac{1}{u}\int_{-\infty}^{\infty}dz\bar{\rho}_f(z)\int_{\frac{z-w}{u_0-u}}^{\frac{z-w}{u_0+u}}dkn_b(k). \tag{2.181}$$

In the case in which the length of the 3-velocity tends to zero, that is $u\to 0$, we have

$$\underset{p_0}{\mathrm{Disc}}\,\Sigma_{ar}(p_0)=\frac{\alpha}{\pi}\int_{-\infty}^{\infty}dz\bar{\rho}_f(z)(p_0-m-z)(1+n_b(p_0-m-z)). \tag{2.182}$$

For $u\neq 0$ we obtain

$$\underset{p0}{\mathrm{Disc}}\,\Sigma_{ar}(w)=\frac{\alpha}{2\pi}\int_{-\infty}^{\infty}dz\bar{\rho}_f(z)\frac{T}{u}\ln\frac{1-e^{-\beta\frac{z-w}{u_0-u}}}{1-e^{-\beta\frac{z-w}{u_0+u}}}. \tag{2.183}$$

We set $m=0$, this can be done without the loss of generality since the two expressions in Eq. (2.182) and Eq. (2.183) depends on the variable $w=up-m$ only. That means the theory is not sensitive where the mass-shell is being placed; it can be anywhere on the real line.

2.4.4 2PI results

We are implementing the same numerical method that we used for the zero-temperature case (**step 1 - step 5** in Section 2.2.2.2), using the finite temperature form of Eq. (2.65), which is given in Eqs. (2.182) and (2.183). In the numerical procedure, we fix the value of the coupling and the numerical value of the temperature and perform the iteration until it converges. The physical temperature is a dimensionful quantity; therefore, dimensionless quantities must depend on the temperature only through the other dimensionful parameter. If there were not for the renormalisation, then the only quantity, which can make the temperature dimensionless, would be w, and the results would depend on βw. However, the renormalisation leads to the appearance of a quantum scale through dimensional transmutation (for the BN model; see Section 2.2.3). This can be characterised, for example, by the value of the Landau pole Λ_{BN}; then, the results will implicitly depend on $\beta\Lambda_{BN}$. In the numerics, this shows up as a dependence of the physical results not only on βw, but also separately on the numerical value of the temperature. We will refer to this numerical value as "dimensionless temperature", knowing that only ratios of these dimensionless temperature values have physical meaning.
The result of the iteration is the finite temperature spectral function. First, we observe that a small thermal mass Δm_T is generated, in dimensionless units in the order of $\Delta m_T \sim T \sim 10^{-3}$. Interestingly, this thermal mass is negative; it shifts the spectral function to the left. In the exact solution in Section 2.3, we found a zero thermal mass, and thus we can consider it as an artefact of the 2PI approximation, which can be incorporated into the mass and finally into $w = up - m - \Delta m$.

2.4.5 The zero velocity case

By applying the algorithm described in Section 2.2.2.2 we can obtain the spectral function derived from the 2PI approximation for the theory, using Eq. (2.182) as the self-energy input. In Fig. 2.12 we can see the spectral function for different coupling values and for different temperatures. The spectrum has a peak, its width is growing with increasing coupling constant and with increasing temperature, likewise in the exact case. In the Dyson-Schwinger approach the exact spectral function can be derived in a closed form (at least in the the zero velocity case). We wish to compare the 2PI results to our analytical expression in Eq. (2.139) obtained in Section 2.3. To benchmark the 2PI approximation, we can compare the resulting spectral function with the exact one. The comparison can be seen in Fig. 2.13. We can see immediately that the two spectra are not very similar. The reason is that the 2PI approximation do not sum up all the diagrams, in particular the coupling constant corrections.

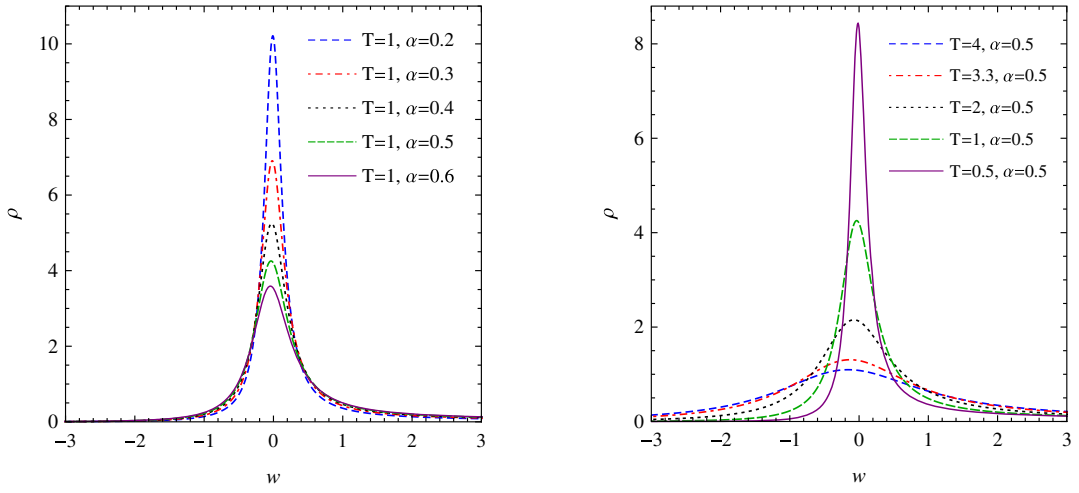

(A) (B)

FIGURE 2.12: The coupling constant dependence of the spectral function in the 2PI approximation (A) at temperature $T = 1$, and (B) at fixed fixed coupling value, $\alpha = 0.5$. The curves widen with growing coupling and growing temperature.

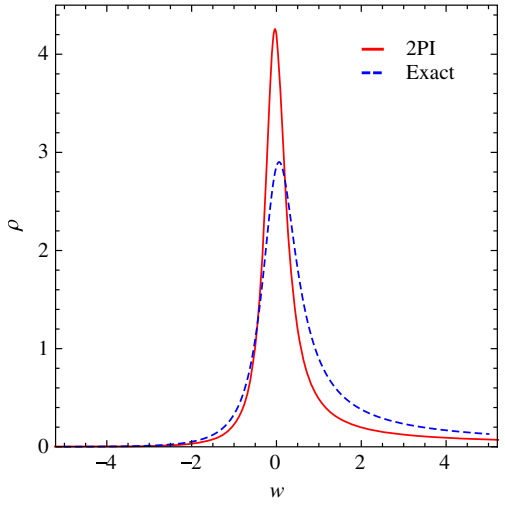

FIGURE 2.13: Comparing the 2PI resummed spectral function to the exact one. The solid red line is obtained from the 2PI resummation, while the dashed blue line is the exact spectral function. Both of them are at T=1 and the couplings are $\alpha_{ex} = \alpha_{2PI} = 0.5$.

Therefore, to improve the 2PI calculation we can try to take into account the resummation of these diagrams effectively in a renormalisation group inspired way, as a temperature dependent coupling constant. We should use a non-perturbative matching procedure, and choose that value of α_{2PI} which reproduces the exact result the most accurately. For a perfect matching not only the coupling constant, but also the higher point functions should also be resummed. But we may hope that the most important effect comes from the relevant couplings, in this case from α_{2PI}.

Therefore, our strategy will be to find the best, temperature dependent value of the coupling constant α_{2PI} that yields the best match between the exact and the 2PI spectral functions. As we can see in Fig. 2.14, there exist such a value, where the matching is almost perfect. We can observe that the fit is excellent not just at the close vicinity of the peak region, but also for much larger momentum regime, and it can give an account also for the asymmetric form of the exact spectral function. For asymptotically large momenta, we expect that the two curves do not agree, according to Section 2.2.2.2, this can also be observed in Fig. 2.14. This result is a strong argument in favor of the usability of 2PI technique at finite temperature also for gauge theories.

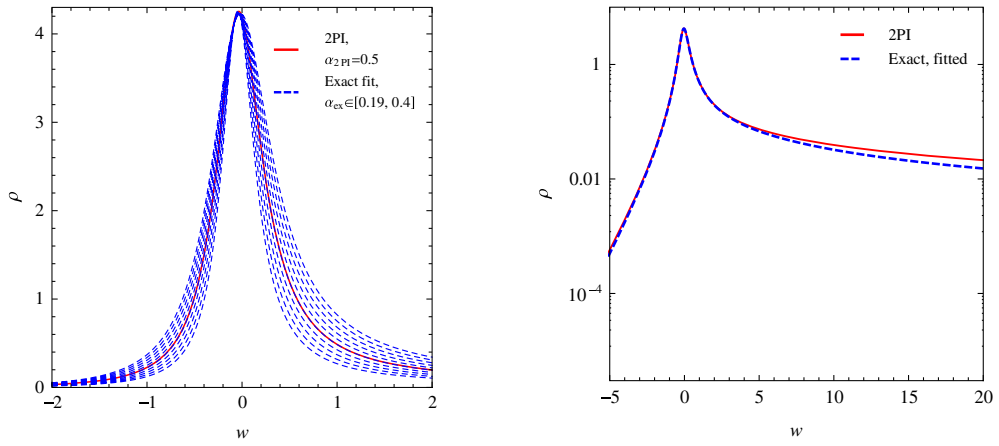

(A) (B)

FIGURE 2.14: The fitting of the exact spectral function on the 2PI spectrum in linear (A) and logarithmic (B) plot. We can see an exact match at the peak and a small deviation in the asymptotics. The fit yields $\alpha_{2PI} = 0.5$ for $\alpha_{ex} = 0.293$ at $T = 1$.

Hence, we can say that the coupling which takes the value of $\alpha_{2PI} = 0.5$ in the 2PI resummation at $T = 1$ is equivalent to an $\alpha_{ex} = 0.293$ in the D-S calculation at the same temperature. One can also conclude that the vertex corrections (which are absent in the 2PI self-energy calculations) have a role to modify the value of the renormalised coupling. In the following, we are going to look for a general relation between α_{2PI} and α_{ex}.

We can repeat the strategy above for different temperatures. In this way we can determine a relation $\alpha_{2PI}(\alpha_{ex}, T)$ (technically it is simpler to obtain $\alpha_{ex}(\alpha_{2PI}, T)$ and invert this relation). This provides the finite temperature dependence, or finite temperature "running" of the 2PI coupling constant.

We expect that for small couplings the exact and the perturbative values agree, since the perturbation theory gives $\alpha_{ex} = \alpha_{2PI} + \mathcal{O}(\alpha_{2PI}^2)$. This is indeed the case. For larger couplings, however, the linear relation changes. Interestingly, we can observe that, depending on the temperature, two different type of functions describe the relation between the couplings. The first type of function which gives the mapping between

the two couplings is valid in the interval $T \in [0, 12.03]$. This relation can be obtained by a one-parameter fit between the 2PI and the exact couplings, namely:

$$\alpha_{2PI} = A_T(e^{\frac{\alpha_{ex}}{A_T}} - 1). \tag{2.184}$$

The result is shown in Fig. 2.15a., the fit parameters (A_T) are listed in Tables 2.1 and 2.2. From this relation we immediately see that for small α_{2PI} the relation of the couplings is linear

$$\alpha_{2PI} \approx \alpha_{ex} + \mathcal{O}\left(\frac{\alpha_{ex}^2}{A_T}\right). \tag{2.185}$$

This tells us that the 2PI and the exact couplings are the same for the perturbative region, meaning that we can rely on the results obtained by 2PI calculations in this regime.

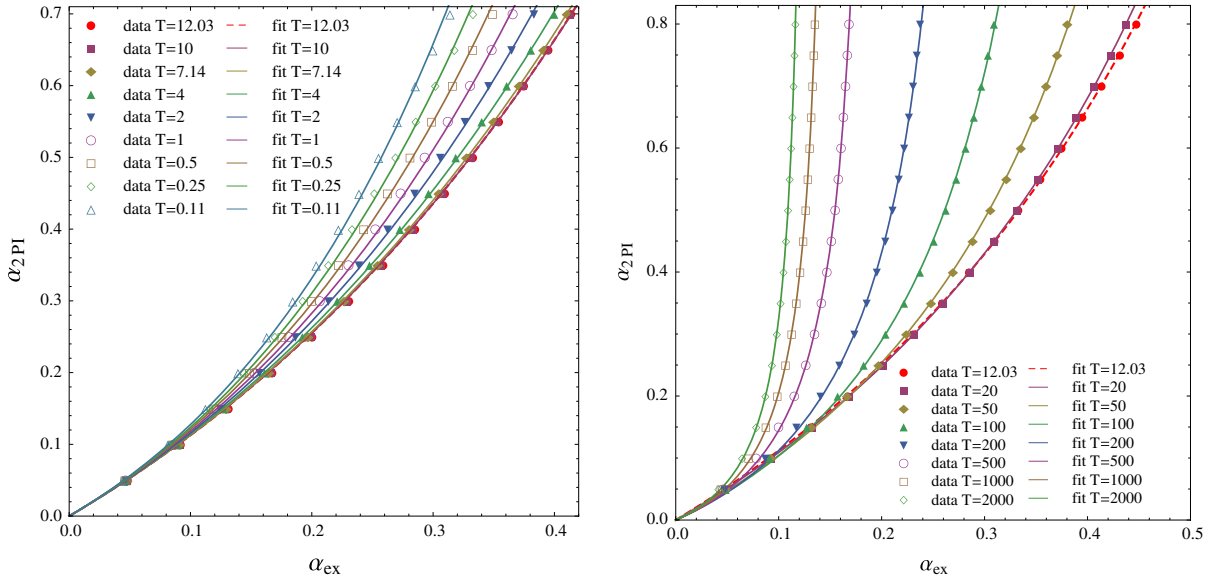

(A) (B)

FIGURE 2.15: The relation between the 2PI and the exact coupling for $u = 0$ at temperatures (A) $T \in [0, 12.03]$ and (B) $T \in [12.03, \infty)$, respectively. The dashed red line indicates the limiting function at $T = 12.03$, for details see the text.

T	0.11	0.25	0.5	1	2	4	7.14	10	12.03
A_T	0.213	0.242	0.27	0.305	0.343	0.384	0.414	0.426	0.429

TABLE 2.1: The fit parameters in the low temperature case. The error of the parameters is ± 0.001.

T	20	50	100	200	500	1000	2000
B_T	1.03 ± 0.003	1.118 ± 0.008	1.217 ± 0.014	1.312 ± 0.017	1.381 ± 0.016	1.38 ± 0.012	1.3 ± 0.006
C_T	1.107 ± 0.001	1.668 ± 0.025	2.654 ± 0.054	4.241 ± 0.083	6.937 ± 0.105	8.951 ± 0.1	9.991 ± 0.055

TABLE 2.2: The fit parameters in the high temperature case.

Thus, if we are using couplings, which are in the order of the fine structure constant of QED ($\alpha = 1/137$) for instance, one does not even have to worry about the temperature dependence of Eq. (2.184). From Eq. (2.184) it is obvious that the relation depends on the temperature through the fit parameter A_T: this is shown in Fig. 2.16a. We can fit the temperature dependence in the following form:

$$A_T = a(\tanh Tb)^c, \tag{2.186}$$

where $a = 0.438 \pm 0.002$, $b = 0.123 \pm 0.01$, and $c = 0.17 \pm 0.002$.

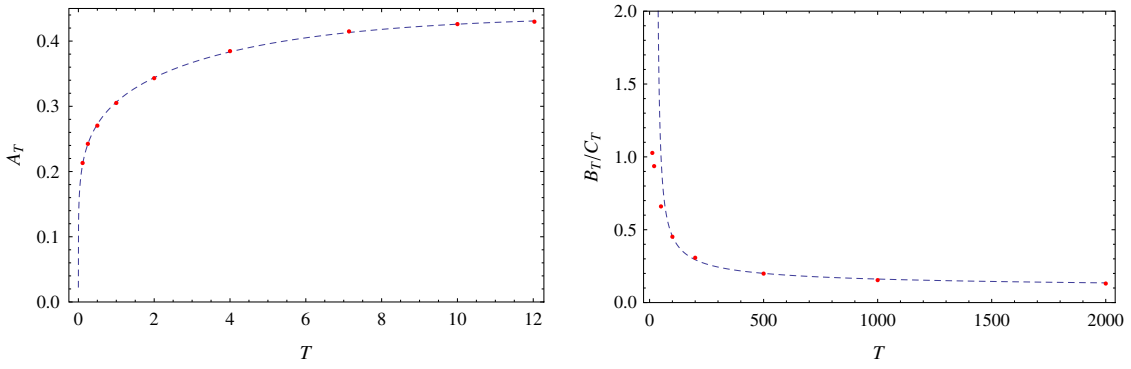

(A) (B)

FIGURE 2.16: The running of (A) A_T and (B) B_T/C_T with respect to the temperature. This latter quantity is the position of the pole (cf. Eq. (2.188)). One can see that the best matching occurs at higher temperatures.

Let us consider the zero temperature limit: $\lim_{T\to 0} A_T = 0$. This tells us that in the zero temperature limit all α_{ex} corresponding to any α_{2PI} by Eq. (2.184) vanish. To see this it is easier to invert the relation and then take the limit, i.e. $\lim_{T\to 0} A_T \ln(\alpha_{2PI}/A_T + 1) = 0$. This is consistent with the fact that at $T = 0$ the coupling drops out from the 2PI propagator [40]. More precisely at $T = 0$ close to the peak:

$$\mathcal{G}_{2PI}(w) \propto \frac{1}{w} \quad \text{, while} \quad \mathcal{G}_{ex}(w) \propto \frac{1}{w^{1+\frac{\alpha_{ex}}{\pi}}}\bigg|_{\alpha_{ex}=0} = \mathcal{G}_{2PI}. \tag{2.187}$$

Therefore the diverging α_{2PI}/α_{ex} relation does not signal a physical singularity, it just means that in order to match the exact theory we have to take into account other diagrams not included in the 2PI resummation.

The relation in Eq. (2.186) is valid up to the dimensionless temperature $T = 12.03$. Above this temperature the trend of the curves can be seen in Fig. 2.15a, namely that they are more and more shallow for increasing temperature. The $\alpha_{2PI}(\alpha_{ex})$ curve becomes steeper and steeper as it can be seen in Fig. 2.15b. We find for small couplings the expected universal linear relation $\alpha_{2PI} = \alpha_{ex} + \dots$. We can also observe that the

$\alpha_{2PI}(\alpha_{ex})$ curves diverge at some limiting value of α_{ex}. This can also be seen from the following fit which describes the numerically determined curve quite well:

$$\alpha_{2PI} = \frac{\alpha_{ex}}{B_T - C_T \alpha_{ex}}. \tag{2.188}$$

The fit parameters can be seen in Table 2.2. This function has a pole at B_T/C_T at each temperature. This is a temperature dependent quantity, the running of the position of the pole can be seen in Fig. 2.16b. Equation (2.188) can be interpreted from the point of view of the scale dependence of the coupling constant. For the BN model the one-loop running is exact which can bee seen from Eq. (2.88), and provides a Landau pole. The value of the coupling for which we find the pole is $\alpha(\mu_0) = \frac{\pi}{\ln \mu/\mu_0}$. If we associate $\mu \sim T$ for high temperatures, this would suggest that the finite temperature dependence also exhibits a Landau-type pole at $\alpha_{ex} \sim (\ln fT)^{-1}$. In fact, a two-parameter fit is

$$\frac{B_T}{C_T} = \frac{d}{\ln(fT)}, \tag{2.189}$$

where $d = 0.576 \pm 0.03$ and $f = 0.035 \pm 0.003$ describes the finite temperature behaviour for large temperatures.

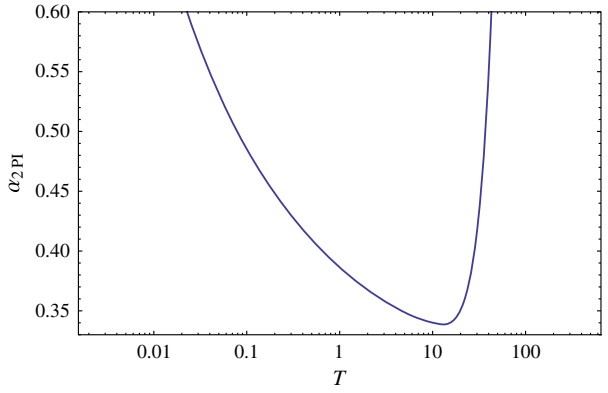

FIGURE 2.17: Finite temperature running of α_{2PI} for fixed α_{ex}. One can observe the high temperature (Landau) pole and the $T \to 0$ divergence.

The finite temperature running of α_{2PI} for fixed α_{ex} can be seen in Fig. 2.17. According to our earlier analysis, we can identify the following characteristic features of this running. For small temperatures, the running of the perturbative coupling is determined by the soft IR physics, the photon cloud. At very small temperatures, seemingly, we find a divergence, but this is not a physical singularity; it just reflects the fact that at zero temperature the 2PI approximation fails to describe the exact spectrum for any couplings, cf. Eq. (2.187). At high temperatures, the perturbative running is the dominant effect with the correspondence $\mu \sim T$. Again, we find there a pole that comes from the Landau pole of the perturbative running. But, again, this singularity is not

a physical one, the exact spectrum is regular for α_{ex} larger than the pole value. But with 2PI calculation with the original action, we cannot reproduce this result, one would need to take into account higher point vertices, too. Between the low temperature and high temperature regimes there is a point where $d\alpha_{2PI}(T)/dT = 0$, in our case this is at the dimensionless temperature value $T = 12.03$. This is a "fixed point" of the running and loosely determines a "critical temperature" separating the two physically different temperature regimes.

2.4.6 The finite velocity case

We can repeat the same analysis for the finite velocity case, too. Since the findings are very similar to the $u = 0$ case, we just shortly overview the results. For the finite velocity case we obtained the exact fermionic spectral function using numerics (see Section 2.3.6.3). In the 2PI approximation we are going to use the same numerical calculation that we used for the $u = 0$ case, and the only difference is that this time we use the formula in Eq. (2.183) for the discontinuity of the self-energy. The spectral functions obtained from 2PI for different $u > 0$, but fixed temperature and coupling constant, can be seen in Fig. 2.18. To fit the spectral functions in the $u > 0$ case, we are applying exactly the same procedure that we used for the $u = 0$ case. For this purpose we choose the value $u = \sqrt{3}$ (or $v = \sqrt{3}/2$).

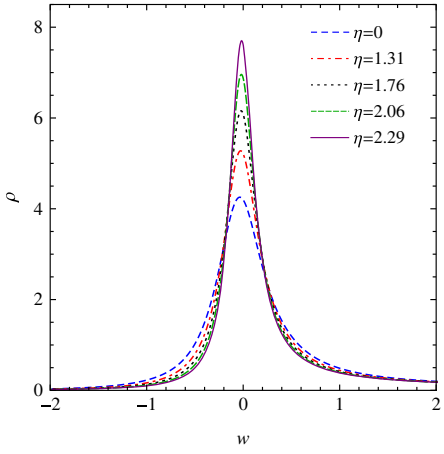

FIGURE 2.18: The 2PI spectral functions with different rapidities ($\eta = \tanh^{-1}(v)$, where $v = u/u_0$) at fixed temperature $T = 1$ and coupling $\alpha = 0.5$. The shrinking of the width can be observed as the velocity grows, which is the same effect that we had for the exact solution in Section 2.3.

In Fig. 2.19 we can find the relation between the 2PI and the exact couplings and in Table 2.3, 2.4 the corresponding fit parameters, but this time for $u = \sqrt{3}$. For the given finite u, we have almost the same picture that we had for the $u = 0$ case, and just the fit parameters, A_T, B_T and C_T, are different. Interestingly, the threshold

temperature stayed at $T = 12.03$, but the running of the parameter as a function of the temperature is slightly modified. Now, we have for $A_T = a\tanh(bA_T)^c$, where this time $a = 0.55 \pm 0.01$, $b = 0.075 \pm 0.01$ and $c = 0.183 \pm 0.004$. For the running of the pole, we have $(B_T/C_T = d/\ln(fT))$ $d = 0.623 \pm 0.04$ and $f = 0.032 \pm 0.003$.

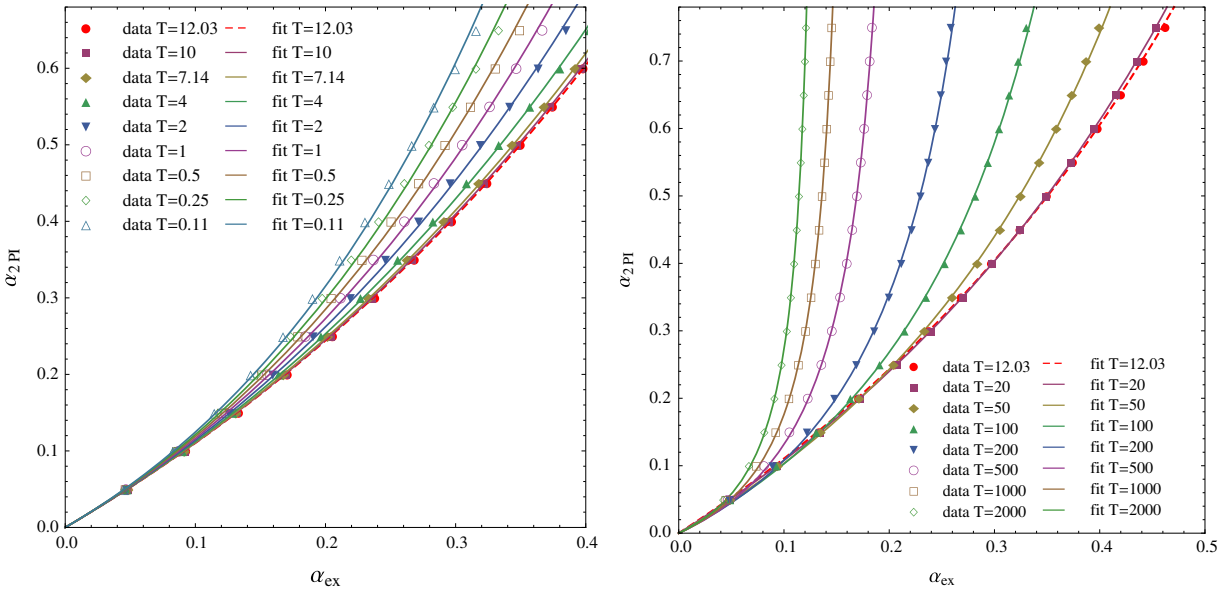

(A) (B)

FIGURE 2.19: The relation between the 2PI and the exact coupling for $u = \sqrt{3}$ at temperatures (A) $T \in [0, 12.03]$ and (B) $T \in [12.03, \infty)$, respectively. The dashed red line indicates the limiting function at $T = 12.03$, for details see the text.

T	0.11	0.25	0.5	1	2	4	7.14	10	12.03
A_T	0.235	0.266	0.298	0.338	0.386	0.442	0.488	0.507	0.517

TABLE 2.3: The fit parameters in the low temperature case for $u = \sqrt{3}$. The error of the parameters is ± 0.001.

T	20	50	100	200	500	1000	2000
B_T	1.016 ± 0.001	1.108 ± 0.007	1.2 ± 0.014	1.29 ± 0.017	1.371 ± 0.0175	1.389 ± 0.0145	1.35 ± 0.009
C_T	0.908 ± 0.002	1.422 ± 0.023	$= 2.275 \pm 0.048$	3.629 ± 0.075	6.113 ± 0.102	8.216 ± 0.105	9.8318 ± 0.079

TABLE 2.4: The fit parameters in the high temperature case for $u = \sqrt{3}$.

2.5 Chapter summary

In this chapter we analysed the IR limit of the QED which is expected to be described accurately by the Bloch-Nordsieck model. The infrared catastrophe can be associated with the presence of infinitely many soft photon excitations around the electron, and as a consequence the perturbation series does not give a reliable result around the mass-shell of the electron. This phenomenon characterises all the massless gauge theories.

However, in the framework of the Bloch-Nordsieck model we are able to derive the full fermionic propagator [31, 32], hence this gives a nice opportunity to benchmark different level of approximations like the one-loop level perturbation theory, the 2PI resummation and the Dyson-Schwinger equations, as we did it in Section 2.2. The one-loop result exhibits an IR sensitivity when we approach the mass-shell, which renders the theory ill-defined. The self-energy (2PI) resummation reorganises the perturbative series in a way that this IR problem disappears. Although the IR sensitivity cannot be seen anymore, but still the 2PI method fails to reproduce the correct result. On the other hand, the Dyson-Schwinger equations, truncated in a way that the Ward identities are satisfied, yield the exact result in the Bloch-Nordsieck model. And, while the original method to obtain the solution is very hard to generalise to other theories, there is a hope to generalise the ideas of the specially truncated Dyson-Schwinger equations method.
In Section 2.3 we studied the Bloch-Nordsieck model at finite temperature; in particular we studied the fermionic spectral function. We used the strategy introduced in Section 2.2 which is based on the Dyson-Schwinger equations, where the infinite hierarchy is closed by using the Ward identity for the vertex function. We worked out the corresponding equations at finite temperature in the real time formalism and solved them. This procedure is exact in the Bloch-Nordsieck model. At zero velocity we were able to obtain fully analytic results for the spectral function. For large momenta and/or zero temperature this formula agrees with the zero temperature result. At finite temperature there appears an asymmetric peak which decreases exponentially below and as a power law above the mass shell.
We gave a numerical implementation of the 2PI resummation for the fermionic spectral function in the BN model at non-zero temperature. In Section 2.3, we showed a derivation of the exact spectral function in an analytic way and obtained a closed form. Hence, this analytic formula provides us with a good basis for the justification of the 2PI approximation. A 2PI approximation missing vertex resummation cannot provide us a full solution, but we can still compare it to the exact result. One of our main results is that the 2PI approximation works excellently at finite temperatures, and the spectrum coming from the 2PI approximation could be fitted to the exact spectrum at high accuracy. The two curves agree well, not just in the vicinity of the peak, but also for a much larger momentum interval. This demonstrates that the 2PI resummation is in fact a physically appropriate approximation for gauge theories, too. Nevertheless, the 2PI and the exact results match each other after properly choosing the 2PI coupling $\alpha_{2PI}(\alpha_{ex}, T)$ as a function of the coupling of the exact formula α_{ex} and the temperature. For a fixed α_{ex}, this describes a temperature-dependent running coupling constant. Another main result is to provide this function for the BN model. The success of the 2PI method extended by a non-perturbative running of the coupling constant encourages one to try this strategy also in the cases of other (gauge) theories. The basis of the temperature

running could be the matching to a non-perturbatively (e.g., in Monte Carlo simulations) determined physical quantity. Then, using temperature-dependent 2PI couplings, one could perform other calculations and give predictions for other, numerically hardly accessible physical quantities.

Chapter 3

The Functional Renormalisation Group Study of the O(N) model

In this chapter we will discuss our second non-perturbative approach to QFT, namely, the Functional Renormalisation Group (FRG) technique. Sometimes it is called the Exact Renormalisation Group, however, despite being non-perturbative we will make several approximations till we get to the real RG equations. This method is based on the Wilsonian idea, that is one starts with an initial theory on a given scale (Lagrangian or Hamiltonian at scale Λ), and step-by-step one integrates out the rapid degrees of freedom, obtaining an effective theory describing the IR physics. Using this strategy provides us a powerful tool to examine second order phase transitions and critical phenomena.

The structure of this chapter is as follows: first we introduce the concept of the Wilson-Kadanoff renormalisation group on statistical systems, discuss why it is useful and how it can describe critical phenomena [14, 62]. Then we move on and study the Functional Renormalisation Group procedure from the point of view of QFT and apply it to the O(N) symmetric N-vector model. We will see from the analysis how the famous Mermin-Wagner theorem emerges, and show that using drastic approximations (like truncating the Taylor-expansion of the effective potential) leads us to a wrong answer to questions related to the phase structure. To cure the inconsistency in the approximated theory we will examine carefully the behaviour of its results and give a statistical argument, which will provide the real description of the phase structure of the O(N) models in arbitrary dimensions and field components. This analysis uses the Vanishing Beta Function curves (VBF) [44], which we will introduce later on, but we can say in advance that they give back all the expectations regarding the O(N) models: they define the right lower and upper critical dimensions and find all the physically relevant fixed points. Interestingly, when $N \to \infty$ in $4 < D < 6$ dimensions, we will find a new fixed point candidate on

the phase space of the model, which was suggested first in recent works of Klebanov *et* al. [52], but also by Percacci in [53] who questioned the validity of this fixed point. With the technique presented here, we will find that the corresponding critical potential associated to this fixed point is metastable. Section 3.4, where we provide a proof of the Mermin-Wagner theorem using analytical considerations, is based on [43] and Section 3.5, where we analyse the phase structure of the O(N) model is based on [44]. Sections 3.1-3.1.4 are based on [63, 76].

3.1 Coarse-graining and the Wilsonian approach

The main idea behind the Wilsonian approach is that we do not care too much about the interactions at small scales (the rapid degrees of freedom), we are only interested in how the system, as a whole, behaves at long distances (IR scales). However, when using this approach, we need to bare in mind that we still need to rely on approximations, that is in general we cannot integrate out all the fluctuations exactly. This is the case in the PT, too, where we calculate loop integrals corresponding to the quantum fluctuations of the theory and sum it up to obtain the full amplitude for the process of interest. Wilson's idea translated to the PT language tells us essentially that we need to reshuffle the perturbation series and organise the summation in a way that will provide reliable answers to the questions regarding the infrared physics. Before going into details, we discuss what we mean by short and long distance physics, and which are the quantities characterising the system at a given scale.

In a strongly correlated system there are basically two relevant scale parameters: (i) the microscopic scale $a \sim \Lambda^{-1}$, which usually corresponds to the lattice spacing, intermolecular distance, the Planck scale, etc., in one word: it provides the natural cut-off scale of the system under consideration. And (ii) the correlation length ξ which also can be thought as the inverse mass. The scales (i) and (ii) are very different, especially at criticality (for example in a ferromagnet without external field at the critical temperature $T = T_c$), and fluctuations in this case exist on all wavelengths between a and ξ. In particle physics the correlation length typically corresponds to the Compton wavelength of the particle and the energy scale of the underlying "fundamental theory" is at the scale of the Grand Unified Theory ($\sim 10^{16}$ GeV) or $\sim 10^{19}$ GeV for quantum gravity. However, to obtain a mathematically consistent QFT one would need to take the continuum limit ($\Lambda \to \infty$), nevertheless, to study the phase structure of such systems we do not need to do so.

In the following we are going present the general procedure through the example of a scalar field $\varphi(p)$ in momentum space. Let us say that we have defined a Hamiltonian at energy scale Λ. Then, the corresponding partition function (which is nothing else but

the generating functional) reads as:

$$Z = \int \mathcal{D}\varphi e^{-H[\varphi,\mathbf{C},\Lambda]}. \tag{3.1}$$

Here, the field $\varphi = \varphi(p)$ considered as the degrees of freedom, $\mathbf{C} = (\lambda_1, \lambda_2, ...)$ represents all the relevant coupling constants introduced at the given scale Λ. By integrating out the rapid degrees of freedom we mean that we perform the functional integration in the partition function, but only for the "high energy modes" $p \in [\Lambda - d\Lambda, \Lambda]$. Schematically to implement this elimination we will divide $\varphi(p)$ into two parts

$$\varphi(p) = \varphi_<(p) + \varphi_>(p), \tag{3.2}$$

where the terms defined as

$$\begin{aligned} \varphi_<(p) &= \{\varphi(p) | p < \Lambda - d\Lambda\}, \\ \varphi_>(p) &= \{\varphi(p) | \Lambda - d\Lambda \leq p \leq \Lambda\}. \end{aligned} \tag{3.3}$$

Hence, we obtain the following integral for the partition functional:

$$Z = \int \mathcal{D}\varphi e^{-H[\varphi,\mathbf{C},\Lambda]} = \int \mathcal{D}_<\varphi\mathcal{D}_>\varphi e^{-H[\varphi_<,\varphi_>,\mathbf{C},\Lambda]}. \tag{3.4}$$

Now, we perform the functional integration only with respect to $\mathcal{D}\phi_>$, which yields :

$$Z = \int \mathcal{D}_<\varphi e^{-H[\varphi_<,\mathbf{C}',\Lambda-d\Lambda]}, \tag{3.5}$$

where we define the new couplings $\mathbf{C}'$ by the equation

$$e^{-H[\varphi_<,\mathbf{C}',\Lambda-d\Lambda]} \equiv \int \mathcal{D}_>\varphi e^{-H[\varphi_<,\varphi_>,\mathbf{C},\Lambda]}. \tag{3.6}$$

We can see that Z was kept unchanged, all we did here is just a redefinition of the partition function with the new effective couplings. Actually, for each new energy scale we can associate a new set of effective couplings. It is more convenient to denote this new scale in the following way: $\Lambda/s \equiv \Lambda - d\Lambda$, with $s > 1$. In this respect we can indicate the effective couplings corresponding to the new scale

$$\begin{aligned} \Lambda &\rightarrow \mathbf{C}, \\ \Lambda/s &\rightarrow \mathbf{C}', \\ \Lambda/s^2 &\rightarrow \mathbf{C}'', \\ &\vdots \end{aligned} \tag{3.7}$$

Thus, we can see that the coupling constant λ_is are naturally associated with an energy scale, while using perturbation theory this can be seen only after removing the infinities and extracting the beta function of the couplings. Wilson's method introduces the concept of renormalisation in the first place without relying on any expansion in the parameters of the theory, hence we expect to go beyond the perturbative results.
There are essentially two distinguished line of thoughts to implement the ideas presented above. One of them is closer to the original idea of the Wilson-Kadanoff block-spin approach, where the RG transformation is carried out by introducing block-spins on the lattice as new sites and redefine the length of the lattice spacing for the new sites. In the meantime the redefinition of the couplings are needed Eq. (3.7). This is what is known as the Wilson-Polchinksi formulation. The other method tackles the problem from the opposite side: it defines an effective average action for those degrees of freedom which we integrate out, thus providing a one-parameter family of effective theories on a given energy scale k. We will use the latter method (Sec. 3.1.3) in our computations, nevertheless, the basics of the first implementation will be also presented (Sec. 3.1.2) in order to understand the differences between the two approach.
Before we proceed to technicalities, we will discuss the the definition of a critical system and its relation to the RG fixed points in the next section.

3.1.1 Criticality and fixed points

As we discussed above, the RG flow takes place in the space of the couplings of the theory. The main advantage of studying the RG flow is that one can extract general informations about the second order phase transitions of the system. At criticality (i.e. one of the couplings is tuned to criticality, e.g. the temperature $T = T_c$) the dimensionful and dimensionless correlation length (which is measured in the unit of the lattice spacing $a \sim 1/\Lambda$) diverges: $\xi = \infty$, $\xi_{dl} = \xi/a = \infty$ (since $a < \infty$), where the former is the dimensionful and the latter is the dimensionless correlation length. If we perform an RG transformation on the critical system that maps $\mathbf{C} \to \mathbf{C}'$, then the new correlation length will be unchanged:

$$\xi_{dl} = \frac{\xi}{a} \to \frac{\xi}{as} = \frac{\xi_{dl}}{s} = \xi'_{dl} = \infty, \qquad \text{if } \xi = \infty. \tag{3.8}$$

Here, $s > 1$ represents the RG transformation by increasing the lattice spacing (in a similar manner as we introduced it in the previous section). This means that the new system, which is obtained through an RG transformation, stayed critical. A critical surface defined by the set of point $\mathbf{C}$s in the space of couplings for which $\xi_{dl} = \infty$. For a second order phase transition only one parameter is needed to be tuned to criticality (e.g. $T \to T_c$), hence the critical surface has a co-dimension one (in the direction of

the tuned coupling). By definition, the critical surface is an invariant subset of the RG transformation.

If we consider a system that is not at criticality (i.e. $\xi_{dl} < \infty$), the RG transformation will result in a new correlation length, i.e. $\xi'_{dl} = \xi_{dl}/s < \infty$, hence the system is "less critical". If we continue the RG steps the system gets further and further away from the critical surface. If one starts applying the RG transformation on a system which is

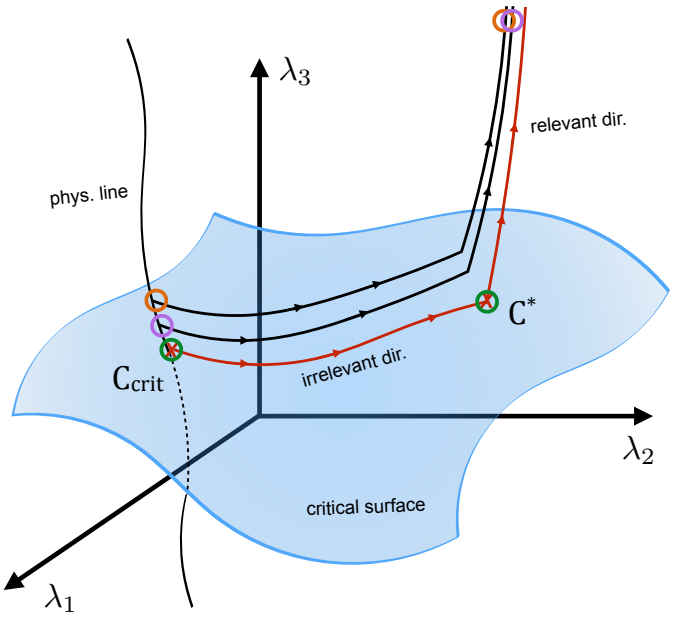

FIGURE 3.1: A schematic picture of a renormalisation group flow in a three-dimensional slice of the infinite-dimensional space of couplings. The vertical line corresponds to the physical line, on which one of the couplings of the system is tuned to criticality (the temperature for instance), i.e. onto the blue surface (critical surface). Various systems with different colours are defined at criticality (green) or close to criticality (orange, purple). The RG transformation governs each system on a different trajectory. The one, which was critical initially (green), stayed critical: it ended up at the fixed point C^*. The other two (orange, purple), which started close to criticality, ended up far from the critical surface, flowing along the only relevant direction that the fixed point has. They can be considered to belong to the same universality class, hence their long-distance behaviour is identical.

on the critical surface it will converge to a fixed point. That is $\mathbf{C} \to \mathbf{C}^*$, when both $\mathbf{C}$ and $\mathbf{C}^*$ are elements of the critical surface, and $\mathbf{C}^* \to \mathbf{C}^*$, i.e. $\mathbf{C}^*$ is invariant under the RG transformation. It is worth to emphasise that the RG transformation does not correspond to an operation which has a physical manifestation: all the systems defined by the RG flow correspond to the same physics, since the partition function remains unchanged.

All systems which are defined with some $\mathbf{C}$ on the critical surface belong to the same

universality class since they have the same long-distance behaviour. However, universality does not only hold for these systems, but also for some systems close to the critical surface. In fact, it can be shown that around the fixed point, the RG flow behaves as power law along its (linearised) eigendirections [62, 63]. There are three possibilities:

- The flow goes away from the fixed point $\mathbf{C}^*$. The direction in which it flows away called the relevant (eigen)direction. The coupling which corresponds to this direction called the relevant coupling.
- The flow approaches the fixed point. This direction corresponds to its irrelevant direction with the irrelevant coupling.
- If one cannot conclude the behaviour of the flow in a given direction from its linearisation, then it is called the marginal direction, and the corresponding coupling is the marginal coupling. In this case one needs to go beyond the linear order to see if the coupling is relevant or irrelevant. The flow in this direction is very slow: instead being power law, it exhibits a logarithmic behaviour.

The number of relevant couplings can be guessed, of course, since it must coincide with the co-dimensions of the critical surface. In the case of a second order phase transition, one parameter is needed to be tuned to criticality, consequently the number of relevant directions must be one. A schematic picture of an RG flow is shown in Fig. 3.1.
From the linearisation of the flow in the vicinity of the fixed point, it is possible to compute the critical exponents of the system, too. It can be shown that the value of the critical exponents classifies different theories into universality classes [62, 106]. Using FRG approach the critical exponents can be obtained with high precision, and they are comparable with the results extracted from lattice simulations. In the present work we will not discuss critical exponents, hence some references are given to the readers who are interested in such computations: [62, 63, 75, 102, 106].

3.1.2 The Wilson-Polchinski approach

As we mentioned above, the Wilson-Polchinski approach [54] is the closest implementation of the coarse-graining procedure originally applied to lattice spin models. We will use here the usual statistical field theory formulation in Euclidean metric. The microscopic physics corresponds to the theory defined on a scale Λ and has the partition function

$$Z[J] = \int d\mu_{K_\Lambda}(\varphi) e^{-\int V_k(\varphi) + \int J\varphi}, \tag{3.9}$$

where we perform the integration using the functional Gaussian measure:

$$d\mu_{K_\Lambda} \equiv \mathcal{D}\varphi e^{-\frac{1}{2}\int_{x,y}\varphi(x)K_\Lambda^{-1}(x-y)\varphi(y)}. \tag{3.10}$$

The kernel $K_\Lambda^{-1}(x-y)$ is defined in momentum space as:

$$K_\Lambda(p) \equiv (1-\theta_\epsilon(p,\Lambda))K(p). \tag{3.11}$$

with $K(p)$ being the free propagator:

$$K(p) = \frac{1}{p^2+m^2}. \tag{3.12}$$

The cut-off function $1-\theta_\epsilon(\Lambda,p)$ is defined to be smooth around the value Λ with a width ϵ. As $\epsilon \to 0$ the quadratic part of the action becomes just the D-dimensional integral of the free propagator with the cut-off Λ. In fact smoothing out the step function is not a necessary requirement for the definition, but for practical reasons it is more convenient to do so. We would like to implement the idea of the separation of the rapid and slow modes that we discussed already at the beginning of this chapter. Let us define again for all p momenta

$$\varphi(p) = \varphi(p)_< + \varphi(p)_>. \tag{3.13}$$

We split the field in slower and faster modes with respect to a scale $k < \Lambda$. Let us associate

$$\begin{aligned} \varphi(p) &\to K_\Lambda(p), \\ \varphi(p)_< &\to K_k(p), \\ \varphi(p)_> &\to K_\Lambda(p) - K_k(p). \end{aligned} \tag{3.14}$$

We need to keep in mind that although $\varphi(p)$ is being written as the sum of $\varphi_<(p)$ and $\varphi_>(p)$, they do not necessarily coincide on the corresponding intervals. Having this expression we are able to rewrite the partition function in terms of $\varphi_<$ and $\varphi_>$, but first we need to show that the functional integration measure can be indeed factorised in the following way:

$$d\mu_{K_\Lambda}(\varphi) = d\mu_{K_k}(\varphi_<)d\mu_{K_\Lambda-K_k}(\varphi_>) \tag{3.15}$$

This can be seen most easily for an analogoues one-dimensional integral:

$$I = \int_{-\infty}^{\infty} dx\, e^{-\frac{x^2}{2\gamma}}, \tag{3.16}$$

where $x = y + z$ and $\gamma = \alpha + \beta$ correspond to $\varphi = \varphi_< + \varphi_>$ and $K_\Lambda = (K_\Lambda - K_k) + K_k$, respectively. Now, let us define

$$J = \int_{-\infty}^{\infty} dy \int_{-\infty}^{\infty} dz e^{-\frac{y^2}{2\alpha}} e^{-\frac{z^2}{2\beta}}. \tag{3.17}$$

Rewriting

$$-\frac{y^2}{2\alpha} - \frac{z^2}{2\beta} = -\frac{1}{2}\frac{\gamma}{\alpha\beta}\left(y - \frac{\alpha}{\gamma}x\right)^2 + \frac{\alpha}{2\beta\gamma}x^2 - \frac{x^2}{2\beta}, \tag{3.18}$$

and using the new variable $u := (y - \frac{\alpha}{\gamma}x)$ and since the Jacobian of the transformation $(y, z) \to (u, x)$ is unity, we will get:

$$J = \int du\, dx e^{-\gamma u^2/2\alpha\beta - x^2/2\gamma} = \sqrt{\frac{2\pi\alpha\beta}{\gamma}} I. \tag{3.19}$$

Not only $I \propto J$, but it can be also shown more generally that

$$\int_{-\infty}^{\infty} e^{-\frac{x^2}{2\gamma} - V(x)} \propto \int dy\, dz e^{-\frac{y^2}{2\alpha}} e^{-\frac{z^2}{2\beta} - V(y+z)}. \tag{3.20}$$

We generalise this result to the functional integrals by writing:

$$\int d\mu_{K_\Lambda}(\varphi) e^{-\int V_k(\varphi)} \propto \int d\mu_{K_k}(\varphi_<)\, d\mu_{K_\Lambda - K_k}(\varphi_>) e^{-\int V_k(\varphi_< + \varphi_>)}. \tag{3.21}$$

From this formula with the integration of the rapid mode we can get the RG scale dependence of the potential V_k:

$$e^{-\int V_k(\varphi_<)} = \int d\mu_{K_\Lambda - K_k}(\varphi_>) e^{-\int V_k(\varphi_< + \varphi_>)}, \tag{3.22}$$

and thus the generating functional is

$$Z = \int d\mu_{K_k}(\varphi_<) e^{-\int V_k(\varphi_<)}. \tag{3.23}$$

We did not include the quadratic term in the field into V_k, this is the reason why we call it the potential. However, in a general case, as soon as $k < \Lambda$ terms with $\varphi_<$ and its arbitrary order of derivatives will be included in V_k. It is possible to derive the

RG equation of the potential which is called the Wilson-Polchinski equation [54], the details can be found in Appendix G . As we emphasised, $V_k(\varphi)$ involves infinitely many couplings contrarily to the PT where there are only the renormalisable ones. But even in very crude approximations, the RG from the Wilson-Polchinski approach can provide non-trivial non-perturbative results. This formulation is mathematically equivalent to the one we will present in the following.

3.1.3 The effective average action

The Wilson-Polchinski approach to the Wilsonian idea of non-perturbative renormalisation provides rather formal results using its RG equation. The Hamiltonians obtained through this type of renormalisation procedure are abstract objects and they are the Hamiltonians of the slow degrees of freedom ($\varphi_<$) which were not yet integrated out. The equivalent formulation of the idea firstly was presented by C. Wetterich and it is called the effective average action [91, 92]. The idea is practically the same, the crucial difference is that instead of computing the sequence of Hamiltonians through the RG equations one considers the effective action $\Gamma[\phi]$ of the rapid modes and builds a one-parameter family of models $\Gamma_k[\phi]$, indexed by the RG scale k, in such a way that:

i When $k = \Lambda$ no fluctuations has been integrated out, and thus we need to get back our initial theory, with the bare action defined at the natural cut-off scale Λ at the microscopic level, hence

$$\lim_{k\to\Lambda} \Gamma_k = S_{bare}. \tag{3.24}$$

ii When $k = 0$ all the fluctuations that were suppressed before are now integrated out. (Actually it would be more appropriate to say "integrated into", that is taking into account in Γ_k.) Hence in this limit we obtain the full quantum effective action:

$$\lim_{k\to 0} \Gamma_k = \Gamma. \tag{3.25}$$

iii In the case when $k < \Lambda$, but non-zero, we will have an effective theory defined with the effective average action at the given scale k.

From these requirements we can immediately see the major difference concerning the role of the scale k in the two approaches. In the Wilson-Polchinski formulation it serves as an ultraviolet cut-off for the slow modes, while it becomes an infrared cut-off for the rapid modes when computing the effective average action. It is crucial that the slow modes play a fundamental role in the Wilson-Polchinski approach, contrary to the

effective average action method, where they are absent and only the rapid modes count. For this reason all the information on the model (RG flow, fixed points, correlation functions, etc.) are incorporated in the main subject of study: $\Gamma_k[\phi]$. This latter feature of the effective average method makes it a more powerful tool compared to the Wilson-Polchinski formulation.

Now that we sketched the idea, we shall proceed to its implementation. We need to decouple the slow modes from the rapid ones, for which the most simple way is to give a large mass to the slow modes. In particle physics this corresponds to a small Compton wavelength which was identified as the a correlation length of such theories ($\hbar/mc$). Thus a large "mass" corresponds to a theory which is far from criticality (since at criticality $\xi \to \infty$), hence the fluctuations are small (suppressed). Now, the idea is to build up a one-parameter family of effective theories using a scale-dependent artificial mass as an infrared regulator:

$$Z_k[J] = \int \mathcal{D}\varphi e^{-S[\varphi]-\Delta S_k[\varphi]+\int J\varphi}, \tag{3.26}$$

where the scale-dependent mass was introduced in the following way:

$$\Delta S_k[\varphi] = \frac{1}{2}\int_q \varphi(q)R_k(q)\varphi(-q). \tag{3.27}$$

Here $R_k(q)$ is the so-called regulator function which has to fulfil the following requirements:

i When $k = \Lambda$ we would like to obtain the bare action. To achieve this, all the fluctuations are needed to be frozen, hence

$$\lim_{k\to\Lambda} R_k(q) = \infty, \qquad \forall q. \tag{3.28}$$

This will ensure that Eq. (3.24) is satisfied. Technically it is more convenient to choose the regulator function as Λ^2 in this limit.

ii When $k = 0$ we need to obtain the full quantum action Eq. (3.25), hence

$$\lim_{k\to 0} R_k(q) = 0, \qquad \forall q. \tag{3.29}$$

iii for $0 < k < \Lambda$ the slow modes in the interval $[0, k]$ are suppressed and the fast modes, which have a momentum in $[k, \Lambda]$, are not modified and the integration can be performed on them, hence

$$R_k(q) \approx \begin{cases} \text{finite} & \text{if } q < k \\ 0 & \text{if } q \geq k. \end{cases} \tag{3.30}$$

There have been extensive studies on a broad class of regulator functions and their optimisation [95, 96]. However, we will use only one regulator function throughout this chapter and we will define this particular regulator function later on, now we just give an example to illustrate their general shape in Fig. 3.2. As we defined the generating

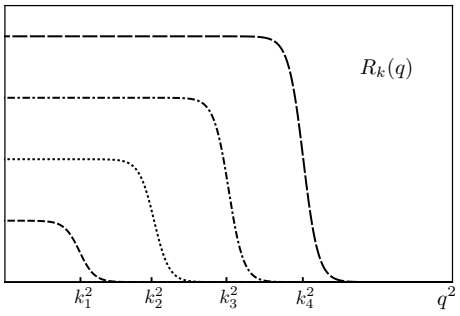

FIGURE 3.2: The typical shape of the regulator function in the effective average action method. Slow modes below the scale k are given a large mass, whereas the fast modes above k are being unaffected. On the figure we can see the regulator function for different k_i values.

functional for the effective theory at scale k we can derive the effective average action from it. It is straightforward to obtain W_k, since it is nothing else but the logarithm of Z_k:

$$W_k = \ln Z_k. \tag{3.31}$$

From here a Legendre transformation would lead us to the corresponding effective action, but this step is not that obvious. Let us first define Γ_k in the usual way but let us call it Γ'_k:

$$\Gamma'_k[\phi] = \sup_J \left(\int J\phi - W_k[\phi] \right), \tag{3.32}$$

where

$$\phi(x) = \frac{\delta W_k}{\delta J}. \tag{3.33}$$

One can check whether this definition fulfils the requirements: when $k \to 0$ the limit of W_k is just W hence $\Gamma'_k \to \Gamma$. This seems to be all right. However, taking the $k \to \Lambda$ limit we can see immediately that it will not give back the bare action because of the large term $\Delta S_{k\to\Lambda}$, thus $\lim_{\mathbf{k}\to 0} \Gamma'_k \neq S_{bare}$. We need to modify the definition of the Legendre transformation of W_k in a way that it will give us the right Γ_k:

$$\Gamma_k[\phi] = \sup_J \left(\int J\phi - W_k[\phi] \right) - \frac{1}{2} \int \phi R_k \phi. \tag{3.34}$$

From this definition we will still get the full quantum action in the limit $k \to 0$ and it will give the right result in the limit $k \to \Lambda$, i.e. $\lim_{\mathbf{k}\to 0} \Gamma_k = S_{bare}$. We will show the latter in the following.

Let us start from the definition of Γ_k and express $J(x)$ from it:

$$J(x) = \frac{\delta \Gamma_k[\phi]}{\delta \phi(x)} + \int_y R_k(x-y)\phi(y). \tag{3.35}$$

Now, we are going to substitute Eq. (3.34) and Eq. (3.35) into the definition of W_k which yields:

$$\begin{aligned} e^{-\Gamma_k} &= \int \mathcal{D}\varphi \exp\left(-S[\varphi] + \int_x \frac{\delta \Gamma_k[\phi]}{\delta \phi(x)}(\varphi(x) - \phi(x))\right) \\ &\quad \exp\left(-\frac{1}{2}\int_{x,y} (\varphi(x) - \phi(x)) R_k(x-y)(\varphi(y) - \phi(y))\right). \end{aligned} \tag{3.36}$$

In the limit $k \to \Lambda$ the regulator function diverges and

$$\lim_{k\to\Lambda} \exp\left(-\frac{1}{2}\int_{x,y} (\varphi(x) - \phi(x)) R_k(x-y)(\varphi(y) - \phi(y))\right) \propto \delta(\varphi - \phi). \tag{3.37}$$

Plugging it back into the Eq. (3.36) and taking the $k \to \Lambda$ limit gives:

$$e^{-\Gamma[\phi]} = \int \mathcal{D}\varphi e^{-S[\varphi] + \int_x \frac{\delta \Gamma_k[\phi]}{\delta \phi(x)}(\varphi(x) - \phi(x))} \delta(\varphi - \phi) = e^{-S[\phi]}. \tag{3.38}$$

This yields indeed $\Gamma_k[\phi] \to S[\phi]$ when $k \to \Lambda$ is performed, hence the right definition of Γ_k is provided by Eq. (3.34).

We are interested in the RG scale dependence of Γ_k. It is being described by the so-called Wetterich equation [91–93], for which we present its derivation in Appendix G. The Wetterich equation is an integro-differential equation for the average effective action and it reads as

$$\partial_k \Gamma_k = \frac{1}{2}\int_q \partial_k R_k(q) \left(\Gamma_k^{(2)}[\phi] + R_k\right)^{-1}(q, -q). \tag{3.39}$$

The inverse in the bracket must be understood in operator sense. There is a more compact form of the Wetterich equation which reads as:

$$\partial_t \Gamma_k[\phi] = \frac{1}{2}\mathrm{Tr}\left[\partial_t R_k \left(\Gamma_k^{(2)}[\phi] + R_k\right)^{-1}\right], \tag{3.40}$$

where we introduced the variable $t = \ln k/\Lambda$ and the trace is there to indicate the integration over the momentum q. There are several properties of this RG equation of the effective action which are worth to mention.

- If at scale Λ the action S is invariant under a group G, then this group must be also a symmetry of the average effective action defined in Eq. (3.36) for all k. Nevertheless, there are theories with gauge symmetry which is broken explicitly when a mass term is introduced. The symmetry breaking term can be controlled by modified Ward identities that become the true Ward identities in the $k \to 0$ limit [76]. However, it remains still an issue to develop a well controlled technique for RG flows in gauge theories.

- The Wetterich equation can also be derived for theories which involve fermions.

- It is worth to mention that the Wetterich equation is very similar to the derivative of the one-loop effective action which can be obtained from PT. In that case we have the following loop expansion of the effective action

$$\Gamma_k = S + \hbar\,\Gamma_k^{1-loop} + \mathcal{O}(\hbar^2). \tag{3.41}$$

To one-loop order $\Gamma_k^{(2)}$ can be replaced by $S^{(2)}$ in the Wetterich equation (RHS of Eq. (3.39)) which yields

$$\partial_t \Gamma_k^{1-loop} = \frac{1}{2}\mathrm{Tr}\left[\partial_t R_k \left(S^{(2)} + R_k\right)^{-1}\right] = \frac{1}{2}\partial_t \mathrm{Tr}\ln(S^{(2)} + R_k). \tag{3.42}$$

Integrating this respect to the scale t gives:

$$\Gamma^{1-loop} = S + \frac{1}{2}\mathrm{Tr}\ln S^{(2)} + \text{const.} \tag{3.43}$$

This is just the formula of the one-loop effective action [9]. Furthermore, if we make the identification of $G_k[\phi] = \left(\Gamma_k^{(2)}[\phi] + R_k\right)^{-1}$ as the full propagator, then we can construct a diagrammatic representation of Eq. (3.39), see Fig. 3.3.

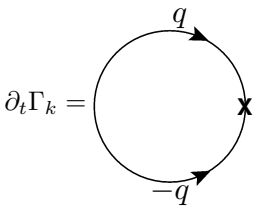

FIGURE 3.3: The one-loop structure of the Wetterich equation Eq. (3.39). On the RHS the line with arrows corresponds to the full propagator with momentum q. The "X" corresponds to the insertion of the operator $\partial_t R_k$.

The $\partial_t R_k$ term in the one-loop integral makes the result convergent in the UV, hence the Wetterich equation is regularised both in the IR and in the UV. All divergencies which show up in PT are avoided and we can obtain the RG flow directly, without computing the relationship between bare and renormalised quantities.

- In the expression of Eq. (3.39) the scale k has the role of an IR regulator scale, hence for $k > 0$ there is no phase transition and as a consequence there is no singularity in Γ_k (which is essentially the Gibbs free energy). If there is a second order phase transition it can be observed only when $k \to 0$.

3.1.4 Approximations of the effective average action

The RG equation (3.39) is of course an extremely complicated expression, thus, apart from a few exceptional cases (e.g. in the large-N O(N) model [94]), we will need approximations in order to solve it. There are two widely used approximations to solve the Wetterich equation. In both cases we are working in a restricted functional space, where we do not use an expansion in some small parameter of the theory. As a consequence, we expect that our result is non-perturbative. The first approximation is called the Green's function approach, where we build up an infinite tower of functional integro-differential equatios for the correlation functions derived from Eq. (3.39) by differentiating it with respect to the field and taking them at some specific field configuration (vanishing or uniform field configuration). At some point we need to truncate these equations, of course. Detailed discussion of this approximation scheme and some improvements can be found in [55, 56, 83].
The second (and the most popular) type of approximation is the so-called derivative expansion, which implicitly assumes the regularity of the effective average action. This eventually should be true when $k > 0$, and hence, it can be expanded in terms of $\partial_\mu \phi$. One can argue beside this approximation that we are interested mostly in the large distance physics, and thus we will keep only the lowest terms in $\partial_\mu \phi$, but we will keep all orders of ϕ:

$$\Gamma_k = \int d^D x \left(U_k(\phi(x)) + \frac{1}{2} Z_k(\phi(x)) (\partial_\mu \phi(x))^2 \right) + \mathcal{O}(\partial^4). \tag{3.44}$$

The most important information from the point of view of the statistical mechanics is contained by the effective potential, $\lim_{k\to 0} U_k$. Therefore, it is still going to give us reliable results if we project the RG equation Eq. (3.39) on the effective potential. This approximation is called the Local Potential Approximation (LPA) and it is defined by taking the fields at uniform field configurations: $\Gamma_k(\phi_{\text{uni}}) = \Omega U_k(\phi_{\text{uni}})$, where Ω is the spatial volume of the system. In this case the effective action will have the form:

$$\Gamma_k = \int d^D x \left(U_k(\phi(x)) + (\partial_\mu \phi(x)^2) \right). \tag{3.45}$$

Here, we also set $Z_k = 1$.
In the next section we are going to briefly discuss the O(N) model and consider its RG equation of the effective potential in the framework of FRG.

3.2 The O(N) model in the framework of FRG

The O(N) or N-vector model is the straightforward generalisation of the φ^4 theory with the quantum field being now $\varphi = (\varphi_1, \varphi_2, ..., \varphi_N)$. Due to its relative simplicity it is one of the most extensively studied models in quantum filed theory and in statistical physics. The action that defines the model has a symmetry under N-dimensional rotations, hence the parameter N can be considered as the dimensionality of a classical spin. In fact, depending on N (the number of components) the model describes for $N = 1$ the Ising model, $N = 2$ the XY model (spins rotating in a plane), $N = 3$ the Heisenberg model (spins rotating in a three-dimensional sphere) (see Fig. 3.4), and for $N = 4$ it serves as a toy model for the Higgs sector in the standard model or for low-energy meson phenomenology. In the following we are going to derive the RG equation of the effective

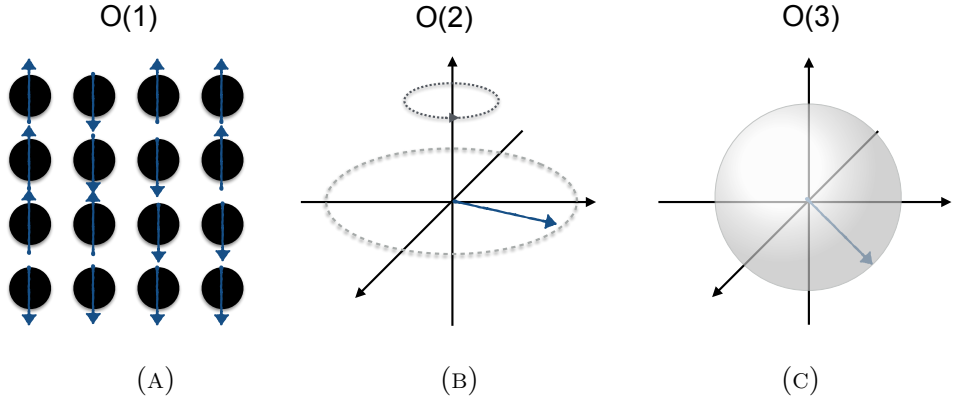

FIGURE 3.4: The spin models corresponding to various O(N) models. (A) is the Ising model with O(1)$\cong \mathbb{Z}_2$ symmetric spins on a lattice, (B) is the XY model with O(2) symmetric spins on the lattice sites and (C) is the Heisenberg model with O(3) symmetric spins defined on each site.

potential for the O(N) model. Every term in the action is invariant under the N-dimensional rotational group, therefore, technically it is more convenient to work with the invariant variable of the theory:

$$\rho = \frac{1}{2}\phi^2. \tag{3.46}$$

Now, there is also another technicality that we need to take care of. Since we wish to study critical systems, where practically we have to work with singular dimensionful quantities, we should use dimensionless quantities instead. This means that in order to

keep the rather simple notations we had so far, by abuse of notation, we will redefine our dimensionful fields and couplings with a "bar" and we will define the dimensionless fields and coupling without bars. For the dimensionful effective potential we will use U_k and the corresponding dimensionless potential is u_k. That is, since we have the canonical dimensions:

$$[U] = k^D, \qquad [\bar{\phi}] = k^{\frac{D-2}{2}} \Rightarrow [\bar{\rho}] = k^{D-2}, \tag{3.47}$$

they will define the following dimensionless quantities:

$$u = \frac{U}{k^D}, \qquad \phi = \frac{\bar{\phi}}{k^{\frac{D-2}{2}}} \Rightarrow \rho = \frac{\bar{\rho}}{k^{D-2}}. \tag{3.48}$$

We start with the Wetterich equation Eq. (3.39) and use the LPA Ansatz Eq. (3.45) for the effective action, which yields (see Appendix G.1.3)

$$\partial_t U_k = \frac{1}{2} \int \frac{d^D q}{(2\pi)^D} \partial_t R_k(q) \left(\frac{N-1}{q^2 + R_k(q) + U_k'} + \frac{1}{q^2 + R_k(q) + U_k' + 2\bar{\rho} U_k''} \right). \tag{3.49}$$

So far, we have not introduced the regulator function R_k explicitly, but we have to do it at this point in order to be able to evaluate Eq. (3.49). By using the optimised (or Litim's) regulator [95],

$$R_k(q^2) = (k^2 - q^2)\, \theta(k^2 - q^2), \tag{3.50}$$

which satisfy the criteria in Sec. (3.1.3), one can evaluate the integral in Eq. (3.49) analytically, which we will show in the following. We can rewrite Eq. (3.49) into D-dimensional spherical coordinates and integrate out the angular part to obtain:

$$\partial_t U_k = v_D \int_0^\infty dx\, x^{\frac{D}{2}-1} \partial_t R_k(q) \left(\frac{N-1}{q^2 + R_k(q) + U_k'} + \frac{1}{q^2 + R_k(q) + U_k + 2\bar{\rho} U_k''} \right), \tag{3.51}$$

where $x \equiv q^2$ and v_D comes from the surface of the D-dimensional unit sphere and the factor of $1/2$, with the explicit expression:

$$v_D = \frac{1}{2^{D+1} \pi^{D/2} \Gamma(D/2)}. \tag{3.52}$$

Both of the terms in the integrand have essentially the same form. Hence, it is more convenient to introduce:

$$\bar{I}(\Omega) = \int_0^\infty dx\, x^{\frac{D}{2}-1} \frac{\partial_t R_k(q)}{q^2 + R_k(q) + \Omega}. \tag{3.53}$$

The term Ω in the denominator is a q independent object. We will use the dimensionless regulator as a function of $y \equiv q^2/k^2$:

$$r(y) = \frac{R_k(q)}{q^2} = \frac{1}{q^2}(k^2 - q^2)\,\theta(k^2 - q^2) = \left(\frac{1}{y} - 1\right)\,\theta\,(1 - y)\,, \tag{3.54}$$

and the logarithmic derivative of R_k by the scale k:

$$\partial_t R_k = \frac{1}{q^2}\frac{\partial r(y)}{\partial y}\frac{\partial y}{\partial t} = \frac{1}{q^2}\frac{\partial r(y)}{\partial y} k\partial_k \left(\frac{p^2}{k^2}\right) = -2q^2 r'(y)y = -2xr'(y)y. \tag{3.55}$$

We continue by substituting Eq. (3.55) into Eq. (3.53):

$$\begin{aligned}
\bar{I}(\Omega) &= \int_0^\infty dx\, x^{\frac{D}{2}-1} \frac{-2xr'(y)y}{q^2 + R_k(q) + \Omega} \\
&= \int_0^\infty dx\, x^{\frac{D}{2}-1} \frac{-2\frac{x}{k^2}r'(y)y}{\frac{x}{k^2}\,(1 + r(y)) + \frac{\Omega}{k^2}} \\
&= \int_0^\infty dx\, x^{\frac{D}{2}-1} \frac{-2y^2 r'(y)}{y + yr(y) + \omega} \\
&= k^D \int_0^\infty dy\, y^{\frac{D}{2}+1} \frac{-2r'(y)}{y + yr(y) + \omega},
\end{aligned} \tag{3.56}$$

where $\omega = \Omega/k^2$. Now, the integrand is being expressed by fully dimensionless quantities, and the dimensionless integral can be denoted by $I(\omega) = \bar{I}(\Omega)/k^D$. Using the definition of Litim's regulator in the dimensionless form given in Eq. (3.54) yields:

$$\begin{aligned}
I(\omega) &= -2\int_0^\infty dy\, y^{\frac{D}{2}+1} \frac{-\frac{1}{y^2}\theta(1-y) + \left(\frac{1}{y} - 1\right)\delta(1-x)}{y + y\left(\left(\frac{1}{y} - 1\right)\,\theta\,(1-y)\right) + \omega} \\
&= 2\int_0^1 dy\, y^{\frac{D}{2}-1} \frac{1}{1+\omega} = \frac{4}{D}\frac{1}{1+\omega}.
\end{aligned} \tag{3.57}$$

Here, in the nominator we used the fact that the derivative of the dimensionless regulator is

$$r'(y) = -\frac{1}{y^2}\theta(1-y) + \left(\frac{1}{y} - 1\right)\delta(1-x). \tag{3.58}$$

Using the result above, we can write down the RG equation for the effective potential given in Eq. (3.49) as

$$\partial_t U_k = A_D \left(\frac{k^D(N-1)}{1 + u_k'} + \frac{k^D}{1 + u_k' + \rho u_k''}\right). \tag{3.59}$$

On the RHS we substituted into ω the corresponding expression from the denominator of Eq. (3.49). We defined the D-dependent factor A_D:

$$A_D = v_D = \frac{1}{2^{D-1}\pi^{D/2}\Gamma(D/2)D}. \tag{3.60}$$

Now, we need to factor out the scale on the LHS of Eq.(3.59), too. Differentiating the potential with respect to the scale gives:

$$k\frac{dU_k(\bar{\rho})}{dk} = k\frac{k^D u_k(\rho)}{dk} = k\left(k^{D-1}Du_k(\rho) + k^D\frac{du_k(\rho)}{dk}\right). \tag{3.61}$$

Now, let us compute the second term in the bracket, where we need to keep in mind that since $\bar{\rho}$ can be arbitrary ρ must depend on the scale:

$$\begin{aligned} k^D\frac{du_k(\rho)}{dk} &= k^D\frac{\partial u_k(\rho)}{\partial k} + k^D\frac{\partial u_k(\rho)}{\partial \rho}\frac{\partial \rho}{\partial k} \\ &= k^D\frac{\partial u_k(\rho)}{\partial k} + k^D\frac{\partial u_k(\rho)}{\partial \rho}\frac{\partial k^{2-D}\bar{\rho}}{\partial k} \\ &= k^D\frac{\partial u_k(\rho)}{\partial k} + k^D\frac{\partial u_k(\rho)}{\partial \rho}k^{1-D}\bar{\rho}(2-D) \\ &= k^{D-1}\left(\partial_t u_k(\rho) + (2-D)u_k'(\rho)\rho\right), \end{aligned} \tag{3.62}$$

where, when we took the partial derivative of the potential respect to k, the dimensionless field variable ρ was understood as a fixed quantity. Now, by substituting Eq. (3.61) with Eq. (3.62) into Eq. (3.59), we will obtain the RG equation for the dimensionless effective potential:

$$\partial_t u_k = -Du_k + (D-2)\rho u_k' + (N-1)\frac{A_D}{1+u_k'} + \frac{A_D}{1+u_k'+\rho u_k''}. \tag{3.63}$$

This equation is going to be our main subject of study. In the following, we will discuss the spontaneous breaking of the symmetry in the O(N) model.

3.3 The O(N) model and the spontaneous breaking of symmetry

Spontaneous symmetry breaking (SSB) is a cornerstone concept in a variety of systems, ranging from field theory and particle physics to statistical mechanics and interacting lattice models. The study of the occurrence of SSB play a crucial role in the theory of phase transitions and in the characterisation of ordered phases and it highlights the interplay between SSB and the dimensionality of the system: this interplay is customarily expressed by defining a lower critical dimension D_L for which SSB cannot occur

[57]. A celebrated exact result connecting SSB and dimensionality is provided by the Mermin-Wagner-Hohenberg-Coleman (MW) theorem [58–60]. According to this theorem a continuous symmetry cannot be spontaneously broken in less than or equal to two dimensions, hence the lower critical dimension is $D_L = 2$. This theorem has been formulated for classical systems [58] and then extended to quantum systems [59, 60]. For magnetic systems with continuous symmetry it rules out the possibility of having a non-vanishing magnetisation at finite temperature in two dimensions, and for $2D$ interacting Bose gases predicts that no Bose-Einstein condensation occurs at finite temperature [59] (for Bose gases this result has been extended to zero temperature [61]). As it is well known, even though the Mermin-Wagner theorem rules out SSB and the existence of a local order parameter in two dimensions, nonetheless the Berezinskii-Kosterlitz-Thouless (BTK) transition may yet occur for the U(1) symmetry and it signaled by the algebraic behaviour of correlation functions in the low temperature phase [62]. The Mermin-Wagner theorem for the O(N)-symmetric scalar field theory states that for $N \geq 2$ in two dimensions no SSB occurs. Although originally formulated in integer dimensions, this result was later extended to graphs with fractional dimensions [64]: in this way one can explicitly show that for $N \geq 2$ there is no SSB for $D \leq 2$, with D being real, while SSB occurs for $D > 2$ [65]. In [66] the study of how O(N) universality classes depend continuously on the dimension D (and as well on N), in particular for $2 < D < 3$ was recently presented. The Ising model, i.e. the $N = 1$ case, is different from O(N) models with continuous symmetry ($N \geq 2$) because the symmetry is discrete: in two dimensions it notoriously has a finite temperature phase transition [67] and it can be shown that this happens for $D \geq 2$ with D real [68]. The large-N limit of O(N) models is also interesting because for $N \to \infty$ it is equivalent to the spherical model [69], which is exactly solvable [70]. The O(N) model represents then an ideal playground to study the interplay of SSB and dimensionality and to test whether (and how) the appearance of SSB depends on the approximation schemes. A powerful method used to consider the phase structure of a model, and consequently to study the appearance of SSB, is the FRG method [14, 71–77]. The O(N) model has been extensively studied using FRG approaches: as relevant for our purposes, we mention that it was used to study, as a function of dimension, the critical exponents of O(N) models [66, 78, 79] and to investigate truncation effects and the regulator-dependence of the FRG equation [80–87], while a FRG study of the critical exponents of the Ising model for $D < 2$ was presented in [78]. The study of single-particle quantum mechanics can be seen as a "low-dimensional" statistical mechanics model: FRG studies addressed double well potential and quantum tunneling [88, 89] and quartic anharmonic oscillators [90].

3.4 Mermin-Wagner-Hohenberg-Coleman theorem for the O(N) model in the framework of FRG

3.4.1 MW theorem for finite N

In this section we will consider the problem of determining the lower critical dimension D_L for the O(N) model for a finite N in LPA. In order to consider the appearance of SSB in the O(N) model for finite N, let us start with the following fixed point equation, which is obtained from Eq. (3.63). By setting $\partial_t u = 0$

$$Du - (D-2)\rho u' = \frac{A_D(N-1)}{1+u'} + \frac{A_D}{1+u'+2\rho u''}. \tag{3.64}$$

The LHS of the RG Eq. (3.64) is linear in the effective potential. The RHS depends on the effective potential and its derivatives non-linearly, thus, we introduce the notation

$$LP \equiv Du(\rho) - (D-2)\rho u'(\rho), \tag{3.65}$$

$$NLP \equiv (N-1)\frac{A_D}{1+u'(\rho)} + \frac{A_D}{1+u'(\rho)+2\rho u''(\rho)}, \tag{3.66}$$

where LP (NLP) stands for the linear (non-linear) part. The fixed point equation (3.64) for the potential, using the notations in Eq. (3.65)-Eq. (3.66), reads then $LP = NLP$. In the large field limit ($\rho \to \infty$) the potential could be diverging or bounded, hence tending to a constant value. However, we need to assume the analyticity of the effective potential for finite field values [109].

Let us consider first the case when $u(\rho)$ is diverging in the large field limit. In this case we need to distinguish three sub-cases according to the behaviour of the derivative, $u'(\rho)$, since it can be diverging, tending to a finite value or to zero. In the case when u' is also diverging NLP tends to zero, hence the asymptotic form of the differential equation is:

$$Du(\rho) - (D-2)\rho u'_{as}(\rho) = 0, \tag{3.67}$$

yielding the solution:

$$u_{as}(\rho) = a\rho^{\frac{D}{D-2}}. \tag{3.68}$$

Due to the stability requirement of the potential, that is u has to be bounded from below, a is forced to be a positive real. We can then write the form of the potential as

$$u(\rho) = g(\rho) + a\rho^{\frac{D}{D-2}}, \tag{3.69}$$

where, $g(\rho)$ vanishes in the large ρ limit. We are looking for the minimum ρ_0: let us differentiate Eq. (3.69) and take it at $\rho = \rho_0$, which is assumed to be the minimum.

Performing this operation one gets

$$0 = g'(\rho_0) + a\frac{D}{D-2}\rho_0^{\frac{D}{D-2}-1}. \tag{3.70}$$

From this ρ_0 can be expressed as

$$\rho_0 = \left(-\frac{g'(\rho_0)}{a}\right)^{\frac{D-2}{2}} \left(\frac{D-2}{D}\right)^{\frac{D-2}{2}}. \tag{3.71}$$

We can now distinguish three sub-cases:

- for $D > 2$ the second factor in the expression of the minimum has a positive real value. We have established already that in the first factor the denominator a is positive. Therefore $g'(\rho_0)$ must be negative or zero in order to fulfil Eq. (3.70). Hence, altogether, the fraction in the bracket must be positive independently of the dimension. So, we found that for $D > 2$ the minimum ρ_0 can be either vanishing or a finite positive number. This latter case indicates that the presence of SSB is possible.

- for $D = 2$ the second factor gives a 0^0, which is indeterminate, or alternatively one can define it as 1 if we consider the $D = 2$ case as a limit ($D \to 2$). In this instance what one can see already from Eq. (3.70) is that if we assume ρ_0 to be a positive real, then $g'(\rho_0)$ should be $-\infty$ to compensate the second term. So, if we consider the limit $D \to 2$ in Eq. (3.71), then $\rho_0 = \infty$, which means there is no finite positive minimum to consider, therefore no SSB occurs in $D = 2$ limit [104]. However, this analysis is not sensitive to the number of the field components N. In the special case, when $N = 1$ (i.e. Ising model) we would need to observe an SSB phase in $D = 2$ as well. From this argument it is not clear how to achieve this. The answer to this question can be found in Section 3.5.1, where the Taylor expansion of the effective potential is used.

- for $D < 2$ one can immediately see that the second factor in Eq. (3.71) is going to have complex value(s). From Eq. (3.70) we can conclude that $g'(\rho_0) \geq 0$ for $D < 2$. The only value for $g'(\rho_0)$ that makes Eq. (3.71) physically sensible is when $g'(\rho_0) = 0$, therefore the potential cannot have a true extremum (minimum) anywhere else than $\rho_0 = 0$. This clearly shows that there exists only a symmetric phase for dimensions $D < 2$ in the LPA.

Now, we will consider those two cases which are left, namely, when $u(\rho)$ diverges and $u(\rho)'$ tends to zero or to a finite constant and the case when $u(\rho)$ itself tends to a constant with the consequence that $u'(\rho)$ is tending to zero. In all of these three cases

the asymptotic form of the fixed point equation (3.64) reads:

$$Du(\rho) - (D-2)\rho u'_{as}(\rho) = c. \tag{3.72}$$

Its solution is

$$u_{as}(\rho) = \frac{c}{D} + a\rho^{\frac{D}{D-2}}. \tag{3.73}$$

Hence, the full potential can be written in the same way as in Eq. (3.69). Now, in the first two cases when $u(\rho)$ is diverging, $g(\rho)$ can have arbitrary behaviour. In this case exactly the same arguments hold as those discussed above for the $u'(\rho) \to \infty$ scenario. On the other hand, when $u(\rho)$ is a constant in the large field limit, we have a more subtle case. From Eq. (3.69) we would demand to tend to a constant, i.e. to c/D, as we see in Eq. (3.73). Here we can have three different situations:

- When $D < 2$:

$$\lim_{\rho\to\infty} u(\rho) = \lim_{\rho\to\infty} g(\rho) + a\rho^{\frac{D}{D-2}} = \frac{c}{D}, \qquad \forall a \geq 0. \tag{3.74}$$

  Thus $g(\rho) \to c/D$. And hence, if we write down Eq. (3.71) we will find the same answer: the only physically sensible solution for it is when $g'(\rho) = 0$, which implies $\rho_0 = 0$, and as a consequence there cannot be a SSB.

- When $D > 2$ the only way to get a constant in the large field limit is to set a to zero:

$$\lim_{\rho\to\infty} u(\rho) = \lim_{\rho\to\infty} g(\rho) + a\rho^{\frac{D}{D-2}} = \frac{c}{D}, \qquad \text{if} \quad a = 0. \tag{3.75}$$

  In this situation in Eq. (3.71) we are going to face the expression of $g'(\rho_0)/0$ which can only be compensated to give a finite value iff $g'(\rho_0) = 0$, too. Since $g(\rho)$ tends to a constant this can be achieved if it converges very fast. This argument is rather handwaving, however, from this analysis this is the most that we can extract. If we assume that $g'(\rho_0) = 0$ in a way that $\lim_{g',a\to 0} g'(\rho_0)/a \in \mathbb{R}^-$ (i.e. $g(\rho)$ is decreasingly approaching the constant value), indeed, we are going to have a finite positive expression for the minimum in Eq. (3.71).

- When $D = 2$ we will face with divergences again, just like in the case when $u(\rho) \to \infty$. The same argument can be done here, as it was done there.

We also need to give a small remark whether the extremum we consider can be truly a minimum. To get the answer to this question, we need to analyse the second derivative of the effective potential. More precisely, we need to show that $u''(\rho_0) > 0$. From

Eq. (3.69) the second derivative of the potential at $\rho = \rho_0$ reads:

$$u''(\rho_0) = \frac{a\left(\frac{D}{D-2} - 1\right) D\rho_0^{\frac{D}{D-2}-2}}{D-2} + g''(\rho_0). \tag{3.76}$$

Now, since we established that $a \geq 0$, the first term provides a positive value whenever $\rho_0 > 0$ (apart from the case when $a = 0$). Hence, the positivity of the expression in Eq. (3.76) depends on the value of $g''(\rho_0)$, which we do not know precisely, but the most important fact, that is the possibility of $u''(\rho_0) > 0$, is not excluded at all. Thus, the analysis we provided above holds.

As a conclusion: the analysis that was presented above in the finite N case when we have a potential that diverges asymptotically, the Mermin-Wagner theorem can be established with the question mark on the case of $D = 2$. When the potential is bounded from both directions (like in the Ising model in $D = 1$ and $D = 2$ [110]) one needs to make a few assumptions to prove the MW theorem in the framework of the FRG at the level of the LPA. In Section 3.5.1 we will show that, indeed $D_L < 2$ when $N = 1$ and $D_L = 2$ when $N \geq 2$. In the next section, however, we will consider the large-N case first.

3.4.2 MW theorem for the spherical model

In this section we consider the O(N) model in the large-N limit which is equivalent to the spherical model [69]: thus we can neglect the terms in Eq. (3.63) which are of order $1/N$. To see this we are going to rescale Eq. (3.63) by an irrelevant parameter ($A_D N$), and considering the new variables $\rho \to \rho/(A_D N)$ and $u \to u/(A_D N)$. The derivative of the potential remains invariant under this rescaling $u' \to \frac{\partial u/(A_D N)}{\partial \rho/(A_D N)} = u'$. As a first step, we divide the RG equation (3.63) by $A_D N$:

$$\partial_t \frac{u}{A_D N} = (D-2)\frac{\rho}{A_D N}u' - D\frac{u}{A_D N} + \frac{1}{1+u'} - \frac{1}{N}\frac{1}{1+u'} + \frac{1}{N}\frac{1}{1+u'+2\rho u''}. \tag{3.77}$$

Next we perform the rescaling

$$\partial_t u = (D-2)\rho u' - Du + \frac{1}{1+u'} - \frac{1}{N}\frac{1}{1+u'} + \frac{1}{N}\frac{1}{1+u'+2\rho u''}. \tag{3.78}$$

By taking the limit $N \to \infty$ the following terms remain:

$$\partial_t u = (D-2)\rho u' - Du + \frac{1}{1+u'}. \tag{3.79}$$

This simplified expression represents the RG equation for the effective potential in the large-N limit of the O(N) model in arbitrary dimension. From Eq. (3.79) we can extract some useful information. First we should differentiate it with respect to ρ in order to

get an equation for the derivative of the potential. It reads then

$$\partial_t u' = (D-2)u' + (D-2)\rho u'' - Du' - \frac{u''}{(1+u')^2}. \tag{3.80}$$

Since in a physically reasonable theory the potential is bounded from below, we can assume that this potential has a global minimum at some $\rho = \rho_0$. For ρ_0 we have the following value for the derivatives of the potential at the fixed point: $u'(\rho_0) = 0$, $u''(\rho_0) \equiv \lambda$. Assuming that the quartic coupling λ is finite, we have then the following equation:

$$0 = (D-2)\rho_0\lambda - \lambda, \tag{3.81}$$

with the solution

$$\rho_0 = \frac{1}{D-2}, \tag{3.82}$$

which determines the cases where the minimum of the potential can be found in the large-N case. There is SSB if the potential has the minimum at some finite $\rho_0 > 0$: in the case of Eq. (3.82) we can satisfy this condition for $D > 2$. For $D < 2$ we find $\rho_0 < 0$, hence in view of Eq. (3.46) there will be no SSB. The $D = 2$ case seems to be undefined again, since $\rho_0 \to \infty$ in this limit. However, if the minimum of the potential is sent to infinity one cannot define a proper real minimum. The absence of a finite minimum indicates the absence of the spontaneous symmetry breaking for $D = 2$ dimensions. This can be also seen by solving Eq. (3.80) using the method of characteristics [104], [94]. The large-N limit is a frequently used technique [53, 105], where the results obtained can be considered as exact ones, since the LPA approximation can be considered as an exact approximation when $N \to \infty$ [94, 106].

3.5 The phase structure of the O(N) model

3.5.1 The Vanishing Beta Function curves

In the following, we are going to use the most common Ansatz for solving the equation 3.63. Namely, it is the Taylor expansion of the effective potential in the field variable. First we are assuming that we can expand the potential in a Taylor-series around vanishing field. That is:

$$u(\rho) = \lim_{n\to\infty} \sum_{i=1}^{n} \frac{u^{(i)}}{i!}\rho^i. \tag{3.83}$$

For the sake of simplicity we are going to use the following notations for the coefficients $\lambda_i \equiv u^{(i)}(0)$. The scale-dependence is encoded into these dimensionless couplings. Most of the times we are also going to use for the quadratic coupling $\lambda_1 \equiv m^2$, sometimes for the quartic coupling $\lambda_2 \equiv \lambda$ and $\lambda_3 \equiv \tau$ for the sextic coupling. Keeping this in mind, we can look at the flow equation of the effective potential and differentiate it once, then evaluate it at $\rho = 0$. So, we get the flow equation for the mass

$$\partial_t m^2 = (\mathrm{D}-2)m^2 - \mathrm{D}m^2 - \frac{3\lambda A_D}{(1+m^2)^2} - \frac{(N-1)\lambda A_D}{(1+m^2)^2}. \tag{3.84}$$

If we are looking for the scale independent solutions (i.e. the fixed point solutions) of this partial differential equation, one can take $\partial_t m^2 = 0$. By doing this, we can express λ by using only the mass term

$$\lambda = -\frac{2m^2\left(1+m^2\right)^2}{(2+N)A_D}. \tag{3.85}$$

This curve defines the value of λ, provided $\partial_t m^2 = 0$, i.e. this relation is only true when the mass stopped running [43], [103]. If one does not have quartic coupling, i.e. $\lambda = 0$, then the solutions for this equation are just the roots of $\lambda(m^2)$, that is $m^2 = -1$ or $m^2 = 0$. Now we derive the flow equation for the quartic coupling, too. To do so, we need to perform the same idea as before, but now we need to differentiate the flow equation of the effective potential twice with respect to ρ and only then evaluate it at $\rho = 0$. One will have then:

$$\begin{aligned}\partial_t \lambda \;=\; & 2(\mathrm{D}-2)\lambda - \mathrm{D}\lambda + A_D\left[\left(\frac{18\lambda^2}{(1+m^2)^3} - \frac{5\tau}{(1+m^2)^2}\right)\right. \\ & \left. +(N-1)\left(\frac{2\lambda^2}{(1+m^2)^3} - \frac{\tau}{(1+m^2)^2}\right)\right].\end{aligned} \tag{3.86}$$

Again, if we are interested in the fixed point of the equation we need to take $\partial_t \lambda = 0$, which enables us to express the sextic coupling as $\tau = \tau(\lambda, m^2)$. If we are looking for the fixed points of both equations Eq. (3.86) and Eq. (3.84) we can express the sextic coupling by only using the mass as an explicit parameter: $\tau = \tau(\lambda(m^2), m^2) = \tau(m^2)$. This looks as follows:

$$\tau = -\frac{2m^2\left(1+m^2\right)^3\left(\mathrm{D}\left(1+m^2\right)(2+N) - 4\left(2+N+2m^2(5+N)\right)\right)}{(2+N)^2(4+N)A_D^2}. \tag{3.87}$$

This function defines the value of τ, provided $\partial_t m^2 = 0$ *and* $\partial_t \lambda = 0$. When we are looking for a fixed point for the whole system of equations we need to set the LHS of Eq. (3.87) to zero (which sets $\partial_t \tau = 0$ automatically), thus providing the values for m^2 where the fixed points are found. The general statement is the following: one can

express the nth coupling simply by using the mass term m^2 as an explicit parameter. This nested formula has the following form:

$$\lambda_n = \lambda_n(\lambda_{n-1}(\lambda_{n-2}(...\lambda_2(m^2))), m^2) = \lambda_n(m^2). \tag{3.88}$$

It is straightforward to prove this using induction (see Appendix H). As a consequence one can find a formula which tells the general form for the nth coupling for $n \geq 2$:

$$\lambda_n = (-1)^{n+1} \frac{2^{[n/2]}}{A_D^{n-1} \prod_{i=1}^{n-1} (2i+N)^{[(n-1)/i]}} m^2 (1+m^2)^n \sum_{i=0}^{n-2} \sum_{j=0}^{n-2} f_{i,j}(N^\alpha)(m^2)^i D^j. \tag{3.89}$$

Here the notation [.] means the integer part of its argument and $f_{i,j}(N)$ is an integer valued function of N^α, where α is an integer, too. From Eq. (3.89) we can conclude that (apart from the prefactor which depends only on N and D) λ_n is a polynomial of m^2 over the integers, which has roots at $m^2 = 0$ and $m^2 = -1$ for every $n \geq 2$. Another interesting consideration is that λ_2 is the greatest common divisor of all the λ_n VBF polynomials, $n \geq 2$. Of course, there are much more roots in the complex numbers domain in general (actually the number of roots are growing with n), but we are only going to consider the real ones, for which the physics is meaningful. However, in special cases like in $D = 4$ and $4 < D < 6$ in the large-N, one can observe a convergent series of the unphysical roots on the complex plane from which the physically sensible results can be extracted. It is worth to emphasise that Eq. (3.89) is the most general form of the couplings $\lambda_n(m^2)$, their qualitative behaviour highly depend on the dimensionality, as we are going to see later on. It also depends on the number of the fields N, of course, but this dependence is rather quantitative.

The coupling $\lambda_n = \lambda_n(m^2)$ in Eq. (3.89) defines a curve in terms of m^2 on which $\partial_t \lambda_{n-1} = 0$, i.e. the beta function of the $(n-1)$th coupling, vanishes. But we know that $\lambda_{n-1} = \lambda_{n-1}(m^2)$ (which we have already in hand, otherwise we could not build up $\lambda_n(m^2)$) defines a curve on which $\partial_t \lambda_{n-2} = 0$, and we can continue this till $n = 1$. For this reason from now on we will refer to the curves defined by Eq. (3.89) as the Vanishing Beta Function (VBF) curves.

As a next step we would like to extract the fixed points of the theory. The VBF curves of course define the possible values of the couplings for the fixed points. In order to find a fixed point we need to perform the following procedure. The VBF λ_n defines a curve where $\partial_t \lambda_{n-1}$ vanishes, but it does not say anything about $\partial_t \lambda_n$ itself. The curve which on $\partial_t \lambda_n$ vanishes is defined by $\lambda_{n+1} = \lambda_{n+1}(m^2)$, and so on. But we need to cut our Taylor expansion at some order, to be able to carry out real computations. Let us say we truncate it at the nth order, but then again we would need the beta function of λ_n to be zero, which is encoded in the VBF defined by λ_{n+1}. Since we expanded

the effective potential in Taylor series until the nth order, clearly we cannot construct that curve. The only way to get $\partial_t \lambda_n = 0$ is to set $\lambda_n(m^2) \equiv 0$ which gives zero for its beta function automatically. In other words, assume that we would like to have an $(n-1)$ order expansion, but before we do so we do not set $\lambda_n = 0$ for the moment. If λ_n were not be zero we would need its beta function to vanish, too, in order to find a fixed point. But we do not want to compute its beta function, because at the end we are satisfied with an $n-1$ order expansion. Since we did not set λ_n to zero yet, we can express it through the vanishing beta function of the $(n-1)$th coupling because its fixed point equation has the form $\partial_t \lambda_{n-1} = 0 = F(m^2) + \lambda_n$, where $F(m^2)$ is a polynomial in m^2. Now, $\lambda_n = -F(m^2)$, which just defines its VBF curve. Since we did not want to have this term (i.e. the nth), we can set $F(m^2) = 0$, which is satisfied at its roots m_0^2s, hence $\lambda_n = 0$, too. Thus, although practically we expanded the effective potential till the order n and we were able to construct the VBF curves all the way till order n, we must find the roots of the nth VBF curve to set the nth coupling to zero, which would imply by construction that $\partial_t \lambda_n \equiv 0$. To make a long story short: we have to solve the following equation

$$\lambda_n(m_0^2) = 0, \tag{3.90}$$

where m_0^2 represents the roots of the VBF curve $\lambda_n(m^2)$. We need to evaluate the other $n-1$ VBF curves at these $m^2 = m_0^2$ points to obtain the value of all the dimensionless couplings at the fixed point, and thus define the truncated effective fixed point potential. So far so good, but let us suppose we find a fixed point potential which is unbounded from below, i.e. defines an unstable theory. That obviously must be wrong, hence we need to bring into play another restriction: since the potential is a polynomial, the asymptotics (i.e. the boundedness from below for large field values) depend on the highest degree term in the polynomial. As a consequence we need to exclude the m_0^2 roots that give $\lambda_{n-1}(m_0^2) < 0$ coupling, which is the coefficient of the highest degree non-zero term in the polynomial expansion.

In general we can sum up all these requirements in the following way. Let us define the set $M = \left\{ m_0^2 \in \mathbb{R} | \lambda_n(m_0^2) = 0 \right\}$. A stable fixed point effective potential can be found by substituting all $m_0^2 \in M$ into the $n-1$ VBF curves $\left\{ \lambda_{n-1}(m^2), \lambda_{n-2}(m^2), ..., \lambda_2(m^2), \lambda_1 \equiv m^2 \right\}$ provided $\lambda_{n-1}(m_0^2) \geq 0$. (If it happens to be zero, too, one need to apply this rule for the VBF $\lambda_{n-2}(m^2)$, and so on). In other words, the set of m_0^2s which defines a true fixed point is

$$M^* = \left\{ m_0^2 \in \mathbb{R} | \lambda_n(m_0^2) = 0 \wedge \lambda_{n-1}(m_0^2) \geq 0 \right\}. \tag{3.91}$$

In the following, some example are presented individually for $D \leq 2$, $2 < D < 4$ and $D \geq 4$, starting with $D \leq 2$.

3.5.2 VBF curves for $D \leq 2$

3.5.2.1 Continuous symmetries ($N \geq 2$)

The Mermin-Wagner theorem essentially states that no spontaneous breaking of continuous symmetry is present in systems of $D \leq 2$. In [66, 79] a numerical evidence was given in the framework of the FRG that the MW theorem indeed holds, here a beyond LPA scheme was used, where the wave function renormalisation was taken into account, too. We have shown in Section 3.4, using analytical considerations, that the MW theorem is not violated even at the LPA level. We will verify the MW theorem for the case of the expanded potential (where this statement cannot be seen directly) by applying the rules that have been settled above. Although the title of this section suggests to include the case of a system with $D = 2$ and $N = 2$, we will perform our analysis using $D = 2$ with $N \geq 3$, since in the former case an infinite order BTK phase transition is present ([97, 98]), as it was mentioned above. To detect this kind of symmetry breaking the LPA is not sensitive enough, as we could see in Section 3.4. However, beyond LPA the BTK phase transition can be observed in the framework of FRG [99–101].

Using Eq. (3.89) for $D = 1$ and $D = 2$ case one can find a simplified expression for the nth coupling

$$\lambda_n \propto (-1)^{n+1} m^2 (1 + m^2)^n \sum_{i=0}^{n-2} g_i(N, D)(m^2)^i. \tag{3.92}$$

Here we only indicated the polynomial structure in m^2, although the prefactors are slightly modified, too. The coefficient functions $g_i(N, D)$ are defined as follows:

$$g_i(N, D) = \sum_{j=0}^{n-2} f_{i,j}(N^\alpha) D^j. \tag{3.93}$$

Interestingly, when setting $D \leq 2$ the finding is that all the g_is are positive for every term, at least till the highest order ($n = 45$), that has been considered in the expansion, this is the observation. This fact suggests that the roots (which are not complex) must be either negative or zero.

Let us find the fixed points according to the rule that has been established in the previous section, using $N = 3$ and $D = 2$. The following VBF curves are found:

$$\begin{aligned}
\lambda_2 &= -\frac{8\pi}{5} m^2(1+m^2)^2, \\
\lambda_3 &= \frac{64\pi^2}{175} m^2(1+m^2)^3(5+27m^2), \\
\lambda_4 &= -\frac{512\pi^3}{7875} m^2(1+m^2)^4\left(25+670m^2+1671(m^2)^2\right), \\
\lambda_5 &= \frac{4096\pi^4}{606375} m^2(1+m^2)^5\left(175+18595m^2+161115(m^2)^2+254799(m^2)^3\right), \\
&\ldots
\end{aligned} \tag{3.94}$$

Considering only the real roots, we can find that they are all situated in the interval $[-1, 0]$. In Fig. 3.5, one can see the plot of the VBF curves versus m^2. The mere fact that we can find roots is against the Mermin-Wagner theorem, because for that to hold true, we should have no roots at all, except at the ending points of the interval $[-1, 0]$.

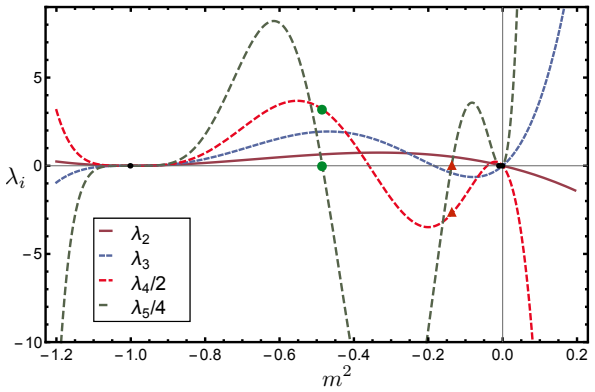

FIGURE 3.5: The VBF curves for the couplings $\lambda_2, \lambda_3, \lambda_4$ and λ_5 in the O(3), $D = 2$ model . Each curve is defined by the vanishing beta functions: $\partial_t m^2 = \partial_t \lambda_2 = \partial_t \lambda_3 = \partial_t \lambda_4 = 0$ respectively. The roots for $\lambda_5(m^2)$ are indicated by black dots. These roots are going to define the fixed point potentials at the truncation level $n = 4$. Two of its roots are indicated by a green dot and a red triangle to demonstrate a valid and a false fixed point, respectively. At the green dot ($m^2 \approx -0.484$) we find that $\lambda_4 > 0$, and evaluating λ_4 at the red triangle ($m^2 = -0.137$) we get $\lambda_4 < 0$, hence defining an unbounded potential, See Fig. 3.6. On λ_4 and on λ_5 a scaling is performed for the sake of the presentation.

We found true fixed point potentials at a finite truncation level according to Fig. 3.5, which should not be there as a consequence of to the MW theorem. The situation is getting worse when we go to higher order in the truncation: indeed, in this case we are going to have more zeros, hence more and more fixed point potentials emerge. How can we resolve this contradiction? One way would be to overcome this situation is that all the roots between -1 and 0 turn into complex valued as we go to higher order. However, from the order of the expansion we used, we cannot put our hope in this. There is another

scenario, too. Let us analyse the VBF curves more carefully. Apparently, one can find a pattern of the roots for the VBF curves: evaluating the λ_{n-1} VBF at each of the roots of λ_n, one will find real numbers alternating in sign starting from the closest root to -1 with $\operatorname{sgn}\lambda_{n-1}(m_1^2) = +1$ (here the 1 in the subscript indicates the closest root of λ_n to -1). For instance in our example in Fig. 3.5 that was $m_1^2 \approx -0.484$ corresponding to the stable potential (Fig. 3.6).

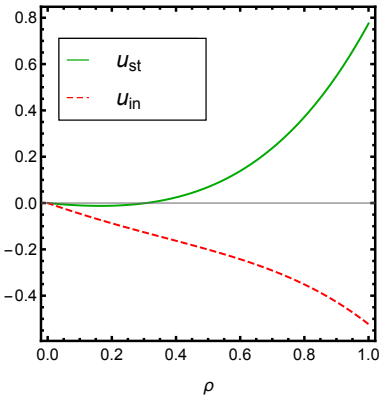

FIGURE 3.6: The fixed point potentials evaluated at the fixed point discussed in Fig. 3.5. A stable potential can be obtained for $m^2 \approx -0.484$ and an instable one for $m^2 = -0.137$, which are indicated on the figure by u_{st}, u_{in}, respectively.

In other words, from the set M defined above, we will consider only $M \setminus \{-1, 0\}$ and the claim is: if we make an ordering from the smallest value to the largest in this set, then every odd element of $M \setminus \{-1, 0\}$ is in the set of $M^* \setminus \{-1, 0\}$, hence for every such element $\lambda_{n-1} > 0$ thus defining a stable potential. So, we are still going to have fixed points even though the number of them is halved by taking into account only the fixed points which define stable potential. It seems that this procedure does not help too much, but, actually, by doing this, we can extract some useful information: each root of the λ_n VBF is surrounded by the roots of the λ_{n-1}, otherwise the alternating signs that was explained above could not be possible. So, it means that by deriving higher and higher order VBF curves the position and the number of roots change in the way that all of the previous roots are around the new ones, see Fig. 3.7. Let us call this interesting pattern of the set of roots the M^* *pattern* for future use. We can do one thing with this without knowing anything about the structure but the root pattern statistics: we can simulate a sequence of sets of points which behave in this way.

Let us consider a randomly generated number X_1 which can take a value in the interval $(-1, 0)$. We generate this number and then we consider two new random numbers: X_2^1 and X_2^2. The first one can take any value in the interval $(-1, X_1)$ and the second in $(X_1, 0)$. After we generate values for X_2^1 and X_2^2, they are going to be the new ending points of the intervals where we define again random numbers but this time three: X_3^1, X_3^2 and X_3^3. We continue this procedure with the random numbers X_n^i with

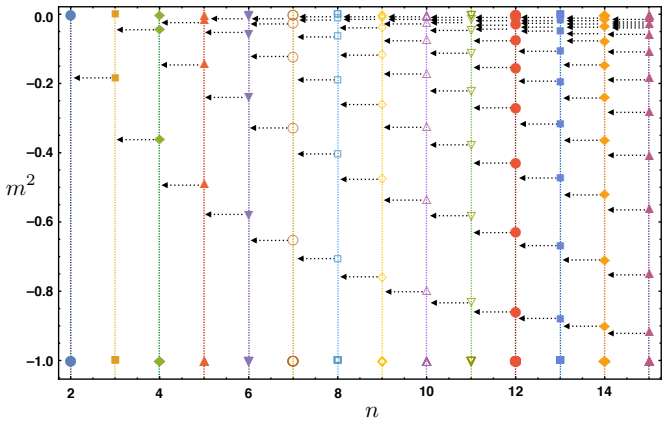

FIGURE 3.7: The roots of the VBF curves $\lambda_2, ..., \lambda_{15}$. Observe the pattern which is given by the following rule: any root of λ_n is between the roots of λ_{n-1} (except for -1 and 0 of course).

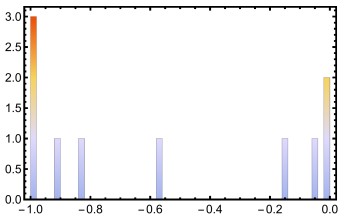

(A) $n = 10$

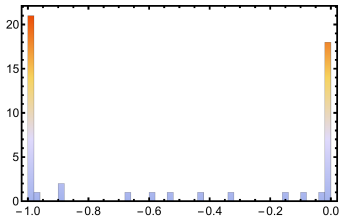

(B) $n = 50$

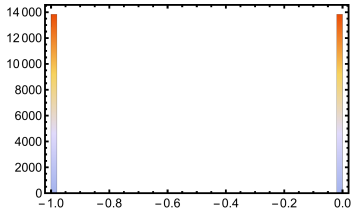

(C) $n = 28000$

FIGURE 3.8: Histograms of the distribution of the points generated in X_n. In the subfigure (A) the distribution of X_{10} in the subfigure (B) the distribution of X_{50} and in the subfigure (C) the distribution of X_{28000} are displayed. Note that the positions of the points are tending to -1 and 0 and at very high n the number of points between the two endpoints is negligible, in other words: the probability of finding a point between the two end points is tending to zero as $n \to \infty$.

$i = 1, 2, ..., n$ and $n \to \infty$, where n indicates that we defined them in the nth step in the interval $(X_{n-1}^{i-1}, X_{n-1}^{i+1})$, including -1 and 0, too. By increasing n we can obtain the distribution of the points created in the way described above; this is shown in Fig. 3.8. From this construction one can see that the distribution of the randomly generated points is changing in a way that they are accumulating at the two ending points of the interval. This suggests that the limit of the probability density for X_n (at least in distributional sense) is:

$$\lim_{n\to\infty} f_{X_n}(x) = \frac{1}{2}(\delta(x+1) + \delta(x)). \tag{3.95}$$

The aim was to simulate the zeros of the VBF polynomials λ_n, and we found that the roots are accumulating at -1 and 0. Thus, if there exists a limit for the VBFs ($\lim_{n\to\infty}\lambda_n = \lambda$), then this will give zero only at -1 and 0, even if this limit is not a continuous function. But this is physically well-justified since this would indicate that we do not find any roots other than the two ending points of the interval, which leads us to the conclusion that no SSB is present in dimensions $D = 2$ with $N = 3$. Indeed, this is a seemingly paradoxical result, namely that we would expect infinitely many number of fixed points as the degree of the VBF polynomials grow, but at the end we will find two actual fixed points defining only one phase, in agreement with the Mermin-Wagner theorem that we wanted to show. We can make another remark on the role of the convexity (or IR) fixed point $m^2 = -1$. From the VBFs one can see that every higher coupling vanishes at this point, i.e. $\lambda_2(-1) = \lambda_3(-1) = ... = 0$, hence the potential, which is defined by this fixed point, is an unstable one, corresponding to the dimensionless potential $u = -\rho^2$. One can now speculate whether this fixed point is a real one or it is just an artefact of the approximations that we use in the FRG. Similar results can be obtained both for the $D = 1$ (see Fig. 3.9). For N dependence and fractional dimensions, see Section 3.5.5 and 3.5.6, respectively.

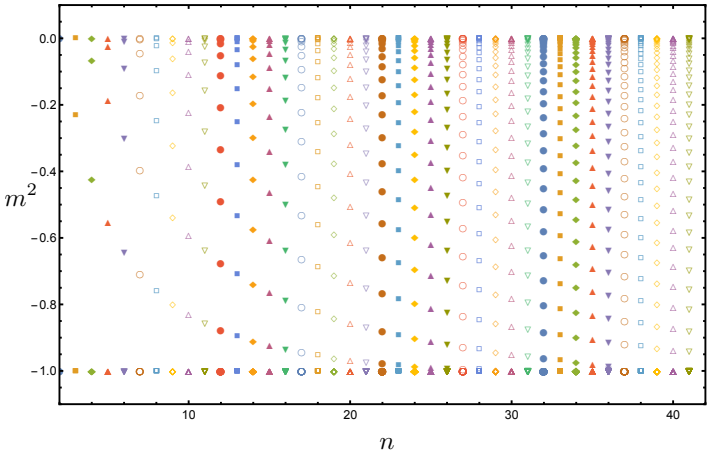

FIGURE 3.9: Roots of a $D = 1$-dimensional theory with $N = 3$ field components. A similar structure can be observed as in Fig. 3.7.

3.5.2.2 $\mathbb{Z}_2$ symmetry ($N = 1$)

In the case of the discrete symmetry the O(N) theory is equivalent to the Ising model, and as the symmetry is being non-continuous, the MW theorem does not necessarily hold for $N = 1$. Indeed, it is well known that in the Ising model we can find a spontaneous symmetry breaking even in the $D = 2$ case, which was carried out in an exact calculation

by Onsager [110]. Here, we are going to see that we can reproduce this result using the technique introduced above.

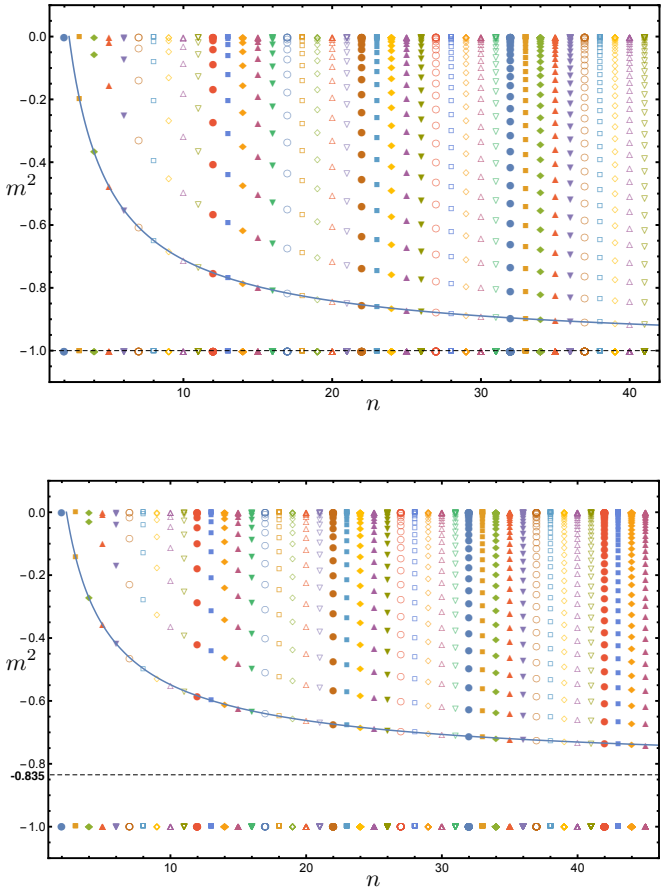

FIGURE 3.10: In the upper (lower) panel the position of the roots of the VBF curves are shown for $N = 1$ in $D = 1$ ($D = 2$). In the one-dimensional case one finds the same pattern that was shown above for $N = 3$ with a convergence to $m^2 = -1$. In two dimensions the roots are converging towards $m^2 = -0.835$ signalling an SSB phase.

In Fig. 3.10 we can see the position of the roots for $D = 1$ and $D = 2$ in a separate plot. The VBF polynomials are described by Eq. (3.92) with different g_i coefficients, of course. We can see qualitative difference between the two figures, namely, in the one-dimensional case, the first root is converging to $m^2 = -1$ and for the two-dimensional case the asymptotic goes to $m^2 = -0.835 \pm 0.001$, defining a threshold for all the roots in higher orders. One can fit a function of the form of $f(x) = a + bx^c$ on the positions of the first roots, with fit parameters $a = -1.00 \pm 0.0002$, $b = 2.08 \pm 0.002$ and $c = 0.85 \pm 0.0006$ in $D = 1$, $a = -0.835 \pm 0.001$, $b = 1.56 \pm 0.004$ and $c = 0.738 \pm 0.003$ in $D = 2$. Now, since the root position pattern is the same as we observed above, we can apply the random number procedure for $D = 1$ in the interval $[-1, 0]$ and for $D = 2$ in the interval $[-0.835, 0]$. The limiting result is the following: in one dimension

the roots are accumulating at $m^2 = -1$ and $m^2 = 0$, thus we can conclude only the stable Gaussian fixed point potential is well defined at the latter. In the case of the two dimensions we will find two fixed points, the Gaussian one ($m^2 = 0$) and another one which is at $m^2 = -0.835$. Now, it is a question whether this fixed point is stable or not. The finding is the following: for every truncation in the present computation (where the highest order was $n = 45$) $\lambda_n(m^2 = -0.835) > 0$, thus we can safely state that it defines a stable fixed point potential, hence indicating a spontaneous symmetry breaking phase. It is interesting that even at LPA level one can observe the SSB for the two-dimensional Ising model contrary to the finding in [43], where even with the numerical spike plot technique [107, 108] it is undetectable, due to its dependence on the numerical precision.

3.5.3 VBF curves for $2 < D < 4$

The O(N) models which belong to the class $2 < D < 4$ have the richest fixed point structure, hence studying them is the most challenging. We are going to perform a detailed analysis for the only integer dimension found in this interval, $D = 3$ restricting ourselves to $N = 2$. We expect here to obtain the well known Wilson-Fisher fixed point in the broken regime, however, we are going to see that there is no clear root structure to be observed for the roots $m^2 > 0$. In this case we have the following generic form for the VBFs in $2 < D < 4$, similarly to the Eq. (3.92)

$$\lambda_n \propto (-1)^{n+1}(m^2)^{1+\Theta(n-4)}(1+m^2)^n \sum_{i=0}^{n-2} g_i(N,D)(m^2)^{i-\Theta(n-4)}. \tag{3.96}$$

Here, $g_i(N, D)$ is defined in a similar way as above in Eq. (3.93), but now, as we can see, the exponent of m^2 has changed, hence in the sum Eq. (3.93) there must be $D^{\alpha(j)}$ rather then D^j, where $\alpha(j)$ represents the remaining exponents, after the prefactor of the sum is factored out. The θ function in the exponent is just the Heaviside step function: $\Theta(n-4) = 1$ if $n \geq 4$ and 0 otherwise. The first few polynomials from the VBFs for $D = 3$ and $N = 2$ are:

$$\begin{aligned}
\lambda_2 &= -3\pi^2 m^2(m^2+1)^2, \\
\lambda_3 &= 3\pi^4 m^2(m^2+1)^3(11m^2+1), \\
\lambda_4 &= -27\pi^6(m^2)^2(m^2+1)^4(23m^2+4), \\
\lambda_5 &= \frac{27\pi^8}{5}(m^2)^2(m^2+1)^5\left(2993(m^2)^2+719m^2+14\right), \\
\lambda_6 &= -\frac{27\pi^{10}}{5}(m^2)^2(m^2+1)^6\left(97167(m^2)^3+27418(m^2)^2+997m^2-14\right), \\
&\ldots
\end{aligned} \tag{3.97}$$

Contrary to the cases of $D \leq 2$, the coefficients g_i can take now negative values, too. From these considerations one can already expect a different root structure from that we had for $D \leq 2$. In Fig. 3.11 we see the VBF curves up to $\lambda_6(m^2)$ and in Fig. 3.12 the root structure up to order $n = 41$. For our analysis we are going to separate the real line of m^2 into three regions. First, we will consider the roots in the interval $[-1, 0]$, then we will turn to the complement set, separately for the intervals $(-\infty, -1)$ and $(0, \infty)$.

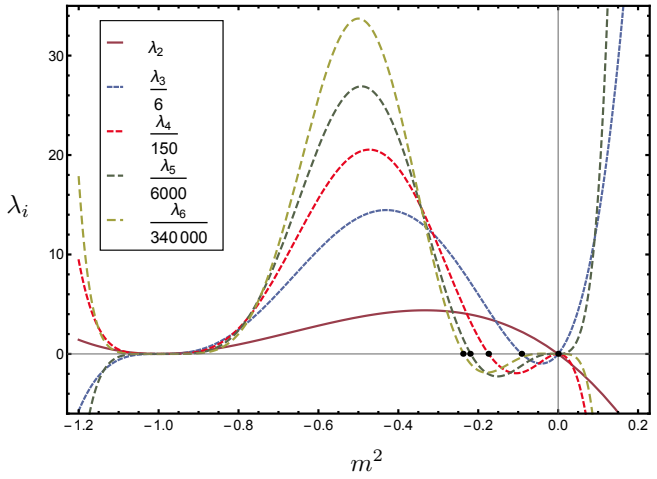

FIGURE 3.11: In this plot the VBFs up to λ_6 are shown for $D = 3$, $N = 2$. For each λ_i the root that is closest to -1 (from above) is indicated with a black dot. Note that, if we consider the position of these points as a sequence then it will converge to a finite value $m^2 = -0.23$, see also in Fig. 3.14.

From Fig. 3.14 it is clear, that in the interval $[-1, 0]$ we have a very similar pattern for the roots (above some n) that we had in the two dimensional case (see Fig. 3.7). However, there is a striking difference between the $D \leq 2$ case and the present $D = 3$ theory: the roots are seemed to be accumulating around the value $m^2 \approx -0.23$, rather than -1. Although this is of course an approximated value, for the sake of simplicity, we will use "equals sign" in the following whenever we consider this value: $m^2 = -0.23$. If one restricts the pattern to the $[-0.23, 0]$ interval, then the random number generating model for the root pattern statistics becomes available again. Since the distribution of the points signals the accumulation at $m^2 = 0$ and $m^2 = -0.23$ the probability density of finding a root in this interval will have the same form as in Eq. (3.95), the only difference is that now the Dirac-deltas now centred at $m^2 = -0.23$ and $m^2 = 0$ rather than $m^2 = -1$ and $m^2 = 0$. We can also check the convergence of the roots by establish an ordering among them: m_1^2, m_2^2 and m_3^2, where the first indicates the root that is the closest, the second is the second closest and the third is the third closest root to $m^2 = -1$ at each order. The root labelled by m_1^2 starts to go towards -1 but at order $n = 6$ it stops and starts to converge to $m^2 = -0.23$ in an oscillatory way.

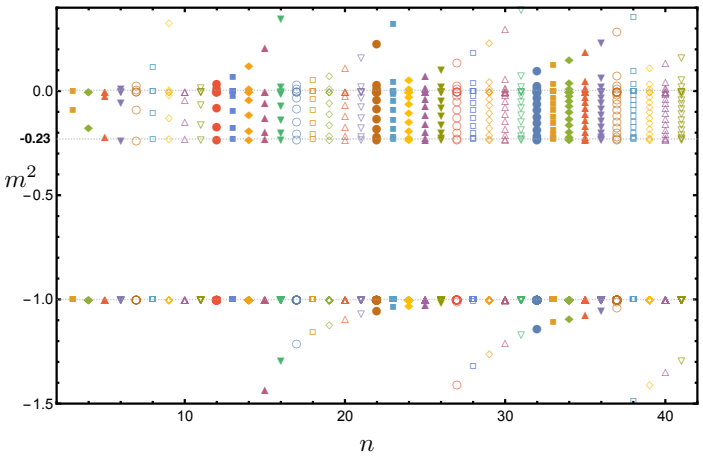

FIGURE 3.12: Here we present the root structure of the VBF curves up to order $n = 41$, in the O(3), D=3 model. Observe that, we can distinguish three regions where the roots are positioned: $m^2 > 0$, $m^2 < -1$ and $m^2 \in [-1, 0]$. For detailed picture see Fig. 3.14.

On the other hand, the roots m_2^2, m_3^2 also converge to this value, and it is possible to fit a curve on them, but this time the fit is an exponentially decaying one, as it can be seen from Fig. 3.14a. The convergence of these roots confirms what we expect from the M^* pattern: the two roots that will remain in this interval for $n \to \infty$ are $m^2 = 0$ and $m^2 = -0.23$, which correspond to the Gaussian and the Wilson-Fisher fixed point, respectively. One needs to check whether the WF fixed point defines a bounded potential. Substituting the value $m^2 = -0.23$ into the VBF polynomials λ_n will give the following result: there are VBF curves for which $\lambda_n(m^2 = -0.23) < 0$ and for which $\lambda_n(m^2 = -0.23) > 0$. This is due to the oscillatory behaviour of the root m_1^2, but we know that this will converge to a finite value, and finally the WF fixed point can be defined as the limit of m_1^2. But until this happens, we will find situations which would give the weird result that the Wilson-Fisher fixed point defines an unbounded potential from below, hence, strictly speaking, we should not consider it as a physical fixed point. This is the case for example with λ_8 and λ_9 (see Fig. 3.13), hence this tells us that there is no Wilson-Fisher fixed point at the truncation level $n = 8$. Even though this is true, we must not forget that the Taylor expansion is an approximation, so the real fixed point structure of the theory will be found when $n \to \infty$, hence the "absence" of the WF fixed point can be considered as an artefact of the expansion.

Let us consider now the region $m^2 < -1$. A magnified picture of it can be seen in Fig. 3.14b. Here, we can observe roots which are running into the convexity fixed point as n grows. The position of the roots would show similar pattern to the M^* pattern, however, here we have difficulties with the unbounded interval $(-\infty, -1]$. We will show how it is possible to overcome such situation in the next section, however, there will be some requirements, which are not fulfiled in the present case.

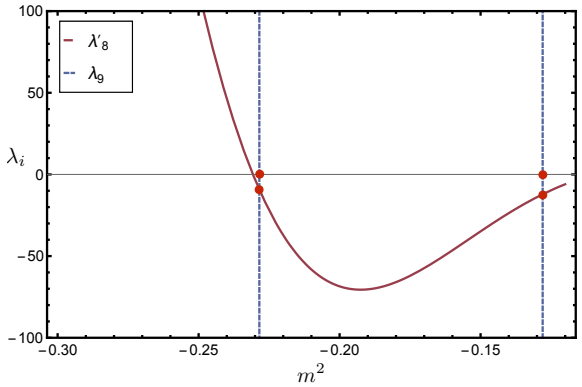

FIGURE 3.13: The absence of the Wilson-Fisher fixed point at the truncation order $n = 8$. We can see that the root of λ_9 to the left define a negative valued $\lambda_8(m^2_{WF})$, which will provide an unphysical potential. Moreover, the second root to the right does not give a sensible potential either. This phenomenon occurs because of the oscillatory nature of m_1^2, but at $n \to \infty$ we expect to see a stable fixed point potential at the WF fixed point. λ_8 has been rescaled with a factor of 2×10^{-7}.

Here, we can only assume that all such roots will converge to $m^2 = -1$ providing us the IR (or convexity) fixed point in the $n \to \infty$ limit. For two of such roots we can show the convergence by doing a fit. Interestingly, in this case the roots are following a different trend to approach -1: the first one is an exponential function $f(x) = a + ce^{b(x-12)}$ with $a = -1.014 \pm 0.005$, $b = -0.39 \pm 0.01$ and $c = -1.43 \pm 0.05$, the second is power law $g(x) = a + c(x - 20)^b$ with $a = -0.885 \pm 0.003$, $b = 1.35 \pm 0.08$ and $c = -7.2 \pm 0.06$. Neither of them goes to -1 precisely, however, these are the best fits that can be found. For large n values, when these roots are very close to -1, they develop an imaginary part, hence they cannot be considered as true fixed points, strictly speaking. One has to go so close to -1 that this effect can be considered as negligible, taking into account that the VBF curves around -1 are extremely flat thanks to the $(1+m^2)^n$ factor in Eq. 3.89. Thus, finding roots around -1 is not always a reliable thing, it might depend on the precision of the root finding algorithm, too.

The remaining region that we need to consider is the half interval $m^2 > 0$. The position of the roots for this region is shown in Fig. 3.14c. One can find again some pattern which could remind us of the M^* pattern, however, in this case beside the fact that the interval is unbounded from above, the roots do not heave a clear bound even from below. The general behaviour of the root positions is that they have the last real value at about $m^2 = 0.01 - 0.02$ (indicated by the red lane in Fig. 3.14c), and below that they will have complex values. Even considering the generated complex roots does not help us to understand this part of the root structure, however, in the case of the four-dimensional O(N) models we can use these complex roots to capture the real physics, as we will see in Section 3.5.4.2.

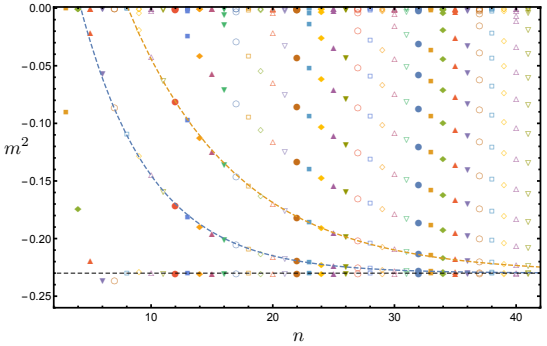

(A) The region $-1 < m^2 < 0$.

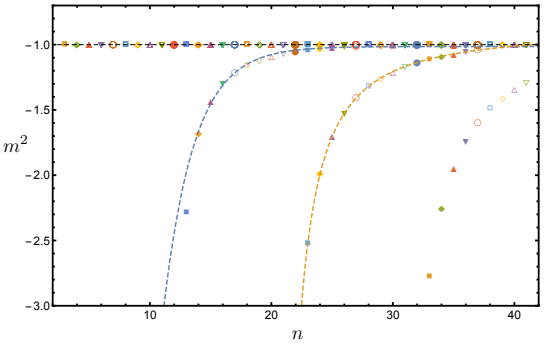

(B) The region $m^2 < -1$.

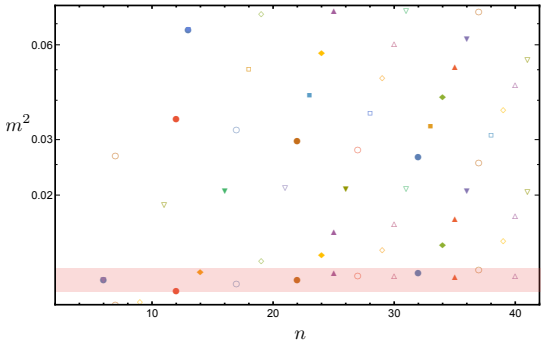

(C) The region $m^2 > 0$

FIGURE 3.14: The root structure of the $D = 3$, $N = 2$ theory separated into different regions. In figure (A) and (B) we can conclude for the $n \to \infty$ limit, that is we will have the following fixed points: Gaussian, Wilson-Fisher and the IR. These suggestions are also confirmed with by functions. Regarding (C) for $m^2 > 0$, no clear answer is found: the red lane indicates the last real root for $m^2 > 0$. For details see the text.

The most important result of this section is the appearance of the Wilson-Fisher fixed point. It may well be possible to find more physical fixed points in other fractal dimensions between two and four dimensions for various N values, but it is beyond the scope of the present study.

3.5.4 VBF curves for $D \geq 4$

So far we considered $D = 1, 2$ and 3. In this section we are going to investigate the theories in $D \geq 4$. Let us look at the first two VBF curves (λ_2 and λ_3) in arbitrary dimensions and field components. We already derived their formula in Section 3.5.1: Eq. (3.85) and Eq. (3.87). Now, we are interested in the roots of the general expressions:

$$\begin{aligned} 0 &= -\frac{2m^2\left(1+m^2\right)^2}{(2+n)A_D}, \\ 0 &= -\frac{2m^2\left(1+m^2\right)^3\left(\mathrm{D}\left(1+m^2\right)(2+N)-4\left(2+N+2m^2(5+N)\right)\right)}{(2+N)^2(4+N)A_D^2}. \end{aligned} \tag{3.98}$$

for λ_2 and λ_3, respectively. The first equation gives zero at $m^2 = -1$ and $m^2 = 0$ independently from the dimension. Among the roots of the second equation in Eq. (3.98) of course we discover again $m^2 = -1$ and $m^2 = 0$, but factorising with respect to these roots, one will be left with the equation for the third root, and it will depend on D. Let us solve it for m^2. The result is the following:

$$m^2 = \frac{-DN - 2D + 4N + 8}{DN + 2D - 8N - 40}. \tag{3.99}$$

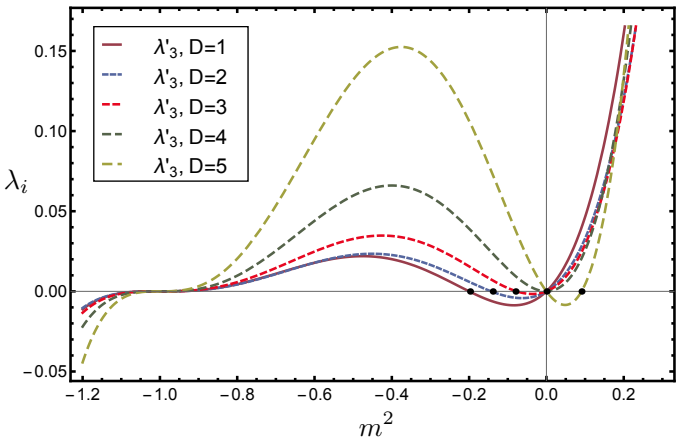

FIGURE 3.15: In this figure one can see how the λ_3 VBF curves change with the dimension. Observe that the only root from the $(-1, 0)$ interval runs into zero as $D \to 4$. For $D \geq 4$ the root obtain a value $m_0^2 > 0$, hence there is no fixed point in the SSB phase but there is one in the symmetric phase, which turns out to be unstable because $\lambda_2(m_0^2) < 0$. Note that, we indicated only integer values for D but the transformation is continuous in the dimension, hence all the values between the integers would define similar curves. For this illustration N was set to 3 and the VBF curves are rescaled as: $\lambda_3' \propto \lambda_3 10^{-\alpha}$, where $\alpha = 0, 4, 4, 5$ and 6 for $D = 1, 2, 3, 4$ and 5, respectively.

This expression shows the "running" of the root (the Wilson-Fisher fixed point) with the dimension. For substituting $D = 1, 2$ and 3 (and $N = 3$), one would get the results that we obtained in the previous sections. However, evaluating it at $D = 4$, we will loose the N dependence completely. In other words: no matter what O(N) model we consider, the WF fixed point coincides with the Gaussian in the $D = 4$ case. In Fig. 3.15 one can see the λ_3 VBF for various dimensions. The observation is the following: the only root in the interval $(-1, 0)$ drifts towards the positive real values. At $D = 4$ it merges into zero, hence, besides the convexity and the Gaussian fixed point, there are no further fixed points present. Above four dimensions the root gets positive values. We can address the question if this is a true fixed point or not. If one substitutes the value of these positive roots into the VBF $\lambda_2(m^2)$, one will immediately see that $\lambda_2(m_0^2) < 0$, thus defining an unstable potential at this truncation level. As a consequence, there are

no any other true fixed points besides the Gaussian and the IR, hence we can call the system trivial. It is possible to derive the dimension dependence for other λ_is, too, with similar qualitative behaviour: the roots start from inside the interval $(-1, 0)$ with $D = 1$ and as the dimension grows, they are tending out from the interval. As D takes the value of 4, the last (i.e. the closest to $m^2 = -1$) root of the VBF under consideration merges into $m^2 = 0$, and all the others have already obtained positive values, see Fig. 3.16, where we illustrate this situation with λ_4.

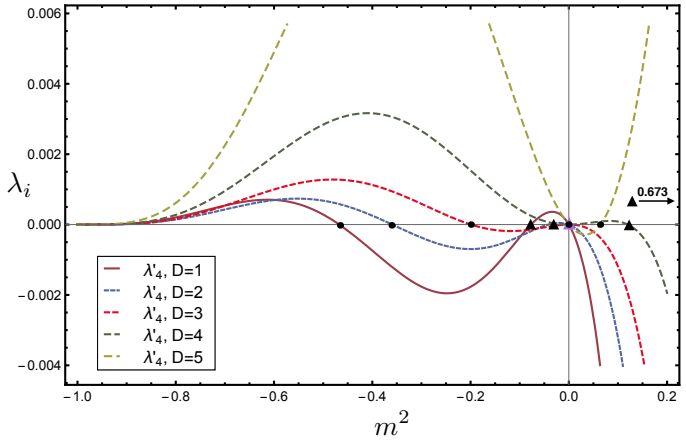

FIGURE 3.16: In this figure one can see the different λ_4 VBF curves for different dimensions. Observe that the two roots from the interval $(-1, 0)$ runs to the right as D grows. For $D = 4$ the root indicated with triangle has got already a positive value and the one which was indicated by a dot, has just melted into zero. For $D = 5$ both of the roots have positive value. The triangle is not present in the plot, since it took the value $m^2 = 0.673$. For this illustration N was set to 3 and the VBF curves are rescaled as: $\lambda'_4 \propto \lambda_4 10^{-\alpha}$, where $\alpha = 5, 6, 7, 8$ and 9 for $D = 1, 2, 3, 4$ and 5, respectively.

In the following, we are going to discuss the VBF curves at a higher truncation level for $D = 5$ in details, as a representative of theories for $D > 4$. However, we need to distinguish the case when $D = 4$, since showing the triviality in this case is not that straightforward as it is for $D > 4$, hence, the four-dimensional case is going to be presented in a separate section. In the last two sections various examples for theories in dimensions $D \geq 4$ are shown.

3.5.4.1 Triviality of the O(N) model in $D > 4$

For any $D > 4$ theories the finding is that the VBF curves has the following structure:

$$\lambda_n \propto (-1)^{n+1}(m^2)(1+m^2)^n \sum_{i=0}^{n-2} g_i(N, D)(m^2)^i. \tag{3.100}$$

Notice that, it has essentially the same structure that we had in the cases $D \leq 2$, but there is one crucial difference. For theories $D \leq 2$ we found the coefficient functions g_is to be always positive, hence defining only negative (and complex) roots for the polynomial, moreover they were inside the interval $(-1, 0)$. In this case likewise to $2 < D < 4$ we can obtain negative values for g_is, too, but contrary to that case, here we do not obtain roots inside the interval (-1,0): all the real roots in this case positioned in the disjoint union of the complement set of (-1,0), i.e. in $(-\infty, -1] \cup [0, \infty)$. The first few VBFs are the following:

$$\begin{aligned}
\lambda_2 &= -24\pi^3 m^2 (m^2+1)^2, \\
\lambda_3 &= \frac{288\pi^6}{7} m^2 (m^2+1)^3 (39m^2 - 5), \\
\lambda_4 &= -\frac{1536\pi^9}{7} m^2 (m^2+1)^4 \left(576(m^2)^2 - 425m^2 + 25\right), \\
\lambda_5 &= \frac{92160\pi^{12}}{539} m^2 (m^2+1)^5 \left(10233(m^2)^3 - 176625(m^2)^2 + 36125m^2 - 1225\right), \\
&\ldots
\end{aligned} \tag{3.101}$$

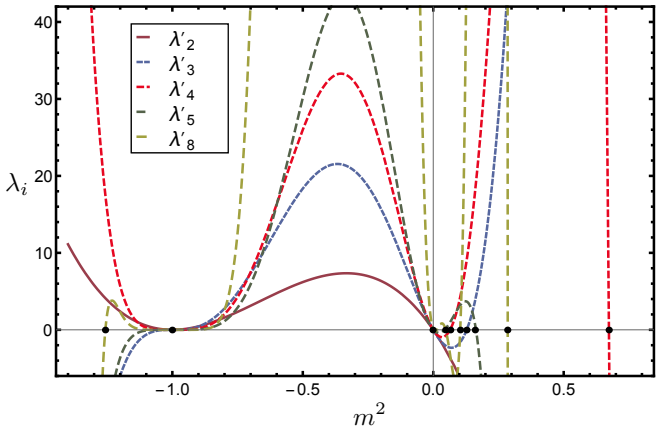

FIGURE 3.17: The VBF curves λ'_i (i=2,...5,8). Observe that the roots of each curve are always outside the interval $(-1, 0)$. For λ_8 we have negative roots, too. For display purposes the VBF curves are rescaled as: $\lambda'_i \propto \lambda_i 10^{-\alpha}$, where $\alpha = 1, 3, 6, 9$ and 19 for $i = 2, 3, 4, 5$ and 8, respectively.

These curves are shown in Fig. 3.17. Now, we are going to analyse their root structure. In the case for theories in $D > 4$ we can clearly identify a pattern of the roots again, just like we did it for $D \leq 2$, i.e. the M^* pattern. For the particular case $D = 5, N = 3$ one can see the position of the VBF roots in Fig. 3.18. What we can observe is just the reverse of what happened in the O(N) models for $D \leq 2$. The roots are situated only outside the interval $(-1, 0)$, and they have a similar pattern to the one we had for the $D \leq 2$ cases, i.e. each root of λ_{n+1} is surrounded by the roots of λ_n.

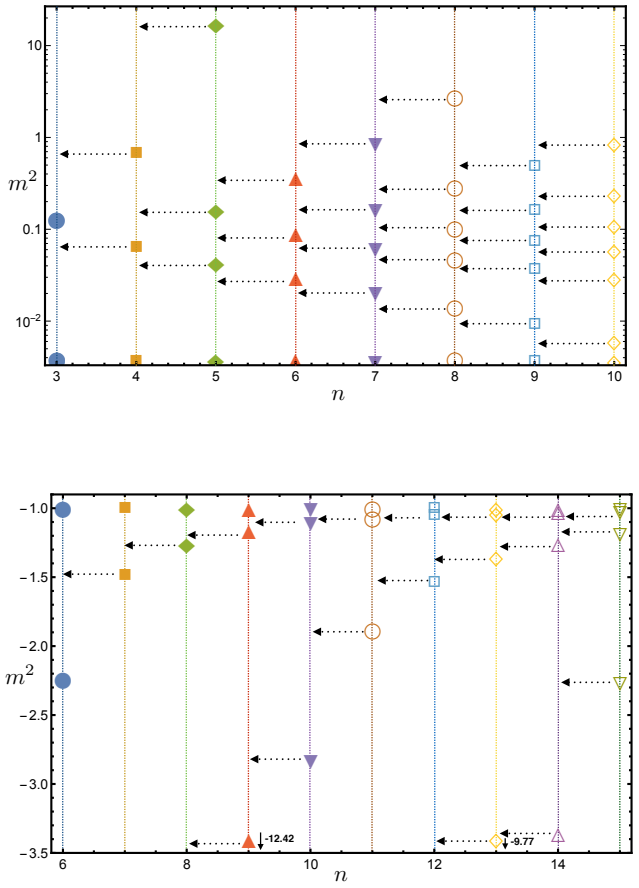

FIGURE 3.18: In the upper (lower) panel the roots of the VBF curves are shown for $\lambda_3, ..., \lambda_{10}$ ($\lambda_6, ..., \lambda_{15}$), for $m^2 \geq 0$ ($m^2 \leq -1$). One can observe a pattern of the roots similar to the $D \leq 2$ case: each root of VBF λ_{n+1} is surrounded by the roots of λ_n. The only problem in this case is, since the interval is unbounded, this pattern is not entirely true: indeed, the highest (lowest) roots of λ_{n+1} now do not have an upper (lower) neighbour from the roots of λ_n. We can overcome this difficulty by one-point compactifying the real line $\mathbb{R}$. For details see the text.

We can call it only similar, since we clearly have a problem in the present case: we are not able to use our random number generating model that we did in Section 3.5.2 for simulating the positions of the roots, because the set $(-\infty, -1] \cup [0, \infty)$ is unbounded. For that reason, the highest (lowest) roots of the VBF λ_{n+1} do not have an upper (lower) neighbour from the set of the roots of the VBF λ_n. However, we are able to do the following trick: let us one-point compactify the real line $\mathbb{R}$, meaning that we "glue" together the points $m^2 \to \pm\infty$, thus creating a closed set for $[0, -1]$. This may look an *ad hoc* idea but we will see that it works. Let us consider for instance the order $n = 6$ and $n = 7$ in Fig. 3.18. The highest valued root in the region $m^2 > 0$ from $n = 7$ would need a root from $n = 6$ to restore the right pattern, but apparently there is no such root.

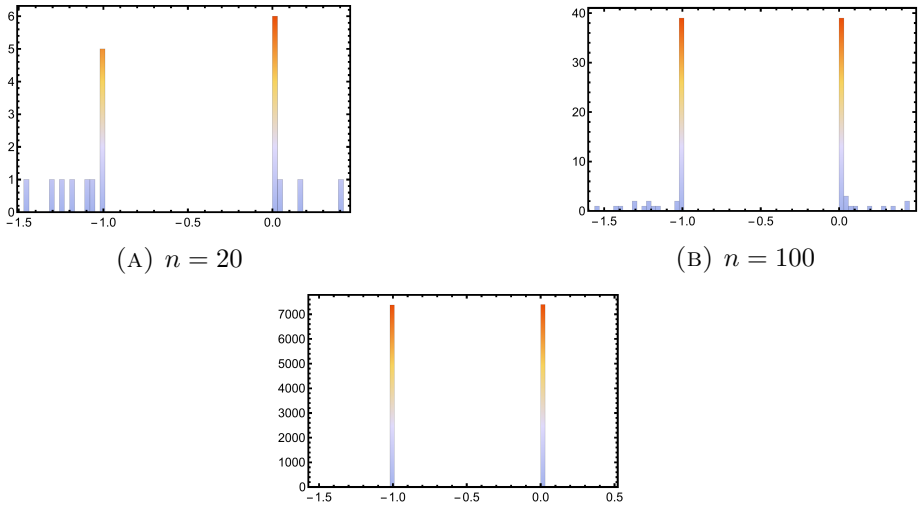

(A) $n = 20$ (B) $n = 100$

(C) $n = 15000$

FIGURE 3.19: Histograms of the distribution of the points generated in X_n. On the subfigure (A) the distribution of X_{20} on the subfigure (B) the distribution of X_{100} and on the subfigure (C) the distribution of X_{15000} are displayed. Observe that the points are accumulating at -1 and 0 but this time from the outside region.

However, if we extend our picture with the compactified real line, we will see that in the region $m^2 < -1$ the right root appears just where we would need it at order $n = 6$, and thus the pattern goes on. This is true for all the other roots (see Fig. 3.18), thus the compactification of the real line is well justified in this way, hence providing us an M^* pattern on the compactified real line. In the interval [0,-1] one can now use the technique that we introduced in Section 3.5.2. The result of such kind of random number procedure is shown in Fig. 3.19.

We can see that the position of the roots are again accumulating at -1 and 0, but now they are approaching from the complement interval of $(-1, 0)$. In this way we can see how the triviality is emerging in the limit $n \to \infty$.

3.5.4.2 Triviality of the O(N) model in $D = 4$

In this section we are going to discuss the $D = 4$ O(N) models, and a special attention will be given to the case $N = 1$, which has been in the centre of interest since triviality is predicted to occur in the ϕ^4 theory. To have a clue on triviality beyond PT we still need to rely on lattice simulations, which actually support the trivial behaviour of such theories [111]. Here, we are going to show a result which suggests that indeed the trivial scenario holds for such models, i.e. no UV fixed point different from the Gaussian is present in the O(N) models taking into account all the symmetry respecting terms in four dimensions (the ϕ^4 case is shown in Fig. 3.15). We are going to present the result

for $N = 1$ but this holds for general N. The VBF polynomials in $D = 4$ have the form:

$$\lambda_n \propto (-1)^{n+1}(m^2)^{1+\Theta(n-3)}(1+m^2)^n \sum_{i=0}^{n-2} g_i(N, D=4)(m^2)^{i-\Theta(n-3)}. \tag{3.102}$$

In particular the first few λ_i for $N = 1$:

$$\begin{aligned}
\lambda_2 &= -\frac{64\pi^2}{3} m^2(m^2+1)^2, \\
\lambda_3 &= \frac{8192\pi^4}{5}(m^2)^2(m^2+1)^3, \\
\lambda_4 &= -\frac{524288\pi^6}{35}(m^2)^2(m^2+1)^4(14m^2-1), \\
\lambda_5 &= \frac{67108864\pi^8}{315}(m^2)^2(m^2+1)^5\left(168(m^2)^2-41m^2+1\right), \\
&\ldots
\end{aligned} \tag{3.103}$$

By analysing the root structure of these equations one will find that all the roots are situated outside the interval of $(-1, 0)$ likewise in the $D > 4$ cases, the only difference is that at the order $n = 7$ the VBF curve λ_7 develops a roots on the complex plane, too, with Re $m^2 > 0$. We have already met such situation in theories defined in $2 < D < 4$ dimensions. In that case, we neglected these roots since we considered them as unphysical. In the present case we still stick to our convention, that is we neglect them as possible fixed point candidates, however we can identify an interesting behaviour for such nonreal roots. Let us look at the root structure of the theory in Fig. 3.21, where we present the position of the real roots for all relevant intervals of m^2.

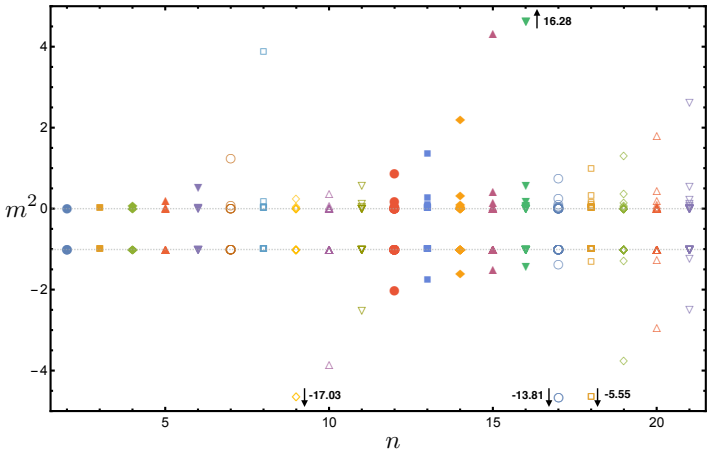

FIGURE 3.20: The real roots of the four-dimensional O(N) model are shown. No root in the interval (-1,0) is found, contrary: all roots are outside this interval. One can see that, just like in the case of the $D > 4$, the roots are approaching -1 and 0 from the outside region. However, more careful analysis is needed in this case. For details see the text.

What we can observe is that the roots are approaching the points -1 and 0, just like in the case for $D > 4$. However, as we indicated above, complex roots are emerging: the first one and its conjugate from $n = 7$, two and their conjugates from $n = 11$, three and the conjugates from $n = 15$ and from $n = 18$ four complex roots plus conjugates. Among these roots, being complex, we cannot make an ordering, however we are able to do that for the real part of them. The real part of the roots are indicated in Fig. 3.21, complex roots with negative real parts does not occur, hence it is enough to consider the Re $m^2 > 0$.

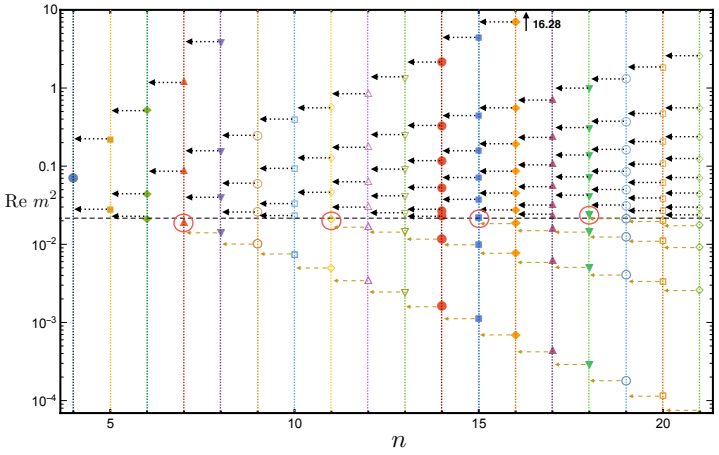

FIGURE 3.21: The real part of the roots. The black dashed line indicates the average threshold between the purely real and complex root values. It is at about $m^2 = 0.022$. For every value of Re m^2 under this line we have an imaginary part for the root. New complex roots are emerging at order $n = 7$, $n = 11$, $n = 15$ and $n = 18$. At these orders we can see a "violation of the pattern" which is being indicated by the arrows: pointed black arrows for the purely real and dashed gold for the complex roots. Apart from the newly emerging complex roots the pattern holds. For details see the text.

The figure shows, that for the real part of the roots, there is indeed a pattern, namely almost the same that we observed both for the cases $D \leq 2$ and $D > 4$, the only differences are in the orders where the complex roots appear. Here, we observe that above and below the real part of the newly appearing complex roots the pattern continues, only at those particular points we find the breaking of the pattern (these are indicated by red circle in Fig. 3.21): no root from real part of the λ_{n+1} goes between the corresponding roots of λ_n. Now, if we consider the limiting distribution of such pattern of the points, we will find that this anomaly will not have an effect on it: after compactification of the real line, as we did it for the $D > 4$, the points are just accumulating at -1 and 0, hence we will find exactly the same result as in Eq. (3.95), but now only for the real part of m^2. We are not done yet, since we have only considered the real part so far. This result on the limiting position of the roots does not make any sense if we find a finite imaginary part of m^2 in this limit. Let us consider therefore the roots on the complex plane. This

is shown in Fig. 3.22. We can see the developing imaginary part at the order $n = 7$ for the first time.

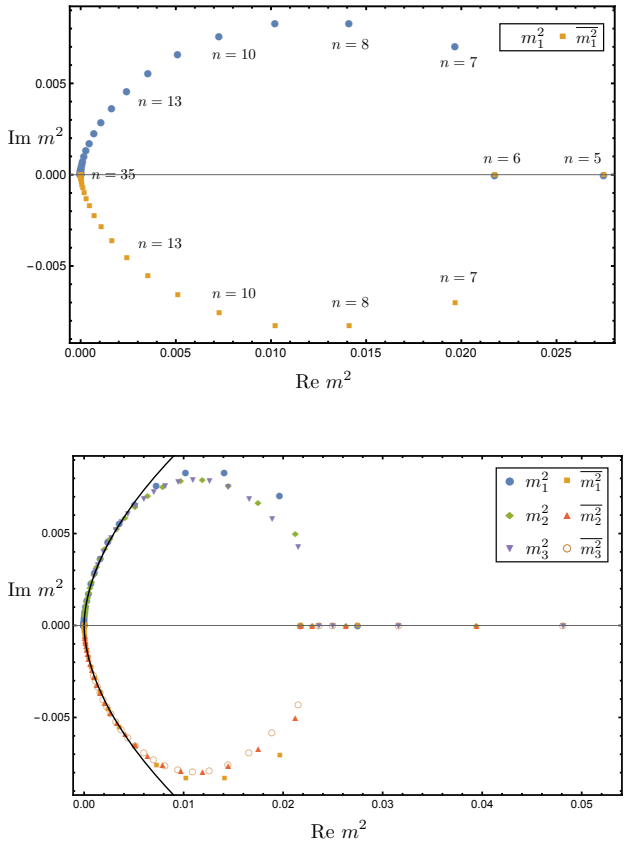

FIGURE 3.22: The roots on the complex plane. In the upper panel one can see the emergence and disappearance of the first complex root (m_1^2). It appears at $n = 7$ and tends to zero as we go higher orders in n. In the lower panel the second and third complex roots are indicated (m_2^2 and m_3^2). They appear at order $n = 11$ and $n = 15$ respectively, and coincide with the curve defined by the complex root m_1^2. The fitted power law curves are defined in the text, and the fitting procedure was performed on 24 data points.

Interestingly, the absolute value of the imaginary part will have a maximum at some point and it is tending to zero just like the real part. We can also express the imaginary part as a power law of the real part close to the origin: Im $m^2 = \pm a(\text{Re } m^2)^b$, where the parameters are $a = 0.162 \pm 0.001$ and $b = 0.589 \pm 0.001$. Now, considering the "running" of the second and the third complex root (m_2^2, m_3^2), which are appearing first at the order $n = 11$ and $n = 18$, respectively, we will find that they behave in a very similar way to the first complex root (m_1^2), moreover, they collapse onto each other close to the origin (see Fig. 3.22), thus approaching 0 with the same exponent. We can see that both the real and the imaginary parts of the roots are approaching zero as the order n grows, hence we can say that the roots, although they are not defined as physical ones when they have complex values, accumulating at -1 and 0 in the $n \to \infty$ limit. It is

interesting that only in the limit the imaginary part is absent entirely, and until we take this limit we will have a gap between $m^2 = 0$ and the last noncomplex valued root in the particular order n. With this procedure we were able to show that only two fixed points are present (with the Gaussian as the only stable one) in the unexpanded O(N) model just like in $D > 4$. Altogether this signals the triviality for the O(N) theories when the dimension is $D \geq 4$. Hence, we were able to show a non-perturbative evidence of the triviality for theories defined in $D \geq 4$.
Regarding to the $D = 3$ case, in Section 3.5.3, the roots on the complex plane does not behave in a way they do in the four-dimensional case (Fig. 3.22), hence we cannot obtain the distribution of the roots by using the random number generating algorithm for the compactified M^* pattern.

3.5.5 The N dependence and the large-N limit

In this section we are going show the effect of changing the number of fields, i.e. N, for particular dimensions. For large-N the RG equation of the effective potential was provided in Eq. (3.79). From this equation one can derive the VBF curves with the usual steps just the N dependence is absent from the formula Eq. (3.89). We cannot show of course the full N dependence, these are only a few checks for particular values of N. One should derive the root structure for each N independently. However, these few examples could give us some ideas what is going on when N is changed.

3.5.5.1 N dependence for O(N) theories in $D \leq 2$

Let us consider three different two-dimensional theories with field components $N = 7$ and $N = 15$ and $N \to \infty$. The position of their roots are shown in Fig. 3.23. We can see in the two finite N cases that there seems to be a problem in the low orders of the expansion: the position of the roots will not satisfy the requirement of the M^* pattern, however, as the order grows the pattern restores.

We need to mention that when a particular root gets very close to -1 in the next order sometimes it becomes complex, but its real part still stays around -1, hence one cannot see this accumulation exactly, but rather we can say this root "melted" into -1. This might be related to the fact what we already explained for the $D = 3$ case: the VBF polynomials get extremely flat close to -1 because of the $(1+m^2)^n$ factor in Eq. (3.89), hence it could mean some problem for the root finding algorithm to provide the right value. One way or another, a complex root does not define a physically sensible theory, thus we can still look at this pattern which will provide Eq. (3.95) as the probability density of the root positions when $n \to \infty$. However, no complex roots occur for the

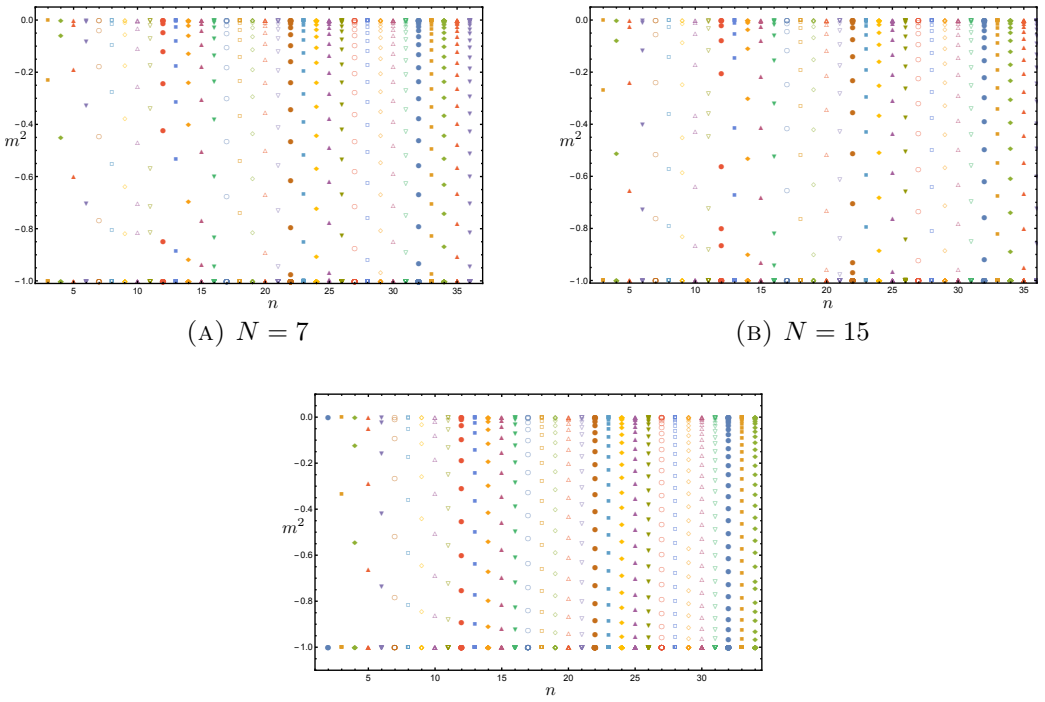

(A) $N = 7$ (B) $N = 15$

(C) $N \to \infty$

FIGURE 3.23: The N dependence of the root positions in $D = 2$. We can see that the M^* pattern restores at larger order of the expansion for various N. Sometimes one will find complex roots close to -1 which can be considered as unphysical. In this way it does not actually matter if we consider the limit of the distribution of the roots or it gets complex providing an unphysical situation. When the $n \to \infty$ limit is taken the only two roots that can be found is -1 and 0. In the large-N limit no complex valued root has been found till the order $n = 34$.

large-N case where, we know that there must be only the symmetric phase present, as it was proven analytically in Section 3.4 in the framework of FRG. The fact that a root gets complex or accumulates at one of the stable fixed points $-1, 0$ is irrelevant from the point of view of the physics: in both of the cases only -1 and 0 survive when $n \to \infty$. For $D = 1$ we can find similar results. These were, of course, only a few checks on the N dependence and it should be considered case by case for every N, however, from our experience we could assume that in the $n \to \infty$ roots inside the interval $(-1, 0)$ either get complex or they are arbitrarily close to -1 or 0 for any field component N.

3.5.5.2 N dependence in $2 < D < 4$

In dimensions $2 < D < 4$ for finite N we will get a very similar result to the one which we obtained in Section 3.5.3. For these values of the dimension, one has the richest fixed point structure of all, hence it should be checked case by case. However, here we will only focus on the integer valued dimension $D = 3$. For the large-N in $D = 3$ the position of the VBF roots show a significant difference comparing them to the finite N

(compare Fig. 3.24 and Fig. 3.12). Here, we can identify the Wilson-Fisher just as we did it in Section 3.5.3, but in this case we cannot see the additional "fake" fixed points at any truncation level. Also for the $m^2 > 0$ roots we can see differences: they start to be organised in the pattern which leads us to the distribution found in Section 3.5.2, Eq. (3.95). In this case it is also remarkable that no complex roots are found unlike for finite N.

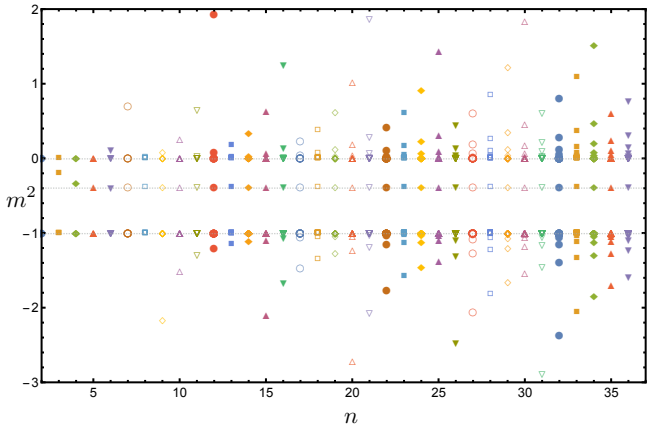

FIGURE 3.24: The roots of the VBF in $D = 3$, $N \to \infty$ are shown. Comparing it to Fig. 3.12 the most striking difference is that there are no "fake" roots between the root which is indicating the Wilson-Fisher ($m^2 = -0.388$) and the one which is for the Gaussian, i.e. $m^2 = 0$. It is equally interesting that in this case we do not find any threshold which after the roots become complex in the $m^2 > 0$ region.

3.5.5.3 N dependence in $D \geq 4$

One of the most important result for theories $D \geq 4$ was the triviality (Section 3.5.4). Our finding is that the modification of the number of the field components N does not give any qualitatively different result for any such theory, when N kept finite. However, we can discover differences between the results when $N < \infty$ and $N \to \infty$ for theories in $D > 4$.

In four dimensions we will see the "compactified" M^* pattern of the real part of the roots as in Fig. 3.21. The only question is wether the convergence on the complex plane towards the origin still holds. We present the results in Fig. 3.25, for $N = 4$, $N = 15$, $N = 40$ and $N \to \infty$. We can observe that the convergence to the origin slows down as N grows, however, for the $N < \infty$ cases, it is possible to fit a curve on them near the origin. The same form of the power law is found for each N, that is $f(x) = ax^b$, just like in the case of $N = 1$ in Section 3.5.4. The parameters are the following $a = 0.193 \pm 0.001$, $b = 0.587 \pm 0.002$ for $N = 4$, $a = 0.249 \pm 0.002$, $b = 0.586 \pm 0.002$ for $N = 15$ and $a = 0.302 \pm 0.006$, $b = 0.584 \pm 0.004$ for $N = 40$.

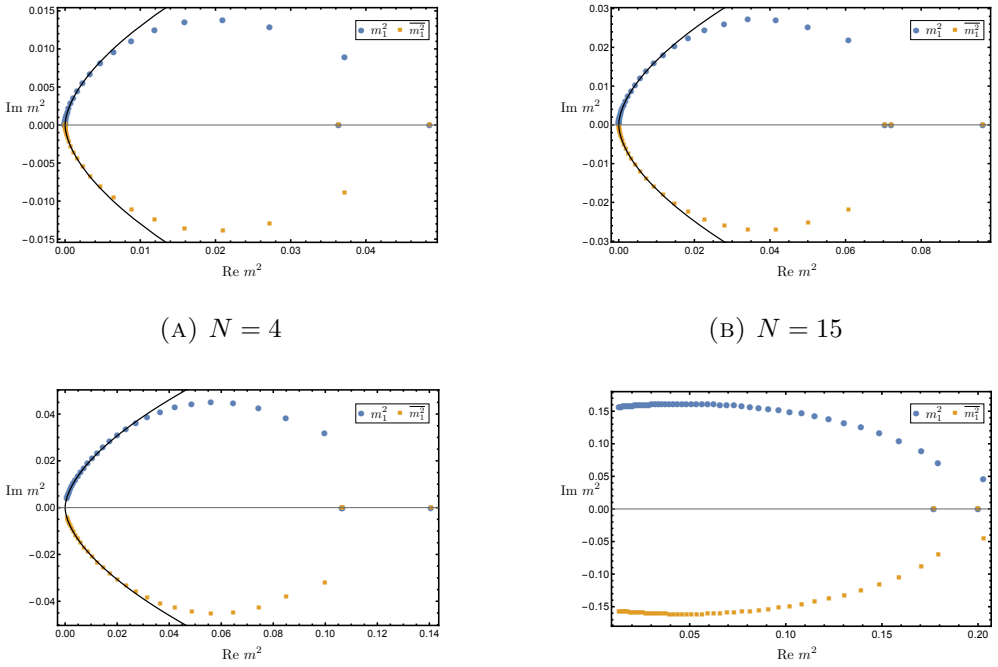

(A) $N = 4$ (B) $N = 15$

(C) $N = 40$ (D) $N \to \infty$

FIGURE 3.25: The convergence to the origin on the complex plane is shown for (A) $N = 4$, (B) $N = 15$ and (C) $N = 40$. On the figure (D) the $N \to \infty$ presented, in this case the number of the data points is not enough to fit a curve on the points near the origin (the expansion order in this case $n = 53$, for the finite N cases $n = 35$). However, the same behaviour is expected: the convergence to the origin slows down as N grows. For the finite N cases a power law fit can be found around the origin (the fit was performed on 24 data points), which exponent seems to be universal. For details see the text.

It is interesting that close to the origin the exponent of the power law seems to take the value 0.586 ± 0.002, and thus one can speculate wether it is universal. Regarding the $N \to \infty$ case, we did not reach the region where we could do the fit, however, the absolute value of the imaginary part reached its maximum and started to decrease. We expect the same behaviour (maybe with different exponent) as for the finite N cases, however, to see that we would need to go to a higher expansion order than that was used in this case ($n = 53$).

For theories in greater than four dimensions the fixed point structure does not change much comparing to the results of Section 3.5.4, only quantitative differences can be observed. We will present a few plots on the roots positions in Fig. 3.26. Arbitrarily we have chosen the cases $\{D = 5, N = 6\}$, $\{D = 8, N = 10\}$ and $\{D = 11, N = 12\}$. The roots are positioned in a way that they accumulate more and more at the two stable roots -1 and 0, which is essential for triviality. There can be minor deviation from the pattern M^*, however, at some point the pattern restores completely, and one can obtain the triviality in a way we did it for the case $D = 5$, $N = 1$.

More interesting case, that can be found, is in the large-N limit. From Eq. (3.79) one can derive again the VBF curves in $D > 4$. In the present section we are going to study only the $D = 5$ theory for the large-N limit. In Fig. 3.27 one can see the root positions for this model. The first thing that we can notice, there is a stable line at $m^2 = 0.139$ which would signal a new fixed point solution. There has been a recent work ([53]) on the topic, wether such fixed point exist in models $4 < D < 6$ and the answer was that, if there is such fixed point it will provide an unphysical fixed point potential. In an earlier work [112] related to holography a similar conclusion was drawn. In the papers [52] an IR fixed point was found for an O(N) symmetric theory with $N+1$ scalars in $D = 6-\epsilon$ for sufficiently large N, including a cubic interaction, too. It was argued that this IR fixed point of the cubic O(N) theory with $N+1$ scalars is equivalent to a UV fixed point of the O(N) model in the large-N, which would imply an unexpected asymptotically safe behaviour of such theories. Now, since we have found such a fixed point, we need to check whether it gives a stable fixed point potential. Substituting the value $m^2 = 0.139$

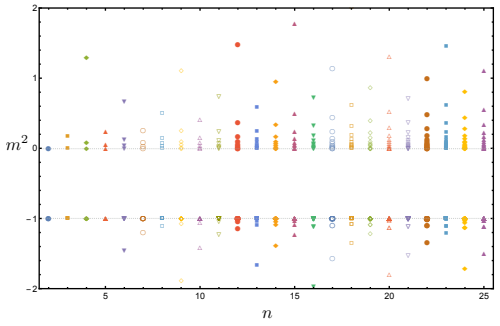

(A) $D = 5$, $N = 6$

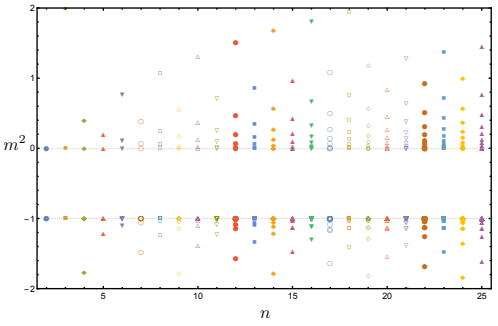

(B) $D = 8$, $N = 10$

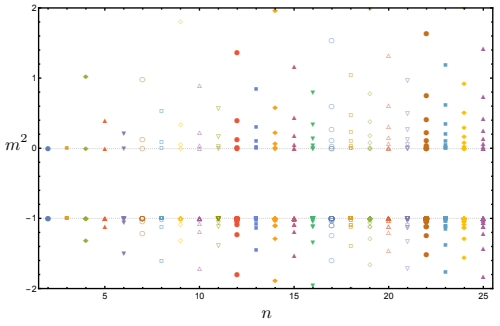

(C) $D = 11$, $N = 12$

FIGURE 3.26: The VBF roots of the O(N) model: (A) in $D = 5$ and $N = 6$, (B) $D = 8$ and $N = 10$, (C) $D = 11$ and $N = 12$. On each plot the accumulation of the roots at $m^2 = -1$ and $m^2 = 0$ can be observed. For the roots $m^2 < -1$ there can be small deviation from the M^* pattern (most likely due to the extreme flatness of the VBFs around -1), but at some point the pattern restores completely.

into the VBF polynomials will provide the exact value for the corresponding coupling at that fixed point, hence defining the fixed point potential. The finding is the following: the highest order in the expansion is $n = 46$, and what we get is $\lambda_n(m^2 = 0.139) \leq 0$ for $2 \leq n \leq 46$. This signals that the fixed point potential defined by this root is unbounded from below in agreement with the findings in [53]. However, a further study is needed to investigate the existence of such fixed point in $4 < D < 6$ at finite N using approximations beyond LPA. In Fig. 3.27 one can also observe that there is a gap between the root corresponding for this newly found unstable fixed point, which can be filled in by considering the real part of the roots. In the same figure considering the lower panel, we can see how the real part of such roots behave. We can fit a power law decaying curve again on the real part of the first root. This curve goes through on the line $m^2 = 0.139$ and in the asymptotic limit goes to zero. The imaginary part behaves pretty much in the same way as in $D = 4$ case (see Fig. 3.25). Here, we can use the same argument as for $D = 4$, $N = 1$: one needs to consider the positions of the roots on the complex plane in order to catch the physics behind. According to our findings, the real part of these roots exhibit the same M^* pattern, hence for $n \to \infty$ we can expect them to accumulate at $m^2 = 0$, leaving us with three fixed points, which are defined by the roots: $m^2 = -1$ (since for $m^2 < -1$ the root structure is the same as it was for the finite N case), $m^2 = 0$ and $m^2 = 0.139$. Out of these three roots only the Gaussian ($m^2 = 0$) seems to provide a stable fixed point potential, thus triviality was found again.

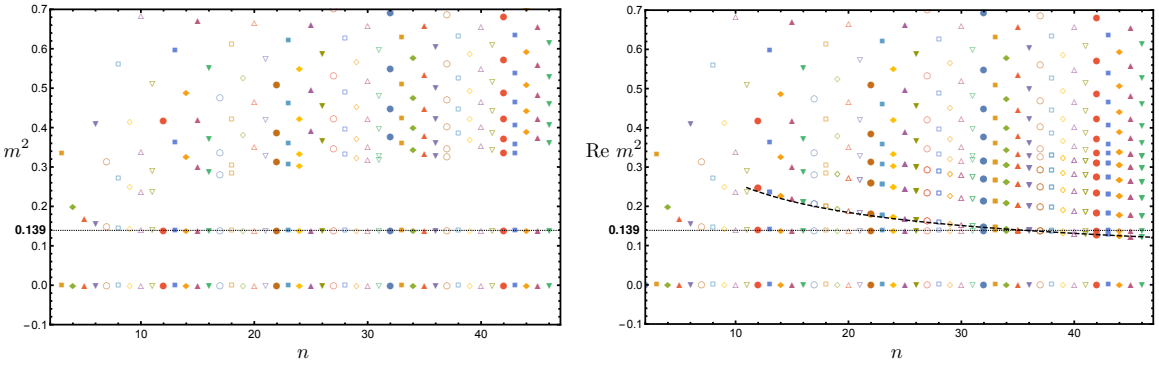

FIGURE 3.27: In the left panel the root structure provided by the real roots are shown. A stable line of the roots can be observed at the value $m^2 = 0.139$. In the right panel the same root structure is shown, but now the real part of the complex roots has been taken into account, too. The real part of the complex roots show the M^* pattern, and also a power law curve can be fitted on them: $f(x) = ax^b$, with $a = 0.807 \pm 0.005$ and $b = -0.492 \pm 0.002$. In the $n \to \infty$ we expect to find triviality again. For details see the text.

3.5.6 The fractal dimensions

We will present a few example on the fractal-dimensional cases in the intervals of the dimension that we have investigated. In Fig. 3.28 the results are shown for $\{D = 1.3, N = 1\}$, $\{D = 2.6, N = 1\}$, $\{D = 3.1, N = 1\}$ and $\{D = 4.6, N \to \infty\}$. In the first three cases the usual fixed points are found, however it, could be possible to find additional fixed points for $2 < D < 4$, but that would require a more detailed study of this interval of the dimension. For the two D values, which are in this interval, we found the WF fixed point, too, and it can be observed that they are situated at different values of m^2: for $D = 2.6$ $m^2_{WF} = -0.34$ and for $D = 3.1$ it oscillates around $m^2_{WF} = -0.16$. The most remarkable case is when we set $N \to \infty$ and choose $D = 4.6 \in (4, 6)$. Just as we saw it for the large-N in $D = 5$, here, we find again a fixed point candidate at the value $m^2 = 0.108$. However, again in agreement with [53], this fixed point found to be an unphysical one, i.e. the root $m^2 = 0.108$ defines an unstable fixed point potential. (More precisely, it is a metastabe potential.)

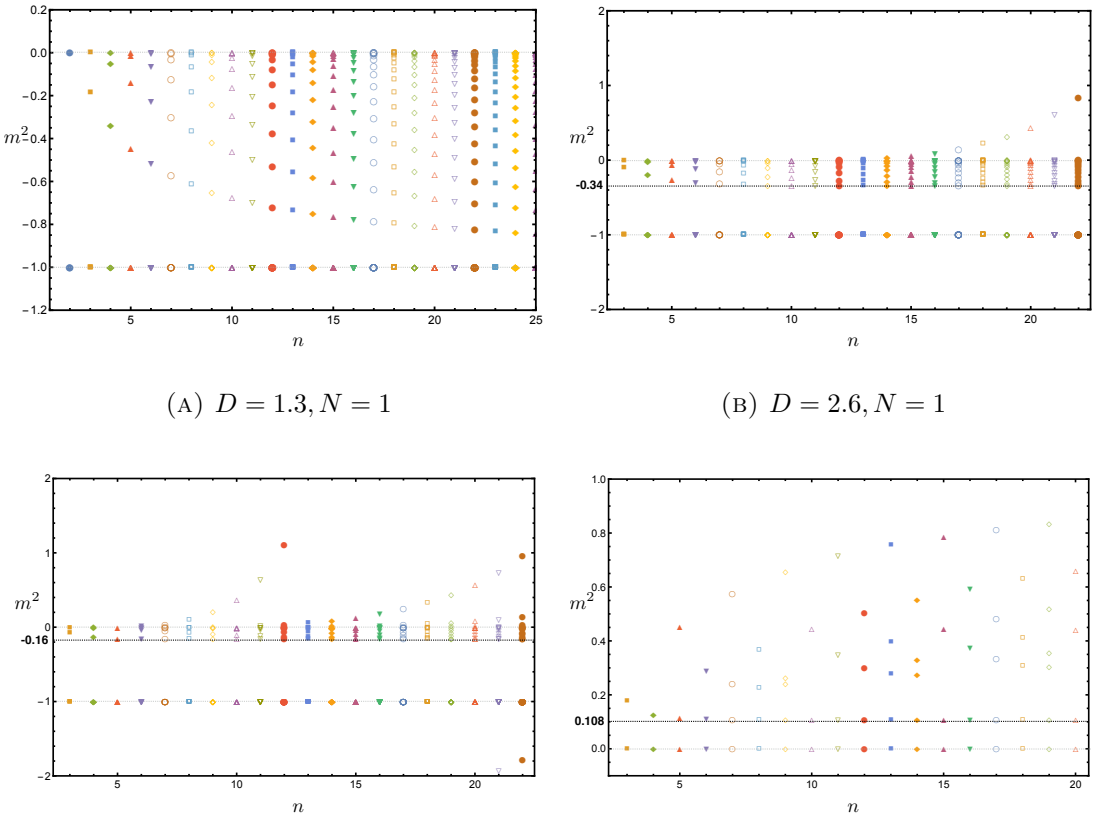

(A) $D = 1.3, N = 1$

(B) $D = 2.6, N = 1$

(C) $D = 3.1, N = 1$

(D) $D = 4.6, N \to \infty$

FIGURE 3.28: The root structure is shown for some fractal-dimensional cases. The usual fixed points are found for $4 < D$, thus the most remarkable is figure (D), where we obtain a fixed point candidate for $D = 4.6$ in the large-N. However, it turned out to define an unstable fixed point potential just like it is shown in [53].

3.6 Chapter summary

In this chapter we studied the phase and fixed point structure of the O(N) model in the framework of FRG. After a short introduction was given, we examined the fixed point equation on the LPA level using analytical considerations. In Section 3.4 we showed that the LPA fixed point equation for the effective potential gives qualitatively correct results regarding the existence of SSB phase. For systems with continuous symmetry ($N \geq 2$) LPA gives no SSB for $D \leq 2$ and shows SSB for $D > 2$ in agreement with the Mermin-Wagner theorem and its extension to systems with fractional dimension. In particular, simple analytical expressions are found in the large-N limit, correctly retrieving the expected results for the spherical model. However, from the analytical study did not turn out what is the situation in the case of the discrete symmetry, i.e. for the Ising model. The answer to that question was given in the subsequent section.
In Section 3.5 we investigated the fixed point structure of the O(N) model for various dimensions an filed components. For our analysis we used the LPA again with a Taylor-expanded potential around zero VEV of the field. In this case from the fixed point equation one is able to express all the fixed point couplings through a polynomial in the mass of the theory, see Eq. (3.89). Each nth polynomial is obtained from the fixed point equation of the $(n+1)$th coupling, that is the equation for $\partial_t \lambda_{n+1}(\lambda_n, m^2) = 0$ can be solved for $\lambda_n = \lambda_n(m^2)$, hence the name VBF (Vanishing Beta Function) curve. A general property of these polynomials is that they have always a root at $m^2 = -1$ and $m^2 = 0$ corresponding to the convexity (or IR) and the Gaussian fixed point, respectively. These polynomials can be obtained for arbitrarily components of the field N and dimension D. To find a true fixed point at a given level of truncation, we established the following rule: let m_0^2 be a root of the polynomial $\lambda_n(m^2)$, then a physically well defined (i.e. bounded from below) fixed point potential is given by the set of couplings $\{\lambda_{n-1}(m_0^2), \lambda_{n-2}(m_0^2), ..., \lambda_1(m_0^2) = m_0^2\}$, provided $\lambda_{n-1}(m_0^2) \geq 0$ (if it happens to be a root for the $(n-1)$th polynomial, too, then the same rule holds for the $(n-2)$th polynomial, and so on). Using this rule to find fixed points at a truncation level n gave us a nice opportunity to make considerations about theories in different dimensions.
First, we considered theories for $D \leq 2$, and in particular, we analysed the case of $D = 2$ in detail. The finding is that for all the theories we considered up to and including dimension two behave qualitatively in the same way for $N \geq 2$. In such theories for continuos symmetries the Mermin-Wagner theorem must hold as we showed in Section 3.4. We provided a statistical approach to show the validity of the theorem by considering the statistics of the root patterns. It was found that for such systems ($D \leq 2$) all the roots are in the closed interval $[-1, 0]$. Since at every truncation level a new root appears, it seems to be paradoxical to prove the Mermin-Wagner theorem: we would not expect any root inside the interval but practically there appears (countably)

infinitely many. A true fixed point in this interval signals an SSB phase, hence the MW theorem seemed to be violated. However, it turned out that is only the case for finite n truncation. As $n \to \infty$ we can recover the MW theorem, by simulating the position of the roots and derive their distribution in the infinite limit, see Section 3.5.2. For discrete symmetry $N = 1$ the O(N) model is equivalent to the Ising model which has an SSB phase in $D = 2$. This result is also shown as a part of this section.

In Section 3.5.3 we investigated the theory for $D = 3$ with $N = 2$, and in $2 < D < 4$ the finding is that the theories that has been considered have similar properties. We found the an additional fixed point beside the Gaussian and the IR fixed point, namely, the Wilson-Fisher fixed point. Although these fixed points have been found, we could not clearly analyse the root structure for the $m^2 > 0$ region. It is also possible that one could find additional fixed points in $2 < D < 4$ for fractional dimensions, but it would require more detailed study. The main result of this section was that we were able to show the appearance of the Wilson-Fisher fixed point.

For $D \geq 4$ we found two qualitatively different results (see Section 3.5.4), however, essentially they lead us to the same physics, namely, to the triviality of the model, that is only the Gaussian fixed point exist for such theories. For theories $D > 4$ we analysed the $D = 5$ case, where the fixed point structure shows similarity to the $D = 2$ case, but now the roots only appear outside of the interval (-1,0), however, for the the root pattern the statistical simulation can be used again if we compactify the real line of m^2. In this way triviality can be shown. The situation for $D = 4$ is different: here, we need to consider the complex roots that appear during the calculations, but it can be shown that both the real and the imaginary part converges to the origin on the complex plane, hence leading to the triviality of the model.

In Section 3.5.5 we showed some results considering different values of N. The most interesting outcome is connected to the recent results in [52, 53], where it was argued that in the O(N) model for $N \to \infty$ if a non-trivial fixed point exist in dimensions $4 < D < 6$, then it defines an unstable fixed point potential. From our analysis we found this particular fixed point, and indeed, it can be shown that it defines an unbounded effective potential. In the last section we gave some results for fractional dimensions, obtaining similar behaviour to the integer-dimensional cases.

According to our findings, we can draw the conclusion that although we used the Local Potential Approximation during our computations, that seems to be enough to obtain the right qualitative physical results (Mermin-Wagner theorem, the presence of the Wilson-Fisher fixed point and triviality), when one extrapolates to infinite order the results obtained in a given order of the Taylor expansion. On the other hand, one has to be careful with such expansions, since as we saw, at finite level of the truncation it can generate "fake" fixed points from the physical point of view.

Chapter 4

Summary and thesis statements

In this dissertation we studied two different non-perturbative methods, namely, the 2PI (Two-Particle Irreducible) functional technique and the Functional (or Exact) Renormalisation Group (FRG) method. The former is based on resumming a particular class of Feynman diagrams, in a well-controlled, systematic way. The latter is using the Wilsonaian idea of renormalisation, that is we integrate out the rapid degrees of freedom of the system in order to obtain its large distance behaviour.

In general, the truncated 2PI resummation works as a non-perturbative approximation technique, and the system of self-consistent equations it provides between the two-point function and the self-energy, cannot be solved exactly. However, in the case of the Bloch-Nordsieck (BN) model, which was designed to mimic the infrared limit of Quantum Electrodynamics in order to prevent the infrared catastrophe, we showed that, if we include the Ward-Takahashi identities as a further input in the equations, one obtains an integral equation equivalent to the Dyson-Schwinger equation, which can be solved exactly. The new approach also makes it possible to extend our computation to finite temperature. In the finite temperature analysis of the BN model the Closed Time Path formalism is used, and we compute the fermionic spectral function of the theory. In this case the model remains exactly solvable, providing a closed formula for the finite temperature spectral function in the rest frame of the fermion. For the finite temperature theory, we derive the 2PI equations, too. Matching its solution to the exact one, gives the running of the 2PI coupling with respect to the temperature.

In the second part of my dissertation, we study the occurrence of spontaneous symmetry breaking for O(N) models using FRG techniques. We show that even the Local Potential Approximation (LPA), when treated the effective potential exactly, is sufficient to give qualitatively correct results for systems with continuous symmetry, in agreement with the Mermin-Wagner theorem and its extension to systems with fractional dimensions. We discussed the derivation of the so called Vanishing Beta Function curves,

which can be used to explore the fixed point structure of the theory under consideration, for arbitrary field components N and dimensions D. The technique is based on the most popular approximation scheme, namely, the polynomial expansion of the effective potential in the LPA. In this case, as an artefact of the approximation, spurious fixed points show up. Using statistical arguments, we can extract the physical fixed points of the theory in accordance with earlier results regarding $D < 4$. For $D \geq 4$ triviality of the O(N) model was shown which is a new result using FRG in LPA. For the large-N O(N) model in dimensions $4 < D < 6$, we found a new interacting fixed point, that defines a metastable critical potential. The existence of this fixed point is a subject of current studies in connection with the asymptotic safe scenario of the model.
The thesis statements are listed below.

I It turned out that in the BN model the Ward-Takahashi identities make a a one-to-one correspondence between the fermion propagator and the vertex function. As a consequence, it is possible to extend the 2PI self-energy equation with the vertex function by expressing it with the fermion propagator. The result is an integro-differential equation equivalent to the Dyson-Schwinger (DS) equation. This equation is linear in the fermion propagator, and taking good care of renormalisation, it is possible to solve analytically, providing the exact solution of the BN model. This is a new way of obtaining the exact solution in the Bloch-Nordsieck model. And, while the original solution method is very hard to generalise to other theories, the generalisation of the Ward identity improved 2PI equations, could be easier. The results are published in [40].

II After generalising the Ward identities to finite temperature the a Dyson-Schwinger equation similar to the $T = 0$ case can be obtained in the BN model. The exact fermionic spectral function of the BN model is derived at finite temperature. Analytic results are presented for some special parameters, namely when we perform the computation in the rest frame of the fermion, for other values we have numerical results. The spectral function is finite and normalisable for any non-zero temperature values. The real time dependence of the retarded Green's function is power-like for small times and exhibits exponential damping for large times. Treating the temperature as an infrared regulator, a safe interpretation of the zero temperature result is also given. The results are published in [41].

III The BN spectral function was numerically determined at finite temperature in the framework of the 2PI approximation. The finding is that the results of the 2PI computation nicely agree with the exact one, provided that a matching of the coupling constant is performed. The mapping between the two parameters results in the finite temperature running of the 2PI coupling constant. This result may apply to

the finite temperature behaviour of the coupling constant in QED, too. The results are published in [42].

IV The occurrence of spontaneous symmetry breaking (SSB) was studied for O(N) models using FRG. It is shown that even the Local Potential Approximation, when treated exactly, is sufficient to give qualitatively correct results for systems with continuous symmetry, in agreement with the Mermin-Wagner theorem. This was shown analytically both for $N < \infty$ and $N \to \infty$. The results are published in [43].

V We discussed the derivation of the so-called Vanishing Beta Function curves, which can be used to explore the fixed point structure of the theory under consideration, for arbitrary field components N and dimensions D. The technique is based on the most popular approximation scheme, namely, the polynomial expansion of the effective potential in the LPA. In this case, as an artefact of the approximation, spurious fixed points show up. Using statistical arguments, we can extract the physical fixed points of the theory in accordance with earlier results regarding $D < 4$. For $D \geq 4$ triviality of the O(N) model was shown which is a new result using FRG in LPA. For the large-N O(N) model in dimensions $4 < D < 6$, we found a new interacting fixed point, that defines a metastable critical potential. The existence of this fixed point is a subject of current studies in connection with the asymptotically safe scenario of the model [52, 53]. The results are published in [44].

Appendix A

One-loop integral in the Bloch-Nordsieck model

The one-loop contribution to the self-energy reads, with a generic u vector in Feynman gauge:

$$\Sigma = -ie^2u^2\int\frac{d^4k}{(2\pi)^4}\,\frac{1}{k^2+i\varepsilon}\,\frac{1}{u^\mu(p_\mu-k_\mu)-m+i\varepsilon}. \tag{A.1}$$

This is Lorentz-invariant, if we do a Lorentz transformation both on u and p. So we may choose a special frame where $\Lambda u=(u_0,0,0,0)$. If u is a proper 4-velocity, then $u_0=1$; if it is $u=(1,\mathbf{v})$, then $u_0=\sqrt{1-\mathbf{v}^2}$, but still constant, since $\mathbf{v}$ is a parameter of the theory. We find then

$$\Sigma = e^2u_0I_0(\frac{m}{u_0}-p_0-i\varepsilon),\qquad I_0(a)=i\int\frac{d^4k}{(2\pi)^4}\,\frac{1}{k^2+i\varepsilon}\,\frac{1}{a+k_0}. \tag{A.2}$$

Thus it is enough to consider I_0 only. There we transform to positive frequency integrals

$$\begin{aligned} I_0(a) &= \frac{ia}{\pi}\int_0^\infty dk_0\int\frac{d^3\mathbf{k}}{(2\pi)^3}\,\frac{1}{k_0^2-\mathbf{k}^2+i\varepsilon}\,\frac{1}{a^2-k_0^2} \\ &= \frac{a}{\pi}\int_0^\infty dk_0\int\frac{d^3\mathbf{k}}{(2\pi)^3}\,\frac{1}{k_0^2+\mathbf{k}^2}\,\frac{1}{a^2+k_0^2}, \end{aligned} \tag{A.3}$$

where in the last step we performed Wick rotation (the choice of the imaginary part of a is crucial for the direction of the rotation on the complex plane).

Now we can write up the integral in k_0 and $\mathbf{k}$ space, in the latter using $3-2\varepsilon$ dimensions:

$$I_0 = a\,\mu^{2\varepsilon}\int_0^\infty\frac{dk_0}{\pi}\int\frac{d^{3-2\varepsilon}\mathbf{k}}{(2\pi)^{3-2\varepsilon}}\,\frac{1}{k_0^2+\mathbf{k}^2}\,\frac{1}{a^2+k_0^2}. \tag{A.4}$$

We use the relation

$$\begin{aligned}\mu^{2\varepsilon}\int\frac{d^{d-2\varepsilon}k}{(2\pi)^{d-2\varepsilon}}\,f(k^2) &= \frac{2(4\pi\mu^2)^{\varepsilon}}{(4\pi)^{d/2}\Gamma(d/2-\varepsilon)}\int_0^\infty dk\,k^{d-1+2\varepsilon}f(k^2)\\ &= \frac{(4\pi\mu^2)^{\varepsilon}}{(4\pi)^{d/2}\Gamma(d/2-\varepsilon)}\int_0^\infty dz\,z^{\frac{d}{2}-1-\varepsilon}f(z)\end{aligned}\tag{A.5}$$

to proceed as

$$\begin{aligned}I_0 &= \frac{a}{\pi}\int_0^\infty dk_0\,\frac{1}{a^2+k_0^2}\,\frac{(4\pi\mu^2)^{\varepsilon}}{(4\pi)^{3/2}\Gamma(\frac{3}{2}-\varepsilon)}\int_0^\infty dz\,z^{\frac{3}{2}-1-\varepsilon}(k_0^2+z)^{-1}\\ &= \frac{a(4\pi\mu^2)^{\varepsilon}\Gamma(-\frac{1}{2}+\varepsilon)}{8\pi^2\sqrt{\pi}}\int_0^\infty dk_0\,\frac{k_0^{1-2\varepsilon}}{a^2+k_0^2}\\ &= \frac{a\Gamma(-\frac{1}{2}+\varepsilon)\Gamma(1-\varepsilon)}{16\pi^2\sqrt{\pi}}\left(\frac{4\pi\mu^2}{a^2}\right)^{\varepsilon}\Gamma(\varepsilon)\\ &= \frac{-a}{8\pi^2}\left[\frac{1}{\varepsilon}-2\ln\frac{a}{\mu}+2+\ln\pi-\gamma_E\right].\end{aligned}\tag{A.6}$$

We write it as

$$I_0=\frac{-a}{4\pi^2}\left[\mathcal{D}_\varepsilon-\ln\frac{a}{\mu}\right],\tag{A.7}$$

where

$$\mathcal{D}_\varepsilon=\frac{1}{2\varepsilon}+1+\frac{\ln\pi-\gamma_E}{2}.\tag{A.8}$$

Therefore

$$\Sigma=(u_0p_0-m)\frac{e^2}{8\pi^2}\left[\frac{1}{\varepsilon}-2\ln\frac{u_0p_0-m}{u_0\mu}+2+\ln\pi-\gamma_E\right].\tag{A.9}$$

We also need to compute

$$\begin{aligned}I_1(a) &= i\int\frac{d^4k}{(2\pi)^4}\,\frac{1}{k^2+i\varepsilon}\,\frac{1}{k_0}\,\frac{1}{a+k_0}\\ &= \frac{-i}{\pi}\int_0^\infty dk_0\int\frac{d^3\mathbf{k}}{(2\pi)^3}\,\frac{1}{k_0^2-\mathbf{k}^2+i\varepsilon}\,\frac{1}{a^2-k_0^2}\\ &= -\frac{1}{a}I_0(a)=\frac{1}{4\pi^2}\left[\mathcal{D}_\varepsilon-\ln\frac{a}{\mu}\right].\end{aligned}\tag{A.10}$$

Appendix B

The 2PI functional technique

The generating functional $Z[J]$ discussed in the Introduction has a functional dependence only on one local source $J(x)$. There is no restriction which could prevent introducing non-local sources in the functional. In particular, adding a bilocal source $K(x,y)$ yields the following form for the generating functional in Euclidean metric:

$$Z[J,K] = \int \mathcal{D}\varphi e^{-S+J_i\varphi_i+\frac{1}{2}\varphi_i K_{ij}\varphi_j}. \tag{B.1}$$

Here, we generalised the partition function for a vector variable $\varphi(x) = (\varphi_1(x), ..., \varphi_n(x))$ with a source $J = (J_1(x), ..., J_n(x))$. The products are $J_i\varphi_i \equiv \sum_i \int d^D x J_i(x)\varphi_i(x)$ and $\varphi_i K_{ij}\varphi_j \equiv \sum_{i,j} \int d^D x \int d^D y \varphi_i(x) K_{ij}(x,y)\varphi_j(y)$. Similarly to the case of $Z[J]$, we can define the generating functional for the connected correlation functions corresponding to the partition function $Z[J,K]$:

$$W[J,K] \equiv \ln Z[J,K]. \tag{B.2}$$

However, in this case the connectedness only holds for the differentiation with respect to J, since differentiating by the bilocal source K will generate disconnected diagrams, too:

$$\begin{aligned}
\frac{\delta^2 W}{\delta J_i(x)\delta J_j(y)} &= \frac{1}{Z[J,K]} \int \mathcal{D}\varphi\varphi_i(x)\varphi_j(y) e^{-S+J_i\varphi_i+\frac{1}{2}\varphi_i K_{ij}\varphi_j} - \phi_i^{J,K}(x)\phi_j^{J,K}(y) \\
&= \langle \varphi_i(x)\varphi_j(y)\rangle_c^{J,K} \equiv G_{ij}^{J,K}(x,y), \\
\frac{\delta W}{\delta K_{ij}(x,y)} &= \frac{1}{2}\frac{1}{Z[J,K]} \int \mathcal{D}\varphi\varphi_i(x)\varphi_j(y) e^{-S+J_i\varphi_i+\frac{1}{2}\varphi_i K_{ij}\varphi_j} \\
&= \frac{1}{2}\left(G_{i,j}^{J,K}(x,y) + \phi_i^{J,K}(x)\phi_j^{J,K}(y)\right).
\end{aligned} \tag{B.3}$$

Where $\phi_i^{J,K}(x) \equiv \delta W[J,K]/\delta J_i(x)$ is just the field VEV in the presence of the two source J and K. In the following, both ϕ and G are understood in the presence of the

sources, however, we will neglect the upper indices which are indicating it. Now, we can define the 2PI effective action by a double Legendre transformation with respect to both sources:

$$\begin{aligned}\Gamma[\phi, G] &= W[J,K] - J_i \frac{\delta W[J,K]}{\delta J_i} - K_{ij}\frac{\delta W[J,K]}{\delta K_{ij}} \\ &= W[J,K] - J_i\phi_i - \frac{1}{2}K_{ij}(\phi_i\phi_j + G_{ij})\end{aligned} \tag{B.4}$$

Here, we used the usual sign convention for the Legendre transformation, whereas in the Introduction we defined it with opposite sign. The latter convention is used by the FRG community. We also neglected the fact that all these quantities are a function of space-time, but we should keep it in mind, of course. From this definition we are able to derive the useful relations:

$$\begin{aligned}\frac{\delta\Gamma[\phi,G]}{\delta\phi_i} &= -J_i - K_{ij}\phi_j, \\ \frac{\delta\Gamma[\phi,G]}{\delta G_{ij}} &= -\frac{1}{2}K_{ij}.\end{aligned} \tag{B.5}$$

In the former equation we used the fact that K_{ij} is symmetric. These are the "quantum equation of motion" from the 2PI effective action with external sources. Via variational principle we can find the stationary mean field and the propagator solution from the equations:

$$\begin{aligned}\left.\frac{\delta\Gamma[\phi,G]}{\delta\phi}\right|_{\phi=\phi_s, G=G_s} &= 0, \\ \left.\frac{\delta\Gamma[\phi,G]}{\delta G}\right|_{\phi=\phi_s, G=G_s} &= 0.\end{aligned} \tag{B.6}$$

These two equations called the "field" and the "gap" equations, respectively. It is easy to see that the defining 2PI effective action at the stationary point of the propagator, i.e. for $G = G_s$, will give us the 1PI effective action for any ϕ defined in the Introduction (just with opposite sign due to the convention which we will not indicate here):

$$\Gamma_{2\mathrm{PI}}[\phi, G_s] = \Gamma_{1\mathrm{PI}}[\phi]. \tag{B.7}$$

It can be also shown that the 2PI effective action can be written in a compact form in terms of the diagrammatic expansion (see in [15])

$$\Gamma[\phi,G] = -S_0[\phi] - \frac{1}{2}\mathrm{Tr}\ln G^{-1} - \frac{1}{2}\mathrm{Tr}\left(G_0^{-1}G - 1\right) + \Gamma_{int}[\phi,G]. \tag{B.8}$$

In this notation $S_0[\phi] = (1/2)\phi_i G_0^{ij}\phi_j$ is the free action, G_0 is the free propagator, G corresponds to the full propagator and the term $\Gamma_{int}[\phi,G]$ contains all the closed 2PI

skeleton (without self-energy insertion) diagrams constructed with the vertices defined in $S_{int}[\phi+\varphi]$ (where only the higher than quadratic terms in φ are found).
The description of the 2PI functional technique above, of course, leads us to an exact expression of the 2PI effective action in Eq. (B.8). However, we always need to truncate $\Gamma[\phi, G]$ at some point to be able to perform calculations. Hence, we will have the equations

$$\begin{aligned} \left.\frac{\delta\Gamma^{tr}[\phi,G]}{\delta\phi}\right|_{\phi=\phi_s,G=G_s} &= 0, \\ \left.\frac{\delta\Gamma^{tr}[\phi,G]}{\delta G}\right|_{\phi=\phi_s,G=G_s} &= 0, \end{aligned} \tag{B.9}$$

where $\Gamma^{tr}[\phi, G]$ is the truncated 2PI effective action. Applying the first one to the truncated version of Eq. (B.8) yields:

$$\phi_s^i = -G_0^{ij} \left.\frac{\delta\Gamma^{tr}_{int}[\phi,G]}{\delta\phi^j}\right|_{\phi=\phi_s,G=G_s}, \tag{B.10}$$

where Γ^{tr}_{int} is the truncated interaction term. Now, applying the second one to Eq. (B.8) gives for the propagator:

$$G_s^{-1} = G_0^{-1} - 2\left.\frac{\delta\Gamma^{tr}_{int}[\phi,G]}{\delta G}\right|_{\phi=\phi_s,G=G_s}. \tag{B.11}$$

From the equation of the propagator we can immediately identify the self-energy by using the usual Dyson equation

$$G^{-1} = G_0^{-1} - \Sigma. \tag{B.12}$$

Hence, from Eq. (B.11) and Eq. (B.12) we get

$$\Sigma[G] = 2\frac{\delta\Gamma^{tr}_{int}[\phi,G]}{\delta G}. \tag{B.13}$$

The Dyson equation from Eq. (B.12) together with the self-energy from Eq. (B.13) represents a self-consistent system of equations, which serves as a basis for the 2PI resummation schemes.

Appendix C

Basics of the finite temperature field theory in CTP formalism

The appropriate quantity that contains both the quantum and the statistical fluctuations is the density matrix of the given system, which we will denote by ρ. Given the density matrix, one is able to compute correlation functions with the formula:

$$\langle O(x_1)O(x_2)...O(x_n)\rangle \equiv \frac{\mathrm{Tr}[\rho O(x_1)O(x_2)...O(x_n)]}{\mathrm{Tr}[\rho]}. \tag{C.1}$$

For a general density matrix we can define the partition function as follows:

$$Z[\rho] = \mathrm{Tr}[\rho] = \sum_{\phi} \langle \phi \,|\, \rho \,|\, \phi \rangle \,, \tag{C.2}$$

where $|\phi\rangle$s are state vectors in the Heisenberg picture, and they form a complete set. For the time evolution operators one can define a path integral representation [49], using a time contour integral on the complex plane. If the same external source can be found in the forward as well as in the backward evolution, then the two operators cancel (since they are complex conjugates) and the initial value remained. Nevertheless, in general we cannot assume this situation, thus different sources can be introduced for each direction of the evolution: J_1 for the forward and J_2 for the backward. In the path integral representation this time-dependent generating functional can be written as

$$Z[\rho, J_1, J_2] = \int \mathcal{D}\varphi^{(1)}\mathcal{D}\varphi^{(2)} \,\langle \phi_1, 0 \,|\, \rho \,|\, \phi_2, 0\rangle \, e^{i[\int_0^t ds \int d^3x (\mathcal{L}(\varphi^{(1)}) + J_1\varphi^{(1)}) - (\mathcal{L}(\varphi^{(2)}) + J_2\varphi^{(2)})]}. \tag{C.3}$$

Here $|\phi_{1,2}, 0\rangle$ are the initial Hilbert space states corresponding to the initial field configurations: $\varphi_H \,|\phi_{1,2}, 0\rangle = \varphi_0^{(1),(2)} \,|\phi_{1,2}, 0\rangle$. It is more convenient to write this integral on

the domain of the complex plane of the time on a given contour. Let us call this contour $\mathcal{C} = \mathcal{C}_1 \cup \mathcal{C}_2$, where the $\mathcal{C}_1$ runs from 0 to t and $\mathcal{C}_2$ from t to 0. The corresponding time evolution operator is:

$$U_J^{\mathcal{C}} = U_{J_2}^{\dagger}(t,0)U_{J_1}(t,0) \equiv \mathrm{T}^{\mathcal{C}} e^{i\int_{\mathcal{C}} dsd^3xJ(s,x)\varphi(s,x)}. \tag{C.4}$$

The contour $\mathcal{C}$ is called the Schwinger-Keldysh closed time path, and $\mathrm{T}^{\mathcal{C}}$ is for contour time path ordering, which is the ordinary time ordering if one considers $\mathcal{C}_1$ but it is the anti-time ordering on $\mathcal{C}_2$. Thus the time integration along the contour $\mathcal{C}$ is

$$\int_{\mathcal{C}} ds = \int_{0,\,\mathcal{C}_1}^{t} ds - \int_{0,\,\mathcal{C}_2}^{t} ds. \tag{C.5}$$

Then the partition function can be written in a compact way:

$$Z[\rho,J] = \int \mathcal{D}\varphi_0^{(1)}\mathcal{D}\varphi_0^{(2)} \left\langle \phi_1, 0 \,|\, \rho \,|\, \phi_2, 0 \right\rangle \int_{\varphi_0^{(1)}}^{\varphi_0^{(2)}} \mathcal{D}\varphi e^{i[\int_{\mathcal{C}} ds \int d^3x(\mathcal{L}(\varphi)+J\varphi)]}. \tag{C.6}$$

This form of the generating functional is very similar to the usual vacuum case. Variation of the partition function respect to the source J will provide the correlation functions which are specified by the initial density matrix ρ.

C.1 Propagators

Here, we are only going to consider the most simple scalar case. Since we introduced the contour $\mathcal{C}$, the correlation functions will have a matrix structure:

$$iG_{ab}(x-y) \equiv \left(\frac{1}{Z[0]} \frac{\delta^2 Z[\rho,J]}{\delta i J_a(x)\, \delta i J_b(x)} - \frac{1}{Z[0]} \frac{\delta Z[\rho,J]}{\delta i J_a(x)} \frac{1}{Z[0]} \frac{\delta Z[\rho,J]}{\delta i J_b(x)} \right) \Bigg|_{J_1=J_2=0}, \tag{C.7}$$

where $a, b \in \{1,2\}$. Each field variable is living on one of the given branch of the time contour $\mathcal{C}$, hence we will use the notation $\varphi^{(i)}(t_j)$ to indicate the fact that $t_j \in \mathcal{C}_i$. In what follows, will not use the spatial coordinate of the space-time, but the dependence on them as variables are understood implicitly. This definition gives a 2×2 matrix for

the propagator with the following elements:

$$\begin{aligned}
iG^{12}(t_1,t_2) &= \left\langle \mathrm{T}^{\mathcal{C}}\varphi^{(1)}(t_1)\varphi^{(2)}(t_2)\right\rangle = \langle\varphi(t_2)\varphi(t_1)\rangle\,,\\
iG^{21}(t_1,t_2) &= \left\langle \mathrm{T}^{\mathcal{C}}\varphi^{(2)}(t_1)\varphi^{(1)}(t_2)\right\rangle = \langle\varphi(t_1)\varphi(t_2)\rangle\,,\\
iG^{11}(t_1,t_2) &= \left\langle \mathrm{T}^{\mathcal{C}}\varphi^{(1)}(t_1)\varphi^{(1)}(t_2)\right\rangle = \langle\mathrm{T}\varphi(t_1)\varphi(t_2)\rangle\\
&= \theta(t_1-t_2)iG^{21}(t_2,t_1)+\theta(t_2-t_1)iG^{12}(t_1,t_2),\\
iG^{22}(t_1,t_2) &= \left\langle \mathrm{T}^{\mathcal{C}}\varphi^{(2)}(t_1)\varphi^{(2)}(t_2)\right\rangle = \langle\mathrm{T}^{*}\varphi(t_1)\varphi(t_2)\rangle\\
&= \theta(t_2-t_1)iG^{21}(t_2,t_1)+\theta(t_1-t_2)iG^{12}(t_1,t_2).
\end{aligned} \tag{C.8}$$

Where T^{*} is the anti-time ordering. The contour propagators are not independent, and as a consequence, we can write down the following identity:

$$G^{11}+G^{22}=G^{12}+G^{21}. \tag{C.9}$$

Sometimes it is more convenient to work in the R/A basis which is defined as:

$$\begin{aligned}
\varphi^{(r)} &= \frac{\varphi^{(1)}+\varphi^{(2)}}{2},\\
\varphi^{(a)} &= \varphi^{(1)}-\varphi^{(2)}.
\end{aligned} \tag{C.10}$$

Now, we can define the propagator in this new basis, too:

$$\begin{aligned}
iG^{rr} &= \left\langle \mathrm{T}^{\mathcal{C}}\varphi^{(r)}\varphi^{(r)}\right\rangle = \frac{1}{4}\left(iG^{11}+iG^{12}+iG^{21}+iG^{22}\right) = \frac{iG^{12}+iG^{21}}{2},\\
iG^{ra} &= \left\langle \mathrm{T}^{\mathcal{C}}\varphi^{(r)}\varphi^{(a)}\right\rangle = \frac{1}{2}\left(iG^{11}-iG^{12}+iG^{21}-iG^{22}\right)\\
&= iG^{11}-iG^{12}=\theta(t_1-t_2)\rho(t_1,t_2),\\
iG^{ar} &= \left\langle \mathrm{T}^{\mathcal{C}}\varphi^{(a)}\varphi^{(r)}\right\rangle = \frac{1}{2}\left(iG^{11}+iG^{12}-iG^{21}-iG^{22}\right)\\
&= iG^{11}-iG^{21}=-\theta(t_2-t_1)\rho(t_1,t_2),\\
iG^{aa} &= \left\langle \mathrm{T}^{\mathcal{C}}\varphi^{(a)}\varphi^{(a)}\right\rangle = iG^{11}-iG^{12}-iG^{21}+iG^{22}.
\end{aligned} \tag{C.11}$$

Here, we introduced the spectral function which is the commutation relation of the fields (for fermions it is the anticommutation relation):

$$\rho(t_1,t_2)=iG^{21}-iG^{12}=iG^{ra}-iG^{ar}=\langle\varphi(t_1)\varphi(t_2)-\varphi(t_2)\varphi(t_1)\rangle\,. \tag{C.12}$$

Some remarks on the R/A formalism: the propagator aa is always zero; G^{ra} and G^{ar} is the retarded and advanced propagator, respectively; G^{rr} sometimes called the Keldysh propagator.

C.2 Equilibrium

In the special case, when the system initially is in equilibrium, the density matrix is given as

$$\rho_{eq} = \frac{1}{Z[0]} e^{-\beta H}, \qquad Z[0] = \mathrm{Tr} e^{-\beta H}, \tag{C.13}$$

where β is the inverse temperature and H is the Hamiltonian. The prefactor in the partition function in Eq. (C.6), thus can be given as

$$\langle \phi_1, 0 \,|\, \rho \,|\, \phi_2, 0 \rangle = \int \mathcal{D}\varphi^{(3)} e^{i \int_0^{-i\beta} dt \int d^3x \, \mathcal{L}(\varphi^3)}, \tag{C.14}$$

where this path integral is over field configurations satisfying the boundary conditions:

$$\varphi^{(3)}(0, \mathbf{x}) = \varphi_0^{(1)}, \qquad \varphi^{(3)}(-i\beta, \mathbf{x}) = \varphi_0^{(2)}. \tag{C.15}$$

Thus, we found a path integral representation for the partition function Z in which the time integral runs along the imaginary axis from $t = 0$ to $t = -i\beta$. Hence, the contour is given now as $\mathcal{C} = \mathcal{C}_1 \cup \mathcal{C}_2 \cup \mathcal{C}_3$, where $\mathcal{C}_3$ represents the new section of the contour on the imaginary axis (Fig. C.1). In equilibrium the system has the property of time

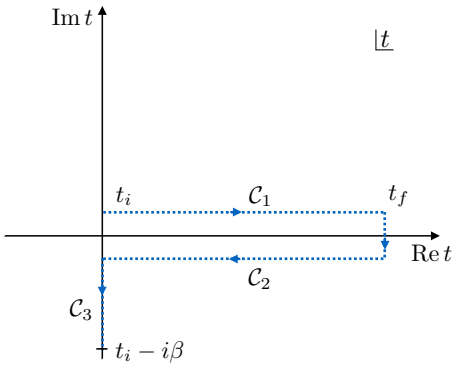

FIGURE C.1: The time integration contour in the equilibrium. In this case the system has a time translation invariance, hence the initial time (t_i) and final time (t_f) time can be shifted arbitrarily.

translation invariance, hence it is possible to set the initial time to $t \to -\infty$ instead of $t = 0$. This gives an enormous simplification in the description of the system. For instance, if we have a correlation function, which is defined by operators living on $C_{1,2}$ and on C_3, the propagation between the "real" and "imaginary" sections of the contour takes infinite time. Now, in every realistic system there is a damping, which ensures for such correlation functions to always be zero. This means that computations involving the contour section C_3 decouples from the calculations performed on the real contour

lines, and hence there is no need to extend the matrix structure of the propagator. Nevertheless, G^{33} can be computed.

In the following, we will give the propagators in equilibrium. Here, we can make a simplification by setting $t_1 = 0$ and $t_2 = t$ using the translation invariance in time:

$$\begin{aligned}
iG^{12}(t) &= \left\langle \mathrm{T}^{\mathcal{C}}\varphi^{(1)}(t)\varphi^{(2)}(0)\right\rangle = \frac{1}{Z[0]}\mathrm{Tr}[e^{-\beta H}\varphi(0)\varphi(t)], \\
iG^{21}(t) &= \left\langle \mathrm{T}^{\mathcal{C}}\varphi^{(2)}(t)\varphi^{(1)}(0)\right\rangle = \frac{1}{Z[0]}\mathrm{Tr}[e^{-\beta H}\varphi(t)\varphi(0)], \\
iG^{11}(t) &= \left\langle \mathrm{T}^{\mathcal{C}}\varphi^{(1)}(t)\varphi^{(1)}(0)\right\rangle = \frac{1}{Z[0]}\mathrm{Tr}[e^{-\beta H}\mathrm{T}\varphi(t)\varphi(0)] \\
&= \theta(t)iG^{21}(t) + \theta(-t)iG^{12}(t), \\
iG^{22}(t) &= \left\langle \mathrm{T}^{\mathcal{C}}\varphi^{(2)}(t)\varphi^{(2)}(0)\right\rangle = \frac{1}{Z[0]}\mathrm{Tr}[e^{-\beta H}\mathrm{T}^{*}\varphi(t)\varphi(0)] \\
&= \theta(t)iG^{12}(t) + \theta(-t)iG^{21}(t), \\
G^{33}(t) &= \left\langle \mathrm{T}^{\mathcal{C}}\varphi^{(3)}(t)\varphi^{(3)}(0)\right\rangle = \frac{1}{Z[0]}\mathrm{Tr}[e^{-\beta H}\mathrm{T}_{\tau}\varphi(-i\tau)\varphi(0)] \\
&= \theta(\tau)iG^{21}(-i\tau) + \theta(-\tau)iG^{12}(-i\tau).
\end{aligned} \tag{C.16}$$

The formulae in the R/A formalism are straightforward to obtain using Eq. (C.11). In fact it, is enough to consider G^{12} and G^{21} only, since everything can be expressed by these two correlation functions. A famous identity was given by Kubo, Martin and Schwinger, which is usually being referred as the KMS relation. It reads:

$$\begin{aligned}
iG^{12}(t) &= \frac{1}{Z[0]}\mathrm{Tr}[e^{-\beta H}\varphi(0)\varphi(t)] = \frac{1}{Z[0]}\mathrm{Tr}[e^{-\beta H}e^{\beta H}\varphi(t)e^{-\beta H}\varphi(0)] \\
&= \frac{1}{Z[0]}\mathrm{Tr}[e^{-\beta H}\varphi(t-\beta)\varphi(0)] = iG^{21}(t-i\beta).
\end{aligned} \tag{C.17}$$

More details about finite temperature field theory can be found in [49].

Appendix D

Local operator equations

D.1 The Dyson-Schwinger equation

The operator equations of motion give relations of the different Green's functions, formulated as the Dyson-Schwinger equations. These equations are *local*, and so they are valid in generic non-equilibrium situations, and, of course, in a thermal medium, too. The generating form of the Dyson-Schwinger equations for generic fields ϕ_i reads [7]

$$\left\langle \frac{\delta S}{\delta \phi_i(y)} \phi_{a_1}(x_1) \dots \phi_{a_n}(x_n) \right\rangle = i \sum_{k=1}^{n} \delta_{i a_k} \delta(y - x_k) \left\langle \prod_{l=1}^{k-1} \phi_{a_l}(x_l) \prod_{m=k+1}^{n} \phi_{a_m}(x_m) \right\rangle . \tag{D.1}$$

We can define the fermionic self-energy in the usual way using Eq. (D.1)

$$\mathcal{G}(x,y) = \mathcal{G}^{(0)}(x,y) + \int d^4x' d^4y' \, \mathcal{G}^{(0)}(x,x') \Sigma(x',y') \mathcal{G}(y',y), \tag{D.2}$$

Then we find in the Bloch-Nordsieck model

$$\Sigma(x,y) = ie^2 u_\mu \int d^4w d^4z \, \mathcal{G}(x,w) G^{\mu\nu}(x,z) \Gamma_\nu(z;w,y), \tag{D.3}$$

where the tree level vertex is eu_μ, the proper vertex is denoted by $e\Gamma_\mu$. At finite temperature we use the same definitions, but we need to take care of which time contour do we perform the integration:

$$\mathcal{G}(x,y) = \mathcal{G}^{(0)}(x,y) + \int_C d^4x' d^4y' \, \mathcal{G}^{(0)}(x,x') \Sigma(x',y') \mathcal{G}(y',y), \tag{D.4}$$

where the symbol $\int_C$ means time integration over the contour. In the Bloch-Nordsieck model

$$\Sigma(x,y) = i\alpha(x_0)e^2 u_\mu \int_C d^4w d^4z\, \mathcal{G}(x,w) G^{\mu\nu}(x,z)\Gamma_\nu(z;w,y), \tag{D.5}$$

where $\alpha(x_0)$ is 1 if $x_0 \in C_1$ and -1 if $x_0 \in C_2$. This factor appears because we expressed the functional derivative $\frac{\delta S}{\delta\phi_i(y)}$ through the derivatives of the Lagrangian, which, however, changes sign on C_2. For details of the finite temperature formalism see Appendix C.

D.2 The vertex function

The second use of the Dyson-Schwinger equation is to have a form for the vertex function. From Eq. (D.1) we find for any gauge theories

$$\left\langle \frac{\delta S}{\delta A^\mu(x)} O(\bar\psi,\psi) \right\rangle = 0, \tag{D.6}$$

where O is any local operator containing $\bar\psi$ and ψ. This implies, in particular

$$\left\langle A_\mu(x)\psi(y)\bar\psi(z)\right\rangle = \int_{(C)} d^4x' G_{\mu\nu}(x,x') \left\langle j^\nu(x')\psi(y)\bar\psi(z)\right\rangle, \tag{D.7}$$

where j_μ is the conserved current. The vertex function shows up in the $A\psi\psi^\dagger$ correlator as

$$\left\langle A_\mu(x)\psi(y)\bar\psi(z)\right\rangle = \int_{(C)} d^4x' d^4y' d^4z'\, iG_{\mu\nu}(x,x') i\mathcal{G}(y,y')(-ie)\Gamma^\nu(x',y',z') i\mathcal{G}(z',z). \tag{D.8}$$

From here, we find

$$\int_{(C)} d^4y' d^4z'\, i\mathcal{G}(y,u)\, e\Gamma^\mu(x;u,v) i\mathcal{G}(v,z) = \left\langle j^\mu(x)\psi(y)\bar\psi(z)\right\rangle. \tag{D.9}$$

In the BN model the fermion propagator is a scalar, moreover $j_\mu = eu_\mu\psi^\dagger\psi$ is proportional to u_μ. Therefore, the vertex function is proportional to u^μ, too. This is written in the Fourier space as

$$\Gamma^\mu(k;p,q) = u^\mu \Gamma(k;p,q)\,(2\pi)^4\delta(k+p-q), \tag{D.10}$$

where we also used the energy-momentum conservation. The C in the parenthesises as a subscript of the integral stands for the time contour in case of finite temperature computations. The vertex has the form of Eq. (D.10) at finite temperature, too, with

the corresponding additional indices. For the contour integration in finite temperature calculations see Appendix C.

D.3 Ward identities

The local equations expressing current conservation can be used in a similar manner. The generating form reads

$$\frac{\partial}{\partial x^\mu}\left\langle j^\mu(x)\phi_{a_1}(x_1)\dots\phi_{a_n}(x_n)\right\rangle = -i\sum_{k=1}^{n}\delta_{ia_k}\delta(x-x_k)\left\langle\prod_{l=1}^{k-1}\phi_{a_l}(x_l)\Delta\phi_i(y)\prod_{m=k+1}^{n}\phi_{a_m}(x_m)\right\rangle, \tag{D.11}$$

where $\Delta\phi_i$ is the transformation of the ith field generated by the conserved charge $Q=\int d^3\mathbf{x}j^0(t,\mathbf{x})$. This means, in particular

$$\frac{\partial}{\partial x^\mu}\left\langle j^\mu(x)\psi(y)\bar\psi(z)\right\rangle = e\delta(x-z)\mathcal{G}(y,z)-e\delta(x-y)\mathcal{G}(y,z). \tag{D.12}$$

We can write the corresponding equation for the vertex function, using Eq. (D.9):

$$\frac{\partial}{\partial x^\mu}\int_{(C)}d^4ud^4v\,i\mathcal{G}(y,u)\Gamma^\mu(x;u,v)i\mathcal{G}(v,z)=\delta(x-z)\mathcal{G}(y-z)-\delta(x-y)\mathcal{G}(y-z). \tag{D.13}$$

In momentum space we have:

$$k_\mu\Gamma^\mu(k;p-k,p)=\mathcal{G}^{-1}(p)-\mathcal{G}^{-1}(p-k). \tag{D.14}$$

Which holds for finite temperature case, too, with the corresponding additional indices. The C in the parenthesis again stands for the contour integration for nonzero temperature calculations (see Appendix C).

Appendix E

BN model calculations at $T > 0$

E.1 The calculation of Eq. (2.116)

Using the free form of the photon propagator G_{21}, we can write:

$$
\begin{aligned}
\bar{\mathcal{J}}(w) &= -e^2U^2\int\frac{d^4k}{(2\pi)^4}\,\frac{1}{uk}\,(1+n(k_0))\frac{2\pi}{2k}(\delta(k_0-k)-\delta(k_0+k))\,\bar{\mathcal{G}}_{ra}(w-uk) = \\
&= \frac{-e^2U^2}{2}\int\frac{d^3\boldsymbol{k}}{(2\pi)^3}\,\frac{1}{k}\left[\frac{1+n(k)}{u_0k-\boldsymbol{uk}}\bar{\mathcal{G}}_{ra}(w-(u_0k-\boldsymbol{uk}))\right. \\
&\quad \left.-\,\frac{1+n(-k)}{-u_0k-\boldsymbol{uk}}\bar{\mathcal{G}}_{ra}(w-(-u_0k-\boldsymbol{uk}))\right] = \\
&= \frac{-e^2U^2}{2}\int\frac{d^3\boldsymbol{k}}{(2\pi)^3}\,\frac{1}{k}\left[\frac{1+n(k)}{u_0k-\boldsymbol{uk}}\bar{\mathcal{G}}_{ra}(w-(u_0k-\boldsymbol{uk}))\right. \\
&\quad \left.-\,\frac{n(k)}{u_0k+\boldsymbol{uk}}\bar{\mathcal{G}}_{ra}(w+(u_0k+\boldsymbol{uk}))\right] = \\
&= \frac{-e^2U^2}{8\pi^2}\int_0^\infty dk\int_{-1}^{1}dx\,\left[\frac{1+n(k)}{u_0-ux}\bar{\mathcal{G}}_{ra}(w-k(u_0-ux))\right. \\
&\quad \left.-\,\frac{n(k)}{u_0-ux}\bar{\mathcal{G}}_{ra}(w+k(u_0-ux))\right] = \\
&= \frac{-e^2U^2}{8\pi^2}\int_0^\infty dk\int_{u_0-u}^{u_0+u}\frac{ds}{us}\,\left[(1+n(k))\bar{\mathcal{G}}_{ra}(w-ks)-n(k)\bar{\mathcal{G}}_{ra}(w+ks)\right] = \\
&= \frac{-e^2U^2}{8\pi^2}\int_0^\infty dq\int_{u_0-u}^{u_0+u}\frac{ds}{us^2}\,\left[\left(1+n\left(\frac{q}{s}\right)\right)\bar{\mathcal{G}}_{ra}(w-q)-n\left(\frac{q}{s}\right)\bar{\mathcal{G}}_{ra}(w+q)\right] = \\
&= \frac{-e^2U^2}{8\pi^2}\int_{-\infty}^\infty dq\,\bar{\mathcal{G}}_{ra}(w-q)\int_{u_0-u}^{u_0+u}\frac{ds}{us^2}\,\left(1+n\left(\frac{q}{s}\right)\right). \qquad \text{(E.1)}
\end{aligned}
$$

E.2 The calculation of Eq. (2.137)

Using basic identities we have:

$$
\begin{aligned}
& \frac{1}{\sin\left(\frac{\alpha}{2} - i\frac{\beta w}{2}\right)} + \frac{(-1)^{\alpha/\pi}}{\sin\left(\frac{\alpha}{2} + i\frac{\beta w}{2}\right)} \\
= \; & \frac{1}{\sin\frac{\alpha}{2}\cosh\frac{\beta w}{2} - i\cos\frac{\alpha}{2}\sinh\frac{\beta w}{2}} + \frac{e^{i\alpha}}{\sin\frac{\alpha}{2}\cosh\frac{\beta w}{2} + i\cos\frac{\alpha}{2}\sinh\frac{\beta w}{2}} \\
= \; & \frac{\left(1+e^{i\alpha}\right)\sin\frac{\alpha}{2}\cosh\frac{\beta w}{2} + i\left(1-e^{i\alpha}\right)\cos\frac{\alpha}{2}\sinh\frac{\beta w}{2}}{\left(\sin\frac{\alpha}{2}\cosh\frac{\beta w}{2}\right)^2 + \left(\cos\frac{\alpha}{2}\sinh\frac{\beta w}{2}\right)^2} \\
= \; & \frac{e^{i\alpha/2}\sin\alpha\left(\cosh\frac{\beta w}{2} + \sinh\frac{\beta w}{2}\right)}{\cosh^2\frac{\beta w}{2}\left(1-\cos^2\frac{\alpha}{2}\right) + \cos^2\frac{\alpha}{2}\sinh^2\frac{\beta w}{2}} \\
= \; & \frac{e^{i\alpha/2}e^{\beta w/2}\sin\alpha}{\cosh^2\frac{\beta w}{2} - \cos^2\frac{\alpha}{2}} = \frac{2e^{i\alpha/2}e^{\beta w/2}\sin\alpha}{\cosh(\beta w) - \cos\alpha}.
\end{aligned}
\tag{E.2}
$$

Appendix F

One-loop correction in the BN model at finite temperature

We are going to use Eq. (2.172) as our starting point. For the one-loop calculation we insert the spectral function of the free theory for both the fermion and gauge fields. The one-loop self-energy discontinuity reads

$$\begin{aligned}
\underset{p_0}{\mathrm{Disc}}\,\Sigma_{ar}(p) &= e^2\int\frac{d^4k}{(2\pi)^4}\,(1+n_b(k_0)-n_f(p_0-k_0)) \\
&\quad\times 2\pi\,\mathrm{sgn}\,k_0\delta(k_0^2-\mathbf{k}^2)2\pi\delta\left(u_0(p_0-k_0)-\mathbf{u}(\mathbf{p}-\mathbf{k})-m\right) \\
&= e^2\int\frac{d^4k}{(2\pi)^4}\,(1+n_b(k_0)-n_f(p_0-k_0)) \\
&\quad\times\frac{(2\pi)^2}{2|\mathbf{k}|}\left[\delta(k_0-|\mathbf{k}|)-\delta(k_0+|\mathbf{k}|)\right]\delta\left(u_0(p_0-k_0)-\mathbf{u}(\mathbf{p}-\mathbf{k})-m\right) \\
&= e^2\int\frac{d^3k}{(2\pi)^3}\,\Bigg(\left(1+n_b(|\mathbf{k}|)-n_f(p_0-|\mathbf{k}|)\right)\frac{2\pi}{2|\mathbf{k}|}\delta\left(u_0(p_0-k)-\mathbf{u}(\mathbf{p}-\mathbf{k})-m\right) \\
&\quad-\left(1-n_b(-|\mathbf{k}|)-n_f(p_0+|\mathbf{k}|)\right)\frac{2\pi}{2|\mathbf{k}|}\delta\left(u_0(p_0+|\mathbf{k}|)-\mathbf{u}(\mathbf{p}-\mathbf{k})-m\right)\Bigg) \\
&= \frac{e^2}{8\pi^3}\int_0^\infty dk\mathbf{k}^2\int_{-1}^{1}dx\frac{(2\pi)^2}{2|\mathbf{k}|}\left[(1+n_b(|\mathbf{k}|)-n_f(p_0-|\mathbf{k}|)\right) \\
&\quad\times\delta\left(u_0p_0-\mathbf{up}-u_0|\mathbf{k}|-|\mathbf{u}||\mathbf{k}|x-m\right)+ \\
&\quad+\left(n_b(|\mathbf{k}|)+n_f(p_0+|\mathbf{k}|)\right)\delta\left(u_0p_0-\mathbf{up}+u_0|\mathbf{k}|-|\mathbf{u}||\mathbf{k}|x-m\right)\Big]\,. \qquad \text{(F.1)}
\end{aligned}$$

In the last step we used that

$$1+n_b(-\omega)=1+\frac{1}{e^{-\omega}-1}=\frac{1}{e^{\omega}-1}=-n_b(\omega). \qquad \text{(F.2)}$$

In the last step we also introduced the variable x which stands for the cosinus of the angle between the two spatial three-vectors $\mathbf{u}$ and $\mathbf{k}$. For the sake of simplicity, in the following we are going to use the notations $pu \equiv p_0 u_0 - \mathbf{pu}$ for the scalar product in Mikowski space, and $k \equiv |\mathbf{k}|, u \equiv |\mathbf{u}|$.
First we would like to integrate out the angle, that is x. The deltas are centered at

$$x = \frac{pu \pm ku_0 - m}{ku}. \tag{F.3}$$

According to the limits of the integral, this means that they will only give nonzero contribution if:

$$|x| = \left|\frac{pu \pm ku_0 - m}{ku}\right| \leq 1 \quad \Rightarrow \quad |pu \pm ku_0 - m| \quad \leq \quad ku. \tag{F.4}$$

In the inequality above we assumed that u^μ is a time-like four vector, since we interpret it as the four-velocity of the fermion. Also, since k^μ is obviously time-like the, the scalar product in Mikowski space of these two time-like four-vectors is definitely time like, i.e. $ku > 0$. Thus, we can neglect the absolute value function. We distinguish two cases corresponding to the two signs in Eq. (F.4).
Let us consider first the case when $|pu + ku_0 - m| < ku$. Here, we need to distinguish again two subcases. Firstly, when we have $pu + ku_0 - m > 0$ then Eq. (F.4) reads as $pu + ku_0 - m < ku$. These two conditions imply

$$\frac{m - pu}{u_0} < k < \frac{m - pu}{u_0 - u}. \tag{F.5}$$

This forces $m - pu > 0$ meaning $pu < m$, i.e. "under the mass-shell". On the other hand, when $pu - m + k_0 < 0$, we have

$$|pu + ku_0 - m| = -pu - ku_0 + m < ku. \tag{F.6}$$

This implies

$$\frac{m - pu}{u_0 + u} < k < \frac{m - pu}{u_0}. \tag{F.7}$$

Since here $m - pu$ needs to be positive again, hence this is again a situation where we have a momentum under the mass-shell.
Now let us consider the other case, when we have a $-$ sign in Eq. (F.4). With a similar reasoning as above we will have two domain of validity again. Firstly, when $pu - ku_0 - m \geq 0$,

$$\frac{pu - m}{u_0 + u} < k < \frac{pu - m}{u_0}, \tag{F.8}$$

and secondly, when $pu - ku_0 - m \leq 0$,

$$\frac{pu-m}{u_0} < k < \frac{pu-m}{u_0-u}. \tag{F.9}$$

The two inequalties describe a situation "above the mass-shell". Evaluating the x-integral in Eq. (F.1), we end up with the expression

$$\begin{aligned}
\underset{p_0}{\mathrm{Disc}}\,\Sigma_{ar}(p) &= \frac{e^2}{4\pi u}\int_0^\infty dk\,[(1+n_b(k)-n_f(p_0-k)) \\
&\quad\times\left(\Theta\left(\frac{pu-m}{u_0+u}<k<\frac{pu-m}{u_0}\right)+\Theta\left(\frac{pu-m}{u_0}<k<\frac{pu-m}{u_0-u}\right)\right) \\
&\quad+(n_b(k)+n_f(p_0+k)) \\
&\quad\times\left(\Theta\left(\frac{m-pu}{u_0+u}<k<\frac{m-pu}{u_0}\right)+\Theta\left(\frac{m-pu}{u_0}<k<\frac{m-pu}{u_0-u}\right)\right)\Bigg] \\
&= \frac{e^2}{4\pi u}\Bigg(\Theta(pu-m)\int_{\frac{pu-m}{u+u_0}}^{\frac{pu-m}{u-u_0}} dk\,(1+n_b(k)-n_f(p_0-k)) \\
&\quad+\Theta(m-pu)\int_{\frac{m-pu}{u+u_0}}^{\frac{m-pu}{u-u_0}} dk\,(n_b(k)+n_f(p_0+k))\Bigg).
\end{aligned} \tag{F.10}$$

Now we have the formula for the discontinuity of the self-energy, therefore we can study its limit in the zero temperature case.

Firstly, we are taking the limit $u \to 0$. It should give us the zero three-velocity case of the fermion, but still on at finite T. The only non-trivial place where u appears in the expression is in the limits of the integration. We consider the two boundaries of the integral and take the limit $u \to 0$:

$$\lim_{u\to 0}\frac{1}{u}\int_{\frac{\pm(pu-m)}{u_0+u}}^{\frac{\pm(pu-m)}{u_0-u}} dk f(k), \tag{F.11}$$

where $f(k)$ is an arbitrary u-independent function. Since the boundaries are approaching each other (the range shrinks to a point), we can evaluate the function $f(k)$ at this particular point. Hence we replace $f(k)$ by $f(\pm p_0 \mp \frac{m}{u_0}) = f(\pm p_0 \mp M)$, where $M \equiv m/u_0$. The integral itself reads as:

$$\lim_{u\to 0}\frac{1}{u}\int_{\pm\frac{(pu-m)}{u_0+u}}^{\pm\frac{(pu-m)}{u_0-u}} dk f(k) = \pm\frac{2}{u_0}(p_0-M)f(\pm p_0 \mp M). \tag{F.12}$$

Using this result we can evaluate Eq. (F.10) in this limit, which gives:

$$\begin{aligned}\underset{p_0}{\mathrm{Disc}}\,\Sigma_{ar}(p_0) &= \frac{e^2}{2\pi u_0}\left[\Theta(p_0-M)(p_0-M)(1+n_b(p_0-M)-n_f(M))\right]. \\ &\quad + \Theta(M-p_0)(M-p_0)(n_b(M-p_0)+n_f(M))] \\ &= \frac{e^2}{2\pi u_0}\left[\Theta(p_0-M)(p_0-M)-(p_0-M)n_b(M)+|p_0-M|n_f(|p_0-M|)\right].\end{aligned} \tag{F.13}$$

We have now the expression for the discontinuity of the self-energy at finite T and $u=0$. In the zero temperature limit we will have the following expression for it:

$$\lim_{T\to 0}\underset{p_0}{\mathrm{Disc}}\,\Sigma_{ar}(p_0)=\frac{e^2}{2\pi u_0}\Theta(p_0-M)(p_0-M). \tag{F.14}$$

This is exactly the discontinuity of the zero temperature self-energy in Eq. (2.46). Thus, this result is consistent with the zero temperature case.
However, if we consider it in general (i.e. for $u\neq 0$) we will have some problems. Let us take first the limit $T\to 0$. This gives for the expressions in the bracket of Eq. (F.10) (note that $k>0$ in any case):

$$\lim_{T\to 0}1+n_b(k)-n_f(p_0-k) = 1-\Theta(k-p_0)=\Theta(p_0-k), \tag{F.15}$$

$$\lim_{T\to 0}n_b(k)+n_f(p_0+k) = \Theta(-p_0-k)=1-\Theta(p_0+k). \tag{F.16}$$

The first line in Eq. (F.15) tells us that the upper boundary of the integration by k cannot exceed p_0 in the first integral of Eq. (F.1). Hence, we need to compare p_0 with the upper limit which is $\frac{pu-m}{u_0-u}$. The prefactor is $\Theta(pu-m)$, which ensures $pu<m$, however, it does not give us enough information, i.e.

$$\mathrm{sgn}\left(p_0-\frac{pu-m}{u_0-u}\right)=\text{undefined}. \tag{F.17}$$

We are facing a similar problem when we try to evaluate the second integral:

$$\mathrm{sgn}\left(p_0-\frac{m-p_0}{u_0+u}\right)=\text{undefined}. \tag{F.18}$$

Since we are unsure in the signs of the expressions above, we are going to have for the complete expression of the discontinuity of the self-energy the following formula:

$$\begin{aligned}
\underset{p}{\mathrm{Disc}}\,\Sigma_{ar}(p_0) &= \frac{e^2}{4\pi u}\Theta(pu-m) \\
&\quad\times\left(\Theta\left(p_0-\frac{p_0-m}{u_0-u}\right)\int\limits_{\frac{pu-m}{u_0+u}}^{\frac{pu-m}{u_0-u}}dk+\Theta\left(\frac{p_0-m}{u_0-u}-p_0\right)\int\limits_{\frac{pu-m}{u_0+u}}^{p_0}dk\right) \\
&\quad-\frac{e^2}{4\pi u}\Theta(m-pu) \\
&\quad\times\left(\left(1-\Theta\left(\frac{m-p_0}{u_0+u}+p_0\right)\right)\int\limits_{\frac{pu-m}{u_0+u}}^{\frac{pu-m}{u_0-u}}dk-\Theta\left(-p_0-\frac{m-p_0}{u_0+u}\right)\int\limits_{-p_0}^{\frac{pu-m}{u_0-u}}dk\right).
\end{aligned} \tag{F.19}$$

Because of Eq. (F.17) and Eq. (F.18) the expression in Eq. (F.19) is not well-defined. To resolve this problem, we need to treat the fermion as a hard probe of the system, i.e. as not being a part of the heatbath. Hence, the only solution to this problem is to set the Fermi-Dirac distribution exactly to zero:

$$n_f(p_0\pm k)\equiv 0. \tag{F.20}$$

In that case Eq. (F.10) simplifies in the following way:

$$\begin{aligned}
\underset{p_0}{\mathrm{Disc}}\,\Sigma_{ar}(p) &= \frac{e^2}{4\pi u}\left(\Theta(pu-m)\int\limits_{\frac{pu-m}{u+u_0}}^{\frac{pu-m}{u-u_0}}dk\,(1+n_b(k))+\Theta(m-pu)\int\limits_{\frac{m-pu}{u+u_0}}^{\frac{m-pu}{u-u_0}}dk n_b(k)\right) \\
&= \frac{e^2}{4\pi u}\left(\Theta(pu-m)\int\limits_{\frac{pu-m}{u+u_0}}^{\frac{pu-m}{u-u_0}}dk\,(1+n_b(k))-\Theta(m-pu)\int\limits_{\frac{pu-m}{u+u_0}}^{\frac{pu-m}{u-u_0}}dk n_b(-k)\right) \\
&= \frac{e^2}{4\pi u}\int\limits_{\frac{pu-m}{u+u_0}}^{\frac{p-m}{u-u_0}}dk\,(1+n_b(k))\,.
\end{aligned} \tag{F.21}$$

Evaluating the integral, one gets a consistent result with the $T=0$ case:

$$\underset{p_0}{\mathrm{Disc}}\,\Sigma_{ar}(p)=\frac{Te^2}{4\pi u}\ln\left(\frac{e^{\beta\frac{pu-m}{u-u_0}}-1}{e^{\beta\frac{pu-m}{u+u_0}}-1}\right)=\frac{e^2}{2\pi}\Theta(pu-m)(pu-m)+\frac{Te^2}{4\pi u}\ln\left(\frac{1-e^{-\beta\frac{pu-m}{u-u_0}}}{1-e^{-\beta\frac{pu-m}{u+u_0}}}\right). \tag{F.22}$$

And taking the limit $T \to 0$, one gets Eq. (2.46):

$$\underset{p_0}{\mathrm{Disc}}\, \Sigma_{ar}(p) = \frac{e^2}{2\pi}\Theta(pu - m)(pu - m). \tag{F.23}$$

Appendix G

Derivation of the RG equations

G.1 The exact RG equations

We are going to consider a simple scalar theory in order to derive the RG equations. We define

$$Z_k[J] = \int \mathcal{D}\phi \, \exp\left(-S[\phi] - \Delta S_k[\phi] + \int J\phi\right),$$

$$\Delta S_k[\phi] = \frac{1}{2}\int_q R_k(q)\,\phi(q)\,\phi(-q),$$

$$W_k[J] = \ln Z_k[J],$$

$$\Gamma_k[\phi] + W_k[J] = \int_x J\phi - \frac{1}{2}\int_{x,y} \phi(x)\,R_k(x-y)\,\phi(y), \tag{G.1}$$

where the definition of $\phi(x)$ is given by:

$$\frac{\delta W_k}{\delta J(x)} = \phi(x) = \langle\phi(x)\rangle. \tag{G.2}$$

When $J(x)$ is k-independent (as in $Z_k[J]$) then $\phi(x)$ computed from W_k is k-dependent. Contrary, if $\phi(x)$ is fixed (as in $\Gamma_k[\phi]$), then $J(x)$ computed from Eq. (G.6) becomes k-dependent.

G.1.1 RG equation for $W_k[J]$

$$\begin{aligned}\partial_k e^{W_k} &= -\frac{1}{2}\int \mathcal{D}\phi \left(\int_{x,y} \phi(x)\,\partial_k R_k(x-y)\,\phi(y)\right) \\ &\quad \times \exp\Big(-S[\phi] - \frac{1}{2}\int_q R_k(q)\phi(q)\phi(-q) + \int J\phi\Big) \\ &= \left(-\frac{1}{2}\int_{x,y} \partial_k R_k(x-y)\frac{\delta}{\delta J(x)}\frac{\delta}{\delta J(y)}\right) e^{W_k[J]}. \end{aligned} \tag{G.3}$$

Therefore, the RG equation for W_k is:

$$\partial_k W_k[J] = -\frac{1}{2}\int_{x,y} \partial_k R_k(x-y)\left(\frac{\delta^2 W_k}{\delta J(x)\,\delta J(y)} + \frac{\delta W_k}{\delta J(x)}\frac{\delta W_k}{\delta J(y)}\right), \tag{G.4}$$

which is equivalent to the Polchinski equation.

G.1.2 RG equation for $\Gamma_k[\phi]$

We first derive the quantum equation of motion. The Legendre transform is symmetric with respect to the two functions that are transformed. Here, in the k-dependent effective theory, the Legendre transform of W_k is $\Gamma_k + 1/2\int \phi R_k \phi$. Thus,

$$\frac{\delta}{\delta\phi(x)}\left(\Gamma_k + \frac{1}{2}\int_{x,y} \phi(x)\,R_k(x-y)\,\phi(y)\right) = J(x), \tag{G.5}$$

and then

$$\frac{\delta\Gamma_k}{\delta\phi(x)} = J(x) - \int_y R_k(x-y)\phi(y). \tag{G.6}$$

In the Polchinski equation Eq. (G.4), the k-derivative is taken at fixed $J(x)$. We must convert it to a derivative at fixed ϕ:

$$\partial_k|_J = \partial_k|_\phi + \int_x \partial_k\phi(x)|_J \frac{\delta}{\delta\phi(x)}. \tag{G.7}$$

Acting on Eq. (G.1) with $\partial_k|_J$, we obtain:

$$\begin{aligned}\partial_k\Gamma_k[\phi]|_J + \partial_k W_k[J]|_J &= \int_x J\,\partial_k\phi|_J \\ -\frac{1}{2}\int_{x,y} \partial_k R_k(x-y)\,\phi(x)\,\phi(y) - \int_{x,y} R_k(x-y)\phi(x)\partial_k\phi(y)|_J \end{aligned} \tag{G.8}$$

Subsituting Eqs. (G.4, G.6, G.7) into this equation we finally obtain

$$\partial_k \Gamma_k[\phi] = \frac{1}{2} \int_{x,y} \partial_k R_k(x-y) \frac{\delta^2 W_k}{\delta J(x)\, \delta J(y)}. \tag{G.9}$$

In the last step we rewrite the RHS of this equation in terms of Γ_k only. We start from Eq. (G.2) and act on it with $\delta/\delta\phi(z)$:

$$\delta(x-z) = \frac{\delta^2 W_k}{\delta J(x)\, \delta J(z)} = \int_y \frac{\delta^2 W_k}{\delta J(x)\, \delta J(y)} \frac{\delta J(y)}{\delta \phi(z)} \ . \tag{G.10}$$

Now, using Eq. (G.6), we get

$$\delta(x-z) = \int_y \frac{\delta^2 W_k}{\delta J(x)\, \delta J(y)} \left(\frac{\delta^2 \Gamma_k}{\delta \phi(y)\, \delta \phi(z)} + R_k(y-z) \right) \ . \tag{G.11}$$

We define

$$W_k^{(2)}(x,y) = \frac{\delta^2 W_k}{\delta J(x)\, \delta J(y)}, \tag{G.12}$$

and thus

$$\delta(x-z) = \int_y W_k^{(2)}(x,y) \left(\Gamma_k^{(2)} + R_k \right)(y,z) \ . \tag{G.13}$$

$\Gamma_k^{(2)} + R_k$ is therefore the inverse of $W_k^{(2)}$ in the operator sense, and this relation is valid for arbitrary ϕ. Note that, although we did not specify it, $W_k^{(2)}$ is a functional of $J(x)$ and $\Gamma_k^{(2)}$ a functional of $\phi(x)$. The RG equation Eq. (G.9) can now be written using Γ_k:

$$\partial_k \Gamma_k[\phi] = \frac{1}{2} \int_{x,y} \partial_k R_k(x-y) \left(\Gamma_k^{(2)} + R_k \right)^{-1}(x,y) \ . \tag{G.14}$$

In Fourier space this equation becomes:

$$\partial_k \Gamma_k[\phi] = \frac{1}{2} \int_q \partial_k \tilde{R}_k(q) \left(\tilde{\Gamma}_k^{(2)} + \tilde{R}_k \right)^{-1}(q,-q) \ . \tag{G.15}$$

G.1.3 The RG equation in the LPA for the O(N) model

We define the potential as $\Gamma_k[\phi]$ evaluated in a uniform field configuration ϕ. By symmetry arguments, we can choose any direction for the N-component vector ϕ. We take

$$\phi = \begin{pmatrix} \phi_1 \\ 0 \\ \vdots \\ 0 \end{pmatrix} . \tag{G.16}$$

The RG equation on the potential in LPA writes as

$$\partial_t U_k = \frac{1}{2} \operatorname{Tr} \left(\partial_t R_k(q) \left(\frac{\partial^2 U_k}{\partial\phi_i \, \partial\phi_j} + (q^2 + R_k)\delta_{ij} \right)^{-1} \right) , \tag{G.17}$$

where the trace means summation over O(N) indices and integration on the variable q. Since

$$\frac{\partial^2 U_k}{\partial\phi_i \, \partial\phi_j} = \frac{\partial U_k}{\partial\rho} \, \delta_{ij} + \frac{\partial^2 U_k}{\partial\rho^2} \, \phi_i \, \phi_j, \tag{G.18}$$

where $\rho = 1/2\phi^2$, we obtain

$$\frac{\partial^2 U_k}{\partial\phi_i \, \partial\phi_j} + (q^2 + R_k)\delta_{ij} = \begin{pmatrix} q^2 + R_k + U_k' + 2\rho \, U_k'' & & & \\ & q^2 + R_k + U_k' & & \\ & & \ddots & \\ & & & q^2 + R_k + U_k' \end{pmatrix} . \tag{G.19}$$

It is straightforward to invert this matrix and to compute the trace. We find:

$$\partial_k U_k \, = \, \frac{1}{2} \int_q \partial_k R_k(q) \left(\frac{N-1}{q^2 + R_k + U_k'} + \frac{1}{q^2 + R_k + U_k' + 2\rho \, U_k''} \right) . \tag{G.20}$$

This equation on the right hand side defines a loop-integral structure with the propagators of the $N-1$ Goldstone modes and the single massive radial mode.

Appendix H

Proof of the nested formula

We would like to prove the nested formula for the coupling constants in Eq. (3.88). The easiest to consider first the case for the large-N, $D = 2$, because the RG equation has the most simple form for these parameters (see Eq. (3.79)), however, it can be generalised to arbitrary N and D, which we will present after this simpler example. Our starting point is the RG equation, and we start to differentiate it with respect to ρ:

$$\begin{aligned}
\partial_t u &= -2u(\rho) + \frac{1}{u'(\rho)+1}, \\
\partial_t u' &= -2u'(\rho) - \frac{u''(\rho)}{(u'(\rho)+1)^2}, \\
\partial_t u'' &= -2u''(\rho) + \frac{2u''(\rho)^2}{(u'(\rho)+1)^3} - \frac{u^{(3)}(\rho)}{(u'(\rho)+1)^2}, \\
\partial_t u''' &= -2u^{(3)}(\rho) - \frac{6u''(\rho)^3}{(u'(\rho)+1)^4} + \frac{6u^{(3)}(\rho)u''(\rho)}{(u'(\rho)+1)^3} - \frac{u^{(4)}(\rho)}{(u'(\rho)+1)^2}, \\
&\ldots
\end{aligned} \tag{H.1}$$

Let us rewrite the last three equation in the following form:

$$\begin{aligned}
\partial_t u' &= F_1(u') + g(u')u'', \\
\partial_t u'' &= F_2(u', u'') + g(u')u^{(3)}, \\
\partial_t u''' &= F_3(u', u'', u''') + g(u')u^{(4)}.
\end{aligned} \tag{H.2}$$

Where we defined:

$$\begin{aligned} F_1(u') &\equiv -2u'(\rho), \\ F_2(u', u'') &\equiv -2u''(\rho) + \frac{2u''(\rho)^2}{(u'(\rho)+1)^3} - \frac{u^{(3)}(\rho)}{(u'(\rho)+1)^2}, \\ F_3(u', u'', u''') &\equiv -2u^{(3)}(\rho) - \frac{6u''(\rho)^3}{(u'(\rho)+1)^4} + \frac{6u^{(3)}(\rho)u''(\rho)}{(u'(\rho)+1)^3}, \\ g(u') &\equiv -\frac{1}{(u'(\rho)+1)^2}. \end{aligned} \tag{H.3}$$

We can find the following relation between F_is:

$$\begin{aligned} F_2(u', u'') &= \frac{\partial F_1}{\partial \rho} + \frac{\partial F_1}{\partial u'}u'' + \frac{\partial g(u')}{\partial u'}u''^2, \\ F_3(u', u'', u''') &= \frac{\partial F_2}{\partial \rho} + \frac{\partial F_2}{\partial u'}u'' + \frac{\partial F_2}{\partial u''}u''' + \frac{\partial g(u')}{\partial u'}u''u'''. \end{aligned} \tag{H.4}$$

Of course, $\partial F_i/\partial\rho = 0$ since in this case there is no explicit ρ dependence, but for the sake of consistency, we will indicate this term, as well. We can make the following statement for $n \geq 1$:

$$\begin{aligned} \partial_t u^{(n)} &= F_n(u', u'', u''', ..., u^{(n)}) + g(u')u^{(n+1)}, \\ F_n(u', u'', u''', ..., u^{(n)}) &= \frac{\partial F_{n-1}}{\partial u'}u'' + \frac{\partial F_{n-1}}{\partial u''}u''' + ... + \left(\frac{\partial F_{n-1}}{\partial u^{(n-1)}} + \frac{\partial g(u')}{\partial u'}u''\right)u^{(n)}. \end{aligned} \tag{H.5}$$

We are going to show this by induction. Let us suppose Eq. (H.5) is true. We are going to show that it holds for $n+1$, too. Let us differentiate Eq. (H.5) once with respect to ρ. It yields:

$$\begin{aligned} \partial_t u^{(n+1)} &= \frac{\partial F_n}{\partial \rho} + \frac{\partial F_n}{\partial u'}u'' + \frac{\partial F_n}{\partial u''}u''' + ... + \frac{\partial F_n}{\partial u^{(n)}}u^{(n+1)} + \frac{\partial g(u')}{\partial u'}u''u^{(n+1)} + g(u')u^{(n+2)}, \\ \partial_t u^{(n+1)} &= \frac{\partial F_n}{\partial \rho} + \frac{\partial F_n}{\partial u'}u'' + \frac{\partial F_n}{\partial u''}u''' + ... + \left(\frac{\partial F_n}{\partial u^{(n)}} + \frac{\partial g(u')}{\partial u'}u''\right)u^{(n+1)} + g(u')u^{(n+2)}, \\ \partial_t u^{(n+1)} &= F_{n+1}(u', u'', u''', ..., u^{(n+1)}) + g(u')u^{(n+2)}, \end{aligned} \tag{H.6}$$

where

$$F_{n+1}(u', u'', u''', ..., u^{(n+1)}) = \frac{\partial F_n}{\partial u'}u'' + \frac{\partial F_n}{\partial u''}u''' + ... + \left(\frac{\partial F_n}{\partial u^{(n)}} + \frac{\partial g(u')}{\partial u'}u''\right)u^{(n+1)}. \tag{H.7}$$

In this way it was shown that the RHS always depend on the highest derivative of $u(\rho)$ linearly, e.g. $u^{(n+1)}$ in Eq. (H.5). Now, if we look for the scaling solution then the LHS vanishes, hence from Eq. (H.5):

$$u^{(n+1)} = -\frac{F_n(u', u'', u''', ..., u^{(n)})}{g(u')}. \tag{H.8}$$

Evaluating this expression at $\rho = 0$ gives:

$$\lambda_{n+1} = -\frac{F_n(\lambda_1, \lambda_2, \lambda_3, ..., \lambda_n)}{g(\lambda_1)}. \tag{H.9}$$

From this expression the nesting is straightforward:

$$\lambda_{n+1} = -\frac{F_n(\lambda_1, \lambda_2, \lambda_3, ..., \lambda_n)}{g(\lambda_1)} = -\frac{F_n(m^2)}{g(m^2)}. \tag{H.10}$$

Here, we used the notation $m^2 \equiv \lambda_1$. Thus, the formula of the nested couplings in Eq. (3.88) is proved for $N \to \infty$ and $D = 2$.

Note that in the finite N case there are terms in the initial RG flow like $\rho u'$ and $\rho u''$. Evaluating the equation at $\rho = 0$ is crucial to be able to neglect these terms, which would prevent us to perform the nesting. Thus, expanding into Taylor series around zero is the only case when we can define VBFs.

In what follows, we will give a proof of the nested formula in Eq. (3.88) for arbitrary field components N and dimensions D. Let us start again by differentiating the RG equation (in this case Eq. (3.63)) with respect to ρ:

$$\begin{aligned}
\partial_t u &= (D-2)\rho u'(\rho) - D u(\rho) + \frac{N-1}{u'(\rho)+1} + \frac{1}{2\rho u''(\rho) + u'(\rho) + 1}, \\
\partial_t u' &= (D-2)\rho u''(\rho) + (D-2)u'(\rho) - D u'(\rho) - \frac{(N-1)u''(\rho)}{(u'(\rho)+1)^2} - \frac{2\rho u^{(3)}(\rho) + 3u''(\rho)}{(2\rho u''(\rho) + u'(\rho) + 1)^2}, \\
\partial_t u'' &= (D-2)\rho u^{(3)}(\rho) + 2(D-2)u''(\rho) - D u''(\rho) + (N-1)\left(\frac{2u''(\rho)^2}{(u'(\rho)+1)^3} - \frac{u^{(3)}(\rho)}{(u'(\rho)+1)^2}\right) \\
&\quad + \frac{2\left(2\rho u^{(3)}(\rho) + 3u''(\rho)\right)^2}{(2\rho u''(\rho) + u'(\rho) + 1)^3} - \frac{2\rho u^{(4)}(\rho) + 5u^{(3)}(\rho)}{(2\rho u''(\rho) + u'(\rho) + 1)^2}.
\end{aligned} \tag{H.11}$$

Let us express the equations above in the following way:

$$\begin{aligned}
\partial_t u' &= F_1(u', \rho u'') + g(u')u'' + h(u', 2\rho u'')(3u'' + 2\rho u^{(3)}), \\
\partial_t u'' &= F_2(u', u'', \rho u^{(3)}) + g(u')u^{(3)} + h(u', 2\rho u'')(5u^{(3)} + 2\rho u^{(4)}),
\end{aligned} \tag{H.12}$$

where

$$\begin{aligned}
F_1(u', \rho u'') &= (D-2)\rho u''(\rho) + (D-2)u'(\rho) - Du'(\rho), \\
F_2(u', u'', \rho u^{(3)}) &= (D-2)\rho u^{(3)}(\rho) + 2(D-2)u''(\rho) - Du''(\rho) \\
&\quad + (N-1)\frac{2u''(\rho)^2}{(u'(\rho)+1)^3} + \frac{2\left(2\rho u^{(3)}(\rho) + 3u''(\rho)\right)^2}{(2\rho u''(\rho) + u'(\rho) + 1)^3}, \\
g(u') &= -\frac{N-1}{(u'(\rho)+1)^2}, \\
h(u', 2\rho u'') &= -\frac{1}{(2\rho u''(\rho) + u'(\rho) + 1)^2}.
\end{aligned} \tag{H.13}$$

We can establish the relation again:

$$F_2(u', u'', \rho u^{(3)}) = \frac{\partial F_1}{\partial \rho} + \frac{\partial F_1}{\partial u'}u'' + \frac{\partial F_1}{\partial u''}\rho u^{(3)} + \frac{\partial g(u')}{\partial u'}u''u'' + \frac{dh}{d\rho}\left(2\rho u^{(3)}(\rho) + 3u''(\rho)\right). \tag{H.14}$$

We can make the following statement for $n \geq 1$:

$$\begin{aligned}
\partial_t u^{(n)} &= F_n(u', u'', ..., \rho u^{(n+1)}) + g(u')u^{(n+1)} \\
&\quad + h(u', 2\rho u'')\left((2n+1)u^{(n+1)} + 2\rho u^{(n+2)}\right), \\
F_n(u', u'', ..., \rho u^{(n+1)}) &= \frac{\partial F_{n-1}}{\partial \rho} + \frac{\partial F_{n-1}}{\partial u'}u'' + ... + \frac{\partial F_{n-1}}{\partial u^n}\rho u^{(n+1)} \\
&\quad + \frac{\partial g(u')}{\partial u'}u''u^{(n)} + \frac{dh}{d\rho}\left(2\rho u^{(n+1)}(\rho) + (2n-1)u^{(n)}(\rho)\right).
\end{aligned} \tag{H.15}$$

Let us suppose that Eq. (H.15) is true for the nth term. Now, we will show it is true for the $n+1$th term:

$$\begin{aligned}
\partial_t u^{(n+1)} &= \frac{\partial F_n}{\partial \rho} + \frac{\partial F_n}{\partial u'}u'' + ... + \frac{\partial F_n}{\partial u^{n+1}}\rho u^{(n+2)} + \frac{\partial g(u')}{\partial u'}u''u^{(n+1)}, \\
&\quad + g(u')u^{(n+2)} + \frac{dh}{d\rho}\left((2n+1)u^{(n+1)} + 2\rho u^{(n+2)}\right), \\
&\quad + h\left((2n+3)u^{(n+2)} + 2\rho u^{(n+3)}\right), \\
&= F_{n+1}(u', u'', ..., \rho u^{(n+2)}) + g(u')u^{(n+2)} + h\left((2n+3)u^{(n+2)} + 2\rho u^{(n+3)}\right),
\end{aligned} \tag{H.16}$$

where

$$F_{n+1}(u', u'', ..., \rho u^{(n+2)}) = \frac{\partial F_n}{\partial \rho} + \frac{\partial F_n}{\partial u'} u'' + ... + \frac{\partial F_n}{\partial u^{n+1}} \rho u^{(n+2)} + \frac{\partial g(u')}{\partial u'} u'' u^{(n+1)} + \frac{dh}{d\rho} \left((2n+1) u^{(n+1)} + 2\rho u^{(n+2)} \right). \tag{H.17}$$

In this way by induction we could show the statement of Eq. (H.15) is true. Here, (in the case of finite N) we have to set $\rho = 0$ and only then it is possible to do the nesting like in Eq. (H.10). From this point it is straightforward to show this.

Bibliography

[1] M.E. Peskin, D.V. Schroeder, *An Introduction to Quantum Field Theory*, (Perseus Books Publishing, 1995.)

[2] G. B. Folland, *Quantum Field Theory: A Tourist Guide for Mathematicians*, (American Mathematical Society, 2008).

[3] J. Butterfield, N. Bouatta, *Renormalization for Philosophers*, arXiv:1406.4532 [physics.hist-ph].

[4] F. Strocchi, *A*n Introduction to Non-Perturbative Foundations of Quantum Field Theory, (Oxford University Press, 2013).

[5] J. Baez, *Renormalization Made Easy*, http://math.ucr.edu/home/baez/renormalization.html

[6] R.P. Feynman, *QED, The strange theory of light and matter*, (Princeton University Press, 1985).

[7] J. Collins, *Renormalization: an introduction to renormalization, the renormalization group and the operator product expansion*, (Cambridge University Press, Cambridge, 1984).

[8] I.J.R. Aitchison, A.J.G. Hey, *Gauge Theories in Particle Physics: Volume I: From Relativistic Quantum Mechanics to QED, 3rd edn.*, (Taylor and Francis, 2003).

[9] R. J. Rivers, *Path Integral Methods in Quantum Field Theory*, (Cambridge University Press, 1987).

[10] I. Montvay, G. Münster *Quantum Fields on a Lattice*, (Cambridge University Press, 1994).

[11] S. Weinberg, *The Quantum Theory of Fields, Volume 1. Foundations*, (Cambridge University Press, 2005).

[12] C. Itzykson, J-B. Zuber, *Quantum Field Theory*, (McGraw-Hill Book Co., 1980)

[13] A. Duncan, *The Conceptual Framework of Quantum Field Theory*, (Oxford University Press, 2012).

[14] K. G. Wilson, Rev. Mod. Phys. **47**, 773 (1975).

[15] J. M. Luttinger and J. C. Ward, Phys. Rev. 118 (1960) 1417. G. Baym, Phys. Rev. 127 (1962) 1391. J. M. Cornwall, R. Jackiw and E. Tomboulis, Phys. Rev. D 10 (1974) 2428.

[16] H. van Hees an J. Knoll, Phys. Rev. D65 (2002) 025010 [hep-ph/0107200]; Phys. Rev. D65 (2002) 105005 [hep-ph/0111193]; Phys. Rev. D66 (2002) 025028 [hep-ph/0203008].

[17] J.-P. Blaizot, E. Iancu and U. Reinosa, Phys. Lett. B568 (2003) 160 [hep-ph/0301201]; Nucl. Phys. A736 (2004) 149 [hep-ph/0312085]

[18] J. Berges, Sz. Borsanyi , U. Reinosa and J. Serreau, Annals Phys. 320 (2005) 344 [hep-ph/0503240].

[19] U. Reinosa, J. Serreau, JHEP 0607 (2006) 028 [hep-th/0605023];

[20] A. Jakovac, Phys. Rev. **D76**, 125004 (2007). [hep-ph/0612268].

[21] A. Patkos, Z. .Szep, Nucl. Phys. **A811**, 329-352 (2008). [arXiv:0806.2554 [hep-ph]].

[22] J. Berges and J. Cox, Phys. Lett. B 517 (2001) 369.

[23] J. Berges, S. Borsanyi and C. Wetterich, Phys. Rev. Lett. 93 (2004) 142002.

[24] J. Berges, S. .Borsanyi, U. Reinosa, J. Serreau, Phys. Rev. **D71**, 105004 (2005). [hep-ph/0409123].

[25] A. Jakovac, Phys.Rev. D78 (2008) 085013, [arXiv:0808.1800 [hep-th]]

[26] G. Fejos, A. Patkos, Z. .Szep, Phys. Rev. **D80**, 025015 (2009). [arXiv:0902.0473 [hep-ph]].

[27] U. Reinosa, J. Serreau, Annals Phys.325:969-1017,2010 [arXiv:0906.2881]

[28] Sz. Borsanyi, U. Reinosa, Phys.Lett.B661:88-94,2008, [arXiv:0709.2316]

[29] J. Berges, S. Roth, Nucl.Phys.B847:197-219,2011, [arXiv:1012.1212]

[30] M.E. Carrington, E. Kovalchuk, Phys.Rev.D76:045019,2007, [arXiv:0705.0162]

[31] F. Bloch and A. Nordsieck, Phys. Rev. **52** (1937) 54.

[32] N.N. Bogoliubov and D.V. Shirkov, *Introduction to the theories to the quantized fields* (John Wiley & Sons, Inc., 1980)

[33] H.M. Fried, *Green's Functions and Ordered Exponentials* (Cambridge University Press, 2002)

[34] J. -P. Blaizot and E. Iancu, Phys. Rev. D **56**, 7877 (1997) [hep-ph/9706397], J. -P. Blaizot and E. Iancu, Phys. Rev. D **55**, 973 (1997) [hep-ph/9607303].

[35] H.A. Weldon, Phys. Rev. D44 (1991) 3955; Phys. Rev. D49 (1994) 1579.

[36] P. Mati, Diploma thesis

[37] A. I. Alekseev, V. A. Baikov and E. E. Boos, Theor. Math. Phys. **54**, 253 (1983) [Teor. Mat. Fiz. **54**, 388 (1983)].

[38] J.O. Andersen, D. Boer, H.J. Warringa, Phys. Rev. D70 (2004), 116007 [hep-ph/0408033], A. Jakovac, Phys. Rev. D **78**, 085013 (2008) [arXiv:0808.1800 [hep-th]], G. Fejos, A. Patkos and Z. .Szep, Phys. Rev. D **80**, 025015 (2009) [arXiv:0902.0473 [hep-ph]].

[39] H. A. Weldon, Phys. Rev. D **44**, 3955 (1991).

[40] A. Jakovac and P. Mati, Phys. Rev. D **85** 085006 (2012), [arXiv:1112.3476 [hep-ph]].

[41] A. Jakovac and P. Mati, Phys. Rev. D **87**, 125007 (2013) [arXiv:1301.1803 [hep-th]].

[42] A. Jakovac and P. Mati, Phys. Rev. D **90**, 045038 (2014), [arXiv:1405.6576 [hep-th]].

[43] N. Defenu, P. Mati, I. G. Marian, I. Nandori, A. Trombettoni, [arXiv:1410.7024 [hep-th]],
The article is under publication at JHEP.

[44] P. Mati [arXiv:1501.00211 [hep-th]],
To be published in PRD (currently under consideration, only minor revisions were required by the referee).

[45] J. -P. Blaizot and E. Iancu, Phys. Rev. D **55** (1997) 973 [hep-ph/9607303].

[46] J. -P. Blaizot and E. Iancu, Phys. Rev. D **56**, 7877 (1997) [hep-ph/9706397], J. -P. Blaizot and E. Iancu, Phys. Rev. D **55**, 973 (1997) [hep-ph/9607303].

[47] H. A. Weldon, Phys. Rev. D **69** (2004) 045006 [hep-ph/0309322].

[48] H. M. Fried, T. Grandou and Y. -M. Sheu, Phys. Rev. D **77** (2008) 105027 [arXiv:0804.1591 [hep-th]].

[49] N. P. Landsman and C. G. van Weert, Phys. Rept. **145**, 141 (1987); M. Le Bellac, *Thermal Field Theory*, (Cambridge Univ. Press, 1996.); A. Arrizabalaga, *PhD thesis: Quantum Field Dynamics and 2PI Effective Action.*

[50] S. -Y. Wang, D. Boyanovsky, H. J. de Vega and D. S. Lee, Phys. Rev. D **62** (2000) 105026 [hep-ph/0005223].

[51] D. Boyanovsky, H. J. de Vega and S. -Y. Wang, Phys. Rev. D **61** (2000) 065006 [hep-ph/9909369].

[52] Lin Fei, Simone Giombi, Igor R. Klebanov, Phys.Rev. **D90** (2014) 025018; Lin Fei, Simone Giombi, Igor R. Klebanov, Grigory Tarnopolsky, arXiv:1411.1099v3 [hep-th]

[53] R. Percacci, G. P. Vacca, Phys.Rev. D **90** (2014) 10, 107702

[54] J. Polchinski, Nucl. Phys. **B231**, 269 (1984)

[55] J.-P. Blaizot, Ramon Mendez Galain, and Nicolas Wschebor. Phys. Rev. E **74**, 051116 (2006)

[56] J.-P. Blaizot, Ramon Mendez Galain, and Nicolas Wschebor. Phys. Rev. E **74**, 051117 (2006)

[57] K. Huang, *Statistical Mechanics* (New York, Wiley, 1987).

[58] N. D. Mermin and H. Wagner . Phys. Rev. Lett. **17**, 1133 (1966).

[59] P. C. Hohenberg, Phys. Rev. **158**, 383 (1967).

[60] S. Coleman, Comm. Math. Phys. **264**, 259 (1973).

[61] S. Stringari, in *Bose-Einstein condensation*, A. Griffin, D. W. Snoke, and S. Stringari eds., p. 86 (Cambridge, Cambridge University Press, 1995).

[62] L. P. Kadanoff, *Statistical physics: statics, dynamics and renormalization* (Singapore, World Scientific, 2000).

[63] B. Delamotte, Lect. Notes Phys. **852** (2012) 49.

[64] D. Cassi, Phys. Rev. Lett. **68**, 3631 (1992); *ibid.*, **76**, 2941 (1996).

[65] R. Burioni and D. Cassi, Phys. Rev. Lett. **76**, 1091 (1996).

[66] A. Codello and G. D'Odorico, Phys. Rev. Lett. **110**, 141601 (2013).

[67] G. Mussardo, *Statistical field theory: an introduction to exactly solved models in statistical physics* (Oxford, Oxford University Press, 2010).

[68] R. Burioni, D. Cassi, and A. Vezzani, Phys. Rev. E **60**, 1500 (1999).

[69] H. E. Stanley, Phys. Rev. Lett. **20**, 589 (1968).

[70] G. S. Joyce, in *Phase Transitions and Critical Phenomena*, Vol. 2, C. Domb and M. S. Green eds., p. 375 (Academic Press, 1972).

[71] D. F. Litim and J. Pawlowski, in *The Exact Renormalization Group*, A. Krasnitz *et al.* eds., p. 168 (World Scientific, Singapore, 1999).

[72] C. Bagnuls and C. Bervillier, Phys. Rep. **348**, 91 (2001).

[73] J. Berges, N. Tetradis, and C. Wetterich, Phys. Rep. **363**, 223 (2002).

[74] J. Polonyi, Central Eur. J. Phys. **1**, 1 (2004).

[75] B. Delamotte, in *Order, disorder and criticality: advanced problems of phase transition theory*, Yu. Holovatch ed., p. 1 (Singapore, World Scientific, 2007) [arXiv:cond-mat/0702365]

[76] H. Gies, Lect. Notes Phys. **852**, 287 (2012).

[77] O. J. Rosten, Phys. Rep. **511**, 177 (2012).

[78] H. Ballhausen, J. Berges, and C. Wetterich, Phys. Lett. B **582**, 144 (2003).

[79] A. Codello, N. Defenu, and G. D'Odorico, arXiv:1410.3308

[80] S.B. Liao, J. Polonyi, and M. Strickland, Nucl. Phys. B **567**, 493 (2000).

[81] D. F. Litim, Nucl.Phys. B **631**, 128 (2002); JHEP **0507**, 005 (2005).

[82] L. Canet, B. Delamotte, D. Mouhanna, and J. Vidal, Phys. Rev. D **67**, 065004 (2003); *ibid*, **68** 064421 (2003).

[83] J.-P. Blaizot, R. Mendez-Galain, and N. Wschebor, Phys. Lett. B **632**, 571 (2006).

[84] C. Bervillier, B. Boisseau, and H. Giacomini, Nucl. Phys. B **789**, 525 (2008); *ibid.*, **801**, 296 (2008).

[85] F. Benitez, J.-P. Blaizot, H. Chate, B. Delamotte, R. Mendez-Galain, and N. Wschebor, Phys. Rev. E **80**, 030103 (2009); *ibid.* **85**, 026707 (2012).

[86] S. Nagy, Phys. Rev. D **86**, 085020 (2012).

[87] J. M. Caillol, Nucl. Phys. B **865**, 291 (2012).

[88] A. Kapoyannis and N. Tetradis, Phys. Lett. A **276**, 225 (2000).

[89] D. Zappalà, Phys. Lett. A **290**, 35 (2001).

[90] S. Nagy and K. Sailer, Annals Phys. **326**, 1839 (2011).

[91] A. Ringwald and C. Wetterich, Nucl. Phys. B **334**, 506 (1990); U. Ellwanger, Z. Phys. C **62** 503 (1994).

[92] C. Wetterich, Nucl. Phys. B **352**, 529 (1991); Phys. Lett. B **301**, 90 (1993).

[93] T. R. Morris, Int. J. Mod. Phys. A **9**, 2411 (1994).

[94] N. Tetradis and C. Wetterich, Nucl. Phys. B **422**, 541 (1994).

[95] D. F. Litim, Phys. Lett. B **486**, 92 (2000); Phys. Rev. D **64**, 105007 (2001); JHEP **0111**, 059 (2001).

[96] I. Nándori, JHEP **1304**, 150 (2013).

[97] V. L. Berezinskii, Zh. Eksp. Teor. Fiz. **61**, 1144 (1971) [Sov. Phys. JETP **34**, 610 (1972)]

[98] J. M. Kosterlitz and D. J. Thouless, J. Phys. C **6**, 1181 (1973).

[99] M. Gräter and C. Wetterich, Phys. Rev. Lett. **75**, 378 (1995).

[100] I. Nandori, J. Polonyi, and K. Sailer, Phys. Rev. D **63**, 045022 (2001).

[101] G. v. Gersdorff and C. Wetterich, Phys. Rev. B **64**, 054513 (2001).

[102] N. Tetradis and C. Wetterich, Nucl. Phys. B **383**, 197 (1992).

[103] A. Codello, G. D'Odorico, and C. Pagani, JHEP **1407**, 040 (2014).

[104] An acknowledgement to J. M. Pawlowski for private discussions on this point.

[105] E. Marchais, "Infrared properties of scalar field theories", Ph.D. Thesis , 2012, University of Sussex http://sro.sussex.ac.uk/45244/

[106] J. Zinn-Justin, *Quantum Field Theory and Critical Phenomena*, Oxford, Clarendon (1989).

[107] T. R. Morris, Phys. Lett. B **334**, 355 (1994).

[108] A. Codello, J. Phys. A **45**, 465006 (2012).

[109] T. R. Morris, Int. J. Mod. Phys. **B**, 12, 1343 (1998)

[110] L. Onsager, Phys. Rev. **65** (1944) 117-149.

[111] Ulli Wolf, Phys. Rev. D **79**: 105002 (2009)

[112] Xavier Bekaert, Euihun Joung, Jihad Mourad, Proceedings of the XVII European Workshop on String Theory (Padova, 5-9 September 2011), arXiv:1202.0543 [hep-th]